ELECTROCHEMICAL AND SPECTROELECTROCHEMICAL STUDIES OF SOME BINUCLEAR COMPLEXES OF RUTHENIUM AND OSMIUM

RUTH J. SORBIE

Ph.D. Thesis

University of Edinburgh

1989

DECLARATION

Except where specific reference is made to other sources, the work presented in this thesis is the original work of the author. It has not been submitted, in whole or in part, for any other degree.

To my husband and my mother.

To the memory of my father.

ACKNOWLEDGEMENTS

I would like to thank Dr. L.J. Yellowlees for her help, encouragement and support throughout this work. I would also like to express my gratitude to Dr. A.J. Blake for collecting the crystal structure data and helping with solving the structures reported in this work and to Dr. A.J. Welch for helping me to perform and interpret the molecular orbital calculations discussed in Chapter 4.

In addition I am grateful to: Alison Griffith who performed the initial molecular orbital calculations discussed in Chapter 1 and helped with the work discussed in Chapter 3, Gwenda Kyd for her help with work in Chapter 5, Mr. A. Taylor for performing FAB mass spectra, Mrs. E. McDougall for performing C,H,N microanalyses, S.E.R.C. for their financial support, the University of Edinburgh for use of facilities and Mrs. Liz Glass who typed this thesis.

I would also like to thank Ewan, Ken, Alan and Robert for their help and support; special thanks are due to Alan who gave me some of his tetrabutylammonium tetrakis (pentafluorophenyl) borate.

Finally I would like to thank my husband, Craig, and my mother for their constant support and encouragement throughout this work, without which it would never have been completed.

ABSTRACT

This thesis involves the characterisation of metal-metal interactions in complexes of the type $[L_3M(\mu\text{-}X)_3ML_3]^{n+}$ where M = Ru, Os; L = terminal ligand e.g. PMe_2Ph; X = bridging ligand e.g. Cl^-; n = 1, 2, 3.

These complexes are all prepared in the n = 1 oxidation state. All undergo two one-electron oxidations $[L_3M(\mu\text{-}X)_3ML_3]^+ \overset{-e^-}{\rightleftharpoons} [L_3M(\mu\text{-}X)_3ML_3]^{2+} \overset{-e^-}{\rightleftharpoons} [L_3M(\mu\text{-}X)_3ML_3]^{3+}$.

Of particular interest is the n = 2 oxidation state which is the "mixed-valence" state. The mixed-valence species $[L_3Ru(\mu\text{-}X)_3RuL_3]^{2+}$ are unstable. They can however be studied and characterised by spectroelectochemical techniques as they are indefinitely stable under a suitable applied electro-generation potential. The technique involves studying the species formed by controlled potential electrolysis inside the cavity of a UV/VIS/NIR spectrophotometer using an optically transparent thin layer electrode (O.T.T.L.E.) cell. A detailed spectroelectrochemical study of $[(PMe_2Ph)_3Ru(\mu\text{-}Cl)_3Ru(PMe_2Ph)_3]^{2+}$ indicates that there is a strong metal-metal interaction between the two metal centres. The complex is considered as a Class III species according to the Robin and Day classification. Systematic alterations of M, X, n and L changes the extent of this interaction but it must always be considered to be strong.

In order to observe Class II behaviour we considered two possibilities, introduction of asymmetry and altering the number of bridging ligands. We studied the triple bridged asymmetric complex $[(CS)(PPh_3)_2Ru(\mu\text{-}Cl)_3RuCl(PPh_3)_2]^+$ and

single cyano-bridged complexes of the general type $[CpL_2Ru\text{-}CN\text{-}RuL_2Cp]^{2+}$ where L = soft neutral ligand. The triple chloro bridged asymmetric complex does indeed exhibit Class II behaviour; the cyano-bridged species however all exhibit Class III behaviour except for the complex $[Cp(PPh_3)_2Ru\text{-}CN\text{-}Ru(CO)(PPh_3)Cp]^{2+}$ which is a Class II species.

CONTENTS LIST

LIST OF FIGURES

LIST OF TABLES

LIST OF SCHEMES

C H A P T E R 1

INTRODUCTION OF BINUCLEAR COMPLEXES

AN EXTENDED SPECTROSCOPIC STUDY OF $[(PMe_2Ph)_3M(\mu\text{-}Cl)_3M(PMe_2Ph)_3]^{2+}$

WHERE M = Ru, Os

1.1 INTRODUCTION

This thesis is concerned with the electronic characterisation of metal-metal interactions in complexes containing two transition metal centres. Binuclear complexes where the two metal centres have different formal oxidation states are of considerable current interest because they represent the simplest systems in which to study these metal-metal interactions and also intramolecular electron transfer reactions. Complexes of this type are termed mixed-valence compounds. Their properties are rarely just the sum of the two metal ions taken separately. Usually there is an interaction between the metal ions which results in dramatic changes in the physical properties of the system e.g. $K_4Fe(II)(CN)_6$ and $Fe_2(III)(SO_4)_3$ are both pale yellow complexes; $KFe(II)Fe(III)(CN)_6$ is however deep blue.[1]

The properties of mixed-valence compounds are related very closely to the similarity or difference in symmetry between the ligand fields of the ions of differing valency. Mixed-valence compounds have been placed into three categories by Robin and Day.[2]

Class 1 species have metal centres in different coordination environments e.g. one may be in an octahedral ligand field and the other a tetrahedral ligand field. In complexes of this type there is no interaction between the metal centres. They are termed "trapped" valence complexes. Class II complexes contain metal centres whose ligand fields are of nearly identical symmetry; they are however crystallographically distinguishable. In this case there is a weak interaction between the metal centres. Class III complexes

contain metal ions in identical coordination environments and are thus crystallographically equivalent. There is a strong interaction between the metal centres.

The absorption spectra of Class I species exhibit a superposition of the electronic spectra of their constituent ions. Class II species show the electronic spectra of their constituent ions at similar energy values. The spectra of the constituent ions is not however evident in the electronic spectrum of Class III species.

The assignment of bands in an absorption spectrum to specific electronic transitions is notoriously difficult. It is often helpful, however, though not entirely rigorous, to categorise the electronic excitations in quite a simple way as "metal based", charge transfer or "ligand based" in origin.[3]

A. <u>"Metal-based" or d-d bands</u>

Such bands arise due to the excitation of an electron from one d orbital on the central metal to another d orbital e.g. in the case of an octahedral complex with a d^1 configuration the following transition occurs on absorption of light of the correct frequency.

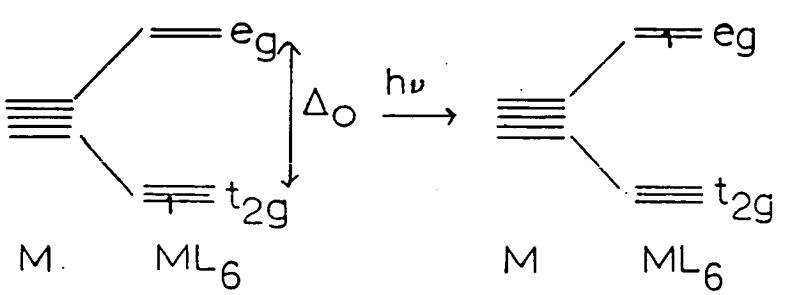

This type of absorption tends to occur in the near infra red or visible region of the electronic spectrum for first row transition metals and is characteristically weak. The intensity of a band is measured by the extinction coefficient, ε, where $\varepsilon = A/cl$; A = absorbance; c = concentration, mol dm^{-3} and l = pathlength, cm, and is usually of the order of 1-10 $mol^{-1}cm^{-1}dm^{3}$ for d-d bands. The intensity of a band is a measure of the probability of a transition and d-d bands are formally forbidden in a strict octahedral environment by Laportes rule which states that $\Delta l = \pm 1$. They are only observed because of vibronic coupling. In tetrahedral complexes there is breakdown of Laportes rule since the p subshell also has t_2 symmetry and hence can mix with the d t_2 set leading to the upper level acquiring some p character. Thus $\Delta l = \pm 1$ holds and the $e \rightarrow t_2$ transition is allowed. However it must be stressed that the bands are still relatively weak. d-d bands are independent of the nature of solvent.

B. Charge Transfer Bands

Absorption bands due to charge transfer transitions involve the transfer of an electron from a molecular orbital centred mainly on the ligand to one centred mainly on the metal (LMCT) or vice versa (MLCT).

They are often of higher energy than d-d transitions and are usually observed at the extreme blue end of the spectrum or in the ultra-violet region. Nearly all charge transfer processes are fully allowed and hence they tend to be very strong, sometimes masking the weak d-d bands (ε is usually of the order 10^3-10^4 $mol^{-1}cm^{-1}dm^3$). LMCT and MLCT processes can

be distinguished by the contrasting behaviour of the energy of the band upon oxidation or reduction of the metal centre. If the absorption band arises due to a LMCT transition then on oxidation of the metal centre, the LMCT absorption band will move to a lower energy and vice versa for MLCT, e.g. in the absorption spectrum of $[OsCl_3(py)_3]^{-4}$ the band at 22,000 cm^{-1} is assigned as a MLCT transition, on oxidation to $OsCl_3(py)_3$ this band shifts to 31,600 cm^{-1}. $[OsCl_6]^{3-4}$ has two bands at 29,600 cm^{-1} and 35,100 cm^{-1} which are assigned as LMCT transitions. On oxidation these shift to 26,400 cm^{-1} and 29,200 cm^{-1} respectively.

The energy of a charge transfer process is dependent on the solvent used for study, because the dipole of the excited state is different from that of the ground state. Thus the orientation of the solvent molecules will not be the same for both the ground state and for the excited state. It is assumed that the electronic transition is a Franck-Condon type transition and therefore takes place many orders of magnitude faster than molecular rearrangements. Depending on the solvent used and the change in dipole, the excited state may be either stabilised or destabilised, that is, the absorption band will move to lower or higher energy respectively.

C. "Ligand based" or Intraligand Bands

Some ligands have low-lying empty orbitals, which are usually antibonding in character. An electronic transition can occur to this orbital from an occupied level also localised primarily on the ligand, leading to characteristic absorption

spectra. The ligand-ligand transition will depend on the nature of the metal centre since the metal-ligand band will involve the occupied ligand based orbital and hence the position of the band will be sensitive to the oxidation state of the metal. Usually when the metal centre is oxidised the transition will move to a lower energy, e.g.

	$\nu(cm^{-1})$ for bipy $\pi \rightarrow \pi^*$ transition [5]
$Ru(bipy)_3^{2+}$	34,000
$Ru(bipy)_3^{3+}$	32,300

(free bipy shows the $\pi \rightarrow \pi^*$ transition at 35,400 cm^{-1})

It can be seen that the change in energy of intraligand transitions observed on oxidation is not as large as those for MLCT/LMCT processes.

These transitions usually occur in the higher energy region of the electronic spectrum, in the ultra-violet region, and are fully allowed ($\varepsilon \sim 10^3 - 10^6$ $mol^{-1}cm^{-1}dm^3$) as are the measurable charge transfer transitions.

The intensity of a band is determined largely from selection rules, with more intense bands arising from transitions which are both spin and orbitally allowed. For an allowed charge transfer transition to show an appreciable intensity it must have significant "one centre character". This is expected on the basis of commonplace understanding of the linear combination of atomic orbitals to form molecular orbitals or the "covalency" of coordinate bonds. A further point regarding band intensities is that strictly it is not the extinction coefficient of a band which is the meaningful parameter; rather

it is the oscillator strength, f. This parameter can be approximated by the area under the peak or $\varepsilon \times \Delta_{\frac{1}{2}}$ where $\Delta_{\frac{1}{2}}$ is the band halfwidth.

In addition to these electronic transitions discussed above the mixed-valence Class II and Class III species exhibit a low energy absorption(s) in the electronic spectrum which have been termed intervalence charge transfer transitions, IVCT. Class I species show no such absorption. The potential energy diagrams for Class I, II and III complexes showing the origin of this transition are illustrated in Figure 1.1.1.[6]

In the case of Class II species this low energy absorption occurs due to true intervalence charge transfer, ν_{IT}. This is attributed to an electron transfer from one metal site to another and can be represented as follows:

$$M(II)M^1(II) \xrightarrow{\nu_{IT}} M(III)M^1(II)*$$

This light induced process generates a M(III) ion in the coordination environment of M(II) and vice versa. The excited species reverts back to the ground state configuration by vibrational relaxation. Bands which arise from this process tend to be fairly weak with $\varepsilon \sim 10\text{-}10^3$ $mol^{-1}cm^{-1}dm^3$. e.g. $[(bipy)_2ClRu(pyz)RuCl(bipy)_2]^{3+}$ [7] shows an intervalence charge transfer band at 7700 cm^{-1}, ε = 450 $mol^{-1}cm^{-1}dm^3$. IVCT bands are broad and the band halfwidth, $\Delta_{\frac{1}{2}}$, for symmetrical complexes such as that given above is usually around 5000 cm^{-1}. The band halfwidth is commonly evaluated as the band width when $A/A_{max} = \frac{1}{2}$, where A is the absorbance. They rarely show vibrational structure, however with third row metals such as osmium the band may be split due to a spin coupling effect.

Figure 1.1.1: Potential Energy versus Nuclear Configuration for Class I, II and III Complexes

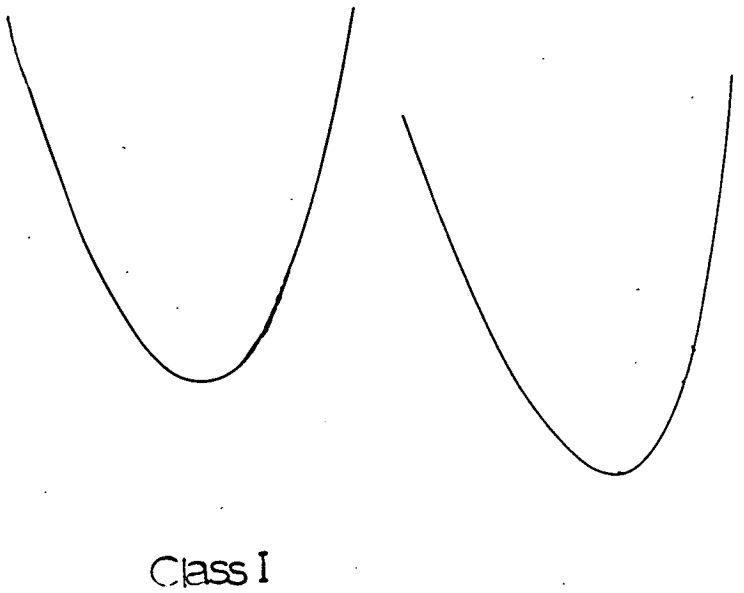

Class I

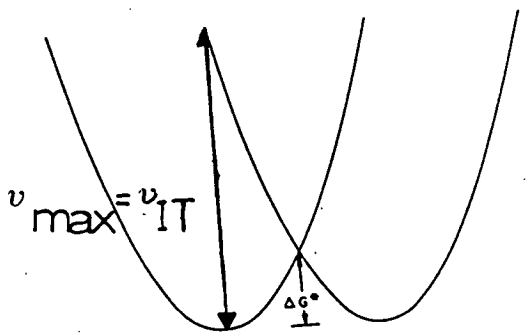

Class II

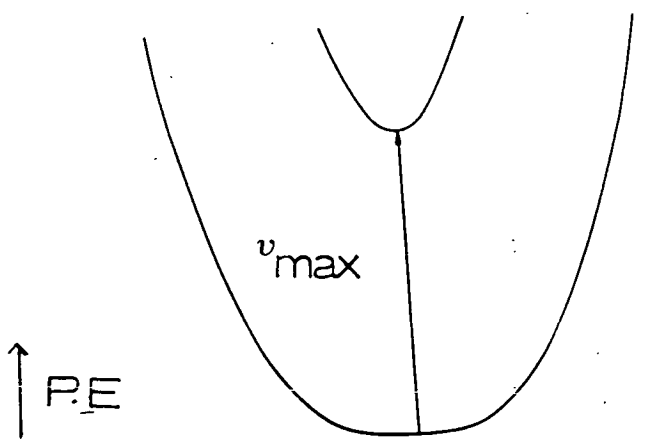

Class III

This effect, which occurs for heavier elements, can lift the degeneracy of otherwise degenerate states leading to more absorption bands than expected and can cause states of different spin to mix which results in the borrowing of intensity by spin forbidden bands from spin allowed bands. Examples of this occur with $[(bipy)_2ClOs(PPh_2CH_2Ph_2P)OsCl(bipy)_2]^{3+}$ [8] and $[(bipy)_2ClRu(pyz)OsCl(bipy)_2]^{3+}$ [9] where the respective IVCT bands are observed at 10,000 cm^{-1}(broad), 6000 cm^{-1}(broad) and 10,900 cm^{-1}(broad), 5900 cm^{-1}(narrow).

In Class III complexes the metal centres are strongly interacting and each metal centre should be considered to have equal charge or average valency. It is necessary in these strongly interacting systems to invoke molecular orbital models in which the low energy bands arise due to transitions within this molecular orbital framework. These bands are often wrongly referred to as IVCT bands also.

Class III low energy bands tend to be more intense than Class II IVCT bands, e.g. the extinction coefficient, ε, for the near infra-red (NIR) band (6370 cm^{-1}) observed for the Creutz-Taube complex[10], designated as a Class III species is 5000 $mol^{-1}cm^{-1}dm^3$. The band halfwidth, $\Delta_{\frac{1}{2}}$, is much narrower. The measured $\Delta_{\frac{1}{2}}$ value for the NIR band in the Creutz-Taube ion is 1500 cm^{-1}. The narrow bands of Class III complexes follows from Figure 1.1.1 as transitions from the turning point of the zero point vibration of the lower potential energy surface fall very close to the corresponding turning points on the upper surface. There may be more than one low energy transition depending on the number which are symmetry allowed. They often show vibrational structure.

Hush[11] has proposed several parameters to distinguish further between Class II and Class III species. Hush theory for species with the two metal centres having the same terminal ligand sets, termed symmetric complexes, will be considered here.

Figure 1.1.1 shows that for a Class II species the vertical process E_{op} corresponds to the intervalence charge transfer process, ν_{IT}. The energy barrier for thermal electron transfer is:

$$E_{th} = {}^{1}/_{4}\, E_{op} \qquad (1)$$

where $$E_{op} = E_{in} + E_{out} \qquad (2)$$

E_{in} is the Franck-Condon term and E_{out} is associated with the reorganisation of the solvent molecules around the metal centres after electron transfer occurs. Directly after electron transfer i.e. M(II)M'(III) → M(III)M'(II), M(III) will have the solvent environment of M(II) and M (II) will have that of M'(III), thus energy is required to reorganise the solvent molecules.

$$E_{out} = e^2 \left(\frac{1}{2a_1} + \frac{1}{2a_2} - \frac{1}{d} \right) \left(\frac{1}{D_{op}} - \frac{1}{D_s} \right) \qquad (3)$$

where $a_{1,2}$ = radii of the two coordination spheres

d = metal-metal distance in Å

D_{op} = optical dielectric constant (equal to the square of the refractive index, n)

D_s = static dielectric constant

The energy of the intervalence charge transfer band is therefore dependent on the solvent used. A plot of ν_{IT} versus ${}^{1}/D_{op} - {}^{1}/D_s$ should be a straight line. The value of

the intercept gives an indication of E_{in}.

The low energy bands observed for Class III species show no solvent dependence as both metal centres have the same charge and coordination environment.

The band halfwidth, $\Delta_{\frac{1}{2}}$, for an intervalence charge transfer band can be calculated using

$$\Delta_{\frac{1}{2}}(\text{calc}) = [\, 2310\ \nu_{IT}\,]^{\frac{1}{2}}\ \text{cm}^{-1} \qquad (4)$$

If the species is a Class II complex then agreement to within 10% of the experimentally observed band halfwidth should be obtained.

The bandhalfwidth for Class II complexes is dependent on temperature tending to decrease as the temperature is lowered. The absorption bands of Class III complexes show no such behaviour.

The degree of delocalisation, α, can be obtained from the intervalence charge transfer band by:

$$\alpha^2 = \frac{4.24 \times 10^{-4}\ \varepsilon\ \Delta_{\frac{1}{2}}}{\nu_{IT}\ d^2} \qquad (5)$$

where ε = extinction coefficient, $\text{mol}^{-1}\text{cm}^{-1}\text{dm}^3$

d = distance between the metal centres in $\mathring{A}$

For a Class II complex $0 < \alpha < 0.25$.

From the above discussion it is apparent that by examination of the low energy region of the electronic spectrum the class of the mixed-valence binuclear complex can be determined. There are many examples of mixed-valence complexes in the literature, particularly for Ruthenium and Osmium.

The most frequent combination of oxidation states is M(II)M'(III) which corresponds to the low spin d^6-d^5 configuration. Examples of complexes of this type include $[(NH_3)_5Ru\text{-}NC\text{-}Ru(CN)_5]^-$ [12] and $[(NH_3)_5Ru(4,4'\text{-bipy})Ru(NH_3)_5]^{5+}$.[13]

There are two main methods that are used for preparing mixed-valence compelxes.

1. Direct combination of two mononuclear species, one of which has a labile coordination site.
2. Electrochemical reduction or oxidation of a binuclear species where the metal centres are M(III)M'(III) or M(II)M'(II) respectively.

The binuclear species we chose to extensively investigate all have three identical bridging ligands (x) and a confacial bioctahedral structure as shown below:

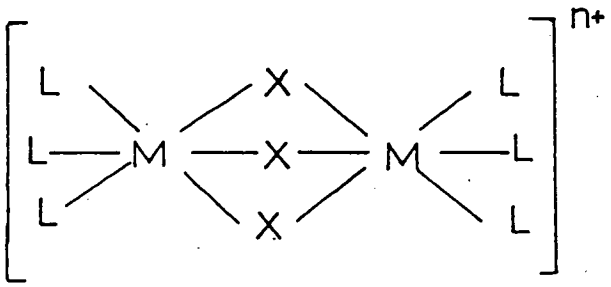

I

The mixed-valence compounds were generated from stable parent complexes by a one-electron exhaustive electrolysis as in method 2 above.

The monocationic species M=Ru, X=Cl and L=PMe_2Ph was first prepared by Chatt in 1961[14] by the interaction of $RuCl_3.3H_2O$ and PMe_2Ph in aqueous methanol.

The complex $[(PMe_2Ph)_3Ru(\mu\text{-}Cl)_3Ru(PMe_2Ph)_3]^+$, undergoes

two reversible one-electron oxidations at +1.23V and +1.75V (versus Ag/AgCl).[15] The two oxidation processes are thus separated by 0.5V. It has been previously suggested that this is indicative of electron delocalisation.[16] Figure 1.1.2 shows the cyclic voltammogram and ac voltammogram for $[(PMe_2Ph)_3Ru(\mu\text{-}Cl)_3Ru(PMe_2Ph)_3]PF_6$. The mixed-valence species $[(PMe_2Ph)_3Ru(\mu\text{-}Cl)_3Ru(PMe_2Ph)_3]^{2+}$ cannot be prepared chemically. It can however be studied and characterised by in situ techniques such as spectroelectrochemistry as it is indefinitely stable at a suitable electrogeneration potential. The spectroelectrochemical technique involves studying the species formed by controlled potential electrolysis inside the cavity of a UV/VIS/NIR spectrophotometer using an optically transparent thin layer electrode cell.

Preliminary spectroelectrochemical studies[17] on the analogous complex where $L=PEt_2Ph$, $X^-=Cl^-$ showed that the mixed-valence species had one low energy band at 4350 cm^{-1}. Initial investigations assigned this complex as a delocalised, Class III, system. In this work the species where $L=PMe_2Ph$, $X^-=Cl^-$ and M=Ru has been thoroughly studied using spectroelectrochemical techniques.

1.2 RESULTS AND DISCUSSION

$[(PMe_2Ph)_3Ru(\mu\text{-}Cl)_3Ru(PMe_2Ph)_3]Cl$ was prepared according to the method of Chatt.[14] The counterion was exchanged for PF_6^- by metathesis because Cl^- has a facile oxidative process which would mask the redox processes of the binuclear species.

Figure 1.1.2: Electrochemistry of $[(PMe_2Ph)_3Ru(\mu\text{-}Cl)_3Ru(PMe_2Ph)_3]^+$ in Methylene Chloride / 0.5M $TBABF_4$

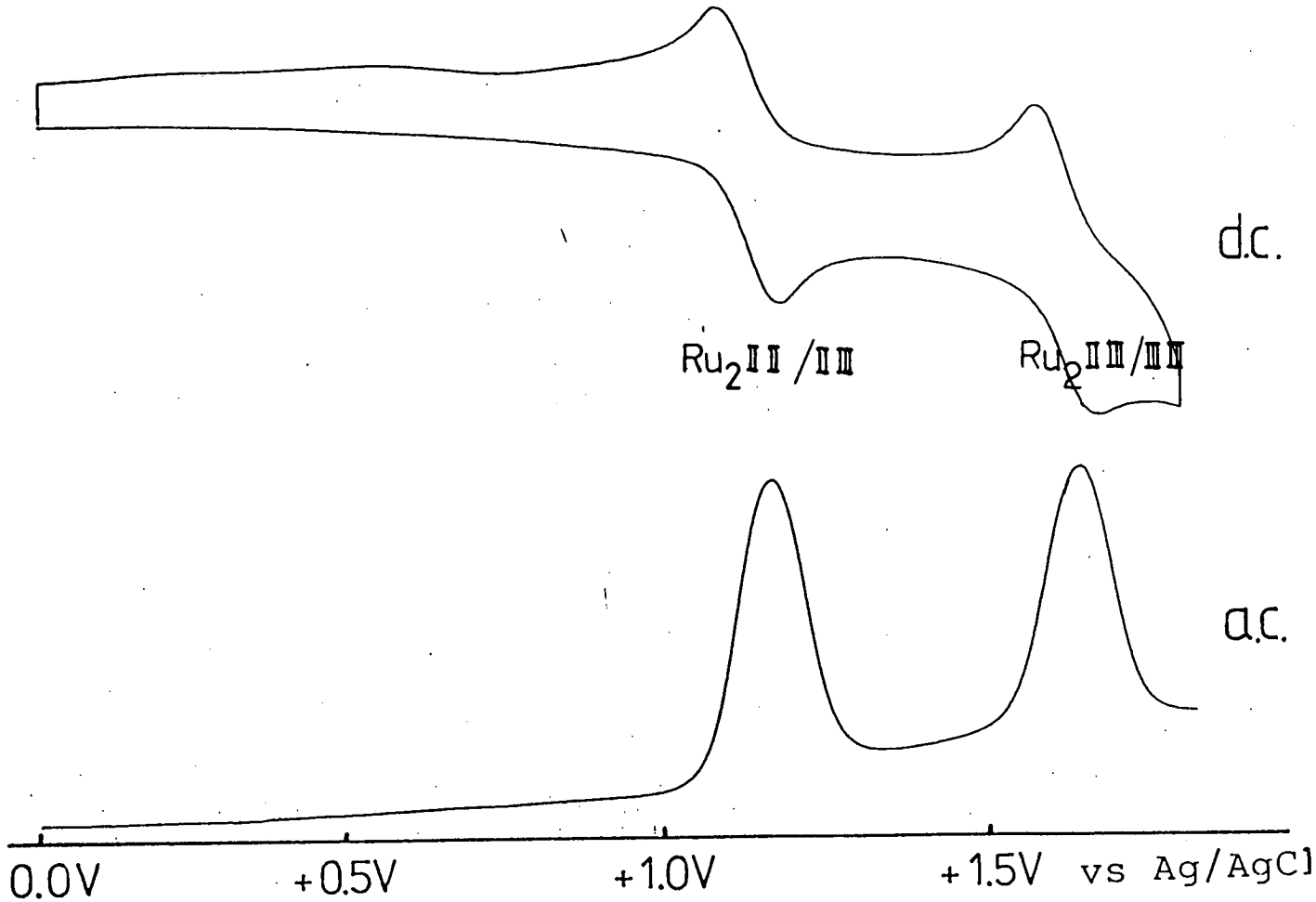

1.2.1 Spectroelectrochemical Studies

The mixed-valence species $[(PMe_2Ph)_3Ru(\mu\text{-}Cl)_3Ru(PMe_2Ph)_3]^{2+}$ was electrogenerated *in situ* in dichloromethane/0.5M $TBABF_4$ at +1.40V using the O.T.T.L.E. cell. The temperature was maintained at 267K throughout the experiment. Spectra were recorded over the range 3125-50,000 cm^{-1}. After recording the change in the spectrum from $[(PMe_2Ph)_3Ru(\mu\text{-}Cl)_3Ru(PMe_2Ph)_3]^{+}$ to $[(PMe_2Ph)_3Ru(\mu\text{-}Cl)_3Ru(PMe_2Ph)_3]^{2+}$ as a function of time the spectrum of the latter species was recorded. It was then reduced back to $[(PMe_2Ph)_3Ru(\mu\text{-}Cl)_3Ru(PMe_2Ph)_3]^{+}$. A requirement of a successful spectroelectrochemical experiment is that the spectrum of the final $[(PMe_2Ph)_3Ru(\mu\text{-}Cl)_3Ru(PMe_2Ph)_3]^{+}$ species is the same in every regard as the starting spectrum. This is indicative of the system being chemically reversible and hence that the spectrum we have observed is a direct consequence of the oxidation process generating the $[(PMe_2Ph)_3Ru(\mu\text{-}Cl)_3Ru(PMe_2Ph)_3]^{2+}$ species. This procedure was followed for every spectroelectrochemical experiment reported in this thesis. Only the near infra-red region of the spectrum will be discussed within this Chapter. Figure 1.2.1. shows the conversion of $[(PMe_2Ph)_3Ru(\mu\text{-}Cl)_3Ru(PMe_2Ph)_3]^{+}$ → $[(PMe_2Ph)_3Ru(\mu\text{-}Cl)_3Ru(PMe_2Ph)_3]^{2+}$ together with the final spectrum of the latter species.

Two bands are observed in the near infra-red region of the spectrum at 7770 cm^{-1} (ε=2864 $mol^{-1}cm^{-1}dm^3$) and 5000 cm^{-1} (ε=2613 $mol^{-1}cm^{-1}dm^3$). We note that only one near infra-red band was observed in the preliminary study. No such bands were observed for related monomeric species as shown in the UV/VIS/NIR spectra of $RuCl_2(P(OMe)Ph_2)_4$ and $RuCl_3(PMe_2Ph)_3$ in

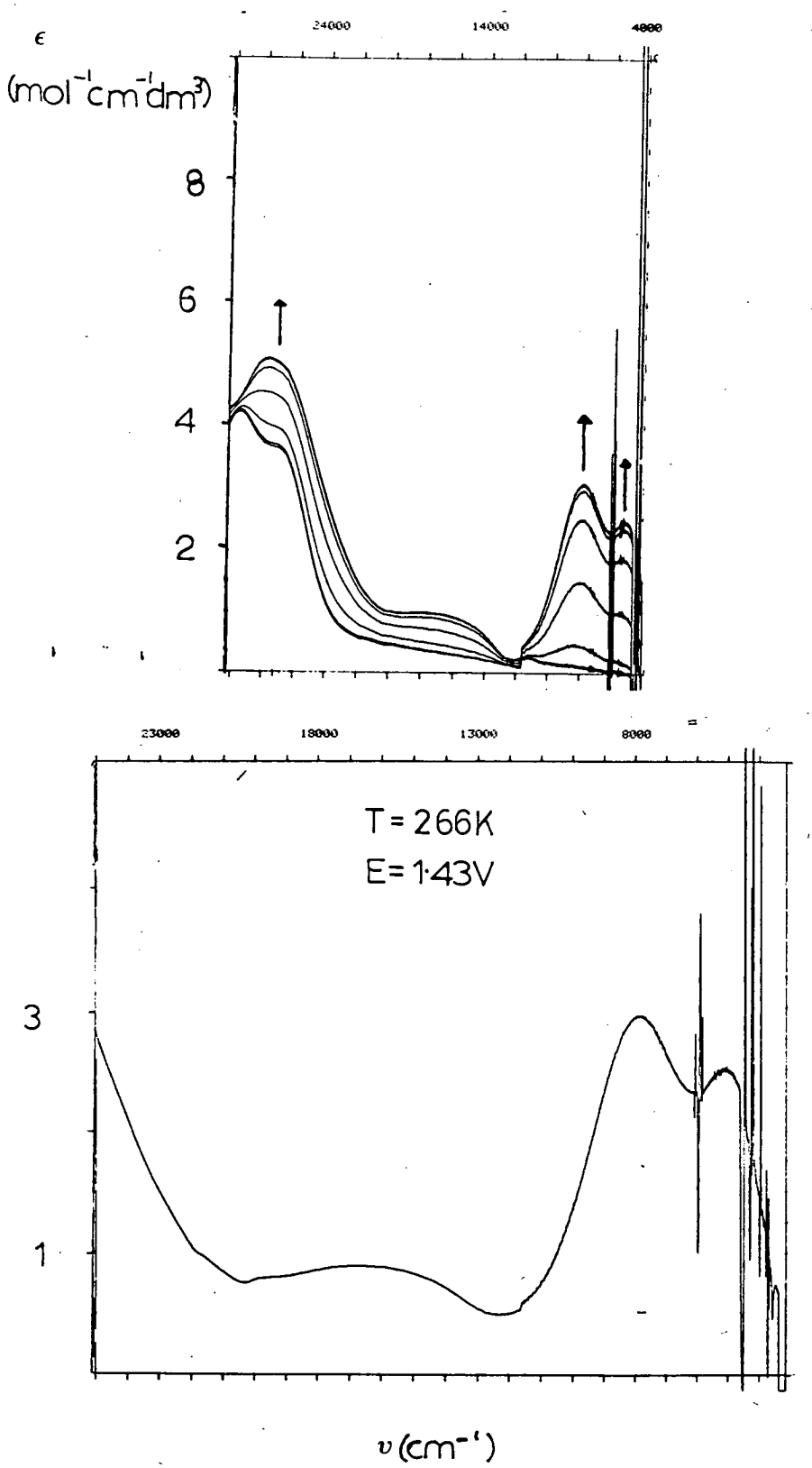

Figure 1.2.1: Spectrum showing conversion of $[(PMe_2Ph)_3Ru(\mu\text{-}Cl)_3Ru(PMe_2Ph)_3]^{+} \rightarrow [(PMe_2Ph)_3Ru(\mu\text{-}Cl)_3Ru(PMe_2Ph)_3]^{2+}$ together with Final Spectrum of $[(PMe_2Ph)_3Ru(\mu\text{-}Cl)_3Ru(PMe_2Ph)_3]^{2+}$

Figure 1.2.2. The monomer, $RuCl_2(PMe_2Ph)_4$ dimerises rapidly in polar media so we were unable to obtain its electronic spectrum whereas $RuCl_2(P(OMe)Ph_2)_4$ requires heating to dimerise. We therefore report the spectrum of the $RuCl_2(P(OMe)Ph_2)_4$ species (Chapter 4 discusses the behaviour of binuclear complexes with different tertiary phosphine ligands. $[(P(OMe)Ph_2)_3Ru(\mu\text{-}Cl)_3Ru(P(OMe)Ph_2)_3]^{2+}$ does however exhibit two low energy bands.). The parent complex $[(PMe_2Ph)_3Ru(\mu\text{-}Cl)_3Ru(PMe_2Ph)_3]^{+}$ shows no near infra-red bands. Unfortunately $[(PMe_2Ph)_3Ru(\mu\text{-}Cl)_3Ru(PMe_2Ph)_3]^{3+}$ could not be successfully electrogenerated. This will be discussed further in Chapter 4.

The band halfwidth, $\Delta_{\frac{1}{2}}$, of the high energy band (taken as twice the energy measure at half height from the high energy side of the band to its centre) at T=300K was measured at 3400 cm^{-1}. Applying Hush theory (equation (4) in section 1.1) to this band gives a $\Delta_{\frac{1}{2}}$ (calc) of 4240 cm^{-1}. Furthermore, $\Delta_{\frac{1}{2}}$ does not vary significantly with temperature, being 3400 cm^{-1} from 300-253K. Further lowering of the temperature to between 243 and 220K causes $\Delta_{\frac{1}{2}}$ to decrease by only 100 cm^{-1} to 3300 cm^{-1}.

The related Osmium complex $[(PMe_2Ph)_3Os(\mu\text{-}Cl)_3Os(PMe_2Ph)_3]^{+}$ which will be discussed in more detail in Chapter 2 also undergoes two one-electron oxidation processes. The absorption spectrum of $[(PMe_2Ph)_3Os(\mu\text{-}Cl)_3Os(PMe_2Ph)_3]^{2+}$ also exhibits two near infra-red bands at 4991 cm^{-1} and 9000 cm^{-1} neither of which show any temperature dependence. Figure 2.2.2 in Chapter 2 show the spectrum of $[(PMe_2Ph)_3Os(\mu\text{-}Cl)_3\text{-}Os(PMe_2Ph)_3]^{2+}$ in methylene chloride/0.5M $TBABF_4$. The

Figure 1.2.2: Spectra of (a) $RuCl_3(PMe_2Ph)_3$ and (b) $RuCl_2(P(OMe)Ph_2)_4$ in Methylene Chloride
T = 290K

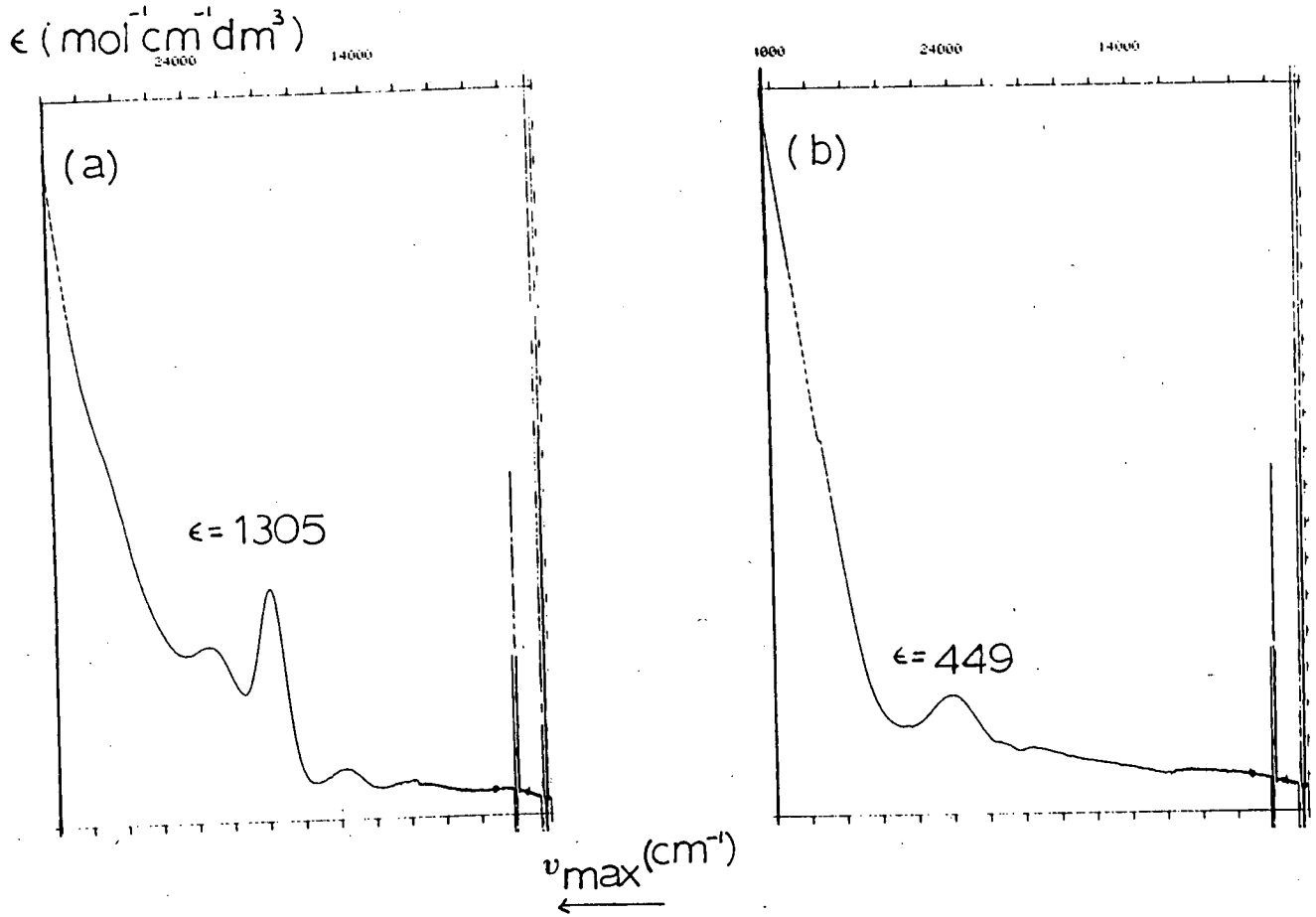

diosmium species has a more accessible first oxidation process as expected (see Chapter 2, Section 2.1); occurring at +1.03V compared with +1.23V in the case of the Ruthenium complex (both are versus Ag/AgCl). Thus a study of the behaviour of the near infra-red absorption band in various solvents was carried out on $[(PMe_2Ph)_3Os(\mu\text{-}Cl)_3Os(PMe_2Ph)_3]^{2+}$. The solvents used were:-

1. Methylene Chloride / 0.5M $TBABF_4$
2. Chloroform / 0.5M $TBABF_4$
3. Dimethylformamide / 0.1M $TBABF_4$
4. Acetone / 0.1M $TBABF_4$
5. Acetonitrile / 0.1M $TBABF_4$

The $[(PMe_2Ph)_3Os(\mu\text{-}Cl)_3Os(PMe_2Ph)_3]^{2+}$ species was generated in each solvent as previously described. Table 1.2.1 gives the values of ν_{max} observed for the most intense band in each solvent together with relevant $^1/D_{op} - {}^1/D_s$ values.

Figure 1.2.3 shows the plot of ν_{max} versus $^1/D_{op} - {}^1/D_s$ for $[(PMe_2Ph)_3Os(\mu\text{-}Cl)_3Os(PMe_2Ph)_3]^{2+}$. On the same graph a plot of ν_{max} versus $^1/D_{op} - {}^1/D_s$ for the well established Class II species $[(bipy)_2ClRu(4_14^1\text{-}bipy)RuCl(bipy)_2]^{3+}$ [18] is shown.

A summary of the observed behaviour for the near-infra red absorption bands of $[(PMe_2Ph)_3M(\mu\text{-}Cl)_3M(PMe_2Ph)_3]^{2+}$, where M=Ru, Os is as follows:

1. The most intense near infra-red band shows no solvent or temperature dependence.

Table 1.2.1 Positions of the most intense low Energy Band in $[(PMe_2Ph)_3Os(\mu\text{-}Cl)_3Os(PMe_2Ph)_3]^{2+}$ in Different Solvents

ν_{max} (cm^{-1})	D_{op}	D_s	Solvent
4,991	2.028	8.9	Methylene Chloride 0.5M $TBABF_4$
5,003	2.085	4.7	Chloroform 0.5M $TBABF_4$
5,000	2.0458	36.7	Dimethyl Formamide 0.1M $TBABF_4$
4,990	1.8413	20.7	Acetone 0.1M $TBABF_4$
5,010	1.8066	36.2	Acetonitrile 0.1M $TBABF_4$

A $X = [(bipy)_2ClRuN\langle\rangle\langle\rangle NRuCl(bipy)_2]^{3+}$

B $\circ = [(PMe_2Ph)_3Os(\mu\text{-}Cl)_3Os(PMe_2Ph)_3]^{2+}$

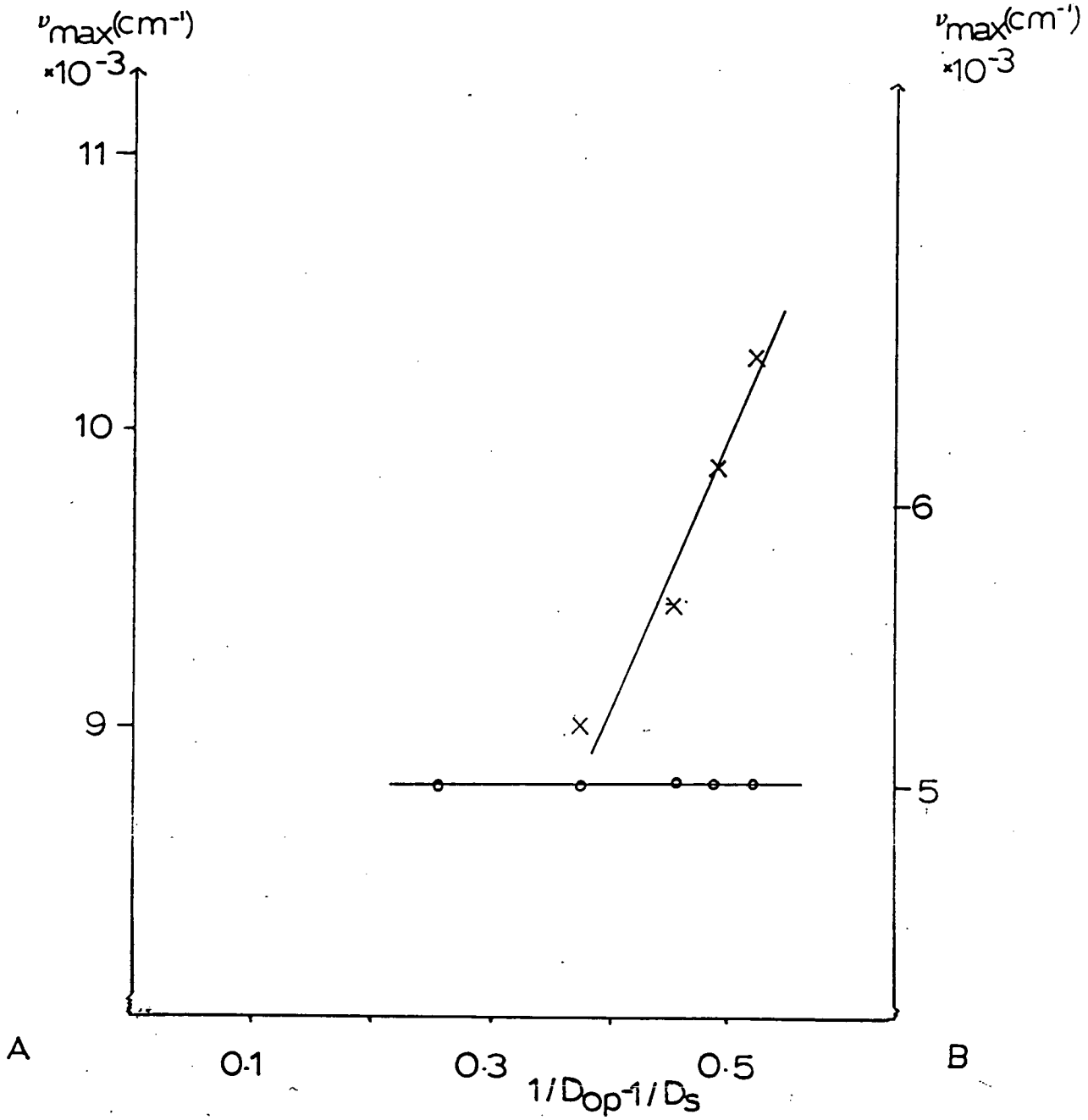

Figure 1.2.3: Graph of ν_{max} versus $^1/D_{op} - {}^1/D_s$ for complexes A and B in various solvents

2. $\Delta_{\frac{1}{2}}$ is narrower than predicted by Hush theory.
3. The band is more intense than expected for an intervalence charge transfer band.

These results suggest that these complexes belong to Class III-type species, that is they must be considered to have strong metal-metal interactions.

The observation of two near infra-red bands must now be addressed.

The molecular orbital scheme for the interaction of metal based d-orbitals within a confacial bioctahedral D_{3h} structure has been described in the literature by Hoffman and others.[19] If the threefold metal-metal axis is taken as the z-axis then the d_{z^2} orbitals interact to form σ and σ^* orbitals with a_1' and a_2'' symmetries respectively. The d_{xy} and $d_{x^2-y^2}$ orbitals interact, presumably weakly, producing δ and δ^* orbitals which have e' and e" symmetries respectively.

A qualitative molecular orbital diagram is shown in Figure 1.2.4.[20] For the Ru(II),Ru(II) parent complex all these orbitals will be full. The related mixed-valence complex $[(NH_3)_3Ru(\mu\text{-}Cl)_3Ru(NH_3)_3]^{2+}$ has been studied by Hush.[20] The electronic spectrum of this species displayed one band in the near infra-red region of the spectrum and one in the visible region. The electronic character of this species was then discussed using the above molecular orbital scheme. The $[(NH_3)_3Ru(\mu\text{-}Cl)_3Ru(NH_3)_3]^{2+}$ species has a formal metal d^6d^5 configuration which leaves the a_2'' orbital singly occupied, thus electronic transitions from the lower

Figure 1.2.4: Molecular orbital scheme for the Interaction of d-orbitals in D_{3h} symmetry

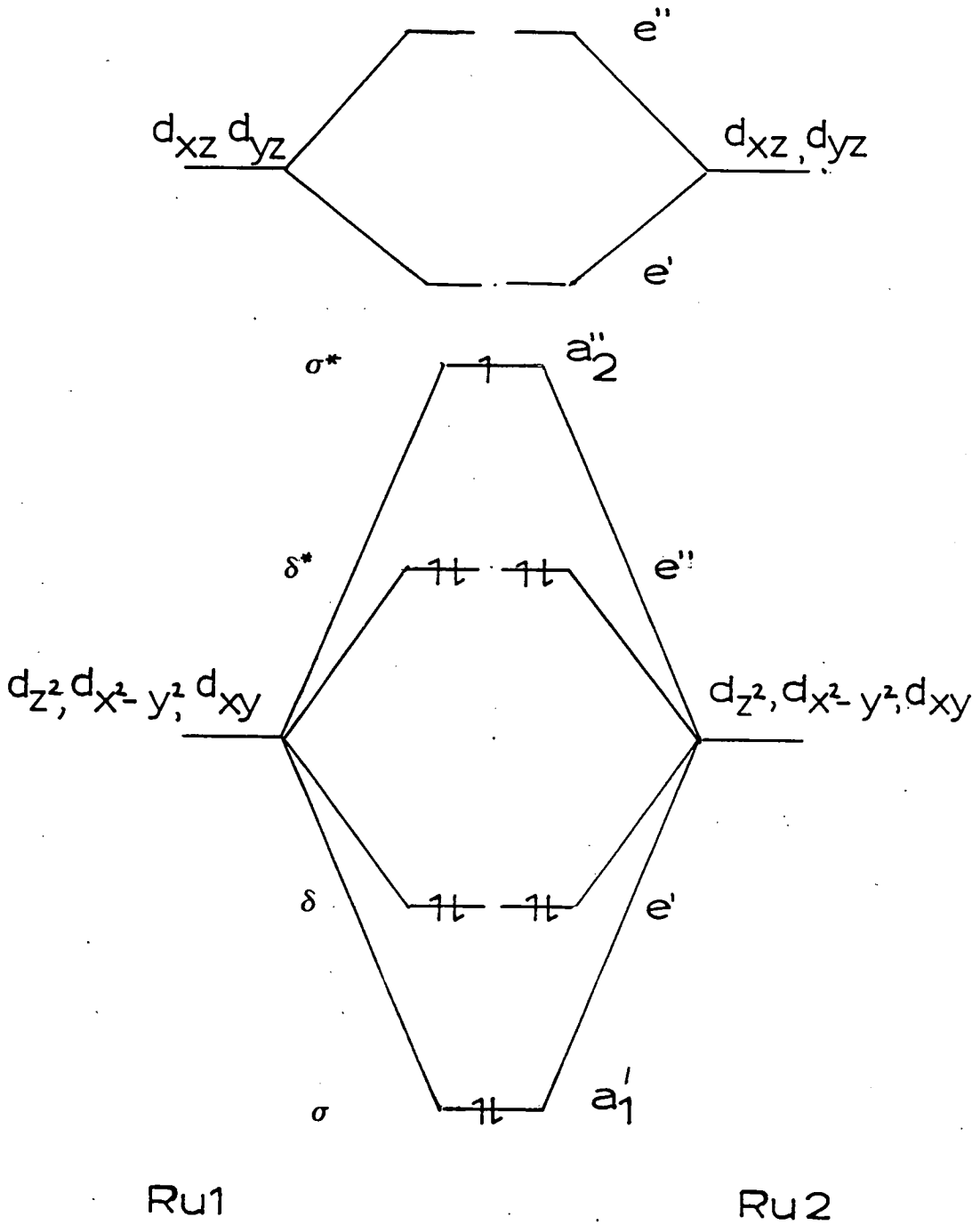

(From reference 20)

levels to the partially occupied $a_2"$ orbital can be envisaged. Symmetry considerations determine that only two transitions are electronically allowed and will thus carry measurable intensities.

$$e" \rightarrow a_2" \quad (x,y \text{ polarised})$$

$$a_1' \rightarrow a_2" \quad (z \text{ polarised})$$

The transition from $e' \rightarrow a_2"$ is symmetry forbidden and will therefore be weak and will probably not be observed.

Electronic selection rules state that for a transition to have appreciable and measurable intensity we must apply the following relationship

$$\sqrt{D} = \int \psi_i \cdot M \cdot \psi_f \, d\zeta \qquad (6)$$

where $\sqrt{D}$ is the transition moment for a transition between two states of a molecule which are described by the wave functions ψ_i (initial level) and ψ_f (final level). M is the dipole moment vector with components $M_x=\Sigma e_j x_j$; $M_y=\Sigma e_j y_j$ and $M_z=\Sigma e_j z_j$ where e_j is the charge of a particle j having coordinates x_j, y_j and z_j.

For a transition to be allowed the integrand must contain the totally symmetric symmetry label A, A_1, A_g or A' of the appropriate point group i.e. have a character of +1 for each symmetry operation.

We can apply this to the system under study, where there are three possible transitions to consider:

1. $a_1' \rightarrow a_2"$
2. $e" \rightarrow a_2"$
3. $e' \rightarrow a_2"$

The symmetry of each of the initial and final wave functions and the components of M are known, so for

1. $a_1' \rightarrow a_2''$

$\psi_i = a_2''$, $\psi_f = a_1'$, $M_{xy} = e'$ and $M_z = a_2''$

Thus ψ_i M ψ_f transforms as e" for M_{xy} and a_1' for M_z which means that the $a_1' \rightarrow a_2''$ transition is electronically allowed.

2. $e'' \rightarrow a_2''$

$\psi_i = a_2''$, $\psi_f = e''$

Product = $a_1' + a_2' + e''$ (xy)

e'' (z)

3. $e' \rightarrow a_2''$

$\psi_i = a_2''$, $\psi_f = e'$

Product = $a_1'' + a_2'' + e''$ (xy)

e'' (z)

so $e'' \rightarrow a_2''$ is allowed in the x,y direction and $e' \rightarrow a_2''$ is forbidden.

Hush therefore assigned the visible absorption band to the $\sigma \rightarrow \sigma^*$ transition ($a_1' \rightarrow a_2''$) and the near infra-red band to the $\delta^* \rightarrow \sigma^*$ transition ($e'' \rightarrow a_2''$).

Intensity arguments also bear this assignment out. The visible band is far more intense than the near infra-red band (ε = 4300 $mol^{-1}cm^{-1}dm^3$ compared to ε = 230 $mol^{-1}cm^{-1}dm^3$) and it is exactly this transition which will have greater amount of "one-centre" character since both the bonding and

antibonding σ orbitals are derived from the same metal based d-orbital.

In order to determine if this explanation is applicable to the system under study extended Hückel molecular orbital (E.H.M.O.) calculations were carried out.

1.2.2 E.H.M.O. Calculations [21]

$[(PMe_2Ph)_3Ru(\mu\text{-}Cl)_3Ru(PMe_2Ph)_3]^{2+}$ was modeled to give ideal D_{3h} symmetry. It was assumed that the Cl-Ru-Cl angle is 90°, Cl-Ru-Ru is 54.74° and P-Ru-P is 90°; with the Ru--Ru distance of 3.16Å and Ru-Cl of 2.74Å. (Assuming the above values for the angles and using an Ru--Ru distance of 3.40Å, which is observed in the monocationic species, would imply that the Ru-Cl bond is 2.94Å which is very long compared to the actual value of 2.50Å, thus the Ru-Ru distance was modified.)

Atomic coordinates for the framework

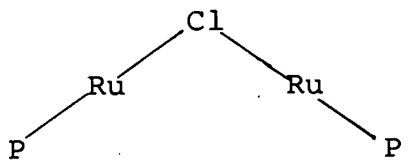

were calculated from average crystallographic data for $[(PMe_2Ph)_3Ru(\mu\text{-}Cl)_3Ru(PMe_2Ph)_3]PF_6$. The alkyl/aryl groups were replaced by H atoms for simplicity. These were generated using the program CALC[22] and the remaining atoms were obtained using the program ROTATION.[22]

The energies of the orbitals were calculated using the ICON8 program[22] and by symmetry considerations they were assigned as follows:

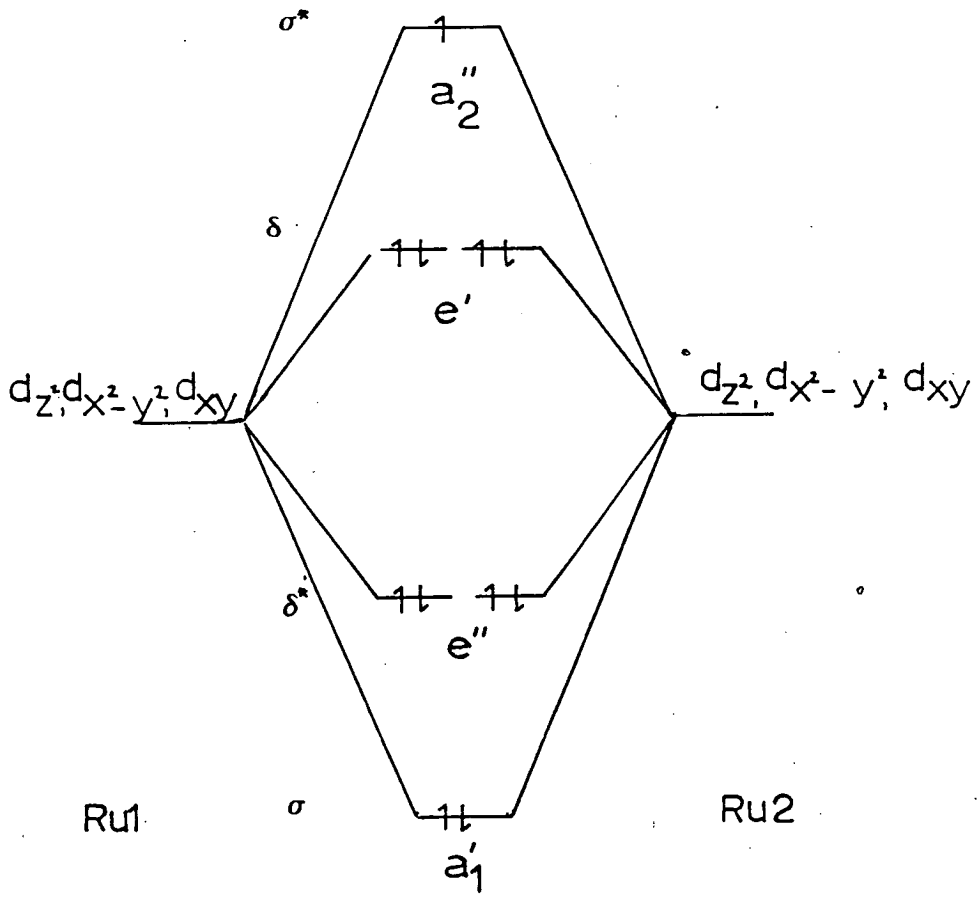

The most obvious difference between our molecular orbital scheme and that of Hush (see Figure 1.2.4) is that the e" pair are lower in energy than e'. The explanation for this switch over and further discussion of the scheme is given in Chapter 4. Once again there is the possibility of three transitions $a_1' \rightarrow a_2''$, $e'' \rightarrow a_2''$ and $e' \rightarrow a_2''$ of which only the first two will carry any measurable intensity.

Theoretically, we predict two allowed intense electronic transitions which agrees with experimental results. The band

at 7770 cm^{-1} is assigned as the $a_1' \rightarrow a_2''$ transition and that at 5000 cm^{-1} as the $e'' \rightarrow a_2''$ transition. The $a_1' \rightarrow a_2''$ transition is likely to be the most intense as this has considerable one-centre character being the bonding and antibonding combination of the d_{z^2} orbital on the metal centres. The e" orbital is composed primarily of the d_{xy} and $d_{x^2-y^2}$ orbitals which will therefore have a much smaller spacial overlap with the partially occupied a_2'' orbital than the a_1' orbital. Thus as the metal-metal interaction increases we would expect a concomittant increase in the overlap of the metal based d-orbitals. This should be reflected in the position of the near infra-red band and its intensity; that is as the metal-metal interaction increases so the absorption band will shift to higher energy and increase in intensity. We therefore suggest using the energy of the most intense near infra-red band as a measure of the metal-metal interaction.

Furthermore the calculations predict a strong metal-metal interaction which is observed experimentally.

1.3 CONCLUSIONS

$[(PMe_2Ph)_3Ru(\mu\text{-}Cl)_3Ru(PMe_2Ph)_3]^{2+}$ is a Class III species with the two metal centres strongly interacting. The E.H.M.O. calculations give qualitative results that agree well with those observed experimentally.

The remainder of this thesis will concentrate on systematically introducing variations into complexes of this type to determine the effect on the metal-metal interaction. The

variations which will be considered in turn are:

1. Metal Centre
2. Oxidation State
3. Bridging Ligand
4. Introduction of Asymmetry
5. Number of Bridging Ligands

1.4 EXPERIMENTAL

Spectroelectrochemical studies were carried out using the O.T.T.L.E. cell. The O.T.T.L.E. cell consists of a fine Pt/Rh gauze working electrode (transparency $\sim$ 40%) fitted into a quartz UV/VIS/NIR cell of 0.05 cm pathlength. At the top of the cell there is a quartz extension which functions as a reservoir for the solution. Into this reservoir a Pt wire counter electrode and Ag/AgCl reference are placed, both protected from the bulk solution by a porous frit.

The cell, together with the electrodes and solution containing the species of interest are fitted into a gas tight PTFE block which is shown in Figure 1.4.1. Temperature control is maintained by passing dry, pre-cooled nitrogen gas between the inner pair of quartz windows and the quartz cell. Monitoring of the temperature is achieved by use of a thermocouple and digital thermometer. To prevent the inner pair of quartz windows from fogging, dry N_2 gas is passed between the inner and outer windows.

The Perkin-Elmer Lambda 9 Spectrophotometer was employed.

Materials

$RuCl_3.3H_2O$ (Aldrich)

PMe_2Ph [23] was made according to the literature method. Methylene chloride was purified by storing over KOH for two weeks, then distilling over P_2O_5. All other solvents were used as obtained.

$[(PMe_2Ph)_3Ru(\mu\text{-}Cl)_3Ru(PMe_2Ph)_3]Cl$ was made according to the method of Chatt.[14] Cl^- was exchanged for PF_6^- by dissolving the complex in methylene chloride then adding methanol/excess NH_4PF_6 and allowing the methylene chloride to evaporate under N_2.

Tetrabutylammonium-tetrafluoroborate ($TBABF_4$) was prepared as follows:

Tetrafluoroboric acid (30 ml, 30% solution) was added slowly to tetrabutylammonium hydroxide (100 ml, 40% by weight), stirring and diluting as required. The pH of the solution was monitored throughout this process using pH paper. At a pH of between 5 and 7 the white solid material was filtered and washed with distilled water (4 x 30 ml). The product was then recrystallised from a water/methanol mixture. A hot filtration was performed and the solution was left to cool. The resulting white needle crystals were then filtered and dried in vacuo at 80°C for 2-3 days.

Figure 1.4.1: Design of the Optically Transparent Thin Layer Electrode (O.T.T.L.E.) Cell

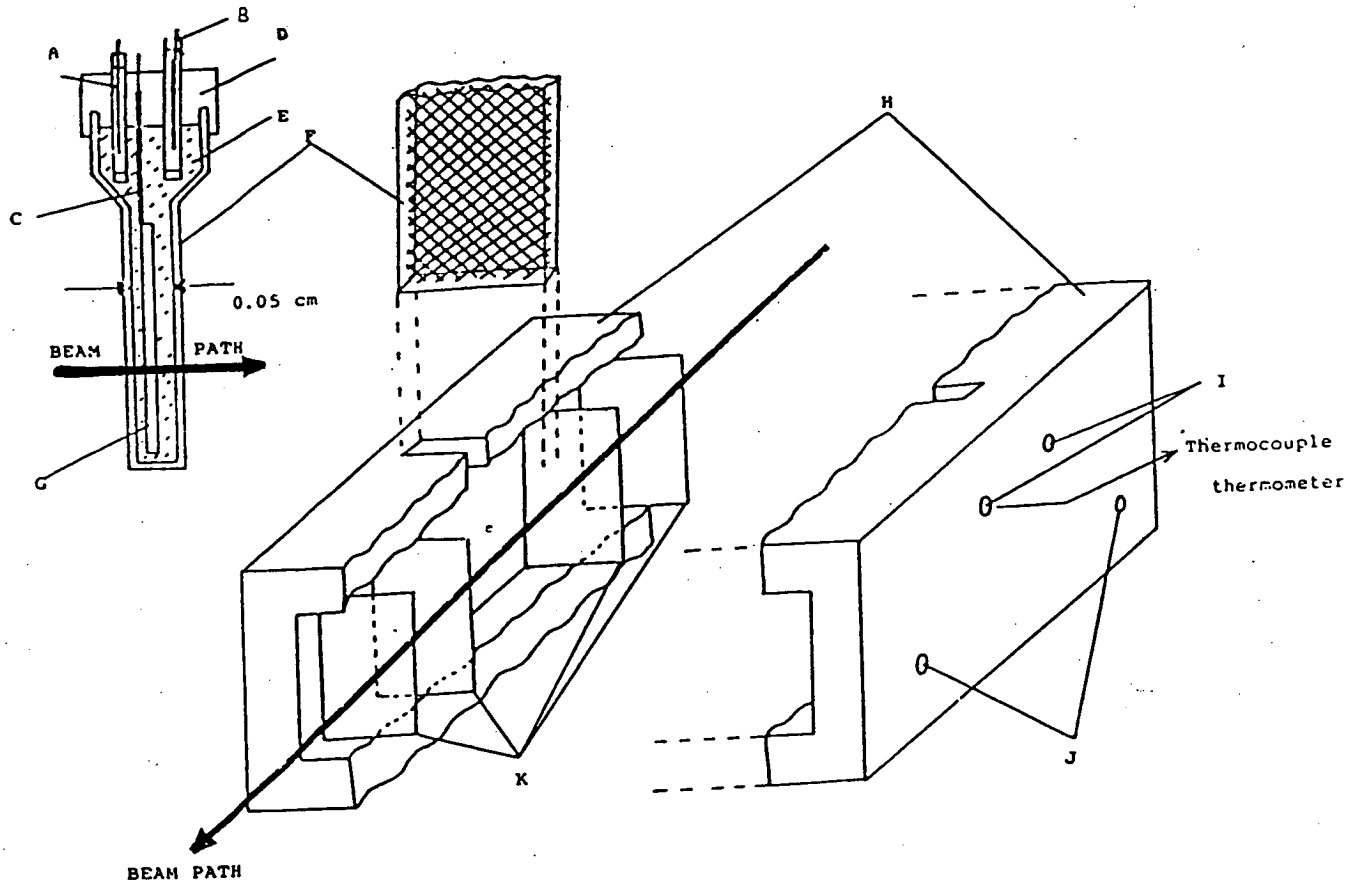

A Counter Electrode

B Reference Electrode

C Working Electrode connection protected from bulk solution by PTFE sleeve

D PTFE cell cap

E Test solution, deoxygenated with Ar or N_2

F 0.1cm Infrasil Quartz cell containing platinum grid working electrode

G Platinum grid working electrode

H PTFE cell block

I Variable Temperature nitrogen inlet ports

J Dry nitrogen inlet ports (to prevent fogging of inner quartz windows)

K Infrasil Quartz cell block windows

1.5 REFERENCES

1. M.B. Robin, Inorg. Chem.; 1962, 1, 337.
2. M.B. Robin and P. Day, Adv.Inorg.Chem. and Radiochem.; 1967, 10, 247.
3. A.B.P. Lever, "Inorganic Electronic Spectroscopy" (Second Edition), 1984, Elsevier.
4. K.J. Taylor, work in progress.
5. L.J. Yellowlees, Ph.D. Thesis, University of Edinburgh, 1982.
6. C. Creutz, Prog.Inorg.Chem.; 1983, 30, 1.
7. R.W. Callahan, G.M. Brown and T.J. Meyer, Inorg.Chem.; 1975, 14, 1443.
8. E.M. Kober, K.A. Goldsby, D.N.S. Narayana and T.J. Meyer, J.Am.Chem.Soc.; 1983, 105, 4303.
9. K.A. Goldsby and T.J. Meyer, Inorg.Chem.; 1984, 23, 3002.
10. C. Creutz and H. Taube, J.Am.Chem.Soc.; 1969, 91, 3988.
11. N.S. Hush, Prog.Inorg.Chem.; 1967, 8, 391.
12. A. Ludi, Chimia; 1972, 26, 647.
13. J.E. Sutton, P.M. Sutton and H. Taube, Inorg.Chem.; 1979, 18, 1017.
14. J. Chatt and R.G. Hayter, J.Chem.Soc.; 1961, 896.
15. A.J. Lindsay, Ph.D. Thesis, University of Edinbrugh, 1982.
16 J. Phelps and A.J. Bard, J.Electroanal.Chem.; 1976, 68, 313.
17. G.A. Heath, A.J. Lindsay, T.A. Stephenson, D.K. Vattis, J.Organomet.Chem.; 1982, 233, 353.
18. M.J. Powers and T.J. Meyer, J.Am.Chem.Soc.; 1980, 102, 1239.

19. R.H. Summerville and R. Hoffmann, J.Am.Chem.Soc.; 1979, 101, 3821.
W.C. Trogler, Inorg.Chem.; 1980, 19, 697.

20. N.S. Hush, J.K. Beattie and V.M. Ellis, Inorg.Chem.; 1984, 23, 3339.

21. A. Griffith, Honours Project, University of Edinburgh, 1988.

22. (a) CALC: "A program for molecular geometry calculations", R.O. Gould and P. Taylor, University of Edinburgh, 1985.
(b) ROTATION: "A program for molecular rotations", A.J. Welch, University of Edinburgh, 1984.
(c) ICON8, J. Howell, A. Rossi, D. Wallace, E. Haraki and R. Hoffmann, Quantum Chemistry Program Exchange, University of Indiana.

23. W.C. Davies and W.J. Jones, Chem.Soc.Journal; 1929, 1, 33.

C H A P T E R 2

VARIATION OF METAL CENTRE (M), M = Ru, Os AND OXIDATION STATE (n), M = Os, n = 1, 2, 3

2.1 INTRODUCTION

The chemistries of complexes of ruthenium and osmium have many similarities. Ruthenium has been more widely studied but its reactions are often typical of both metals. They may be found in a wide range of oxidation states in their complexes. The principal oxidation states of ruthenium in its complexes are 0, II and III whereas for osmium they are 0, II, III and IV.[1]

1. Oxidation State 0 - This has a d electron configuration of d^8. It tends to occur only for mononuclear and polynuclear carbonyls and tertiary phosphine complexes, e.g. $Ru(CO)_3(PPh_3)_2$ and $Os(P(OR)_3)_5$, where R = alkyl or aryl.
2. Oxidation State II - This has a d electron configuration of d^6. It occurs for a wide range of complexes incorporating both π-acceptor and σ/π-donor ligands; examples include $RuCl_3(NO)(PR_3)_2$, R = alkyl or aryl and $[Os(CN)_6]^{4-}$. All Ru(II) and Os(II) complexes are low spin, diamagnetic and octahedral.
3. Oxidation State III - This has a d electron configuration of d^5. This oxidation state is also found in complexes with a wide range of ligands, that is both π-acid and σ-donor ligands, e.g. mer $RuCl_3(PR_3)$, R = alkyl or aryl together with its osmium analogue mer $OsCl_3(PR_3)$, R = alkyl or aryl. Ru(III) complexes tend to be more common than Os(III). They are all low spin with one unpaired electron.

4. Oxidation State IV - This has a d electron configuration of d^4. It is more common for osmium to be in this oxidation state. The most well known example being the hexahaloosmate dianions, $[OsX_6]^{2-}$, X = Cl, Br, I. Similar ruthenium species are also known. Most compounds tend to be neutral or anionic (as above), a few cationic species are however known, e.g. $[Os(diars)_2X_2]^{2+}$ where X = halide, diars = o-$C_6H_4(AsMe_2)_2$.

The wide variety of oxidation states which are found in both ruthenium and osmium compounds generally results in their complexes having a rich redox chemistry. A good example of this occurs with the hexachlorometallates, $[MCl_6]^{n-}$, where the II, III, IV and V oxidation states may be observed electrochemically.[2] Electrochemical studies on $[MCl_6]^{n-}$ have shown that the redox couples for 2nd row transition metal complexes are more anodic than for the corresponding third row species, for example:

n	$[OsCl_6]^{n-}$	$[RuCl_6]^{n-}$	
2,1	+1.28	+1.61	
3,2	-0.64	-0.05	
4,3	-2.0	-1.6	(V versus S.C.E.)

The difference in redox behaviour for analogous 2nd and 3rd row transition metal complexes is at first inspection puzzling. The ionic radii of the 2nd and 3rd row metal ions is roughly equivalent but the nuclear charge of the 3rd row is of course much greater than the 2nd row. Naively, then,

we might expect electrons in 5d orbitals to be more tightly held than electrons in 4d orbitals which would be reflected in the potential required to oxidise or remove an electron from a 5d metal centre being greater than for a 4d metal centre. Experimentally this is not observed.

We can however explain the observations using relativistic arguments.[3] The probability of electrons in s orbitals (and to a lesser extent those in p-orbitals) being in the vicinity of the nucleus is high whereas electrons in d and f orbitals rarely descend to the region near the nucleus. The s and p electrons therefore experience a considerably stronger attractive force than the d and f electrons and the greater the force the greater the velocity of the electrons. Thus the speed of the s and p electrons close to the nucleus is dependent on the mass of the nucleus. We can then use equation 1 which equates the mass of an electron (M) with its speed (V).[4]

$$M = M_o \; / \; \sqrt{(1-(V/C)^2)} \qquad (1)$$

where M_o = rest mass and C = velocity of light. This relationship means that the faster the electron travels the larger its apparent mass. The resulting higher mass of the s and p electrons screens the nuclear attraction more efficiently from the d electrons which therefore experience a weaker effective nuclear charge than might be expected. The higher atomic number of the 3rd row transition metals compared to the 2nd row means that the electrons in the s and p orbitals will all travel faster. Thus the 5d electrons will be better shielded than the 4d electrons from the nucleus and will consequently experience a weaker attractive force.

The 5d electrons will therefore be destabilised energetically and will expand radially compared to electrons in the 4d orbitals. Thus it will be easier to remove electrons from 3rd row transition metals than 2nd row transition metals. Exactly the same arguments apply to explain the easier reduction of the 2nd row transition metal complexes compared with those of the 3rd row; namely, that the effective nuclear charge of 2nd row metals is greater than the corresponding 3rd row metals.

In this study two triple-chloro bridged complexes of the type $[(PMe_2Ph)_3M(\mu\text{-}Cl)_3M(PMe_2Ph)_3]^{n+}$ are studied where M = Ru, Os; n = 1,2 3. Species where n = 1 undergo two one-electron oxidations.[5]

$$[L_3M(II)(\mu\text{-}Cl)_3M(II)L_3]^{+} \overset{-e^-}{\rightleftharpoons} [L_3M(II)(\mu\text{-}Cl)_3M(III)L_3]^{2+} \overset{-e^-}{\rightleftharpoons} [L_3M(II)(\mu\text{-}Cl)_3M(III)L_3]^{3+}$$

The osmium complex being oxidised at less positive potentials than the ruthenium species in accord with the previous discussion.

We have shown in Chapter 1 that when n = 2 the metal centres in the ruthenium complex are strongly interacting. This Chapter addresses the questions of:

1. Does changing ruthenium for osmium in these complexes influence the metal-metal interaction?

and 2. What is the effect of changing the oxidation state from n = 1 to n = 2 then to n = 3 in the case of the osmium complex?

The techniques used to probe the metal-metal interaction are spectroelectrochemistry, X-ray crystallography and kinetic studies.

When an electron transfer reaction takes place, in this case from the complex to an electrode, it is expected that at the very least there will be some change in the structure of the reactant molecule. If this change is not particularly large then the redox process will appear to be a simple one with fast charge transfer kinetics. However sometimes there are more apparent changes taking place e.g. isomerisation.

There are many examples cited in the literature where binuclear species show a change in metal-metal distance on oxidation or reduction.

The complexes 1. $[Cp_2Fe_2(CO)_2(\mu\text{-}SMe)_2]^{n+}$; [6] n = 0, 1 and 2. $[Cp_2Fe_2(CO)_2(\mu\text{-}PPh)_2]^{n+}$; n = 0, 1, 2; [7] have been structurally characterised. It has been shown by Dahl[6,7] and others that significant shortening of the metal-metal distance occurs on oxidation to the cationic species.

	Metal-Metal Distance (pm)		
Complex	Neutral	Cation	Dication
1	339	293	-
2	349.8	314	276.4

The shortening of the metal-metal distance is attributed to electron loss from an antibonding molecular orbital.

The related molybdenum complex 3. $Cp_2Mo_2(\mu\text{-}SMe)_4$ [8] was found to show no change in metal-metal distance on oxidation.

All have well established electron transfer processes.[9,10,11] The Marcus-Hush theory predicts that the rate of electron transfer in the reaction:[12]

$$Ox + e^- \rightleftharpoons red$$

should depend upon the extent of accompanying changes in the internal structures of the oxidised and reduced species.

It has been suggested that larger structural changes will give rise to smaller rates of electron transfer. Geiger[13] attempted to determine values for the heterogeneous electron transfer rate constants (k_s) of the three compounds discussed above. All species studied showed similar values of k_s which on the basis of the structural data is unexpected, since both 1 and 2 would be expected to have lower values of k_s than 3.

The method of Nicholson[14] was used to calculate k_s which is given in equation (2):

$$k_s = \Psi(\pi a D_o)^{\frac{1}{2}} / \gamma^{\alpha} \qquad (2)$$

where $a = nF\nu/RT$

$\gamma^{\alpha} = 1$

D_o = Diffusion Coefficient in cm^2s^{-1}

n = number of electrons

ν = Scan rate in Vs^{-1}

F = Faradays Constant (96487 $Cmol^{-1}$)

R = Gas constant (8.314)

The value Ψ is dependent on scan rate ν and is obtained for a particular ΔE_p value (where $\Delta E_p = E_{pc} - E_{pa}$) from the curve shown in Fig. 2.1.1.

D_o, the diffusion coefficient, must be obtained for the system under study. It is calculated from the Ilkovic equation (3):

$$D_o^{\frac{1}{2}} = i_d / 706nC_o m^{2/3} t^{1/6} \qquad (3)$$

where i_d = limiting current, A

Figure 2.1.1: Graph of Ψ versus ΔE_p [13]

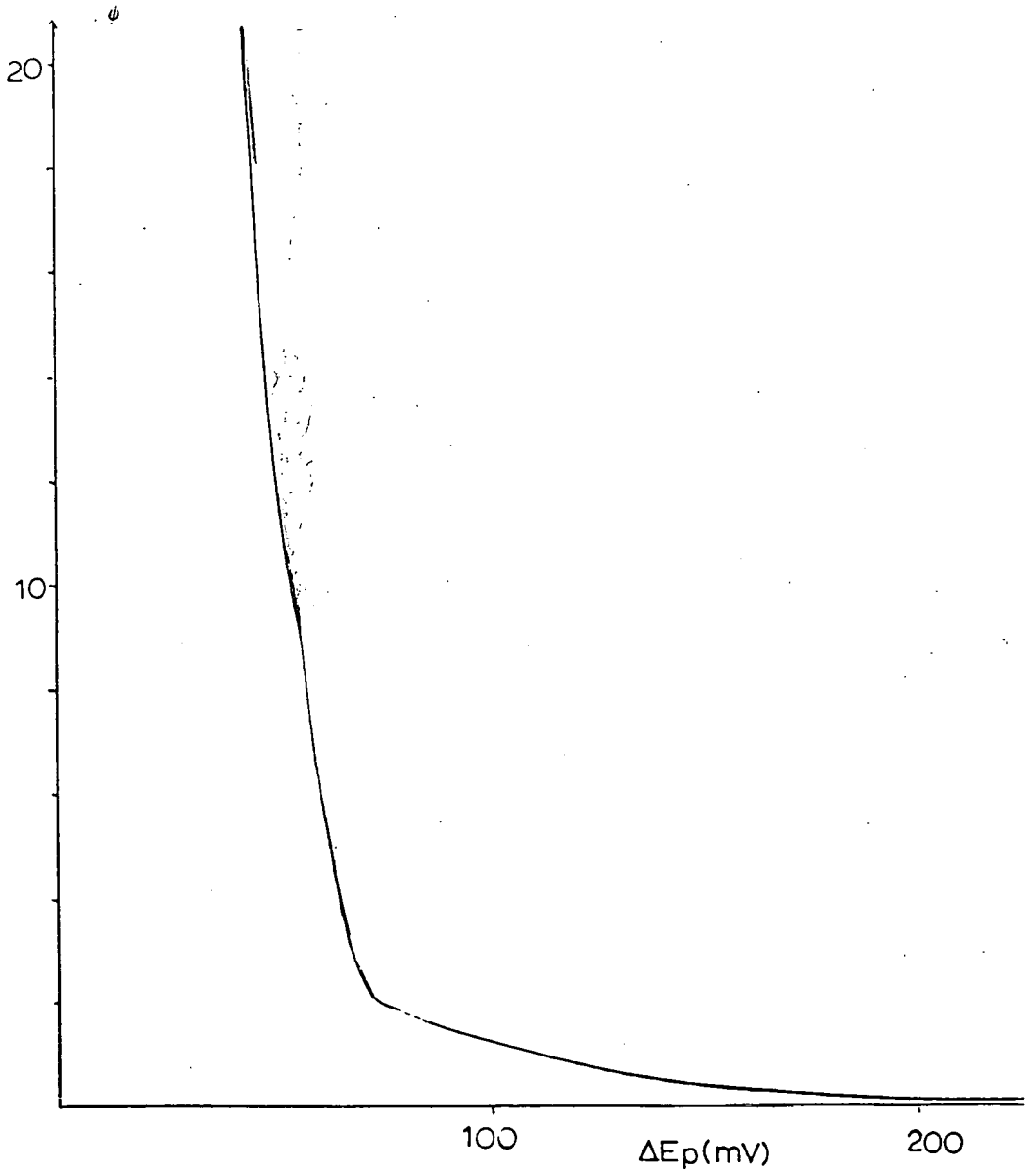

C_O = m molar concentration of compound

m = rate of flow from dropping mercury electrode in mgs^{-1}

t = drop lifetime in s

This equation is limited to use with the dropping mercury electrode. In systems where this cannot be used D_O can be obtained using the Levich equation (4) which involves the use of the rotating disc electrode (see Appendix 1):

$$i_{i,c} = 0.260\, n\, FAD_O^{2/3} \omega^{1/2} \nu_z^{-1/6} C_o^* \qquad (4)$$

where ω = angular frequency of rotation in s^{-1} (2π x rotation rate)

F = Faradays Constant (96487 $Cmol^{-1}$)

ν_z = kinematic viscosity in $cm^2 s^{-1}$

A = area of electrode in cm^2

C_O^* = initial bulk concentration in mol cm^{-3}.

From a plot of i versus $\omega^{1/2}$, the value of D_O can be obtained.

It was concluded in the previous systems studied that calculated rate constants for heterogeneous electron transfer, k_S, are independent of any structural change occurring. It was suggested that the rates were dependent only on the energy of solvent reorganisation as changing the solvent caused the k_S values to be quite different.

There are many other examples of binuclear species where structural characterisations have been undertaken for more than one oxidation state.

Electron transfer can be accompanied by an increasing metal-metal distance, a decreasing distance or very little change at all.

(a) Increasing Metal-Metal Distance

Binuclear species of the type $Fe_2(CO)_6\mu X_2$[15] where X = PR_2, AsR_2, SR , TeR; contain a metal-metal bond in the neutral compound. On reduction to the dianion when X = PPh_2, the Fe--Fe distance increases from 262.3 pm to 363.0 pm. This implies that the lowest unoccupied molecular orbital is antibonding and largely metal based. The metal-based reduction is found to be a reversible two-electron process suggesting that fast electron transfer is occurring even though there is a large structural change in the molecule.

In complexes without bridging ligands similar behaviour has been observed. On reduction of $[Pt_2(NH_3)_4(C_5H_4NO)_2]^{2+}$ to $Pt_2(NH_3)_4(C_5H_4NO)_2$ an increase in the Pt-Pt bond distance from 254.7 pm to 289.9 pm is observed.[16]

(b) Decreasing Metal-Metal Distance

The complex $(C_6H_5)_2Cr_2(\mu dppm)(CO)_4.2C_6H_6$[17] has a metal-metal distance of 482.8 pm. On oxidation to the mixed valence cation $[(C_6H_5)_2Cr_2(\mu dppm)(CO)_4]^+$ the distance is found to shorten to 437.4 pm. This complex has been categorised as a delocalised system.

(c) Little Change in Metal-Metal Distance

In some species behaviour similar to that in the $Cp_2Mo_2(\mu SMe)_4$ complex is observed where no structural change accompanies a redox process. There are three structurally characterised oxidation states of the species $[Re_2Cl_4(PR_3)_4]^{n+}$ where n = 0, 1, 2[18] and R = PMe_2Ph. This system has no bridging ligands. When n = 0 the Re-Re distance is 224.1 pm. A one electron oxidation of the complex involves removal of an electron from an antibonding molecular orbital to give the

complex with a Re-Re distance of 221.8 pm. On further oxidation to $[Re_2Cl_4(PR_3)_4]^{2+}$ the metal-metal distance only decreases by 0.3 pm to 221.5 pm. On removal of electrons the metal centres require to form metal-metal bonds to satisfy their need for electrons. This effect which will bring the metal centres closer together is however balanced by the fact the higher metal charge on oxidation causes contraction of the metal based orbitals thus leading to poorer overlap. $[Tc_2Cl_8]^{3-}$[19] on oxidation to $[Tc_2Cl_8]^{2-}$ shows an increase in metal-metal distance. This is also thought to be a consequence of the higher charge at the metal centres. Wieghardt[20] recently observed similar behaviour in the complex $[LRu(\mu O)(\mu CH_3CO_2)_2RuL]^{3+}$ where L = 1,4,7 trimethyl-1,4,7-triazacyclononone. On oxidation this showed an increase of 8.4 pm in metal-metal distance.

Effects other than changes in metal-metal distance can occur. In the complex $Fe_2(CO)_6(\mu PPh_2)_2$[15] the Fe_2P_2 core is puckered. On reduction to $[Fe_2(CO)_6(\mu PPh_2)_2]^{2-}$ the Fe_2P_2 core becomes planar.

$Rh_2(CO)_4(\mu t\text{-}Bu_2P)_2$[21] in its neutral state has one tetrahedral and one planar metal environment but on reduction both are tetrahedral.

The results obtained for the $[L_3M(\mu\text{-}X)_3ML_3]^{n+}$ systems under study in this work will now be discussed.

2.2 RESULTS AND DISCUSSION

2.2.1 Variation of the Metal Centre

The influence of the metal centre on the extent of metal-metal interaction in the $[(PMe_2Ph)_3M(\mu\text{-}Cl)_3M(PMe_2Ph)_3]^{2+}$ species,[22,23] M = Ru, Os, has been studied using spectroelectrochemical methods.

In order to determine if there are differences in the structure of the complexes when n = 1, crystallographic studies of $[(PMe_2Ph)_3Os(\mu\text{-}Cl)_3Os(PMe_2Ph)_3]PF_6$ were carried out. The equivalent ruthenium complex has been previously structurally characterised.

Attempts were made to chemically prepare the mixed metal complex. Electrochemical and FAB mass spectroscopic results indicate that this was in fact prepared, however we were unable to obtain a pure sample for further studies.

(a) Spectroelectrochemistry

The electrochemical and spectroelectrochemical results are shown in Table 2.2.1 for $[(PMe_2Ph)_3M(\mu\text{-}Cl)_3M(PMe_2Ph)_3]PF_6$ where M = Ru, Os.

Electrochemical studies using cyclic voltammetry (c.v.) and a.c. voltammetry were carried out in methylene chloride/ 0.5M $TBABF_4$ using Pt working and counter electrodes and an Ag/AgCl reference electrode. Electrochemical techniques are discussed in detail in Appendix 1. Figure 2.2.1 shows the cyclic voltammogram obtained for $[(PMe_2Ph)_3Os(\mu\text{-}Cl)_3Os(PMe_2Ph)_3]PF_6$.

Spectroelectrochemical studies were carried out as described in Chapter 1. The mixed-valence

Table 2.2.1: Electrochemical and Spectroelectrochemical Results for $[(PMe_2Ph)_3M(\mu\text{-}Cl)_3M(PMe_2Ph)_3]^+$ in Methylene Chloride / 0.5M $TBABF_4$

M	$E_{\frac{1}{2}}$ (V versus Ag/AgCl) [a]		ν_{max} (cm^{-1})	ε ($mol^{-1}cm^{-1}dm^3$)
	II,II/II,III	II,III/III,III	II,III	
Ru [b]	1.23(0.070) [c]	1.75(0.100)	5,000	2,613
			7,770	2,864
Os [b]	1.05(0.060)	1.57(0.080)	5,000	4,868
			9,200	650

a. Ferrocene / Ferrocinium at +0.56V

b. T = 290K (electrochemistry)
T = 266K (spectroelectrochemistry)

c. E_p^F - E_p^R values are shown in brackets in V (where E_p^F and E_p^R are the potentials at the maximum of the forward and reverse scans).

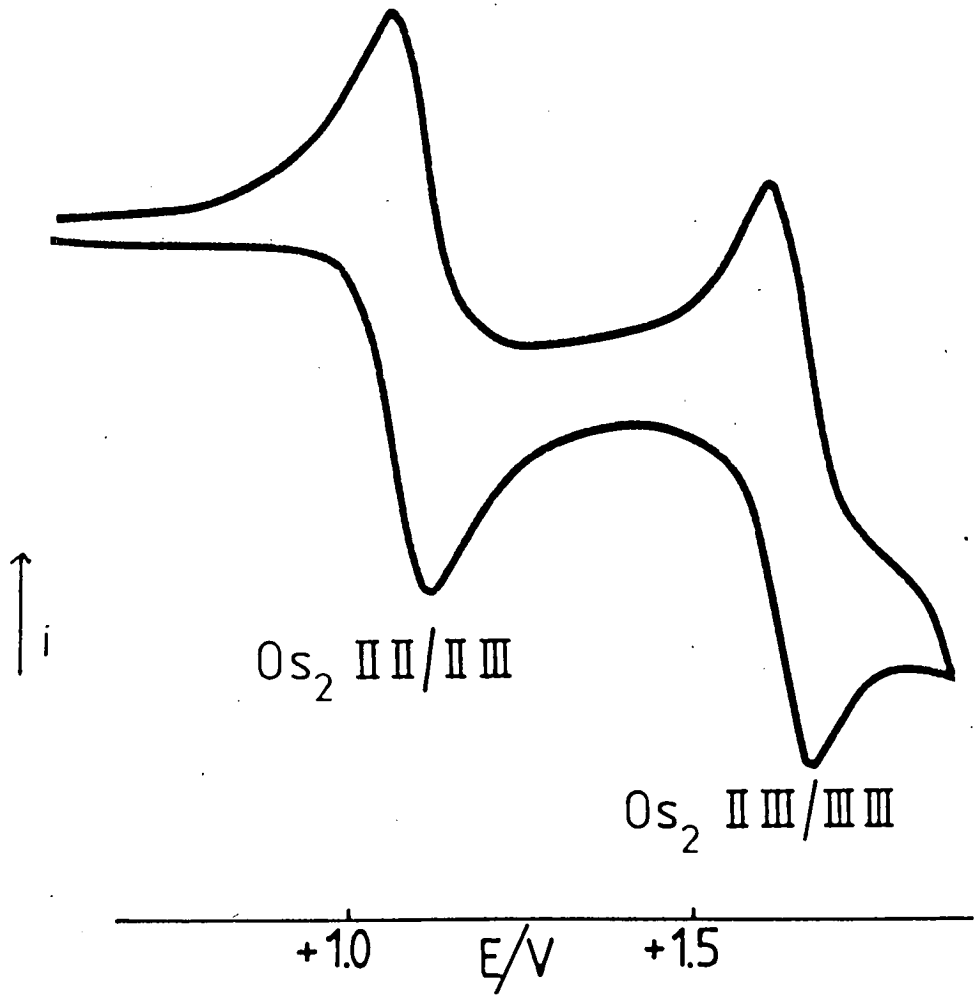

Figure 2.2.1: Cyclic Voltammogram of $[(PMe_2Ph)_3Os(\mu\text{-}Cl)_3Os(PMe_2Ph)_3]^+$ in Methylene Chloride / 0.5M $TBABF_4$ at T = 290K

$[(PMe_2Ph)_3Os(\mu\text{-}Cl)_3Os(PMe_2Ph)_3]^{2+}$ species was generated at a potential of +1.26V. Only the near infra-red region of the spectrum of the mixed-valence species will be discussed in this Chapter. The osmium species showed two near infra-red bands. The position of the bands, ν_{max}, was found to be independent of solvent used and the band halfwidth, $\Delta_{\frac{1}{2}}$, independent of temperature; indicating a strong metal-metal interaction as in the ruthenium complex. On changing the metal centre from ruthenium to osmium there is little difference in the positions of the bands. Figure 2.2.2 shows the spectrum obtained for each. It must be noted that the most intense band is the high energy band in the case of the ruthenium complex and vice versa for the osmium complex. In Chapter 1 the intense band was assigned as the $a_1' \rightarrow a_2''$ transition and is used as a measure of M-M interaction; thus we assign the intense, lower energy near infra-red band (4991 cm^{-1}) in the spectrum of $[(PMe_2Ph)_3Os(\mu\text{-}Cl)_3Os(PMe_2Ph)_3]^{2+}$ to the $a_1' \rightarrow a_2''$ transition and the less intense band at higher energy (9000 cm^{-1}) to the $e'' \rightarrow a_2''$ transition. Considering only the $a_1' \rightarrow a_2''$ transitions then the metal-metal interaction in the case of the osmium species is less than in the ruthenium complex.

(b) Single Crystal X-Ray Structure of $[(PMe_2Ph)_3Os(\mu\text{-}Cl)_3Os(PMe_2Ph)_3]PF_6$

Details of the structure solution are given in the experimental section.

Small, yellow needles were grown by vapour diffusion in methylene chloride and diethylether. A summary of selected

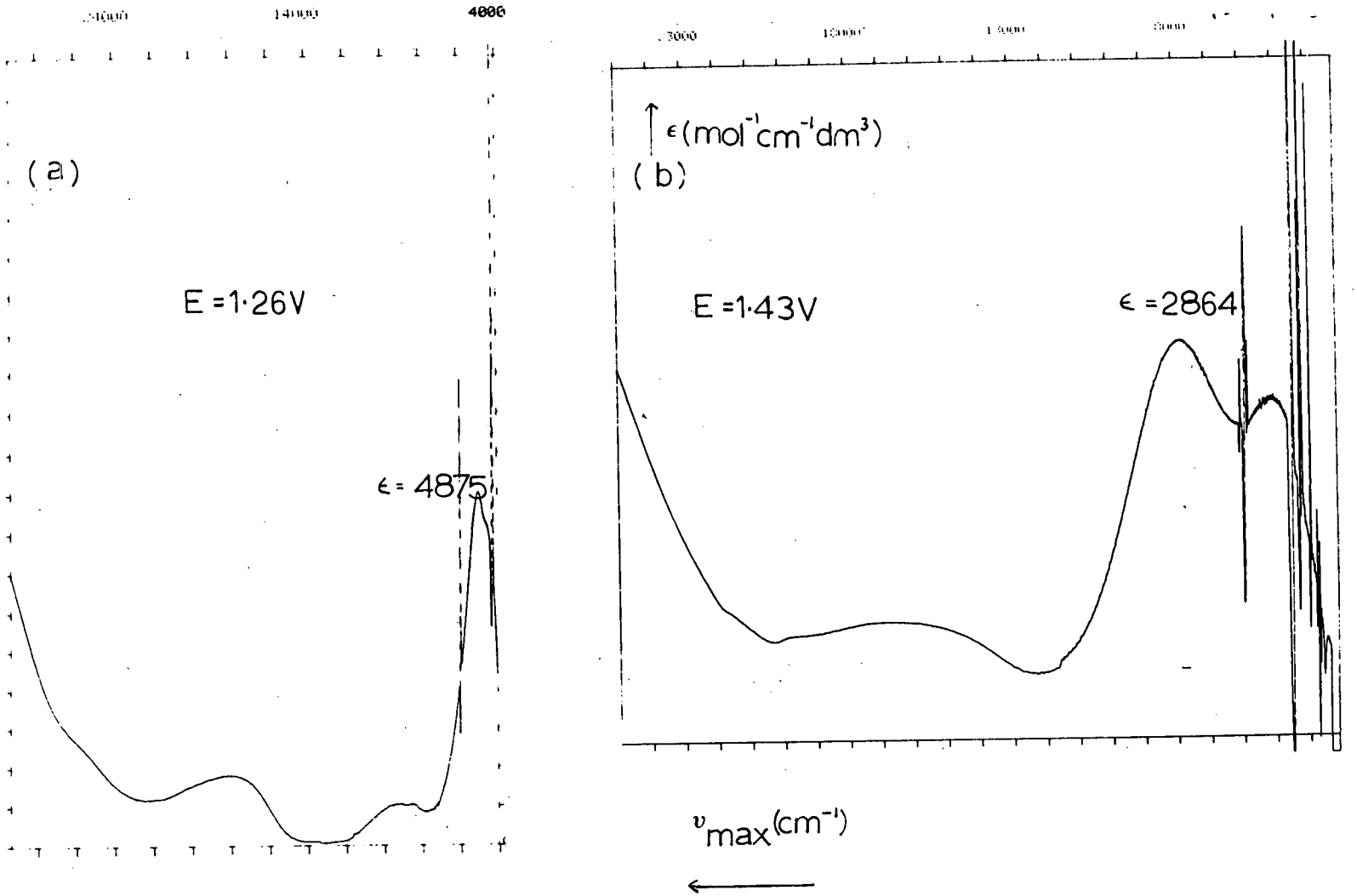

Figure 2.2.2: NIR/VIS Spectra of (a) $[L_3Os(\mu\text{-}Cl)_3OsL_3]^{2+}$ and (b) $[L_3Ru(\mu\text{-}Cl)_3RuL_3]^{2+}$ where L = PMe_2Ph in Methylene Chloride / 0.5M $TBABF_4$ at T = 266K

bond lengths and angles are given in Table 2.2.2.

A view of the $[(PMe_2Ph)_3Os(\mu\text{-}Cl)_3Os(PMe_2Ph)_3]^+$ cation is shown in Figure 2.2.3 (without H atoms).

The metal-metal distances, average M-$\hat{Cl}$-M and P-$\hat{M}$-P angles are compared below for the two complexes $[(PMe_2Ph)_3Os(\mu\text{-}Cl)_3Os(PMe_2Ph)_3]^+$ and $[(PMe_2Ph)_3Ru(\mu\text{-}Cl)_3Ru\text{-}PMe_2Ph)_3]^+$.

M	M--M (Å)	M-$\hat{Cl}$-M (°)	P-$\hat{M}$-P (°)
Os	3.440(1)	87.0	95.6
Ru	3.39	86.0	95.3

The data indicate that a weaker M--M interaction would be expected in $[(PMe_2Ph)_3Os(\mu\text{-}Cl)_3Os(PMe_2Ph)_3]^{2+}$ than in $[(PMe_2Ph)_3Ru(\mu\text{-}Cl)_3Ru(PMe_2Ph)_3]^{2+}$.

(c) Conclusions

We observe a decrease in the metal-metal interaction on changing the metal centre from ruthenium to osmium.

This result can be understood in the light of the discussion at the beginning of this chapter (section 2.1). We have argued that on relativistic grounds we would expect metal-based oxidations of osmium complexes to be at less positive potentials than corresponding complexes containing ruthenium. This is indeed observed with these binuclear species. A further consequence of the discussion was that the d-orbitals should be more radially diffuse on 3rd row transition metals than 2nd row and hence we might expect there to be poorer overlap of the d-orbitals of osmium than ruthenium.

Table 2.2.2: Selected Bond Lenths and Angles for

$[(PMe_2Ph)_3Os(\mu\text{-}Cl)_3Os(PMe_2Ph)_3]^+$

Bond Lengths(A) with standard deviations

Os(1) -Cl(1)	2.4811(20)	P(2) -C(21)	1.849(6)
Os(1) -Cl(2)	2.5060(21)	P(2) -C(27)	1.829(10)
Os(1) -Cl(3)	2.4974(20)	P(2) -C(28)	1.813(11)
Os(1) - P(1)	2.2878(24)	P(3) -C(31)	1.842(6)
Os(1) - P(2)	2.2738(24)	P(3) -C(37)	1.807(10)
Os(1) - P(3)	2.2909(25)	P(3) -C(38)	1.835(11)
Os(2) -Cl(1)	2.4680(20)	P(4) -C(41)	1.852(7)
Os(2) -Cl(2)	2.5042(21)	P(4) -C(47)	1.837(11)
Os(2) -Cl(3)	2.5287(20)	P(4) -C(48)	1.839(11)
Os(2) - P(4)	2.2854(25)	P(5) -C(51)	1.841(6)
Os(2) - P(5)	2.276(3)	P(5) -C(57)	1.824(12)
Os(2) - P(6)	2.2959(25)	P(5) -C(58)	1.825(12)
P(1) -C(11)	1.843(6)	P(6) -C(61)	1.845(6)
P(1) -C(17)	1.842(10)	P(6) -C(67)	1.819(11)
P(1) -C(18)	1.810(11)	P(6) -C(68)	1.832(11)

Angles(degrees) with standard deviations

Os(1) -Cl(1) -Os(2)	88.07(6)
Os(1) -Cl(2) -Os(2)	86.72(6)
Os(1) -Cl(3) -Os(2)	86.38(6)
P(1) -Os(1) - P(2)	98.06(9)
P(1) -Os(1) - P(3)	94.28(9)
P(2) -Os(1) - P(3)	95.12(9)
P(4) -Os(2) - P(5)	98.49(9)
P(4) -Os(2) - P(6)	94.42(9)
P(5) -Os(2) - P(6)	93.49(9)

Figure 2.2.3: View of the $[(PMe_2Ph)_3Os(\mu\text{-}Cl)_3Os(PMe_2Ph)_3]^+$ Cation

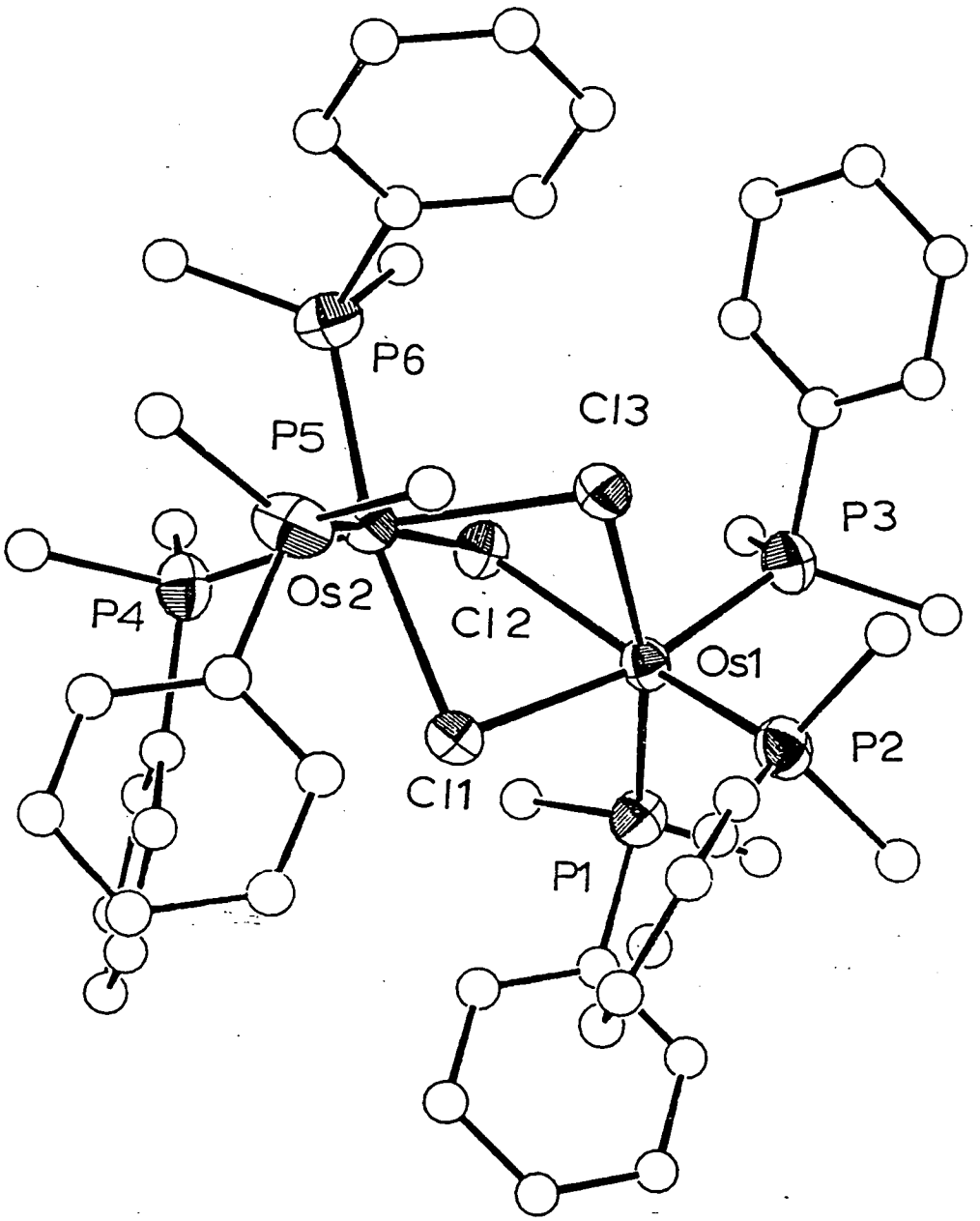

2.2.2 Variation of the Oxidation State, n

The effect of varying the oxidation state of the complex on the metal-metal interaction was studied using:

(a) Spectroelectrochemistry

(b) Kinetics

(c) X-ray Crystallography

(a) Spectroelectrochemistry

The spectroelectrochemical results for M = Os are shown in Table 2.2.3. The absorption spectrum of the $[(PMe_2Ph)_3Ru(\mu\text{-}Cl)_3Ru(PMe_2Ph)_3]^{3+}$ species was not observed. The reasons for this will be discussed in Chapter 4. The effect of changing n will therefore only be discussed for osmium.

The n = 3 state was electrogenerated in a similar manner to n = 2 at a potential of E = +1.84V (versus Ag/AgCl). The temperature used was 233K. After electrogeneration the n = 3 state was reduced back to the n = 2 state to check on the chemical stability of the oxidised product. Figure 2.2.4 shows the changes observed in the UV/VIS/NIR spectrum on oxidation from n = 1 to n = 2 and n = 2 to n = 3.

When n = 1 , no near infra-red bands are observed. By increasing the oxidation state from n = 1 to n = 2, we observe two bands in the near infra-red region of the spectrum. As previously discussed these are due to absorptions within the molecular orbital framework of the two strongly interacting metal centres. The low energy d-orbitals interact to give molecular orbitals with symmetry labels as shown on page 54. An electron has been removed from antibonding

Table 2.2.3: Positions of the Bands (ν_{max}) in the Low Energy Region of the Electronic Spectrum of $[(PMe_2Ph)_3Os(\mu\text{-}Cl)_3Os(PMe_2Ph)_3]^{n+}$ (where n=1,2,3) in Methylene Chloride / 0.5M $TBABF_4$

n	ν_{max} (cm^{-1})	ε ($mol^{-1}cm^{-1}dm^3$)
1	No low energy bands observed	-
2 [a]	4,991	4,875
	9,000	670
3 [b]	11,480	7,220
	15,000	2,116

a. T = 243K, Electrogeneration Potential = +1.26V (versus Ag/AgCl at which ferrocene is oxidised at +0.56V)

b. T = 233K, Electrogeneration Potential = +1.84V (versus Ag/AgCl)

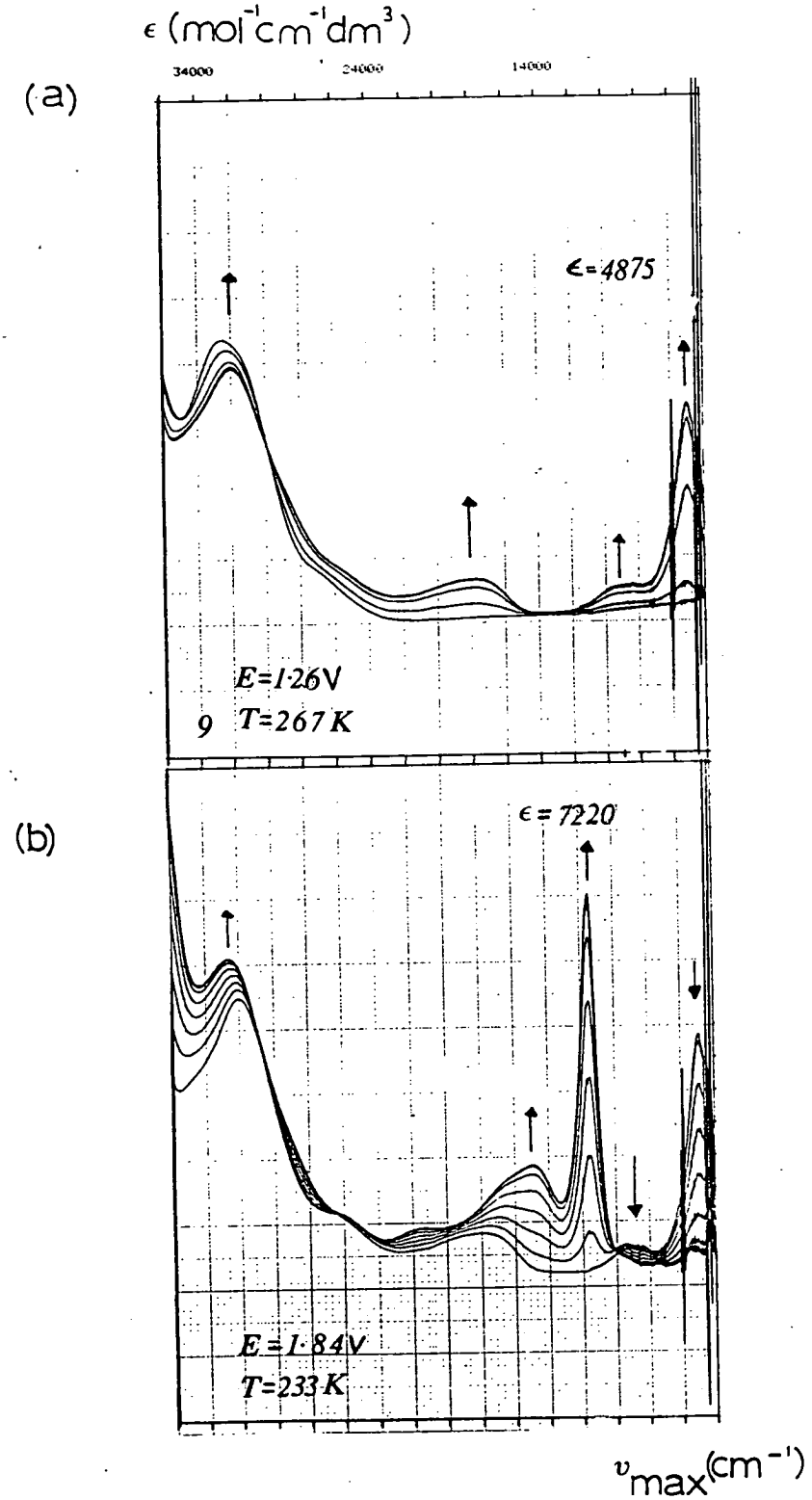

Figure 2.2.4: Spectra showing (a) the oxidation of $[(PMe_2Ph)_3Os(\mu\text{-}Cl)_3Os(PMe_2Ph)_3]^{+} \rightarrow [(PMe_2Ph)_3Os(\mu\text{-}Cl)_3Os(PMe_2Ph)_3]^{2+}$ and (b) $[(PMe_2Ph)_3Os(\mu\text{-}Cl)_3Os(PMe_2Ph)_3]^{2+} \rightarrow [(PMe_2Ph)_3Os(\mu\text{-}Cl)_3Os(PMe_2Ph)_3]^{3+}$ in Methylene Chloride/0.5M $TBABF_4$

molecular orbital a_2" to give:

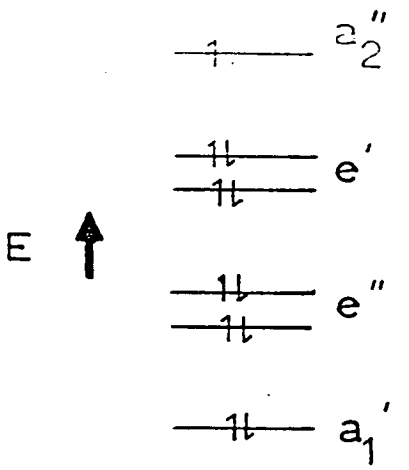

The electronic selection rules result in only the e" → a_2" and a_1' → a_2" transitions having appreciable intensity.

In going from n = 2 to n = 3 we still only observe two bands in the low energy region of the electronic spectrum which have moved to higher energy and become more intense. Both these observations indicate an increasing metal-metal interaction as a further electron has been removed from the complex. This electron has been removed from an antibonding molecular orbital to give: (see over page)

Once again the electronic selection rules indicate only two fully allowed transitions, namely e" → a_2" and a_1' → a_2".

These studies suggest that we are seeing an increase in metal-metal interaction on removal of antibonding electrons. It is therefore likely that the metal-metal separation is decreasing, i.e. we are seeing a structural change upon

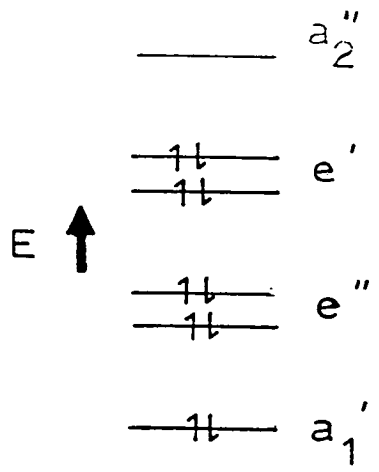

oxidation. In order to probe the suggested structural change we undertook kinetic studies of the first oxidation process of the osmium species.

(b) Kinetic Studies - Determination of the Heterogeneous Electron Transfer Rate Constant, k_s

Following the method of Nicholson[14] where,

$$k_s = \frac{\psi(\pi a D_o)^{\frac{1}{2}}}{\gamma^{\alpha}} \quad (1)$$

the differences in forward and reverse peak potentials, ΔE_p, were obtained at high scan rates, 30-70Vs^{-1} for the $[(PMe_2Ph)_3Os(\mu\text{-}Cl)_3Os(PMe_2Ph)_3]^{+/2+}$couple and the ferrocene/ferrocinium couple in methylene chloride/0.5M $TBABF_4$. Values of ψ were obtained from the graph of ψ versus ΔE_p shown in Figure 2.1.1. This was carried out at 286.6K.

The diffusion coefficient, D_o, for each system was obtained from the Levich equation:

$$i = 0.620nFA D_O^{2/3} \omega^{1/2} \nu^{-1/6} C_O^* \quad (3)$$

using the rotating disc electrode on the same solvent system as was used in the preceding kinetic study.

The graph of i versus $\omega^{1/2}$ is shown in Figure 2.2.5 for $[(PMe_2Ph)_3Os(\mu\text{-}Cl)_3Os(PMe_2Ph)_3]^{+/2+}$ and in Figure 2.2.6 for ferrocene/ferrocinium. The slopes, $i/\omega^{1/2}$ were found to be 0.3×10^{-6} and $67.5\times10^{-6} As^{1/2}$ respectively.

So for $[(PMe_2Ph)_3Os(\mu\text{-}Cl)_3Os(PMe_2Ph)_3]^{+/2+}$

$$D_O = 0.87\times10^{-6} \text{ cm}^2\text{s}^{-1}$$

and for ferrocene/ferrocinium

$$D_O = 2.20\times10^{-5} \text{ cm}^2\text{s}^{-1}$$

Values of k_S at different scan rates for both $[(PMe_2Ph)_3Os(\mu\text{-}Cl)_3Os(PMe_2Ph)_3]^{+/2+}$ and ferrocene/ferrocinium are shown in Table 2.2.4.

The average value for the heterogeneous electron transfer rate of the osmium complex is lower than for ferrocene/ferrocinium.

k_S $[(PMe_2Ph)_3Os(\mu\text{-}Cl)_3Os(PMe_2Ph)_3]^{+/2+} = 0.031 \text{ cms}^{-1}$

k_S Ferrocene / Ferrocinium $= 0.438 \text{ cms}^{-1}$

This result suggests that we are seeing a structural change taking place on oxidation of

$[(PMe_2Ph)_3Os(\mu\text{-}Cl)_3Os(PMe_2Ph)_3]^{+}$ to

$[(PMe_2Ph)_3Os(\mu\text{-}Cl)_3Os(PMe_2Ph)_3]^{2+}$.

In order to investigate this further X-ray crystallographic studies were carried out.

Figure 2.2.5: Graph of i(A) versus $\omega^{1/2}(s^{-1/2})$ to determine D_o for $[(PMe_2Ph)_3Os(\mu\text{-}Cl)_3Os(PMe_2Ph)_3]^{+/2+}$

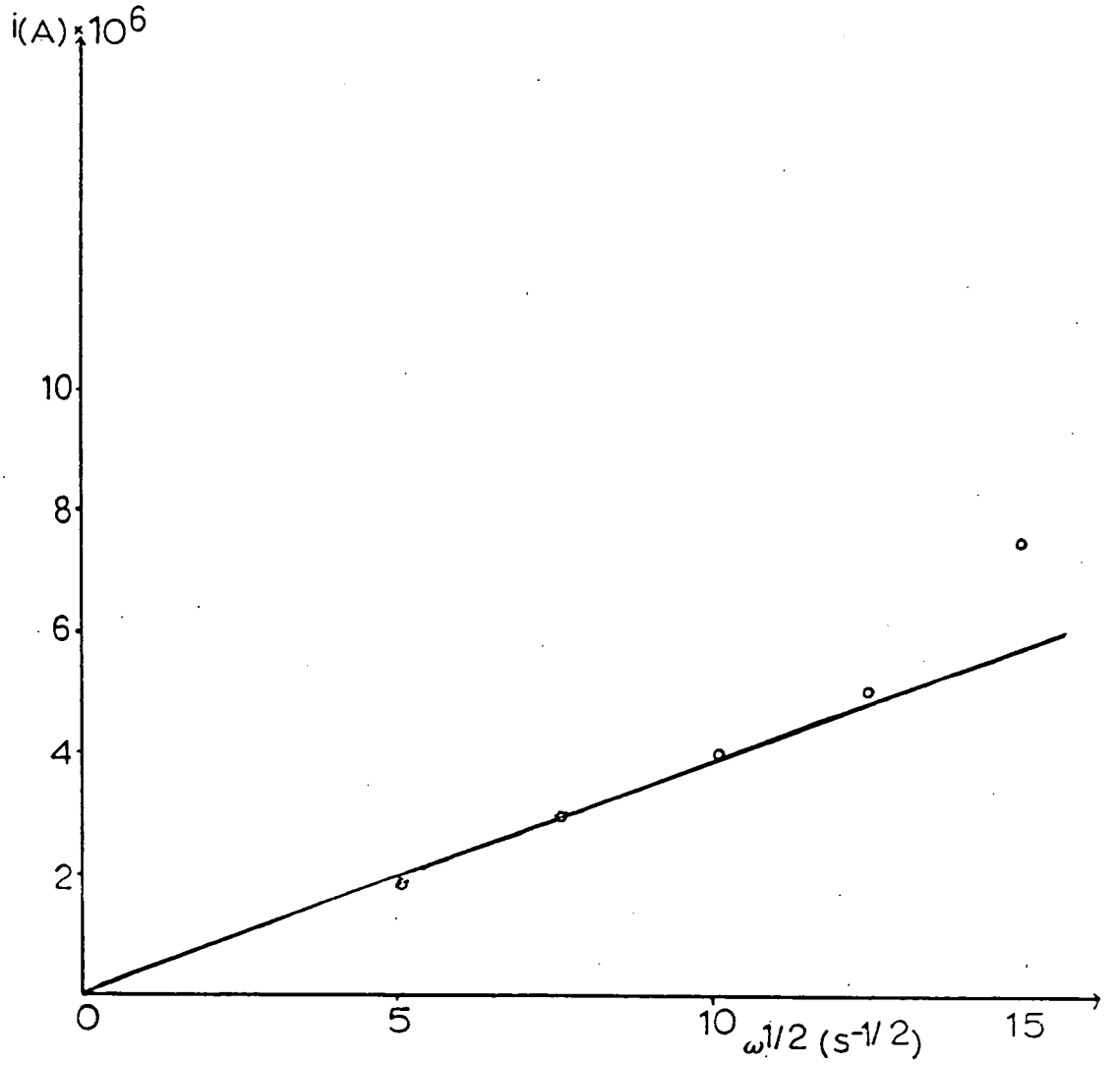

Figure 2.2.6: Graph of i(A) versus $\omega^{1/2}$ ($s^{-1/2}$) to determine D_o for Ferrocene/Ferrocinium

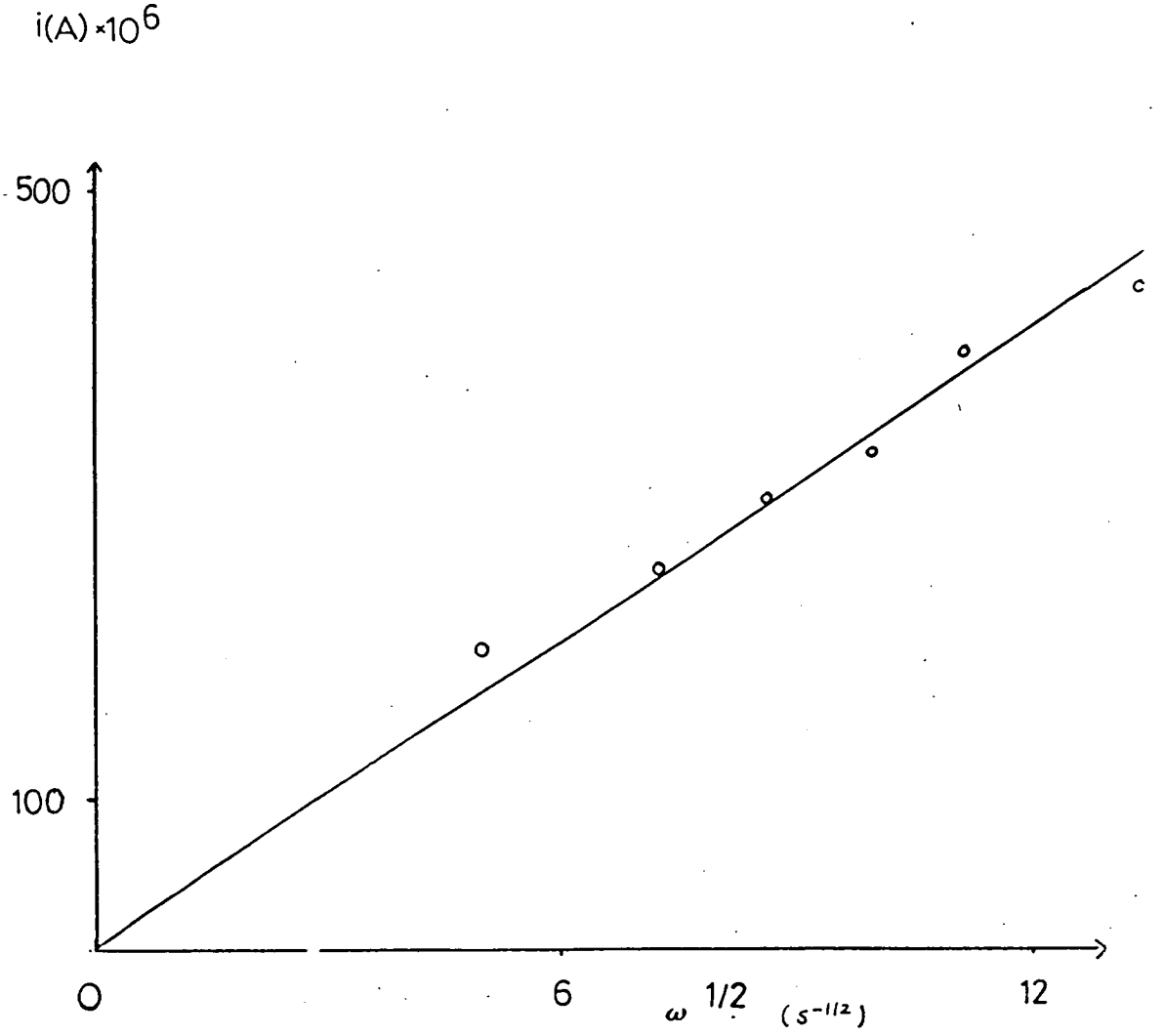

Table 2.2.4: Heterogeneous Rate Constant Values (k_s) for (a) $[(PMe_2Ph)_3Os(\mu\text{-}Cl)_3Os(PMe_2Ph)_3]^{+/2+}$ and (b) Ferrocene/Ferrocinium at different Scan Rates (ν) in Methylene Chloride/0.5M $TBABF_4$ at 286.6K

(a) $[(PMe_2Ph)_3Os(\mu\text{-}Cl)_3Os(PMe_2Ph)_3]^{+/2+}$

$\nu(vs^{-1})$	$\Delta E_p(mV)$	Ψ	$k_s(cms^{-1})$
30	86	1.375	0.079
40	95	0.750	0.050
50	125	0.356	0.026
60	154	0.250	0.020

(b) Ferrocene/Ferrocinium

$\nu(vs^{-1})$	$\Delta E_p(mV)$	Ψ	$k_s(cms^{-1})$
30	84	1.96	0.568
40	89	1.00	0.335
50	85	1.85	0.692
60	85	1.85	0.758
70	97	0.625	0.276

(c) X-ray Crystallographic Studies

$[(PMe_2Ph)_3Os(\mu\text{-}Cl)_3Os(PMe_2Ph)_3]^+$ on oxidation to $[(PMe_2Ph)_3Os(\mu\text{-}Cl)_3Os(PMe_2Ph)_3]^{2+}$ on the basis of spectro-electrochemical and kinetic studies is expected to undergo a structural change. This is thought to occur as a decrease in metal-metal distance together with changes in M-$\hat{Cl}$-M angles etc. Crystallographic studies would obviously confirm this. The compound can be oxidised electrochemically but separation from the vast excess of inert electrolyte is a problem. Oxidation was therefore carried out chemically using a variety of oxidants; 60% $HClO_4$, concentrated HNO_3 and $NOBF_4$. The resulting purple complex was shown to be $[(PMe_2Ph)_3Os(\mu\text{-}Cl)_3Os(PMe_2Ph)_3]^{2+}$ by UV/VIS/NIR spectroscopy. Unfortunately it was found to be unstable unless in the presence of excess oxidant. Crystals were grown in the presence of oxidising agent and methylene chloride and attempts were made to mount the crystals in Lindemann tubes with oxidant and then to seal the tubes. They were however found to be too small for crystallographic studies.

The $[(PEt_3)_3Os(\mu\text{-}Cl)_3Os(PEt_3)_3]^+$ complex was prepared[22] as it was expected to have a more accessible first oxidation (see Chapter 4). This was found to be the case, $E_{\frac{1}{2}}$ = +0.90V versus Ag/AgCl where ferrocene/ferrocinium is at 0.56V. It shows similar spectroelectrochemical behaviour to the $[(PMe_2Ph)_3Os(\mu\text{-}Cl)_3Os(PMe_2Ph)_3]^+$ species and is discussed in more detail in Chapter 4. Oxidation of this species in methylene chloride with 60% $HClO_4$ yielded an orange material. The UV/VIS/NIR spectrum confirmed it to be the $[(PEt_3)_3Os(\mu\text{-}Cl)_3Os(PEt_3)_3]^{2+}$ species. Fig. 2.2.7 shows

Figure 2.2.7: Spectra showing (a) $[(PEt_3)_3Os(\mu\text{-}Cl)_3Os(PEt_3)_3]^{2+}$ generated chemically using 60% $HClO_4$ and (b) $[(PEt_3)_3Os(\mu\text{-}Cl)_3Os(PEt_3)_3]^{2+}$ generated electrochemically in Methylene Chloride / 0.5M $TBABF_4$

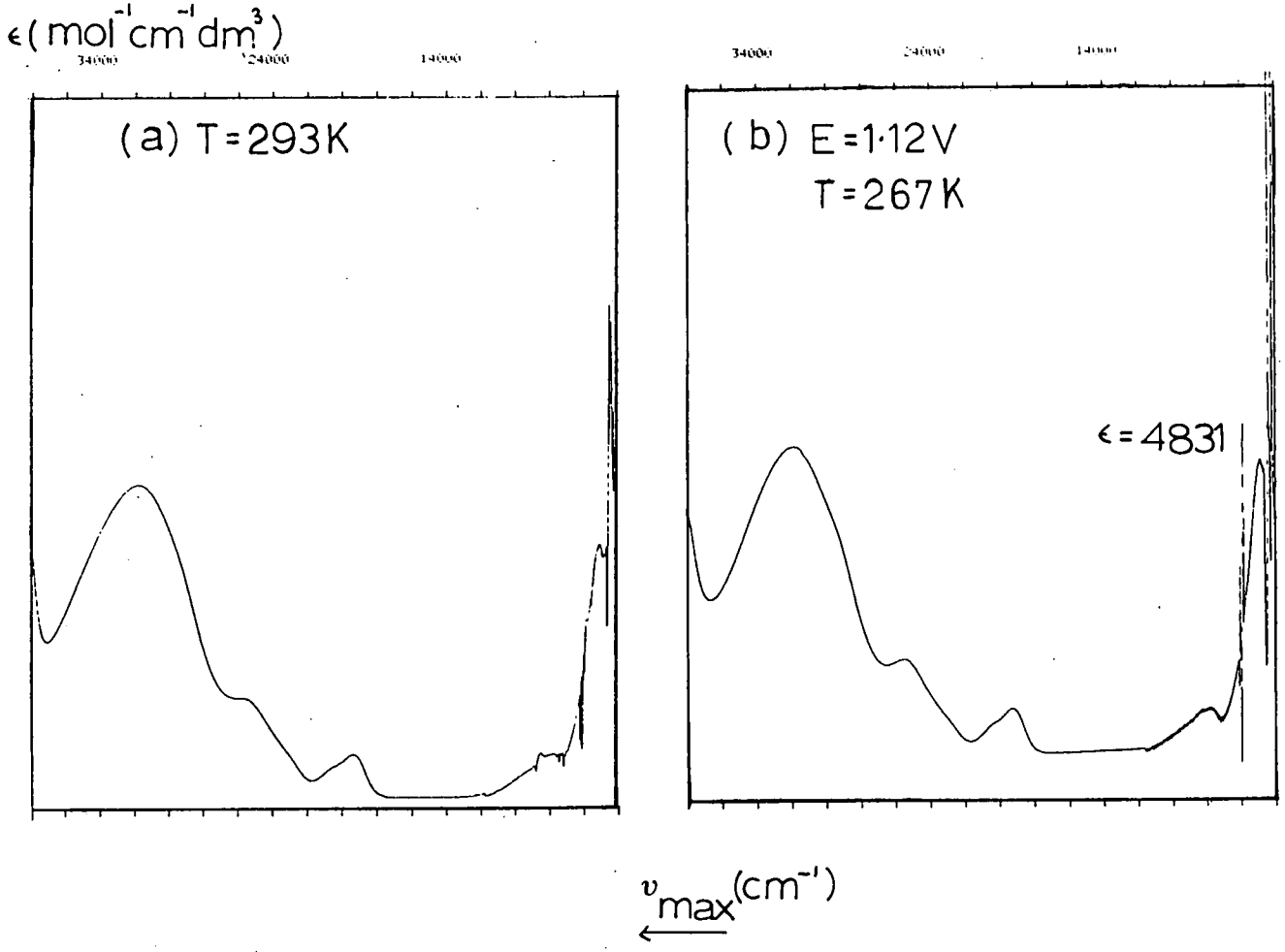

the spectrum obtained together with that of the electrogenerated $[(PEt_3)_3Os(\mu\text{-}Cl)_3Os(PEt_3)_3]^{2+}$ species. This was found to be stable in the absence of oxidant. Crystals were grown from methylene chloride/diethyl ether. They appeared to be single, but attempts to photograph them failed. It was eventually decided after using different solvents that the crystals were in fact layers of crystals on top of each other.

Finally different counterions were used:
1. $OsCl_6^{2-}$, 2. $B(C_6F_5)_4^-$ and 3. $CH_3\text{-}(C_6H_4)\text{-}SO_3^-$.
The monocationic complex was oxidised as described previously then the anions 1, 2 and 3 were added respectively to methylene chloride solutions containing the dicationic species. Using 2 single crystals were obtained suitable for X-ray crystallographic studies. The X-ray crystal structure of the monocationic species had also to be carried out in order to make a direct comparison. These will now be discussed.

Single Crystal Structures of the Binuclear Monocationic species (A) $[(PEt_3)_3Os(\mu\text{-}Cl)_3Os(PEt_3)_3]PF_6$ and (B) $[(PEt_3)_3Os(\mu\text{-}Cl)_3Os(PEt_3)_3](B(C_6F_5)_4)(ClO_4)\cdot\frac{1}{2}CH_2Cl_2$

Single crystals of species B were obtained as described previously from a methylene chloride/diethyl ether solution. Complex A was prepared by literature methods;[22] crystals were obtained from a methylene chloride/methanol solution by slow evaporation of methylene chloride.

Crystal data and the method of solving and refining each structure is detailed in the experimental section (section 2.3).

A view of the monocation is shown in Figure 2.2.8 and that of the dication in Figure 2.2.9. Tables 2.2.5 and 2.2.6 give a selection of bond lengths and angles.

On oxidation the Os--Os distance decreases from 3.473(1)Å to 3.406(1)Å. The average Os-Cl bond length decreases (from 2.492 to 2.472Å) and the average Os-P bond length increases (2.304 to 2.350Å). The average Os-$\hat{Cl}$-Os angle decreases by 1.24° from 88.25° to 87.01°.

Spectroelectrochemical studies on $[(PEt_3)_3Os(\mu\text{-}Cl)_3Os(PEt_3)_3]^{2+}$ have shown the metal centres to be strongly interacting i.e. Class III species with strong delocalisation (see Chapter 4). The two metal centres are indistinguishable crystallographically in the $[(PEt_3)_3Os(\mu\text{-}Cl)_3Os(PEt_3)_3]^{2+}$ species supporting delocalisation.

On oxidation of $[(PEt_3)_3Os(\mu\text{-}Cl)_3Os(PEt_3)_3]^{+}$ to $[(PEt_3)_3Os(\mu\text{-}Cl)_3Os(PEt_3)_3]^{2+}$ an electron is removed from a metal based antibonding molecular orbital, thus a decrease in metal-metal distance would be expected which is indeed observed. The average Os-Cl bond length decreases as expected for a π-donating ligand-metal bond. The average Os-P distance increases which would be expected for a metal-π-acceptor ligand bond but PEt_3 is a σ/π donor (see Chapter 4). We therefore suggest that the reason for the M-P bonds increasing is steric. The steric effect occurs across the bridge (see Chapter 4). As the metal centres move closer together due to the increasing interaction upon oxidation the PEt_3 ligands can only pack efficiently with minimal steric crowding and retention of the confacial bioctahedral structure if the M-P bond lengths increase. This has the

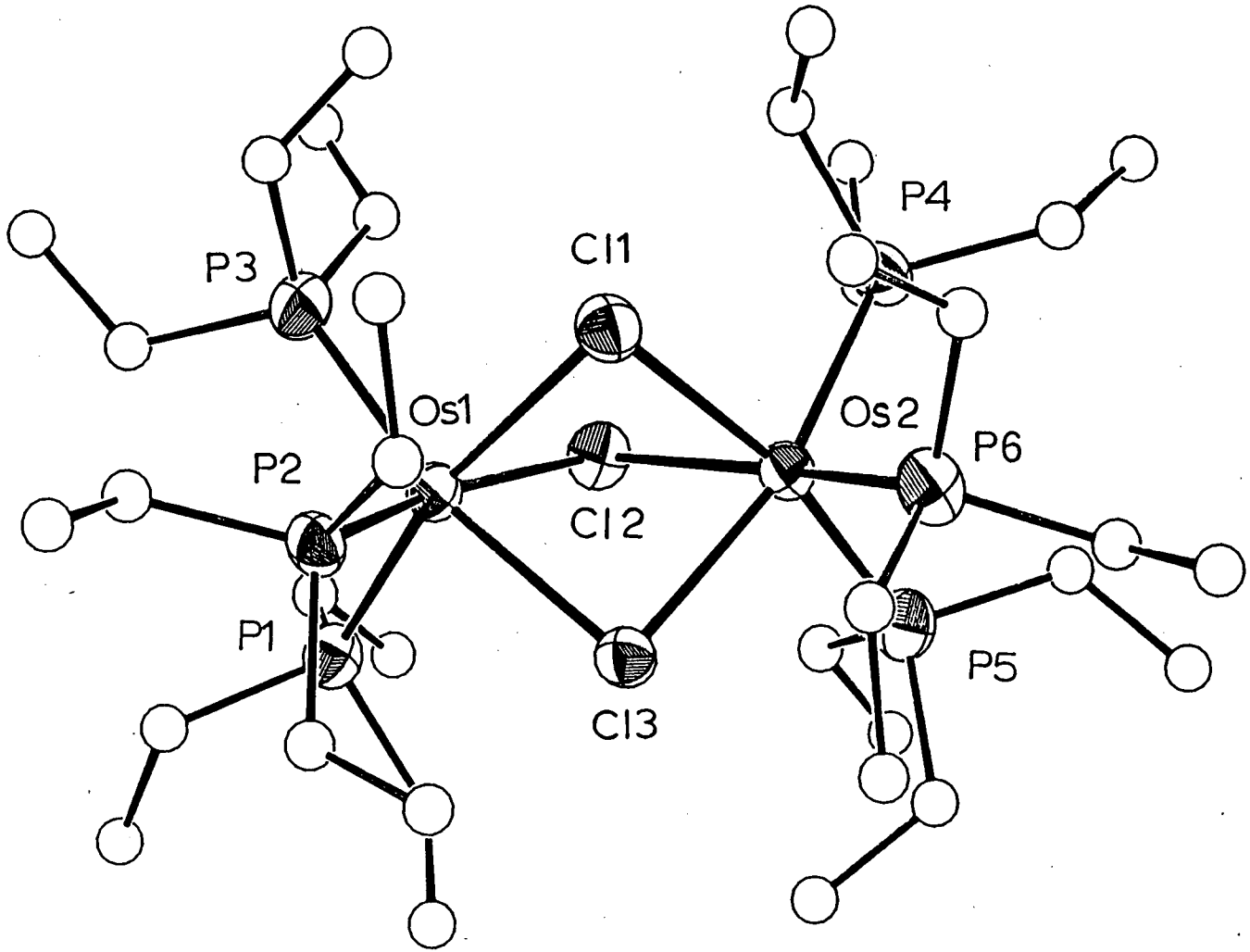

Figure 2.2.8: View of the $[(PEt_3)_3Os(\mu\text{-}Cl)_3Os(PEt_3)_3]^+$ monocation

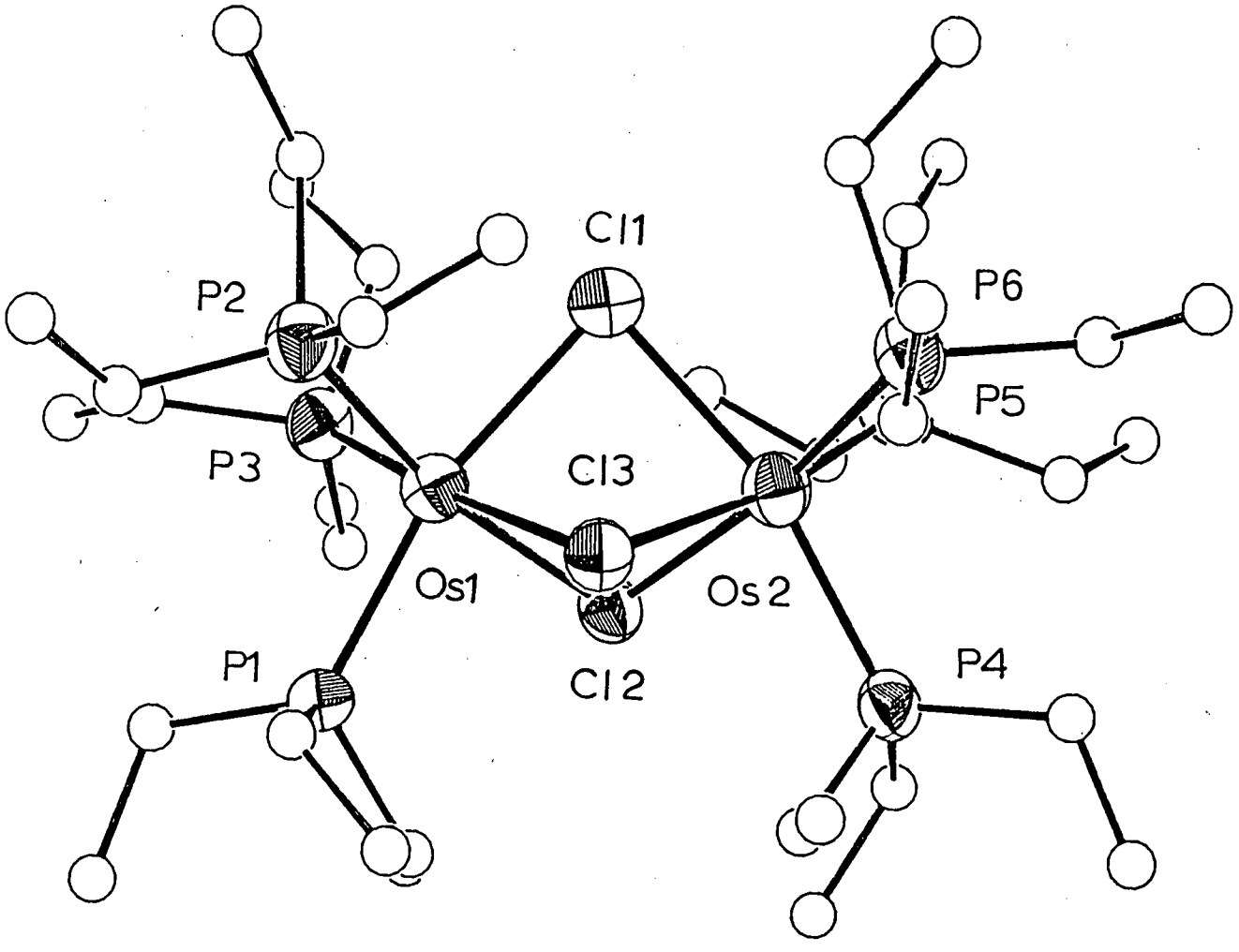

Figure 2.2.9: View of the $[(PEt_3)_3Os(\mu\text{-}Cl)_3Os(PEt_3)_3]^{2+}$ dication

Table 2.2.5: Selected Bond Lenths and Angles for

$[(PEt_3)_3Os(\mu\text{-}Cl)_3Os(PEt_3)_3]^+$

Bond Lengths(Å) with standard deviations

Os(1) -Cl(1)	2.484(5)	P(2) -C(211)	1.830(25)
Os(1) -Cl(2)	2.463(5)	P(2) -C(221)	1.868(23)
Os(1) -Cl(3)	2.486(6)	P(2) -C(231)	1.81(3)
Os(1) - P(1)	2.344(6)	P(3) -C(311)	1.87(3)
Os(1) - P(2)	2.354(6)	P(3) -C(321)	1.843(23)
Os(1) - P(3)	2.356(6)	P(3) -C(331)	1.89(3)
Os(2) -Cl(1)	2.458(5)	P(4) -C(411)	1.860(24)
Os(2) -Cl(2)	2.486(5)	P(4) -C(421)	1.828(23)
Os(2) -Cl(3)	2.464(6)	P(4) -C(431)	1.840(25)
Os(2) - P(4)	2.348(6)	P(5) -C(511)	1.825(23)
Os(2) - P(5)	2.344(6)	P(5) -C(521)	1.845(24)
Os(2) - P(6)	2.356(6)	P(5) -C(531)	1.88(3)
P(1) -C(111)	1.83(3)	P(6) -C(611)	1.877(25)
P(1) -C(121)	1.88(3)	P(6) -C(621)	1.82(3)
P(1) -C(131)	1.782(25)	P(6) -C(631)	1.851(24)

Angles(degrees) with standard deviations

Os(1) -Cl(1) -Os(2)	87.12(17)
Os(1) -Cl(2) -Os(2)	86.96(17)
Os(1) -Cl(3) -Os(2)	86.96(18)
P(1) -Os(1) - P(2)	94.16(22)
P(1) -Os(1) - P(3)	95.93(22)
P(2) -Os(1) - P(3)	97.88(22)
P(4) -Os(2) - P(5)	98.13(21)
P(4) -Os(2) - P(6)	93.72(21)
P(5) -Os(2) - P(6)	96.22(21)

Table 2.2.6: Selected Bond Lengths and Angles for $[(PEt_3)_3Os(\mu\text{-}Cl)_3Os(PEt_3)_3]^{2+}$

Bond Lengths(Å) with standard deviations

Os(1)	-Cl(1)	2.487(4)	P(2)	-C(211)	1.883(18)
Os(1)	-Cl(2)	2.501(4)	P(2)	-C(221)	1.839(17)
Os(1)	-Cl(3)	2.489(4)	P(2)	-C(231)	1.828(17)
Os(1)	- P(1)	2.301(4)	P(3)	-C(311)	1.839(22)
Os(1)	- P(2)	2.300(4)	P(3)	-C(321)	1.861(19)
Os(1)	- P(3)	2.306(4)	P(3)	-C(331)	1.837(23)
Os(2)	-Cl(1)	2.499(4)	P(4)	-C(411)	1.856(18)
Os(2)	-Cl(2)	2.511(4)	P(4)	-C(421)	1.850(18)
Os(2)	-Cl(3)	2.477(4)	P(4)	-C(431)	1.851(20)
Os(2)	- P(4)	2.319(4)	P(5)	-C(511)	1.855(19)
Os(2)	- P(5)	2.304(4)	P(5)	-C(521)	1.877(19)
Os(2)	- P(6)	2.291(4)	P(5)	-C(531)	1.854(20)
P(1)	-C(111)	1.861(18)	P(6)	-C(611)	1.821(17)
P(1)	-C(121)	1.818(17)	P(6)	-C(621)	1.863(20)
P(1)	-C(131)	1.845(17)	P(6)	-C(631)	1.851(20)

Angles(degrees) with standard deviations

P(1)	-Os(1) -	P(2)	97.87(14)
P(1)	-Os(1) -	P(3)	96.21(14)
P(2)	-Os(1) -	P(3)	96.88(14)
P(4)	-Os(2) -	P(5)	94.61(15)
P(4)	-Os(2) -	P(6)	97.92(15)
P(5)	-Os(2) -	P(6)	96.59(15)
Os(1)	-Cl(1)	-Os(2)	88.29(12)
Os(1)	-Cl(2)	-Os(2)	87.71(12)
Os(1)	-Cl(3)	-Os(2)	88.76(12)

effect of relieving steric crowding across the bridge. Space filling diagrams[24] illustrate this, as shown in Figures 2.2.10 and 2.2.11.

Conclusions

Changing the oxidation state, n, from 1 to 2 to 3 causes the metal centres to become more strongly interacting. Kinetic studies support the idea that we are seeing a structural change taking place. This is indeed observed in the X-ray crystallographic studies of the monocationic and dicationic species where changes in the metal-metal distance M-P and M-Cl bond lengths are observed.

2.3 EXPERIMENTAL

Electrochemical studies were performed using the PAR model 170 potentiostat and programmer with provision for iR compensation. A platinum working and counter electrode were employed together with an Ag/AgCl reference electrode against which ferrocene is oxidised at $E_{\frac{1}{2}} = +0.56V$. Scan rates used were from 20-500 mVs^{-1} (c.v.) and 20 mVs^{-1} (a.c.v.). The temperature was controlled using the Haake F3 temperature controller and Haake Q bath.

Kinetic studies were performed using the PAR model 170 potentiostat and programmer with provision for iR compensation, HITEK transient store, Tektronix Oscilloscope model D66A and Hewlett-Packard XY recorder model 7035B. The Haake bath and temperature controller were used to control the temperature as above. Scan rates used were from 30-70 Vs^{-1}.

D_O was determined by use of the rotating disc electrode,

Figure 2.2.10: Space Filling Diagram of $[(PEt_3)_3Os(\mu\text{-}Cl)_3Os(PEt_3)_3]^{+}$ [24]

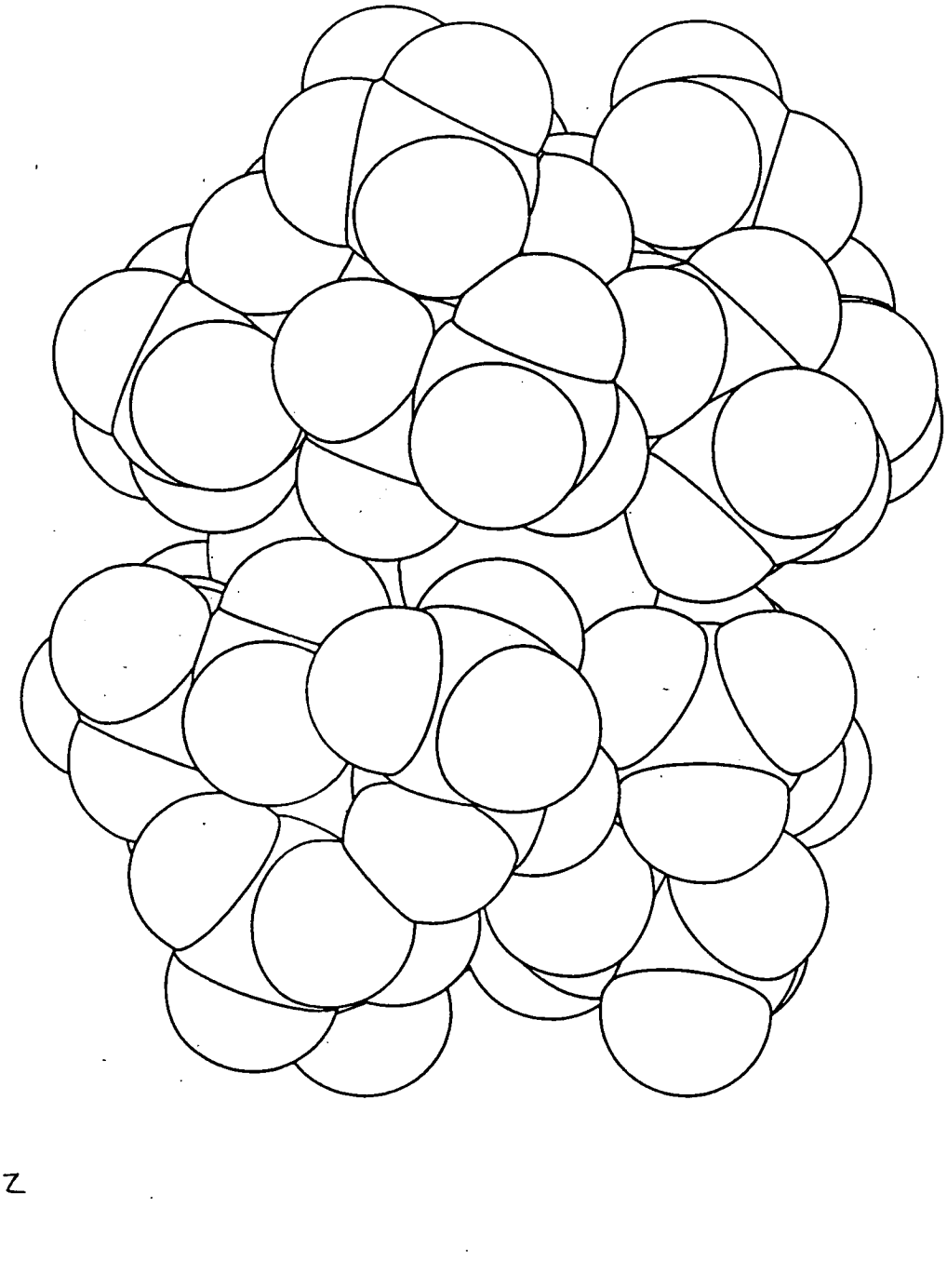

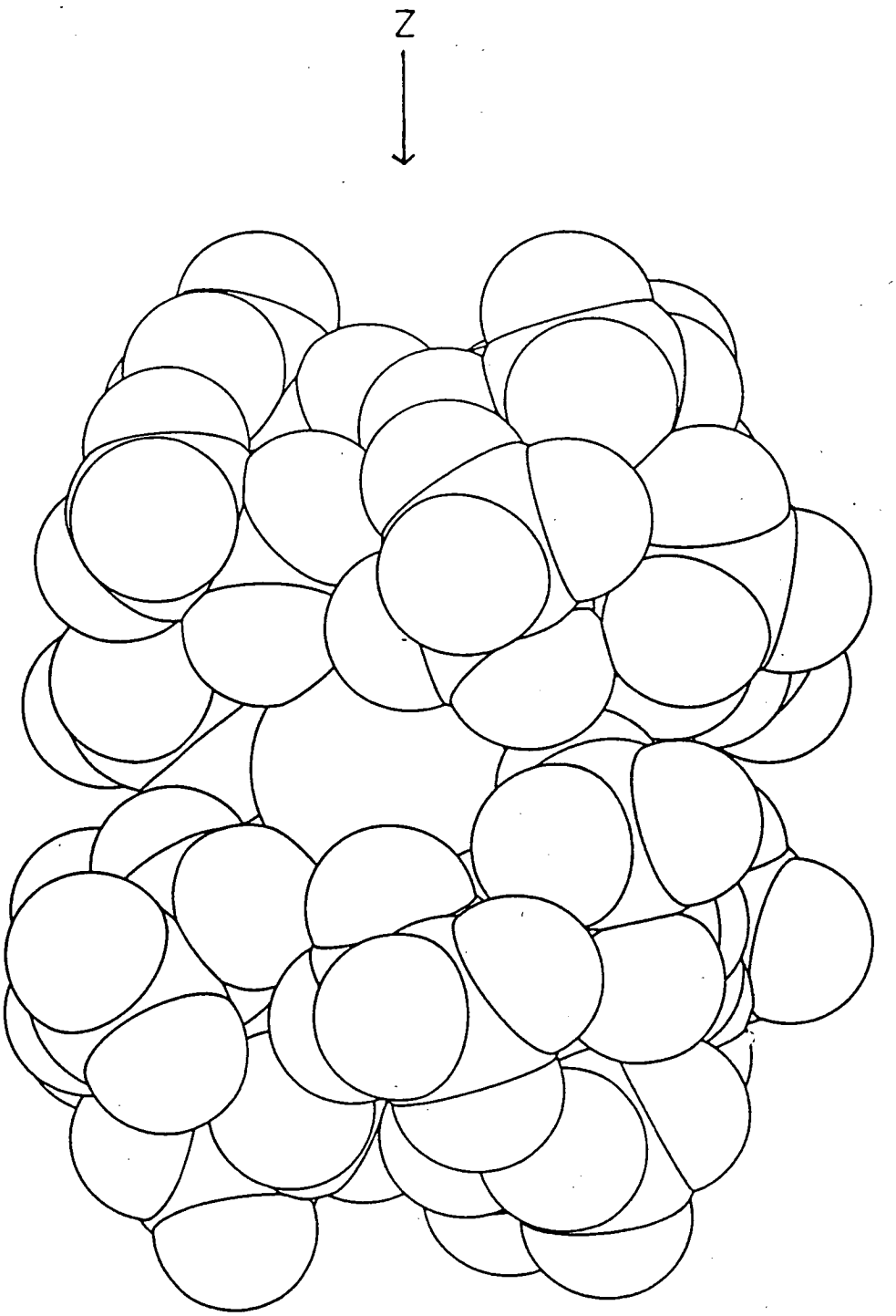

Fig. 2.2.11: Space Filling Diagram of

$[(PEt_3)_3Os(\mu\text{-}Cl)_3Os(PEt_3)_3]^{2+}$ 24

where A = 0.3848 cm^2. The temperature was controlled as above.

Spectroelectochemical studies were carried out using the optically transparent thin layer electrode as described previously. Temperature control was achieved as described previously. The Perkin Elmer Lambda 9 spectrophotometer was employed for these studies. Spectra were recorded over the range 3,125-50,000 cm^{-1}.

Materials

$RuCl_3 \cdot 3H_2O$ and K_2OsCl_6 were obtained from Aldrich. Methylene Chloride was purified as described previously. All other solvents were used as supplied without further purification.

$TBABF_4$ was prepared as described previously.

PMe_2Ph was prepared according to the literature method.[25]

$[(PMe_2Ph)_3M(\mu\text{-}Cl)_3M(PMe_2Ph)_3]PF_6$ were prepared according to literature methods.[22,23], M=Ru,Os

$[(PEt_3)_3Os(\mu\text{-}Cl)_3Os(PEt_3)_3]PF_6$ was prepared according to the literature method.[22]

Reaction of Cis $OsCl_2(PMe_2Ph)_4$ with Cis $RuCl_2(PMe_2Ph)_4$

To a warm degassed butan-2-ol solution (20ml) of cis $OsCl_2(PMe_2Ph)_4$[23] (0.085g), cis $RuCl_2(PMe_2Ph)_4$[26] (0.076g) in degassed butan-2-ol (10ml) was added dropwise.

This mixture was heated to reflux under N_2 for 24 hours. On cooling yellow crystals formed. These were filtered and washed with methanol and diethyl ether and dried in vacuo.

Assuming the presence of the ionic dimer $[(PMe_2Ph)_3M(\mu\text{-}Cl)_3M(PMe_2Ph)_3]Cl$; the Cl^- anion was exchanged for PF_6^- as previously described. Experimental results suggest that a mixture of $[(PMe_2Ph)_3Ru(\mu\text{-}Cl)_3Ru(PMe_2Ph)_3]PF_6$, $[(PMe_2Ph)_3Ru(\mu\text{-}Cl)_3Os(PMe_2Ph)_3]PF_6$ and $[(PMe_2Ph)_3Os(\mu\text{-}Cl)_3Os(PMe_2Ph)_3]PF_6$ were obtained.

FAB Mass Spectrum: Found $M^+ = 1316$ (20%)

$M^+ = 1228$ (100%)

$M^+ = 1139$ (25%)

Calculated for $[(PMe_2Ph)_3Os(\mu\text{-}Cl)_3Os(PMe_2Ph)_3]^+$

$M^+ = 1314.35$

$[(PMe_2Ph)_3Ru(\mu\text{-}Cl)_3Os(PMe_2Ph)_3]^+$

$M^+ = 1225.35$

and $[(PMe_2Ph)_3Ru(\mu\text{-}Cl)_3Ru(PMe_2Ph)_3]^+$

$M^+ = 1136.35$

Electrochemistry

Cyclic voltammetry (c.v.) and a.c. voltammetry studies (a.c.) showed peaks at:-

1. +1.07V
2. +1.29V
3. +1.59V
4. +1.82V

(versus Ag/AgCl on which ferrocene is oxidised at +0.56V)

Peaks 1 and 4 are twice as intense as those of 2 and 3. This is consistent with there being the three species present. The diosmium complex shows two one-electron oxidations at 1.07V and 1.59V; the diruthenium at +1.29V and +1.82V. The mixed osmium/ruthenium complex would be expected to show two

oxidations; the osmium centre being oxidised first at +1.07V and then ruthenium centre being oxidised at +1.89V.

Attempts to separate the complexes failed due to similarities in solubility and mass.

Single Crystal Structure of $[(PMe_2Ph)_3Os(\mu\text{-}Cl)_3Os(PMe_2Ph)_3]PF_6$

This complex was prepared as described previously. Crystal Data: $[C_{48}H_{66}Cl_3Os_2P_6]PF_6$, M = 1460.56, monoclinic, space group $P2_1/c$, a = 14.4399 (9), b = 16.3484(11), c = 23.9188(20)Å, β = 97.048(7)°, V = 5616.3Å^3 (from setting angles for 43 reflections with 2θ = 25-26, λ = 0.71073Å), z = 4, D_{calc} = 1.727g cm^{-3}, T = 293K, pale yellow needles, 0.77x0.13x0.077 mm, μ = 49.19 cm^{-1}, $F(000)$ = 2864.

Data Collection and Processing

Stöe STADI-4 diffractometer, graphite monochromated Mo-K_α X-radiation, T = 293K, $\omega/2\theta$ scans using learnt profile method,[27] 6683 reflections measured ($2\theta_{max}$ 45°, h-15→7 k-0→17, l 0→25), 5685 unique data (R_{int} = 0.0292), giving 4710 with $F > 6\sigma(F)$ for use in all calculations. No significant crystal decay or movement. Initial corrections for absorption based on ψ scans were applied, minimum and maximum transmission factors are 0.0454 and 0.0736 respectively.

Structure Solution and Refinement

Using the fractional coordinates of the isostructural $[(PMe_2Ph)_3Ru(\mu\text{-}Cl)_3Ru(PMe_2Ph)_3]PF_6$ species the positions of all non hydrogen atoms were located. These were refined with anisotropic thermal parameters. H atoms were fixed in calculated positions using AFIX. DIFABS[28] absorption correction was carried out with minimum correction = 0.804

and maximum correction = 1.534.

At final convergence $\underline{R}$ = 0.0303, $\underline{R}_w$ = 0.0374, $\underline{S}$ = 1.076 for 460 refined parameters and the final ΔF synthesis showed no peak above 0.831e$\mathring{A}^{-3}$ or below -0.48e$\mathring{A}^{-3}$. The weighting scheme $\underline{W}^{-1} = \sigma^2(F) + 0.000386F^2$ gave satisfactory agreement analyses and in the final cycle $(\Delta/\sigma)_{max}$ = 0.118.

Atomic scattering factors were inlaid[29] or taken from reference 30. The figure was obtained using ORTEP.[31]

Single Crystal X-Ray Structure of $[(PEt_3)_3Os(\mu\text{-}Cl)_3Os(PEt_3)_3]PF_6$

This complex was prepared and crystallised as described previously.

Crystal Data: $[C_{48}H_{90}Cl_3Os_2P_6]PF_6$, M = 1340.62, triclinic, space group $P\bar{1}$, $\underline{a}$ = 11.1820(14), $\underline{b}$ = 13.8689(17), $\underline{c}$ = 18.5669(23)$\mathring{A}$. α = 84.601(6), β = 82.421(8), γ = 67.194(7)°, $\underline{V}$ = 2631.02$\mathring{A}^3$ (from setting angles for 63 reflections with 31 < 2θ < 32 °, λ = 0.71073$\mathring{A}$), $\underline{z}$ = 3, $\underline{D}_{calc}$ = 2.538g cm^{-3}, $\underline{T}$ = 293K, pale yellow tablet, 0.77x0.27x0.12 mm, μ = 78.62 cm^{-1}, $\underline{F}$(000) = 2004.

Data Collection and Processing

Stöe STADI-4 diffractometer graphite monochromated Mo - $\underline{K}_\alpha$ X-radiation, T = 293K, $\omega/2\theta$ scans with width (0.99 + 0.347 tanθ)°, 6850 data collected ($2\theta_{max}$ 90°, h-11→12, k-14→14, l 0→19, 6289 unique data (R_{int} = 0.0000), giving 5290 with F > 6σ($\underline{F}$) for use in all calculations. No significant crystal decay or movement. Initial corrections for absorption based on ψ scans were applied, minimum and maximum transmission factors are respectively 0.051 and 0.129.

Structure Solution and Refinement

A Patterson synthesis located the Os atoms and subsequent iterative cycles of least squares refinement and difference Fourier synthesis located all non-H atoms. These were then refined using SHELX-76 with anisotropic thermal parameters for Os, Cl and P. H atoms were fixed in calculated positions using AFIX. DIFABS[28] absorption correction was carried out with minimum correction = 0.804 and maximum correction = 1.534. At final convergence $\underline{R}$ = 0.0518, $\underline{R}_w$ = 0.0717, $\underline{S}$ = 1.027 for 311 refined parameters and the final ΔF synthesis showed no peak above 0.632e$\mathring{A}^{-3}$. The weighting scheme $\underline{W}^{-1} = \sigma^2(F) + 0.00634F^2$ gave satisfactory agreement analyses and in the final cycle $(\Delta/\sigma)_{max}$ was 0.101. Atomic scattering factors were inlaid[29] or taken from reference 30. The figure was obtained using ORTEP.[31]

Single Crystal Structure of

$[(PEt_3)_3Os(\mu\text{-}Cl)_3Os(PEt_3)_3][B(C_6F_5)_4][ClO_4]\cdot\frac{1}{2}(CH_2Cl_2)$

This species was prepared as previously described. Crystal Data: $[C_{48}H_{66}Cl_3Os_2P_6][C_{24}B_4F_{20}][ClO_4]\cdot\frac{1}{2}(CH_2Cl_2)$, M = 2010.44, monoclinic, space group $\underline{C2/c}$, $\underline{a}$ = 38.9930(120), $\underline{b}$ = 16.3694(39), $\underline{c}$ = 26.6316(28)$\mathring{A}$, β = 106.140(13), $\underline{V}$ = 16328.7$\mathring{A}^3$ (from setting angles for 29 reflections with $43 < 2\theta < 45$, λ = 1.5134$\mathring{A}$), $\underline{z}$ = 8, $\underline{D}_{calc}$ = 1.635g cm^{-3}; $\underline{T}$ = 293K, orange plates, 0.46x0.46x0.16 mm, μ = 92.32 cm^{-1}, $\underline{F}(000)$ = 7960.

Data Collection and Processing

Stöe STADI-4 diffractometer, graphite monochromated Cu-$\underline{K}_\alpha$ X-radiation, T = 293K, $\omega/2\theta$ scans with width (0.99 + 0.347 tanθ)°, 9173 data collected ($2\theta_{max}$ = 100°, h-38→34, k-0→16, l-0→26), 7545 unique data (R_{int} 0.0163), giving 5849 with $\underline{F} > 6\sigma(\underline{F})$ for use in all calculations. No significant crystal movement or decay. Initial corrections for absorption based on ψ scans were applied, the minimum and maximum transmission factors are 0.0073 and 0.0895 respectively.

Structure Solution and Refinement

A Patterson synthesis located the Os atoms and subsequent iterative cycles of least squares refinement and difference Fourier synthesis located all non H-atoms. These were then refined by least squares using SHELX-76[29] with anisotropic thermal parameters for Os, P, Cl. DIFABS[28] absorption correction using SHELX-86[32] was carried out with minimum correction = 0.687 and maximum correction = 1.334. H atoms were fixed in calculated positions using AFIX. The $-C_6F_5$ rings were fixed as rigid groups. At final convergence $\underline{R}$ = 0.0747, $\underline{R}_w$ = 0.0980, $\underline{S}$ = 1.097 for 364 refined parameters and the final ΔF synthesis showed no peak above 0.845e$\mathring{A}^{-3}$. The weighting scheme $\underline{W}^{-1} = \sigma^2(F) + 0.000578F^2$ gave satisfactory agreement analyses and in the final cycle $(\Delta/\sigma)_{max}$ = 0.034.

Atomic scattering factors were inlaid[29] or taken from reference 30. The figure was obtained using ORTEP.[31]

2.4 REFERENCES

1. F.A. Cotton and G. Wilkinson, "Advanced Inorganic Chemistry", 4th Edition, 1980, John Wiley and Sons, Inc.
2. K.H. Moock, Ph.D. Thesis, University of Glasgow, 1985.
3. P. Pyykkö and J.P. Desclaux, Acc.Chem.Res.; 1979, 12, 279.
4. A. Sommerfield, Ann.Phys.; 1916, 51.
5. A.J. Lindsay, Ph.D. Thesis, University of Edinburgh, 1982.
6. N.G. Connelly and L.F. Dahl, J.Am.Chem.Soc.; 1970, 92, 7472.
7. J.D. Sinclair, Ph.D. Thesis, University of Wisconsin, 1972.
8. N.G. Connelly and L.F. Dahl, J.Am.Chem.Soc.; 1970, 92, 7470.
9. R.E. Dessy, F.E. Story, R.B. King and M. Waldorp, J.Am.Chem.Soc.; 1966, 88, 471.
10. J.A. McCleverty, D. Frisch, M.K. Lloyd and D. Seddon, J.Chem.Soc., Dalton Trans.; 1973, 2268.
11. R.E. Dessy, R. Kornmann, C. Smith and R. Haytor, J.Am.Chem.Soc.; 1968, 90, 2001.
12. (a) R.A. Marcus, J.Chem.Phys.; 1956, 26, 4966; 1965, 43, 79; (b) N.S. Hush, J.Chem.Phys.; 1958, 962.
13. (a) T. Gennett, W.E. Geiger, B. Willett and F.C. Anson, J.Electroanal.Chem.; 1987, 222, 151;
    (b) T. Gennett, Ph.D. Thesis, University of Vermont, 1985.
14. R.S. Nicholson, Anal.Chem.; 1965, 37, 1351.

15. J.P. Collman,R.K. Rothrock, R.G. Finke and F. Rose-Munch, Inorg.Chem.; 1982, 21, 146.

16. L.S. Hollis and S.J. Lippard, Inorg.Chem., 1983, 22, 2605.

17. N. Van Order Jr, W.E. Geiger, T.E. Bitterwolf and A.L. Rheingold, J.Am.Chem.Soc.; 1987, 109, 5680.

18. F.A. Cotton, Chem.Soc.Reviews; 1983, 12, 35.

19. F.A. Cotton, A. Davison, V.W. Day, M.F. Fredrich, C. Orrig and R. Swanson, Inorg.Chem.; 1982, 21, 1211.

20. P. Neubold, K. Wieghardt, B. Nuber and I. Weiss, Inorg.Chem.; 1989, 28, 459.

21. J.G. Gaudiello, T.C. Wright, R.A. Jones and A.J. Bard, J.Am.Chem.Soc.; 1985, 107, 888.

22. J. Chatt and R.G. Hayter, J.Chem.Soc.; 1961, 896.

23. V.T. Coombe, Ph.D. Thesis, University of Edinburgh, 1985.

24. PLUTO: W.D.S. Motherwell, University of Cambridge, England.

25. W.C. Davies and W.J. Jones, Chem.Soc.Journal; 1929, 1, 33.

26. P.W. Armit, T.A. Stephenson and A.S.F. Boyd, J.Chem.Soc., Dalton Trans.; 1975, 1663.

27. W. Clegg, Acta Cryst. A; 1981, 37, 22.

28. DIFABS; N.G. Walker and D. Stuart, Acta Cryst, Sect.A;

29. SHELX-76; "A program for crystal structure determination and refinement", G.M. Sheldrick, University of Cambridge, England, 1976.

30. D.T. Cromer and J.L. Mann, Acta Cryst.; 1968, A24, 321.

31. ORTEP; P.D. Mallinson and K.W. Muir, J.Appl.Cryst.; 1985, 18, 51.

32. SHELX-86: "A program for crystal structure determination and refinement", G.M. Sheldrick, University of Göttingen, 1986.

C H A P T E R 3

VARIATION OF BRIDGING LIGAND, X^-

$X = OH^-, Cl^-, Br^-, I^-$; M = Ru

$X = Cl^-, Br^-, I^-$; M = Os

3.1 INTRODUCTION

Triply-bridged species of the type $[L_3M(\mu\text{-}Cl)_3ML_3]^{n+}$ have been known for some time where M = Ru, Os; L = PMe_2Ph, $PMePh_2$, PEt_2Ph, $PEtPh_2$; n = 1. These were first prepared by Chatt in 1961[1] by the interaction of $RuCl_3 \cdot 3H_2O$ or $(NH_4)_2OsCl_6$ in aqueous methanol or ethanol with the appropriate tertiary phosphine ligand. Non-chlorobridged complexes, $[L_3M(\mu\text{-}X)_3ML_3]^{n+}$ are much rarer. In 1968 Shaw et al.[2] reported the first synthesis of complexes of this type where n = 1; X^- = Br^-, I^-; L = PMe_2Ph. The $[L_3Ru(\mu\text{-}Br)_3RuL_3]^+$ complex was prepared by the interaction of $RuCl_3 \cdot xH_2O$ and PMe_2Ph in isopropyl alcohol with an excess of LiBr. The iodo bridged complex was made by the reaction of $[L_3Ru(\mu\text{-}Cl)_3RuL_3]^+$ and NaI in isopropyl alcohol.

The range of complexes of this type has been greatly extended since these studies by using other methods of preparation. Robinson et al.[3,4] reported the preparation of $[L_3Ru(\mu\text{-}X)_3RuL_3][BPh_4]$ where X^- = Br^-; L = $P(OEt)_3$ from the reaction between $[RuBr_2(norb)]_n$ and $P(OEt)_3$ in refluxing methanol. Stephenson prepared triply-bromo bridged complexes by the reaction of $RuBr_2(PPh_3)_3$ and the appropriate tertiary P(III) ligand in methanol.[5] Ashworth[6] further extended the range of ruthenium triply-bridged species to X^- = OH^-; L = PMe_2Ph, $PMePh_2$, $P(OMe)Ph_2$; X^- = F^-, SH^-, SMe^-; L = PMe_2Ph and in our laboratories his method was used to prepare the complex where X^- = SEt^-; L = PMe_2Ph.[7] His method involved first preparing the triply-hydroxy bridged complex by the reaction of $[RuH(COD)(NH_2NMe_2)_3]PF_6$ in a 2:1 mixture of acetone and methanol with the appropriate tertiary

phosphine ligand. By the action of the appropriate acid, HX, on the triply-hydroxy bridged complex the above range of complexes were obtained. It was also found that this method was more satisfactory than that of Shaw for preparing the species where X^- = Br^- and I^-; L = PMe_2Ph.[7] Triply-methylene[8] and hydrido-bridged[9,10] complexes are also known. Wilkinson[8] reported the complex $[(PMe_3)_3Ru(\mu\text{-}CH_2)_3Ru(PMe_3)_3]$. This was prepared by the reaction of $[Ru_3O(O_2CMe)_6(H_2O)_3](O_2CMe)$ with dimethylmagnesium and PMe_3 in tetrahydrofuran. Both the osmium and ruthenium triply-hydrido bridged species are known. The osmium[10] complex where L = PMe_2Ph is prepared by the reaction of $Os_2H_4L_6$ and $HBF_4 \cdot Et_2O$. The ruthenium[9] complex is made in a similar manner by the interaction of $Ru_2H_4(PMe_3)_6$ with HBF_4 in tetrahydrofuran.

There are many examples of triply-bridged complexes where the terminal ligands are not tertiary phosphine ligands. The related complexes $[(NH_3)_3Ru(\mu\text{-}X)_3Ru(NH_3)_3]^{2+}$ where X^- = Cl^- and Br^- are known. These are prepared by the reaction of $[Ru(NH_3)_6]X_2$ and HX.[11,12]

Stephenson prepared complexes of the type $[ArM(\mu\text{-}X)_3MAr]^+$ where M = Os; Ar = C_6H_6, $\underline{p}Me\text{-}C_6H_4CHMe_2$ X^- = Cl^-; M = Ru; Ar = C_6H_6, $C_6H_3Me_3$, $\underline{p}MeC_6H_4CHMe_2$, C_6Me_6; X^- = OPh^-, OMe^-, OEt^-, OH^-, Cl^-, Br^-, I^-.[13,14]

The $[(\eta\text{-}C_6H_6)Ru(\mu\text{-}Cl)_3Ru(\eta C_6H_6)]PF_6$ complex is prepared by the reaction of $[Ru(\eta C_6H_6)Cl_2]$ in methanol at ambient temperatures with excess NH_4PF_6. The other triply-halide bridged species could not be prepared in this way due to the insoluble nature of the starting complexes. It is thought that the mechanism of forming the triply-chloro bridged

species involves intermolecular coupling of the weakly solvated monomers $Ru(\eta C_6H_6)Cl_2(MeOH)$ and $[Ru(\eta C_6H_6)Cl(MeOH)_2]^+$. The reaction of the corresponding pyridine complexes also led to the formation of the triply-bridged complex. The analogous Br^- and I^- monomers give the triply-bridged bromide and iodide complexes respectively. The osmium complexes are prepared in a similar manner. There is spectroscopic evidence to show that by using these methods mixed-bridged complexes have been prepared. The hydroxy- and alkoxo-[15]bridged species are prepared by the reaction of $[M(\eta C_6H_6)Cl_2]_2$; M = Ru, Os with an excess of NaOH or Na_2CO_3 for $X = OH^-$ and NaOR for $X = OR^-$.

Wieghardt has prepared many triply-bridged ruthenium complexes where the terminal ligand set at each metal centre is the macrocyclic ligand; 1,4,7 trimethyl-1,4,7 triaza-cyclononane, L, of which examples include:
1. $[LRu(\mu\text{-}O)(\mu\text{-}CH_3CO_2)_2RuL]^{3+}$,[16] 2. $[LRu(\mu OH)_2(\mu\text{-}CH_3CO_2)RuL]^{3+}$[17] and 3. $[LRu(\mu\text{-}O)_3RuL]^+$.[18] 1 and 2 are both formed by the reaction of $RuLCl_3$ and $Na(O_2CCH_3)$. 3 is obtained from the reaction of the triply-hydroxy bridged complex $[LRu(\mu\text{-}OH)_3RuL]^{3+}$ and NaOH.

Recently Meyer[19] reported the preparation of related ruthenium complexes of the type $[(tpm)Ru(\mu\text{-}O)(\mu\text{-}L)_2Ru(tpm)]^{n+}$ where 1. $L = O_2P(O)(OH)$, $n = 1$; 2. $L = O_2CCH_3$, $n = 2$ and tpm is the tridentate; facial ligand tris(1-pyrazolyl)methane. These are prepared using an analogous method to Wieghardt i.e. by the reaction of $[(tpm)RuCl_3]\cdot 1.5H_2O$ in phosphate buffer with sodium carbonate and sodium acetate solutions respectively.

Another class of triply-bridged binuclear complexes are: $[(C_3N_2R_2)^{\dagger}{}_3Ru(\mu\text{-}X)_3Ru(C_3N_2R_2)_3]X$;[20] $X^- = Cl^-$, I^-; R = Me, Et. These are formed by the reaction of the monomeric $RuCl_2(C_3N_2R_2)_4$ complex in methylene chloride at 40°C for $X^- = Cl^-$ and in acetone at 40°C with NaI for $X^- = I^-$.

The reaction of 1,2 bis (isopropylseleno)ethane, $C_3H_7SeCH_2CH_2SeC_4H_7$ with ruthenium(III) halides gives complexes which have been formulated as triply-bridged complexes of the type hexahalo-tris-μ(1,2 bis(isopropylseleno)ethane)-diruthenium (III).[21]

A triply bridging $-Me_2Ge-$ structure has been proposed for the minor products of the pyrolysis of $(Me_3Ge)_2M(CO)_4$ where M = Ru, Os. The product is thought to be $(CO)_3M(\mu\text{-}GeMe_2)_3M(CO)_3$.[22] The $[(PMe_3)_3Ru(\mu\text{-}X)_3Ru(PMe_3)_3]^+$ complexes where $X^- = OH^-$,[23] H^-,[9] Cl^-[24] and CH_2^{2-}[8] have been characterised crystallographically. The triply-bridged hydroxy-, hydrido- and chloro-complexes are all formally ruthenium (II) species. The metal-metal distance in the case of the hydroxy-bridged species is 3.004Å. On changing the ligand to chloride the metal-metal distance increases by 0.14Å to 3.28Å. These distances are indicative of there being no or very little metal-metal interaction. The triply hydrido-bridged complex has a much smaller metal-metal distance of 2.540Å. It is clear that the overlap requirements of the three bridges will pull the two metal atoms closer together. Since the hydrido-bridging ligand can only be a two-electron donor as opposed to the four-electron donor Cl^- and OH^- bridging ligands, the possibility arises that the metal atoms might be linked by a triple Ru≡Ru bond. This would give a formal 18-electron configuration at each

† ($C_3N_2R_2$ = $\overline{CN(R)CH_2CH_2NR}$.)

metal atom and would account for the short Ru--Ru distance. The decreased M-M distance may also arise because H^- has a smaller ionic radius than Cl^- or OH^-.

The triply methylene-bridged complex, however, has two Ru(III) centres. The metal-metal distance is 2.540Å. The short metal-metal distance has been explained by a metal-metal bond. This suggestion is reinforced by the observed diamagnetism of the complex.

Halogen containing compounds tend to change progressively with increasing size. As in other groups there is a much greater change between the first row element, F, and the second row element, Cl, than between the other elements.

Spectroscopic studies on $[(NH_3)_3Ru(\mu\text{-}X)_3Ru(NH_3)_3]^{2+}$, $X^- = Cl^-$, Br^-, have shown the ruthenium centres to be strongly interacting.[25] In the case of the smaller bridging ligand, Cl^-, the interaction is stronger. Bands due to the $\sigma \rightarrow \sigma^*$ and $\delta^* \rightarrow \sigma^*$ transitions are observed at 17,000 cm^{-1} (strong) and 7150 cm^{-1} (weak) respectively, in the case of $X^- = Cl^-$ and 15,790 cm^{-1} (strong) and 6870 cm^{-1} (weak) respectively for $X^- = Br^-$.

Crystallographic studies of these complexes support the spectroscopic data. When $X^- = Cl^-$ the Ru--Ru distance is 2.753Å.[26] On changing Cl^- for Br^- the distance increases to 2.852Å.[27]

The range of complexes where M = Ru, $X^- = Cl^-$, Br^-, I^-, OH^-, SEt^-; L = PMe_2Ph have been studied electrochemically.[6] It has been discussed previously that the $[(PMe_2Ph)_3Ru(\mu\text{-}Cl)_3\text{-}Ru(PMe_2Ph)_3]^+$ complex undergoes two reversible one electron oxidations:

$$[(PMe_2Ph)_3Ru(\mu\text{-}Cl)_3Ru(PMe_2Ph)_3]^+ \underset{}{\overset{-e^-}{\rightleftharpoons}} [(PMe_2Ph)_3Ru(\mu\text{-}Cl)_3Ru(PMe_2Ph)_3]^{2+}$$

Ru(II)Ru(II) 'Ru(II)Ru(III)'

$$\overset{-e^-}{\rightleftharpoons} [(PMe_2Ph)_3Ru(\mu\text{-}Cl)_3Ru(PMe_2Ph_3)_3]^{3+}$$

Ru(III)Ru(III)

The other halogen containing compounds were found to have similar redox behaviour i.e. they show the expected two one-electron oxidations with ∿0.5V separation. The oxidations all occur at similar potentials versus the Ag/AgCl reference regardless of the bridging halide. The I^- containing complex is oxidised at slightly less positive potentials compared to the Cl^- and Br^- complexes and the second oxidation is irreversible. The triply hydroxy-bridged species also shows two one-electron oxidations, the second being irreversible. The oxidation potentials are approximately 0.4V less positive than the equivalent halogen containing species. Presumably this difference is in part due to the hydroxy ligand being a better π-donor than the halogens. The μ-SEt complex only undergoes one oxidation at +0.67V (versus Ag/AgCl). This is reversible only at low temperatures (T = 233K).

The colour of each complex is dependent on the bridging ligand. When $X^- = OH^-$ the complex is pale yellow; $X^- = Br^-$, orange-yellow and $X^- = I^-$, orange.

We have shown in the previous chapters that complexes of the type $[L_3M(\mu\text{-}Cl)_3ML_3]^{2+}$ where M = Ru, Os; L = PMe_2Ph have a strong metal-metal interaction. The aim of this study is to vary the bridging ligands to determine the effect this has on the metal-metal interactions.

Crystallographic studies of $[(PMe_2Ph)_3Ru(\mu\text{-}X)_3Ru(PMe_2Ph)_3]^+$ where X^- = Cl^-,[28] OH^-,[6] in which there is probably no metal-metal interaction present, have been carried out. These show that for the larger Cl^- ligand the Ru--Ru distance is 3.39Å, 0.31Å greater than in the case of the smaller OH^- ligand, c.f. the data for the related complexes where L = PMe_3 discussed previously.

The decreasing Ru--Ru distance on going from bridging Cl^- to OH^- is believed to reflect the differing ruthenium to bridging ligand distances and angles rather than an increased metal-metal interaction. No data are available for binuclear osmium complexes.

3.2 RESULTS AND DISCUSSION

3.2.1 M = Ruthenium

The complexes where L = PMe_2Ph; X^- = OH^-, I^-; n = 1 were made according to the method of Ashworth,[6] where L = PMe_2Ph, X^- = Cl^-, n = 1 using the method of Chatt[1] and where L = PMe_2Ph; X^- = Br^-; n = 1 by the method of Stephenson.[5]

The electrochemical and spectroelectrochemical results are shown in Table 3.2.1. A crystallographic study of the species where X^- = I^-, L = PMe_2Ph, n = 1 was undertaken to determine the differences in this structure from that where X^- = Cl^-.

Electrochemical studies were carried out in methylene chloride/0.5M $TBABF_4$ when X^- = Cl^- and acetone/0.1M $TBABF_4$ when X^- = OH^-, Br^-, I^-, to avoid halogen exchange, using Pt working and counter electrodes and an Ag/AgCl reference electrode (as described previously).

Table 3.2.1: Electrochemical and Spectroelectrochemical Results for $[(PMe_2Ph)_3Ru(\mu\text{-}X)_3Ru(PMe_2Ph)_3]^+$

X^-	$E_{1/2}$ (V versus Ag/AgCl)[a]		ν_{max} (cm^{-1})	ε ($mol^{-1}cm^{-1}dm^3$)
	II,II/II,III	II,III/III,III	II,III	
OH^-[b]	0.86(0.060)[e]	1.37[d]	8,640	5,625
Cl^-[c]	1.23(0.07)	1.75(0.100)	5,000	2,613
			7,770	2,864
Br^-[b]	1.24(0.060)	1.75(0.070)	5,000	1,917
			7,330	1,534
I^-[b]	1.21(0.060)	1.82[d]	4,850	2,511
			7,000	1,076

a. Ferrocene/Ferrocinium at +0.56V

b. In acetone/0.1M $TBABF_4$ at T = 290K (for electrochemistry) and T = 243K (for spectroelectrochemistry)

c. In Methylene Chloride at T = 290K (for electrochemistry) and T = 243K (for spectroelectrochemistry)

d. Irreversible even at low temperatures (T = 243K)

e. $E_p^F - E_p^R$ (where E_p^F and E_p^R are potentials at the maximum of the forward and reverse scans respectively) are shown in brackets in V.

Spectroelectrochemical studies were carried out by generating the $[(PMe_2Ph)_3Ru(\mu\text{-}X)_3Ru(PMe_2Ph)_3]^{2+}$ mixed-valence species <u>in situ</u> at a suitable electrogeneration potential using the O.T.T.L.E. cell (usually 0.2V beyond the redox process) as described previously. The temperature was maintained at 243K for each experiment. Only the near infra-red region will be discussed.

The electrochemical results have been discussed in Section 3.1. The spectroelectrochemical results will now be discussed.

(a) <u>Spectroelectrochemistry</u>

The complexes where X^- = Cl^-, Br^-, I^- all showed two bands in the near infra-red region of the electronic spectrum. When X^- = OH^- one broad asymmetric band is observed. The near infra-red bands occur due to the $a_1' \rightarrow a_2''$ and $e'' \rightarrow a_2''$ transitions discussed previously. The ultimate spectra of the $[(PMe_2Ph)_3Ru(\mu\text{-}X)_3Ru(PMe_2Ph)_3]^{2+}$ species where X^- = OH^-, Cl^-, Br^- and I^- are shown in Figures 3.2.1 - 3.2.4. The positions of the bands, ν_{max}, were found to be independent of the solvent used and the band halfwidth, $\Delta_{\frac{1}{2}}$, was found to be independent of the temperature and is less than 5000 cm^{-1}.

This indicates that all species have strongly interacting metal centres. The extent of the interaction varies as monitored by the near infra-red absorption spectrum. The positions of the near infra-red bands move to lower energy as the size of the bridging ligand increases which we would argue is reflecting a decreasing metal-metal interaction.

In the case where X^- = Cl^-, the highest energy band is the most intense, however when X^- = Br^-, I^-, it is the lowest

Figure 3.2.1: VIS/NIR Absorption Spectrum of $[(PMe_2Ph)_3Ru(\mu\text{-}OH)_3Ru(PMe_2Ph)_3]^{2+}$ in Acetone / 0.1M $TBABF_4$

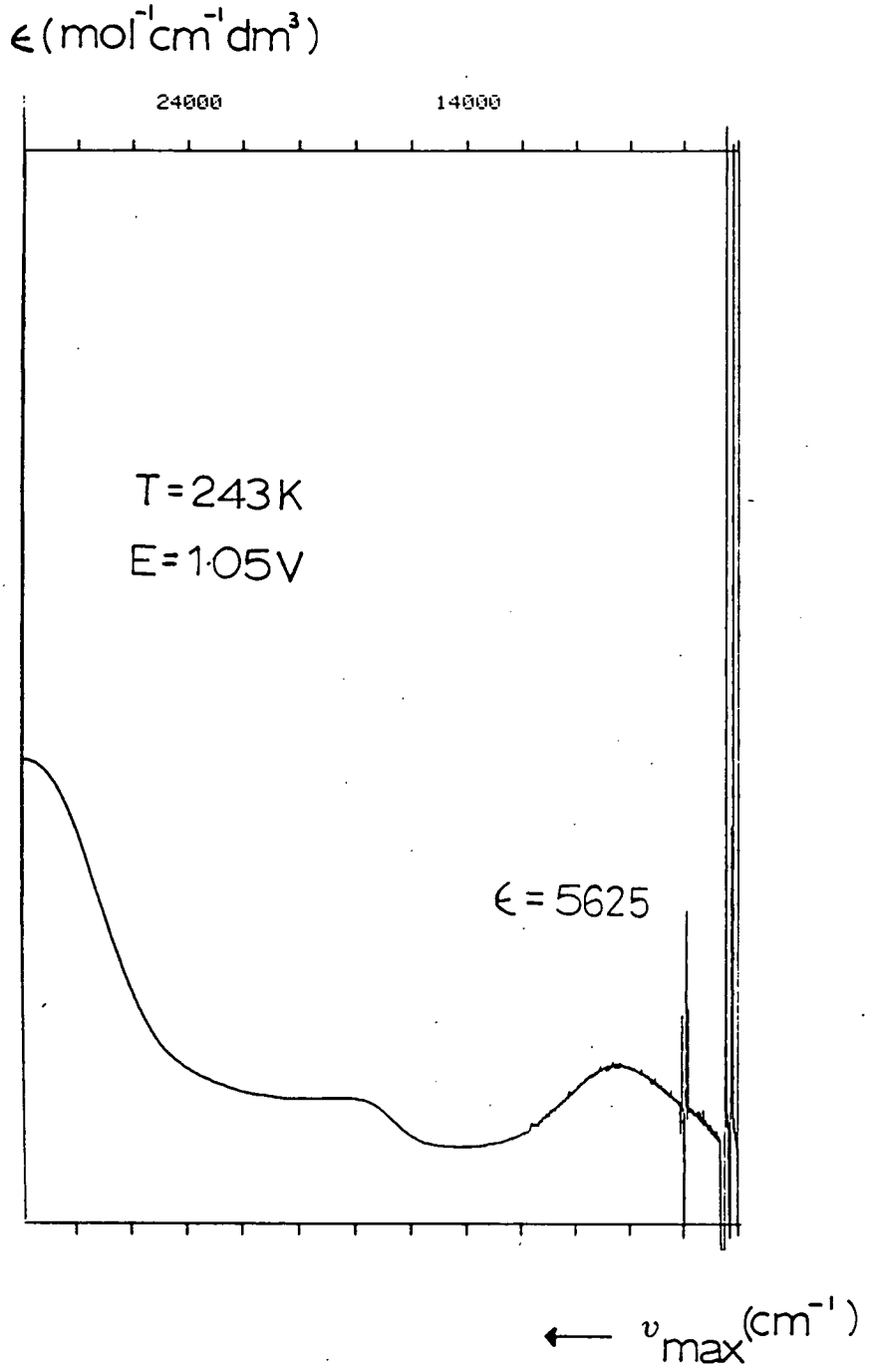

Figure 3.2.2: VIS/NIR Absorption Spectrum of $[(PMe_2Ph)_3Ru(\mu\text{-}Cl)_3Ru(PMe_2Ph)_3]^{2+}$ in Methylene Chloride / 0.5M $TBABF_4$ at T = 243K

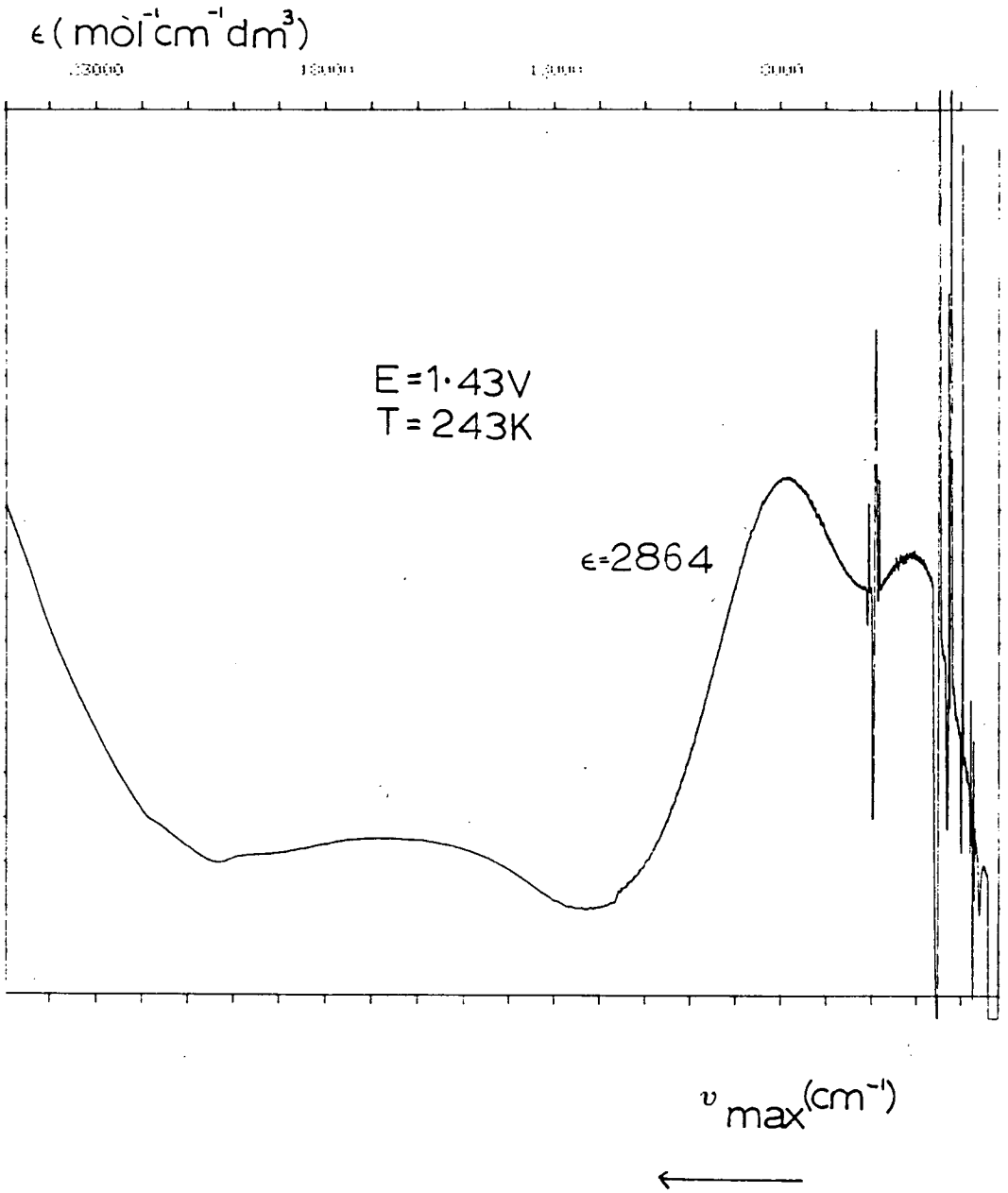

Figure 3.2.3: VIS/NIR Absorption Spectrum of $[(PMe_2Ph)_3Ru(\mu\text{-}Br)_3Ru(PMe_2Ph)_3]^{2+}$ in Acetone / 0.1M $TBABF_4$

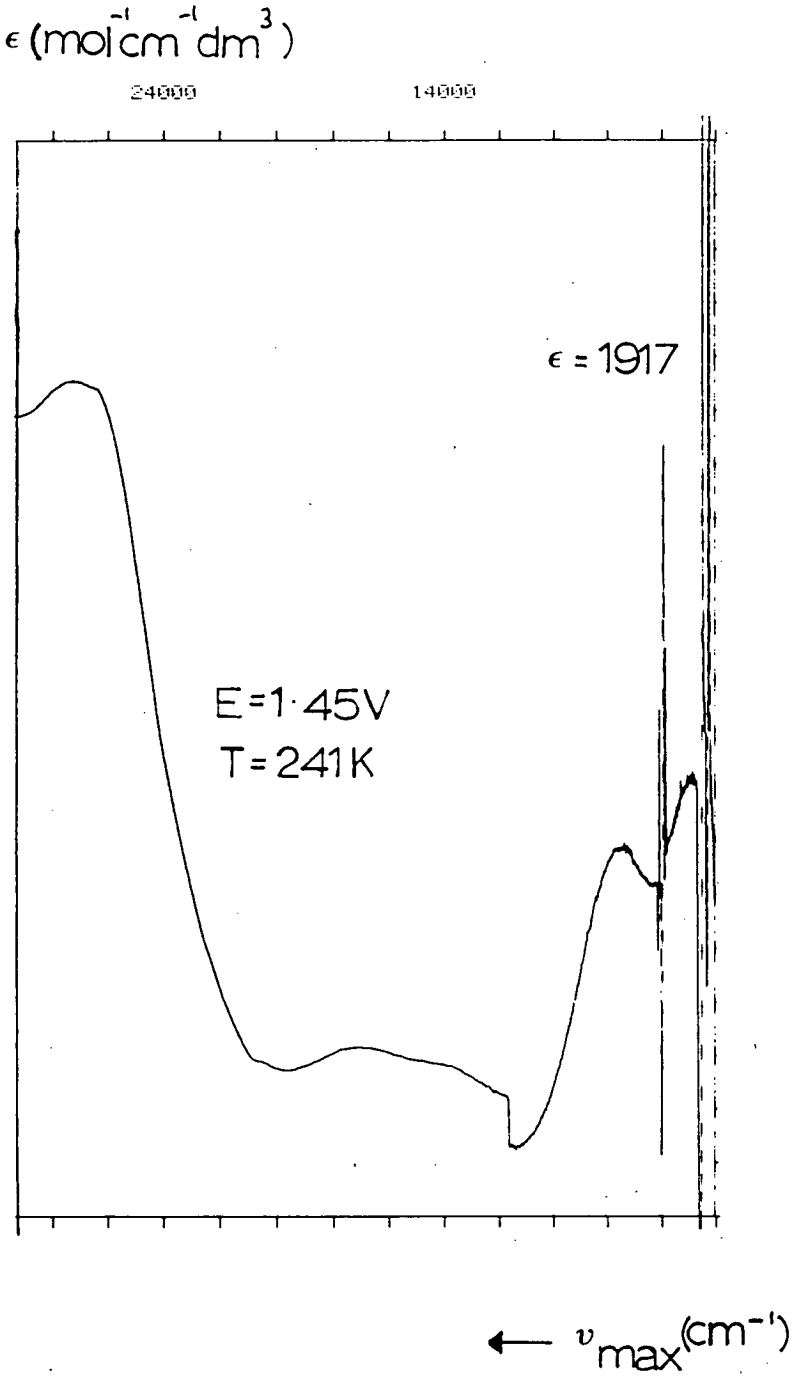

Figure 3.2.4: VIS/NIR Absorption Spectrum of $[(PMe_2Ph)_3Ru(\mu\text{-}I)_3Ru(PMe_2Ph)_3]^{2+}$ in Acetone / 0.1M $TBABF_4$

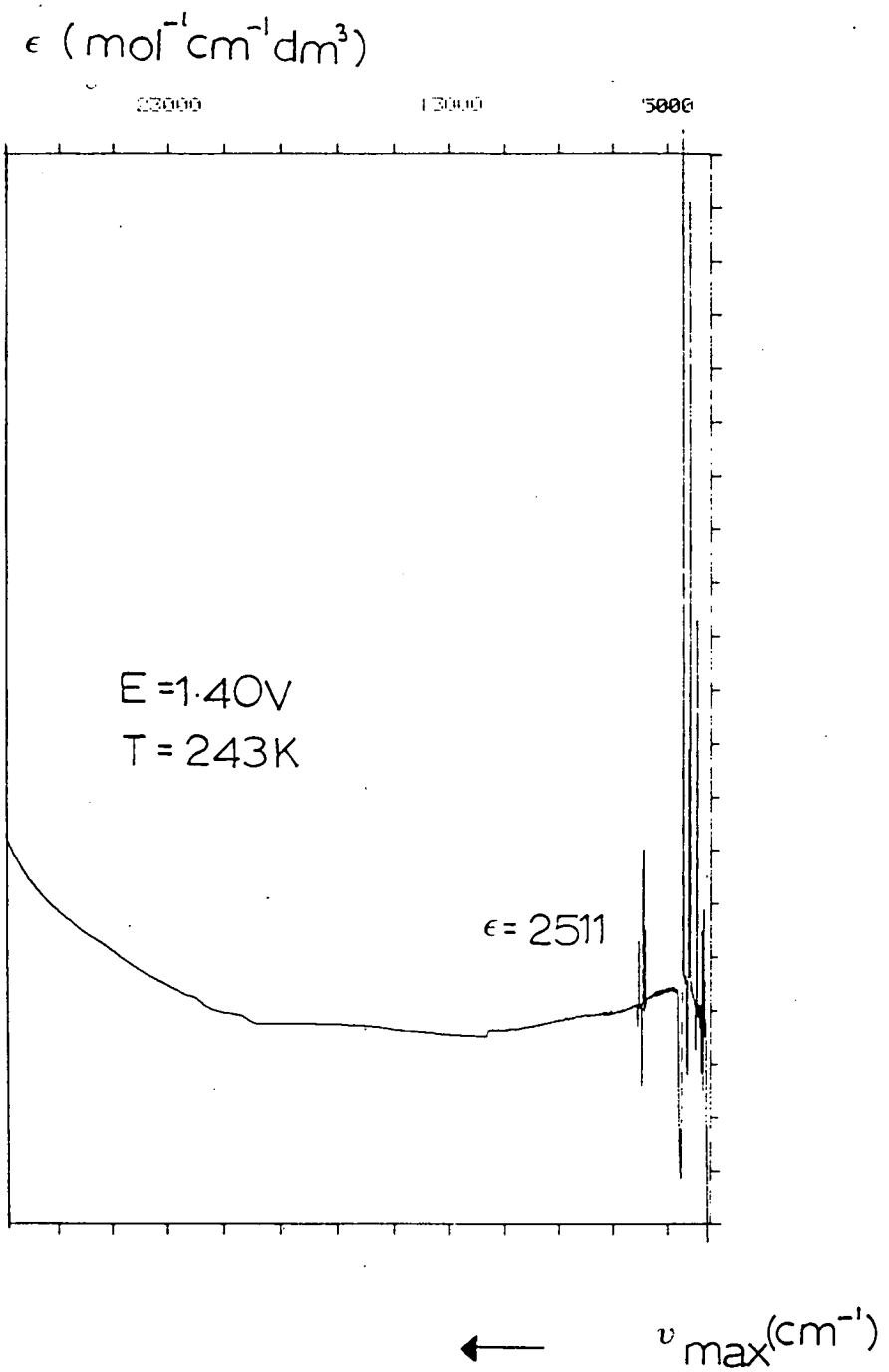

energy band that is the most intense. This band is assigned to the $a_1' \rightarrow a_2''$ transition (see Chapter 1). This implies that as the metal-metal interaction decreases the a_1' orbital is destabilsied compared to the e" orbital. This effect was also observed when the nature of the terminal tertiary P(III) ligand was varied and is discussed in more detail in Chapter 4. This was not however observed in the related $[(NH_3)_3Ru(\mu\text{-}X)_3Ru(NH_3)_3]^{2+}$ [25] complexes where X^- = Cl^-, Br^-. These complexes both have the most intense band at higher energy. This is discussed further in Chapter 4.

(b) Single Crystal X-ray Structure of $[(PMe_2Ph)_3Ru(\mu\text{-}I)_3Ru(PMe_2Ph)_3]PF_6$

Details of the structure solution are given in the experimental section.

The only solvent system which gave single crystals suitable for an X-ray crystallographic study of this species was a methanol/methylene chloride mixture. This unfortunately caused exchange of I^- by Cl^- from HCl present in the methylene chloride thus leading to the formation of $[(PMe_2Ph)_3Ru(\mu\text{-}Cl)_3\text{-}Ru(PMe_2Ph)_3]^+$ and HI. The crystals did not contain any mixed bridged species, that is $\mu\text{-}Cl_2I$ or $\mu\text{-}ClI_2$, as shown by FAB mass spectroscopy data which showed only parent ion peaks for the $\mu\text{-}Cl_3$ and $\mu\text{-}I_3$ species (at 1136 and 1411 amu respectively).

The crystal used for data collection thus contained a mixture of the two species and led to problems with the solution. Refinement showed that there was a 3:1 mixture of μ-Cl to μ-I in the crystal. The e.s.d.'s on each I atom

and each Cl atom were low confirming that there are no mixed bridged species present.

A view of the $[(PMe_2Ph)_3Ru(\mu\text{-}I)_3Ru(PMe_2Ph)_3]^+$ cation is shown in Figure 3.2.5 (without H atoms). Table 3.2.2 gives a selection of bond lengths and angles.

The Ru--Ru distance is 3.499(1)Å. This is 0.109Å longer than in the analogous $\mu\text{-}Cl_3$ species.[28] The average Ru-$\hat{I}$-Ru angle is 82° which is smaller than in the case of the $\mu\text{-}Cl_3$ species (Ru-$\hat{Cl}$-Ru = 86°). The Ru-$\hat{Cl}$-Ru angle in the $[(PMe_2Ph)_3Ru(\mu\text{-}Cl)_3Ru(PMe_2Ph)_3]^+$ cation present in the crystal is 87° which compares with that in the crystal structure of the pure $\mu\text{-}Cl_3$ complex. For $X^- = OH^-$, the average Ru-$\hat{O}$-Ru angle is 90°. It appears that as the size of the bridging ligand increases the Ru-$\hat{X}$-Ru angle decreases.

A similar effect is observed in the related $[(NH_3)_3Ru(\mu\text{-}X)_3Ru(NH_3)_3]^{2+}$ complexes where $X^- = Cl^-$, Br^-. When $X^- = Cl^-$, the average Ru-$\hat{X}$-Ru angle is 70.2°; whereas when $X^- = Cl^-$, the angle is 68.5°.[26,27]

The average Ru-I distance is 2.68Å, and the average Ru-Cl distance is 2.54Å, slightly longer than in the crystal structure of the pure complex.

(c) Conclusions

As the size of the bridging ligand increases the metal-metal interaction decreases. However, in Robin and Day's[29] classification the interaction must always be regarded as strong.

The crystal structure of $[(PMe_2Ph)_3Ru(\mu\text{-}I)_3Ru(PMe_2PH)_3]^+$ shows the expected larger metal-metal distance than when

Figure 3.2.5: View of the $[(PMe_2Ph)_3Ru(\mu\text{-}I)_3Ru(PMe_2Ph)_3]^+$ Cation

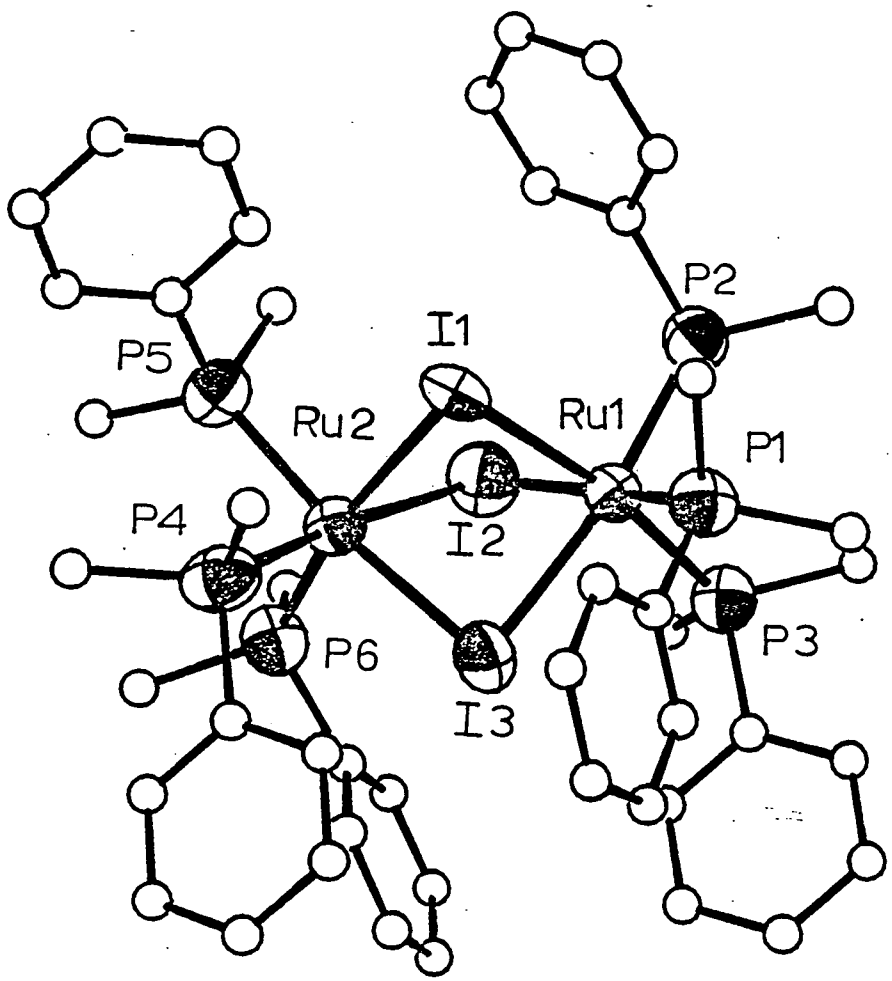

Table 3.2.2: Selected Bond Lengths and Angles for

$[(PMe_2Ph)_3Ru(\mu\text{-}I)_3Ru(PMe_2Ph)_3]^+$

Bond Lengths(A) with standard deviations

Ru(1) - I(1)	2.591(10)	P(1) -C(111)	1.827(8)
Ru(1) - I(2)	2.599(9)	P(1) -C(121)	1.802(14)
Ru(1) - I(3)	2.736(7)	P(1) -C(131)	1.831(14)
Ru(1) -Cl(1)	2.604(9)	P(2) -C(211)	1.845(8)
Ru(1) -Cl(2)	2.562(10)	P(2) -C(221)	1.796(15)
Ru(1) -Cl(3)	2.545(9)	P(2) -C(231)	1.829(15)
Ru(1) - P(1)	2.319(4)	P(3) -C(311)	1.843(8)
Ru(1) - P(2)	2.297(4)	P(3) -C(321)	1.816(16)
Ru(1) - P(3)	2.291(4)	P(3) -C(331)	1.810(15)
Ru(2) - I(1)	2.668(10)	P(4) -C(411)	1.845(8)
Ru(2) - I(2)	2.738(9)	P(4) -C(421)	1.815(13)
Ru(2) - I(3)	2.740(7)	P(4) -C(431)	1.848(14)
Ru(2) -Cl(1)	2.562(9)	P(5) -C(511)	1.844(8)
Ru(2) -Cl(2)	2.483(10)	P(5) -C(521)	1.818(14)
Ru(2) -Cl(3)	2.504(9)	P(5) -C(531)	1.817(16)
Ru(2) - P(4)	2.297(4)	P(6) -C(611)	1.842(8)
Ru(2) - P(5)	2.308(4)	P(6) -C(621)	1.818(14)
Ru(2) - P(6)	2.279(4)	P(6) -C(631)	1.821(14)

Angles(degrees) with standard deviations

Ru(1) - I(1) -Ru(2)	83.4(3)
Ru(1) - I(2) -Ru(2)	81.86(25)
Ru(1) - I(3) -Ru(2)	79.41(18)
Ru(1) -Cl(1) -Ru(2)	85.2(3)
Ru(1) -Cl(2) -Ru(2)	87.8(3)
Ru(1) -Cl(3) -Ru(2)	87.7(3)
P(1) -Ru(1) - P(2)	94.21(13)
P(1) -Ru(1) - P(3)	92.81(13)
P(2) -Ru(1) - P(3)	97.84(13)
P(4) -Ru(2) - P(5)	94.49(13)
P(4) -Ru(2) - P(6)	94.37(13)
P(5) -Ru(2) - P(6)	97.70(12)

X^- = Cl^-. The metal-metal distances increase as the size of the bridging ligand increases but the average M-$\hat{X}$-M angle decreases.

3.2.2 M = Osmium

The complexes where L = PMe_2Ph; X^- = Cl^-, Br^-; n = 1 were made according to the method of Coombe and Stephenson.[25(b)] When L = PMe_2Ph, X^- = I^-; n = 1; a variation of this method was used.

Electrochemical and spectroelectrochemical studies were carried out as in Section 3.2.1. In this case the $[(PMe_2Ph)_3Os(\mu\text{-}X)_3Os(PMe_2Ph)_3]^{3+}$ species could be observed by spectroelectrochemical methods. The oxidation state was not available for study in the case of the ruthenium containing complexes. This enabled the extended study of the dependence of metal-metal interactions on both the nature of the bridging ligand and the overall oxidation state of the complex. The results are shown in Table 3.2.3.

(a) Electrochemistry

All species have similar electrochemical behaviour. All show two reversible one-electron oxidations. The complex where X^- = I^- is oxidised at slightly less positive potentials than when X^- = Cl^-, Br^-. This behaviour is analogous to that observed for the ruthenium compounds.

(b) Spectroelectrochemistry

When X^- = Cl^-, Br^-; n = 2 two near infra-red bands are observed in the electronic spectrum. As in the case of the ruthenium complexes the band halfwidth, $\Delta_{\frac{1}{2}}$, was found to be

Table 3.2.3: Electrochemical and Spectroelectrochemical Results for $[(PMe_2Ph)_3Os(\mu\text{-}X)_3Os(PMe_2Ph)_3]^+$

X	$E_{1/2}$ (V versus Ag/AgCl)[a]		ν_{max} (cm^{-1})		ε ($mol^{-1}cm^{-1}dm^3$)	
	II,II/II,III	II,III/III,III	II,III	III,III	II,III	III,III
Cl^{-}[b]	+1.05(0.060)[d]	+1.57(0.080)	5000	11480	4875	7220
			9200	15000	650	2116
Br^{-}[c]	+1.06(0.060)	+1.56(0.080)	4870	10730	4252	6888
			8350	14501	425	1871
I^{-}[c]	+0.99(0.060)	+1.44(0.080)	4970	9640	2416	2348
			7840	11400	470	1510
			11000	17400	403	839

a. Ferrocene/Ferrocinium at +0.56V

b. In Methylene Chloride/0.5M $TBABF_4$ at T = 290K (for electrochemistry) and T = 243K (for spectroelectrochemistry)

c. In Acetone/0.1M TBABF at T = 290K (for electrochemistry) and T = 243K (for spectroelectrochemistry)

d. $E_p^F - E_p^R$ values are shown in brackets

independent of temperature and the peak position, ν_{max}, is independent of the solvent used. Both of these factors indicate a strong metal-metal interaction in $[(PMe_2Ph)_3Os(\mu\text{-}X)_3Os(PMe_2Ph)_3]^{2+}$. In the case of X^- = I^- three bands are observed in the near infra-red region of the electronic spectrum. This is presumed to be due to a spin orbit coupling effect which has been discussed in Chapter 1, section 1.1. Figures 3.2.6 - 3.2.8 show the spectrum observed for X^- = Cl^-, Br^- and I^- respectively.

The most intense band observed in the near infra-red region is always the low energy band. On changing the bridging ligand the energy of the intense band does not change significantly. The energy of the weaker band does however decrease as the size of the bridging ligand increases. The extinction coefficients of all the bands decrease as the size of the bridging ligand increases. Both of these observations indicate a decrease in metal-metal interaction as X^- increases in size.

Spectroelectrochemical monitoring of the n = 3 oxidation state, $[(PMe_2Ph)_3Os(\mu\text{-}X)_3Os(PMe_2Ph)_3]^{3+}$, shows the near infra-red bands moving to higher energy for X^- = Cl^-, Br^-, I^- indicating an increase in metal-metal interaction as a further electron is removed from the complexes. Figures 3.2.9 - 3.2.11 show the observed spectra for X^- = Cl^-, Br^-, I^- respectively. Thus we are suggesting that as the complexes are oxidised to the n = 3 oxidation state so the metal centres move closer together. To date we have been unsuccessful in growing crystals of $[L_3Os(\mu\text{-}X)_3OsL_3]^{3+}$, where L = tertiary phosphine ligand, suitable for an X-ray crystallographic study.

Figure 3.2.6: VIS/NIR Absorption Spectrum of
$[(PMe_2Ph)_3Os(\mu\text{-}Cl)_3Os(PMe_2Ph)_3]^{2+}$
in Methylene Chloride / 0.5M $TBABF_4$
at T = 243K

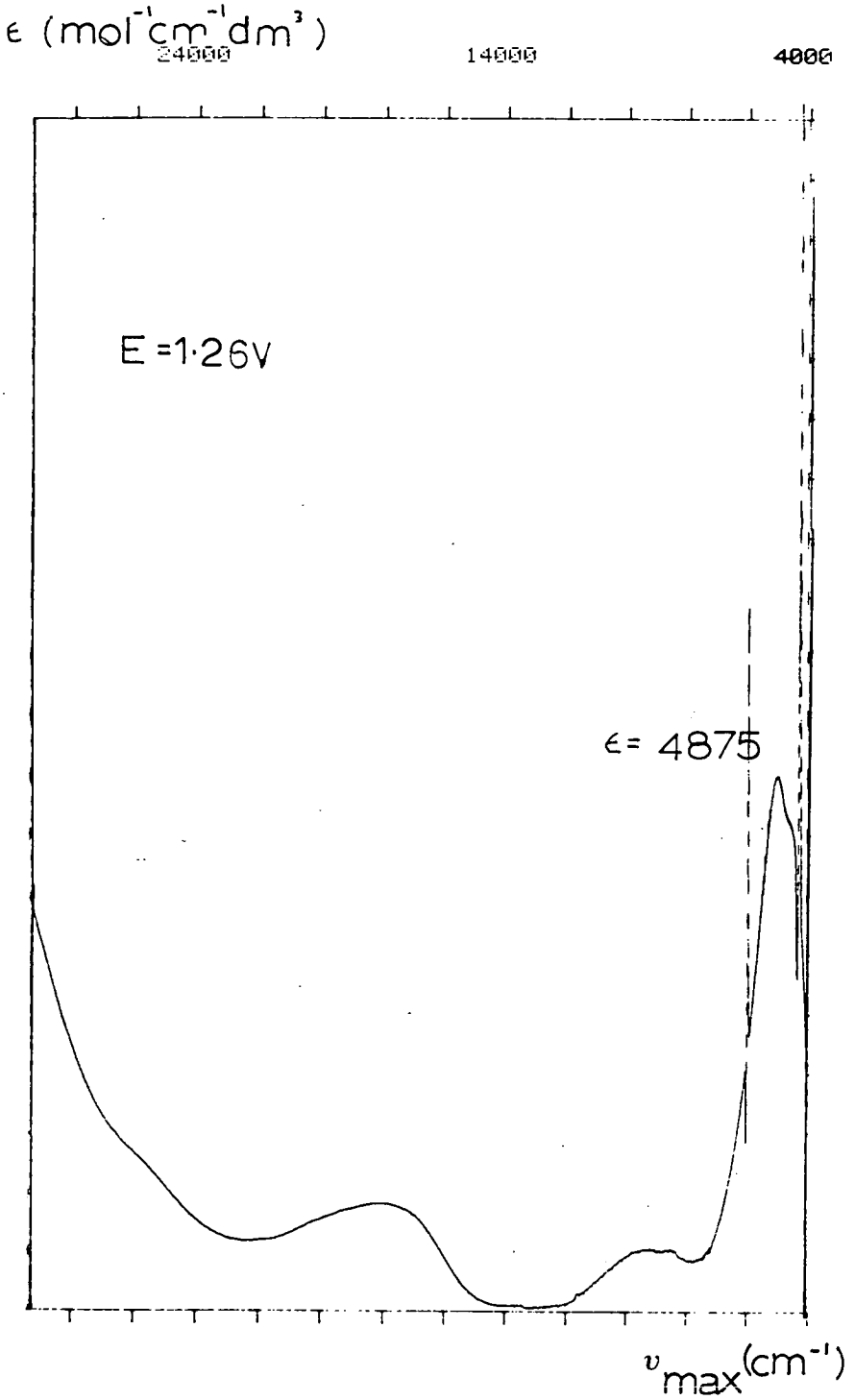

Figure 3.2.7: VIS/NIR Absorption Spectrum of
$[(PMe_2Ph)_3Os(\mu\text{-}Br)_3Os(PMe_2Ph)_3]^{2+}$
in acetone / 0.1M $TBABF_4$ at T = 243K

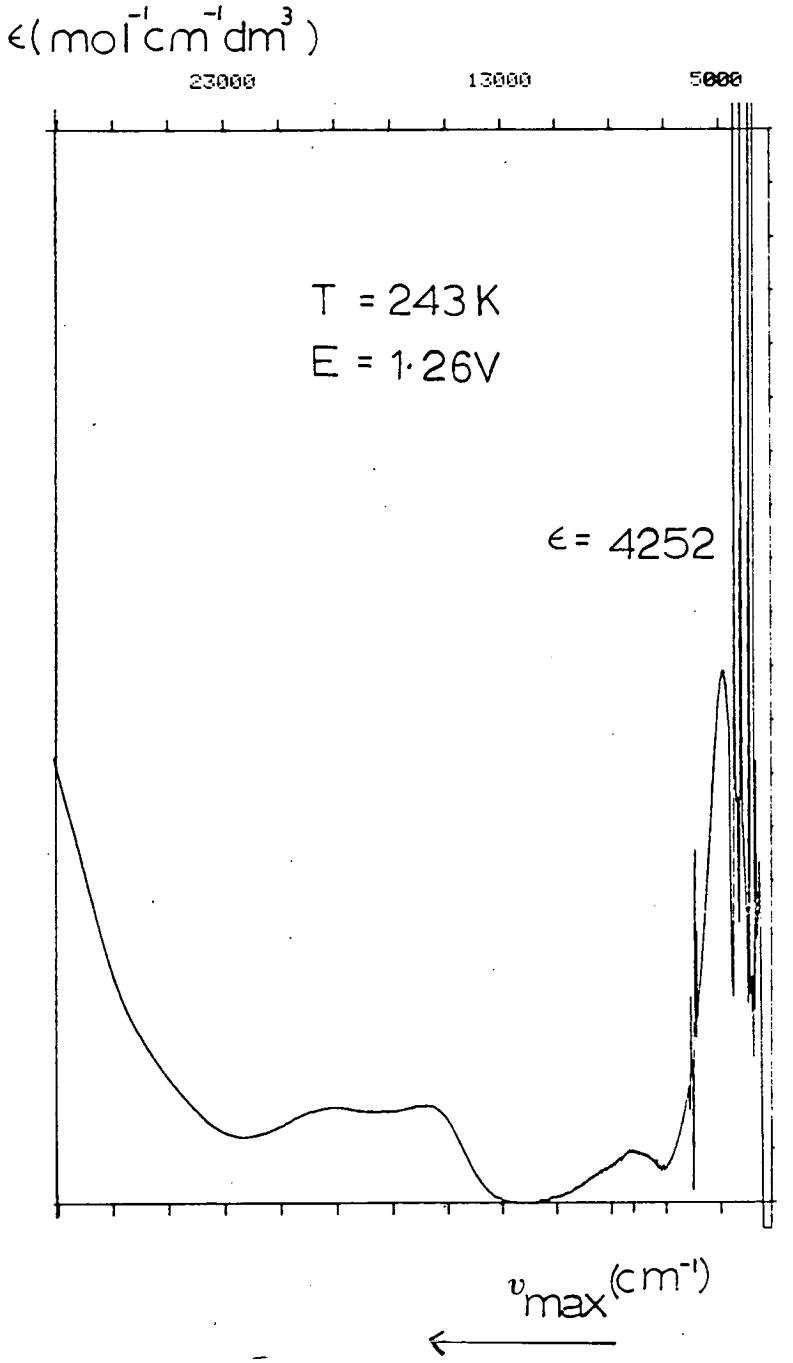

Figure 3.2.8: VIS/NIR Absorption Spectrum of $[(PMe_2Ph)_3Os(\mu\text{-}I)_3Os(PMe_2Ph)_3]^{2+}$ in Acetone / 0.1M $TBABF_4$

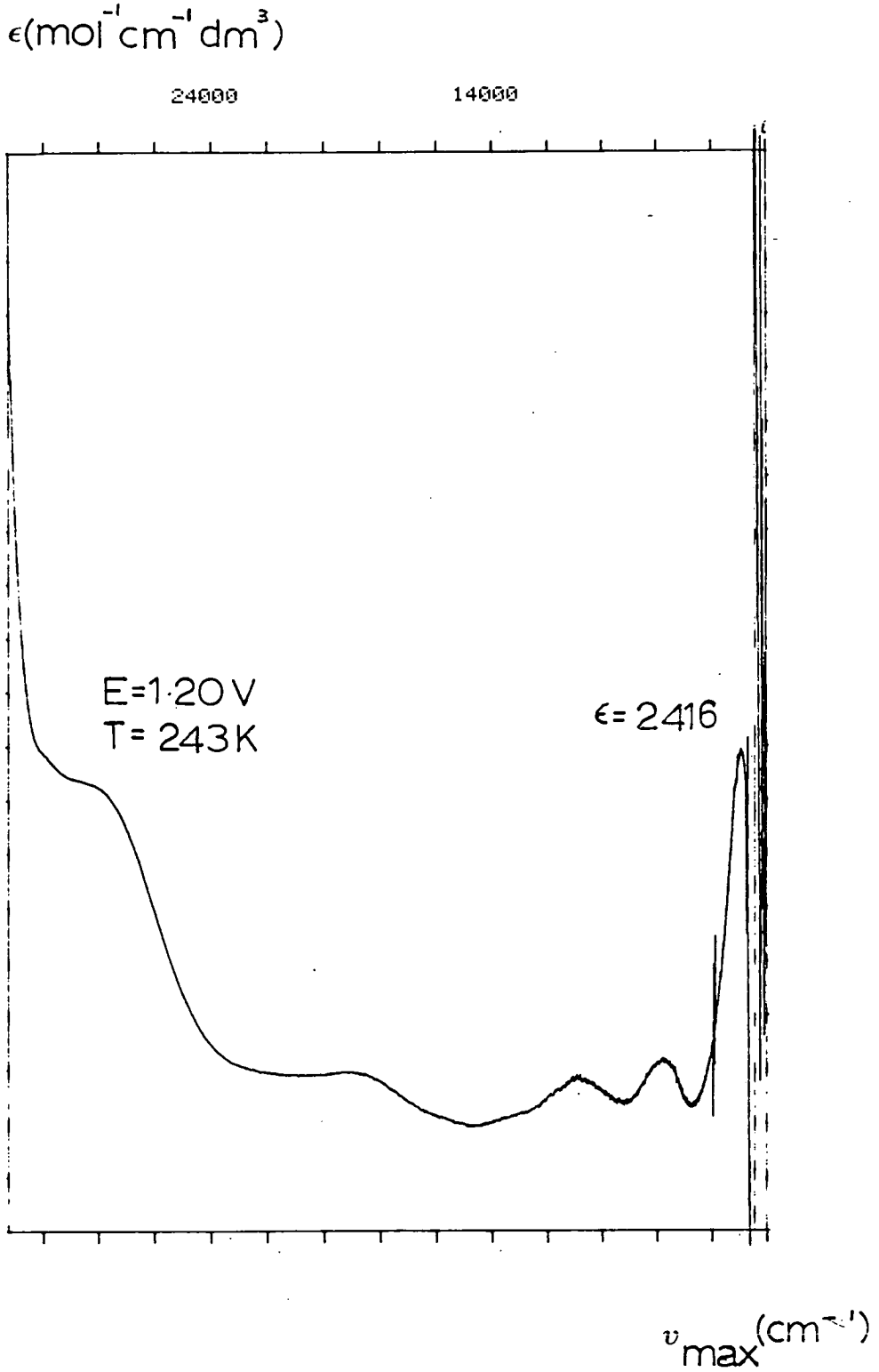

Figure 3.2.9: UV/VIS/NIR Absorption spectrum of $[(PMe_2Ph)_3Os(\mu\text{-}Cl)_3Os(PMe_2Ph)_3]^{3+}$ in Methylene Chloride at T = 243K

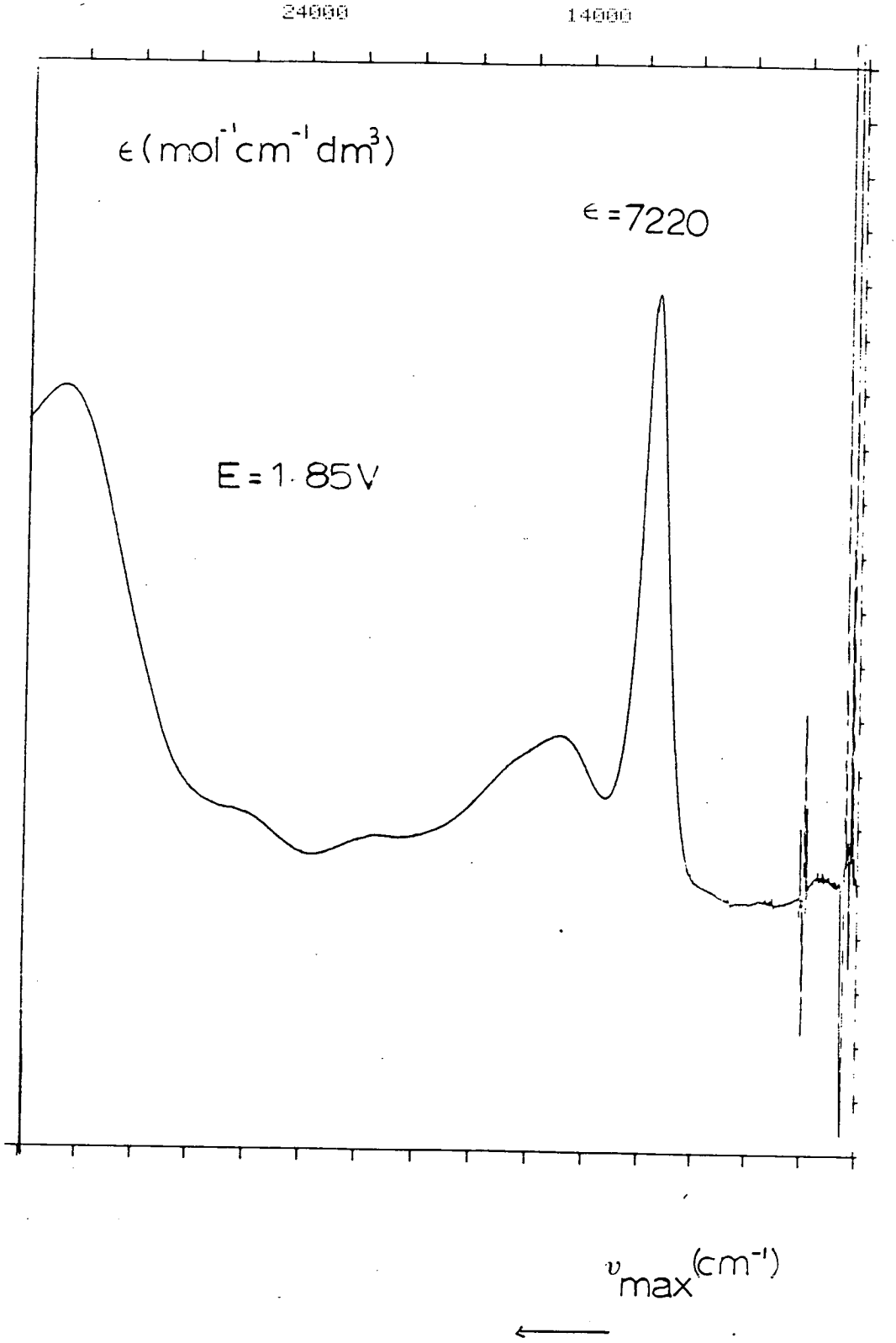

Figure 3.2.10: VIS/NIR Absorption Spectrum of $[(PMe_2Ph)_3Os(\mu\text{-}Br)_3Os(PMe_2Ph)_3]^{3+}$ in Acetone / 0.1M $TBABF_4$ at T = 240K

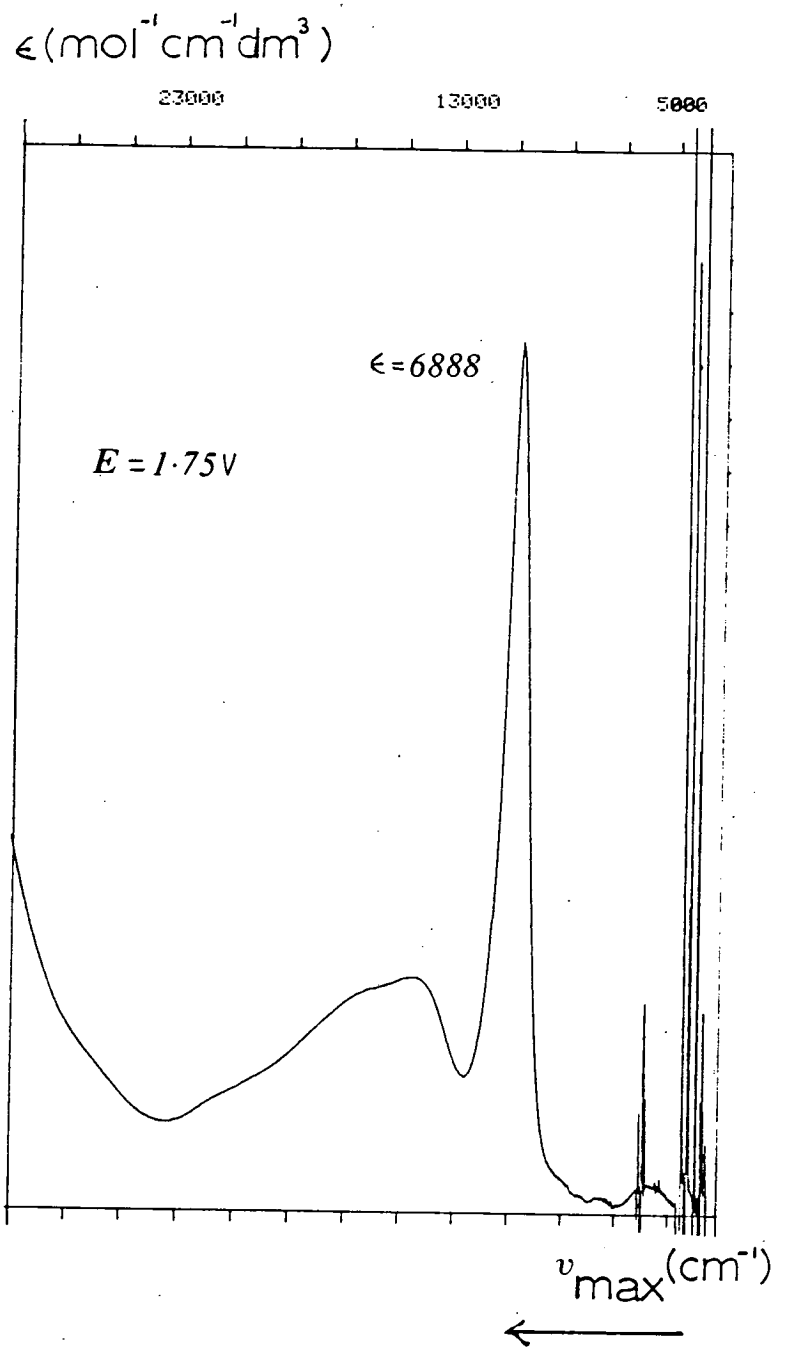

Figure 3.2.11: VIS/NIR Absorption Spectrum of $[(PMe_2Ph)_3Os(\mu\text{-}I)_3Os(PMe_2Ph)_3]^{3+}$ in Acetone / 0.1M $TBABF_4$

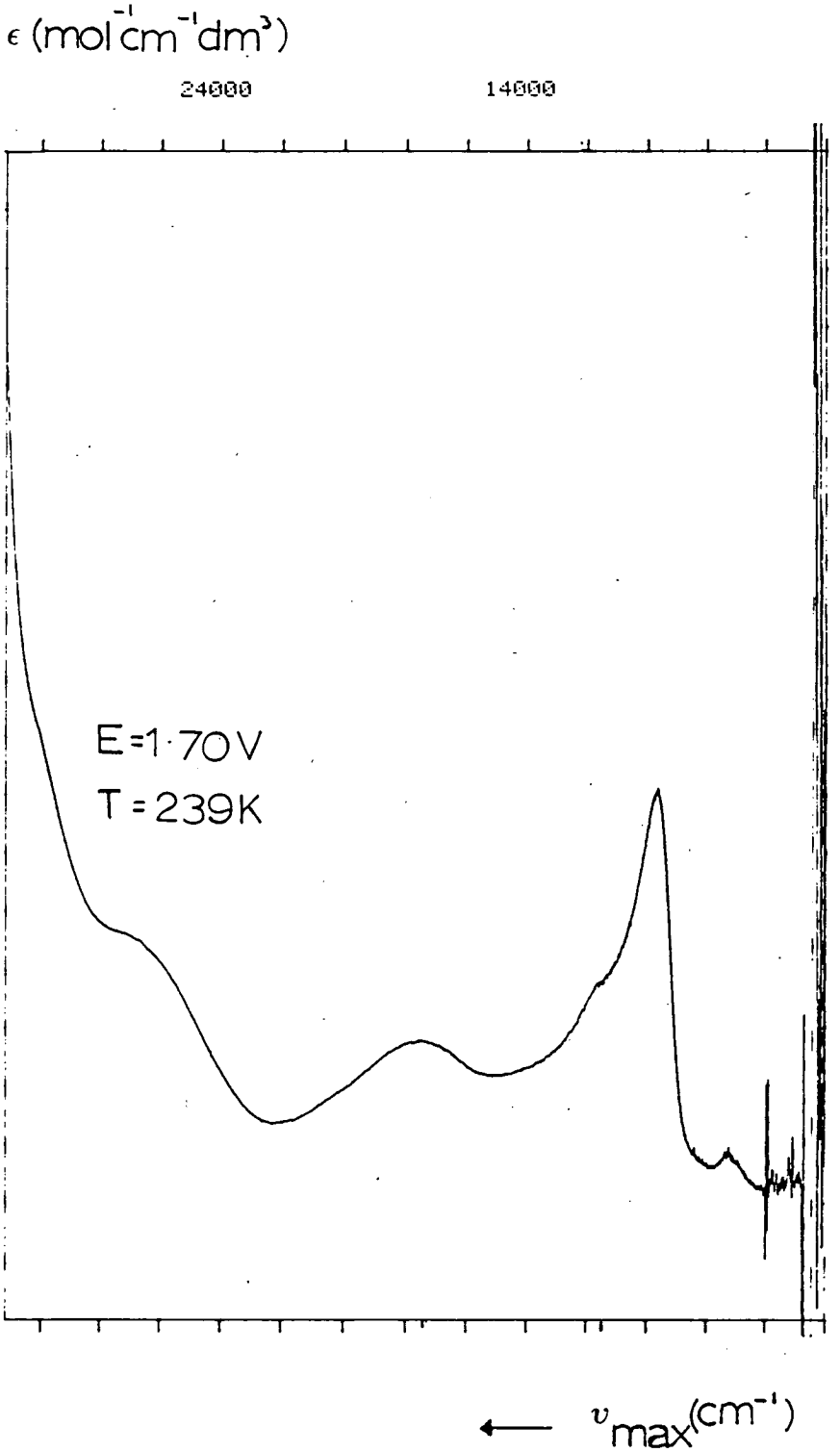

The electronic absorption spectrum shows more extreme differences in the n = 3 oxidation state as the bridging ligand is changed than in the n = 2 state. All near infra-red bands decrease in energy as X increases in size. This is probably due to the fact that the metal centres are closer together than in the n = 2 oxidation state. Again the extinction coefficient of the near infra-red bands decrease as the size of X increases.

In the ruthenium complexes the most intense band observed was not always the low energy one; as X decreased in size the high energy band became more intense until at $X^- = Cl^-$ the most intense band is that at high energy. This effect is not observed in the case of osmium complexes. This observation will be discussed more fully in Chapter 4.

(c) Conclusions

We conclude for the diosmium species that increasing the size of the bridging ligand decreases the extent of metal-metal interaction which is in agreement with the ruthenium complexes. This effect is more apparent in the oxidation state n = 3 than n = 2.

3.3 EXPERIMENTAL

Electrochemical studies were performed using a PAR model 170 potentiostat and programmer as described previously. Temperature control was achieved as previously described.

Spectroelectrochemical studies were carried out as described previously using the O.T.T.L.E. cell. The temperature was controlled as described previously. The Perkin-Elmer

Lambda 9 Spectrophotometer was employed for these studies. Spectra were recorded over the range 3,125-50,000 cm^{-1}. Elemental analyses were performed by the Chemistry Department, University of Edinburgh. FAB mass spectra were recorded by the Chemistry Department, University of Edinburgh, using the Kratos-50TC Spectrometer, using 3-nitrobenzylalcohol (3-NOBA) as the matrix.

Materials

Methylene chloride was purified as described previously. All other solvents were used as supplied without further purification.

$RuCl_3 \cdot 3H_2O$, K_2OsCl_6 and OsO_4 were obtained from Johnson Matthey.

$TBABF_4$ was prepared as previously described. PMe_2Ph[30] was prepared according to the literature method.

$[(PMe_2Ph)_3M(\mu\text{-}X)_3M(PMe_2Ph)_3]PF_6$ where M = Ru, X^- = OH^-, Cl^-, Br^-, I [1,6]; M = Os, X^- = Cl^-, Br^- [5] were prepared according to literature methods.[5]

1. Preparation of Tri-μ-iodohexakis (dimethylphenylphosphine) diosmium (II,II) hexafluorophosphate

$OsI_3(PMe_2Ph)_3$ (0.1g) (see 2. for preparation of this complex) and PMe_2Ph (0.0625 ml) were stirred together for a short while in degassed 2-methoxyethanol under N_2. The colour remained dark green/blue. The mixture was warmed to 50°C. After 30 minutes the solution was yellow in colour. The solution was maintained at this level of heating for a further hour. No further change

in colour occurred. It was expected that the yellow solution contained the $OsI_2(PMe_2Ph)_4$ complex on the basis of the known reaction of $OsCl_3(PMe_2Ph)_3$ and PMe_2Ph in 2-methoxyethanol giving $OsCl_2(PMe_2Ph)_4$. Following this method, the volume of the solution was reduced and acetone was added. No solid however formed. The solution was left overnight with no formation of solid. The volume of the solution was reduced to dryness and diethylether was added. A yellow solid then formed. A FAB mass spectrum suggested that this complex was the desired triple iodo-bridged complex.

The counterion was exchanged for PF_6^- by dissolving the compound in acetone and adding methanol/excess NH_4PF_6 to this. Slow evaporation yielded yellow/orange crystals. These were washed with water, methanol and diethylether and dried in vacuo (0.052g, 59% yield).

Elemental Analysis Found C: 33.51%, H: 4.02%, N: 0%

Calculated for $[C_{48}H_{66}I_3Os_2P_6]PF_6$

C: 33.22%, H: 3.81%, N: 0%

FAB mass spectrum Found M^+ = 1591 (100%)

1450 (5%)

1315 (15%)

Calculated for $[(PMe_2Ph)_3Os(\mu\text{-}I)_3Os(PMe_2Ph)_3]^+$

M^+ = 1589

$[(PMe_2Ph)_3Os(\mu\text{-}I)_3Os(PMe_2Ph)_2]^+$

M^+ = 1451

$[(PMe_2Ph)_3Os(\mu\text{-}I)_3Os(PMe_2Ph)]^+$

M^+ = 1313

2. Preparation of Tris(dimethylphenylphosphine) tri-iodo osmium(III)

To a mixture of OsO_4 (0.1g), ethanol (5 ml) and concentrated HI (0.71 ml), PMe_2Ph (0.3 ml) was added. The red/brown solution immediately turned blue/black. This was left stirring for 1 hour and was then left for a few hours, after which blue/black solid formed. This was filtered and washed with water, cold ethanol and hexane and was dried in vacuo (0.22g, 57% yield).

Elemental Analysis Found C: 28.92%, H; 3.24%, N: 0%

Calculated for $C_{24}H_{33}I_3P_3Os$

C: 29.23%, H: 3.35%, N: 0%

FAB mass spectrum Found M^+ = 985 (4%)

860 (100%)

846 (5%)

734 (100%)

Calculated for $OsI_3(PMe_2Ph)_3$

M^+ = 985

$OsI_2(PMe_2Ph)_3$

M^+ = 860

$OsI_3(PMe_2Ph)_2$

M^+ = 846

and $OsI(PMe_2Ph)_3$

M^+ = 734

Single Crystal X-Ray Structure of $[(PMe_2Ph)_3Ru(\mu\text{-}I)_3Ru(PMe_2Ph)_3]PF_6$

This complex was prepared as described previously.

Crystal Data: $[C_{48}H_{66}I_{0.81}Cl_{2.19}P_6Ru_2]PF_6$, M = 1355.46, monoclinic, space group $P2_1/c$, a = 14.510(6), b = 16.493(6), c = 23.949(10)Å, β = 97.026(33), V = 5694.1Å^3 (from setting angles for 11 reflections with $30 < 2\theta < 35$, λ = 1.54184Å), z = 4, D_{calc} = 1.581g cm^{-3}, T = 293K, orange tapered plate, 0.693 x 0.154 x 0.015 mm, μ = 111.654 cm^{-1}, $F(000)$ = 2723.

Data Collection and Processing: Stöe STADI-4 diffractometer, graphite monochromated Cu-K_α X-radiation, T = 293K, $\omega/2\theta$ scans with scan width $(0.99 + 0.347 \tan\theta)°$, 8303 data collected ($2\theta_{max}$ 120°, h-16→16, k-0→26, l 0→26), 7322 unique data (R_{int} = 0.0521), giving 5744 with $F > 6\sigma(F)$ for use in all calculations. No significant crystal decay or movement.

Structure Solution and Refinement: A Patterson synthesis located the heavy atoms and subsequent iterative cycles of least-squares refinement using SHELX-76[31] and difference Fourier synthesis located all non-H atoms. Refinement showed that there was 72% $[(PMe_2Ph)_3Ru(\mu\text{-}Cl)_3Ru(PMe_2Ph)_3]PF_6$ and 28% of $[(PMe_2Ph)_3Ru(\mu\text{-}I)_3Ru(PMe_2Ph)_3]PF_6$ in the crystal used for data collection. All non-H atoms were refined (by least squares on F^2) with anisotropic thermal parameters. The phenyl rings were fixed to be rigid hexagons. H atoms were fixed in calculated positions using AFIX. DIFABS[32] absorption correction was carried out with minimum correction = 0.881 and maximum correction = 1.056. At final convergence

$\underline{R}$ = 0.0711, $\underline{R}_w$ = 0.0968, $\underline{S}$ = 1.005 for 309 refined parameters and the final ΔF synthesis showed no peak above 0.714e$\mathring{A}^{-3}$ or below 0.624e$\mathring{A}^{-3}$. The weighting scheme $\underline{W}^{-1} = \sigma^2(F) + 0.001329F^2$ gave satisfactory agreement analyses and in the final cycle $(\Delta/\sigma)_{max}$ was 0.144.

Atomic scattering factors were inlaid[31] or taken from reference 32. Molecular geometry calculations utilised CALC.[34] The figure shown in section 3.2.1 was produced using ORTEP.[35]

3.4 REFERENCES

1. J. Chatt and R.G. Hayter, J.Chem.Soc.; 1961, 896.
2. M.S. Lupin and B.L. Shaw, J.Chem.Soc.; A, 1968, 741.
3. D.A. Couch and S.D. Robinson, Inorg.Chem.; 1974, 13(2), 456.
4. D.A. Couch and S.D. Robinson, Inorg.Chim.Acta; 1974, 9(1), 39.
5. P.W. Armit, T.A. Stephenson and A.S.F. Boyd, J.Chem.Soc., Dalton Trans.; 1975, 1669.
6. T.V. Ashworth, N.J. Nolte and E. Singleton, J.Chem.Soc., Chem.Comm.; 1977, 936.
7. A.J. Lindsay, Ph.D. Thesis, University of Edinburgh, 1982.
8. M.B. Hursthouse, R.A. Jones, K.M.A. Malik and G. Wilkinson, J.Am.Chem.Soc.; 1979, 101, 4128.
9. R.A. Jones, G. Wilkinson, I.J. Colquhoun, W. McFarlane and A.M.R. Galas, J.Chem.Soc., Dalton Trans.; 1980, 2480.
10. M.A. Green, J.C. Huffmann and K.G. Caulton, J.Organomet. Chem.; 1983, 243, C78.
11. F. Bottomley and S.B. Tong, Can.J.Chem., 1971, 49, 3739.
12. E.E. Mercer and L.W. Gray, J.Am.Chem.Soc.; 1972, 94, 6426.
13. T. Arthur and T.A. Stephenson, J.Organomet.Chem.; 1981, 208, 369.
14. T. Arthur, Ph.D. Thesis, University of Edinburgh, 1980.
15. T. Arthur, D.R. Robertson, D.A. Tocher and T.A. Stephenson, J.Organomet.Chem.; 1981, 208, 389.
16. P. Neubold, K. Wieghardt, B. Nuber and J. Weiss, Inorg. Chem.; 1989, 28, 459.

17. K. Wieghardt, W. Herrmann, M. Köppen, I. Jibril and G. Huttner, Z. Naturforsch; 1984, 39B, 1335.

18. P. Neubold, B.S.P.C. della Vedora, K. Wieghardt, B. Nuber and J. Weiss, Angew.Chem., Int.Ed.Engl.; 1989, 28, 763.

19. A. Llobet, M.E. Curry, H.T. Evans and T.J. Meyer, Inorg.Chem.; 1989, 28, 3131.

20. R.B. Hitchcock, M.F. Lappert and P.L. Pye, J.Chem.Soc., Chem.Comm.; 1976, 644.

21. G. Hunter and R.C. Massey, Inorg.Nucl.Chem.Lett.; 1973, 9, 727.

22. S.A.R. Knox and F.G.A. Stone, J.Chem.Soc. (A); 1971, 2874.

23. R.A. Jones, G. Wilkinson, A.M.R. Galas, M.B. Hursthouse and K.M.A. Malik, J.Chem.Soc., Dalton Trans.; 1980, 1771.

24. J.A. Statler, G. Wilkinson, M. Thornton-Pett and M.B. Hursthouse, J.Chem.Soc., Dalton Trans.; 1984, 1731.

25. (a) N.S. Hush, J.K. Beattie and V.M. Ellis, Inorg.Chem.; 1984, 23, 3338.

(b) V.T. Coombe, Ph.D. Thesis, University of Edinburgh, 1985.

26. M.N. Hughes, D. O'Reardon, R.K. Poole, M.B. Hursthouse, and M. Thornton-Pett, Polyhedron; 1987, 6, 1711.

27. J.K. Beattie, P. Del Favero, T.W. Hambley and N.S. Hush, Inorg.Chem.; 1988, 27, 2000.

28. M. Laing and L. Pope, Acta Cryst.; 1976, B32, 1547.

29. M.B. Robin and P. Day, Adv.Inorg.Chem. and Radiochem.; 1967, 10, 247.

30. W.C. Davies and W.J. Jones, Chem.Soc.J.; 1929, 1, 33.

31. G.M. Sheldrick, SHELX-76, "Program for Crystal Structure Refinement", University of Cambridge, England, 1976.

32. N.G. Walker and D. Stuart, Acta Cryst., Sect.A; 1983, 39, 158.

33. D.T. Cromer and J.L. Mann, Acta Cryst.; 1976, A24, 321.

34. R.O. Gould and P. Taylor, CALC, "Program for Molecular Geometry Calculations", University of Edinburgh, Scotland, 1985.

35. ORTEP; P.D. Mallinson and K.W. Muir, J.Appl.Cryst.; 1985, 18, 51.

C H A P T E R 4

VARIATION OF TERMINAL LIGAND, L

L = TERTIARY PHOSPHINE LIGAND

4.1 INTRODUCTION

It has been widely observed that altering the substituents on P(III) ligands markedly changes the behaviour of the ligands themselves and their transition metal complexes, in particular in their structural, spectroscopic and chemical properties. This was originally rationalized entirely in terms of electronic effects.

A general view of how PX_3 ligands, X=halide, bind to transition metals was proposed by Chatt.[1] He suggested that the lone pair on the phosphorous forms a σ-bond with the metal and that unfilled phosphorous 3d orbitals accept electron density from the metal to form a π-bond. This can be represented as follows:

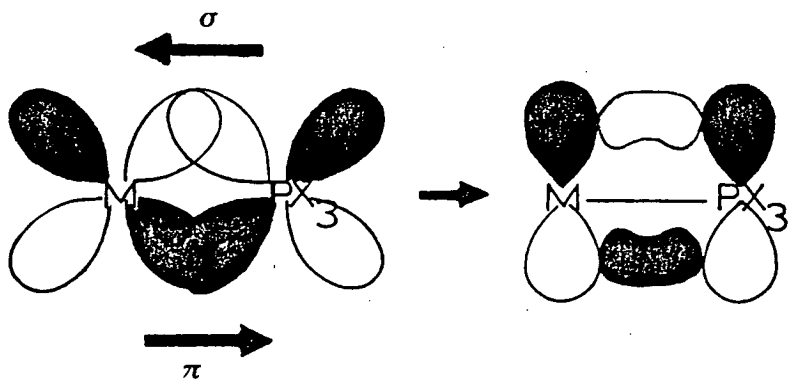

This view excludes PR_3 and PH_3, R=alkyl group, as only strongly electronegative atoms can cause sufficient contraction of the phosphorous 3d orbitals to make them suitable for π-bonding thus; PH_3 and PR_3 were originally classified as strong σ-donors and weak π-acceptors; whereas $P(OR)_3$ and PF_3 were considered to be weaker σ-donors and very strong π-acceptors.

This explanation of transition metal-phosphorous bonding has been a subject of much controversy over the years. The

question being whether phosphorous can actually be involved in π-back bonding and if so does it use its d-orbitals. The π-acceptor theory above has been used to explain the properties of the transition metal-phosphorous bond.

It was however widely accepted that the extent of π-back bonding varied from ligand to ligand. Many groups have been involved in determining the extent of π-acceptance in tertiary P(III) ligands by measuring the ν(CO) stretching vibration in complexes such as $Mo(CO)_3L_3$[2] and $Co(CO)_3(NO)L$,[3] where L=tertiary P(III) ligand. The ν(CO) stretching vibration is used as a measure of π-acceptance because the bonding of CO to a metal centre can be viewed in a similar manner to that described for tertiary P(III) ligands except that in CO the acceptor orbital is an unfilled π*-orbital. When both CO and P are bound to the same metal they compete for the electron density in the filled metal d-orbital. Weak π-accepting tertiary P(III) ligands allow more donation to the CO π*-orbital hence causing the ν(CO) stretching vibration to be lowered and vice versa for strongly π-accepting tertiary P(III) ligands. The following order of π-acidity resulted from these studies:

$$NO > CO > PF_3 > PCl_3 > P(OPh)_3 > P(OMe)_3 > PPh_3 > PMe_3 > PEt_3 > P(NC_5H_{10})_3$$

Cotton[4] stated that measuring differences in the ν(CO) stretching vibration was not as good a method of measuring π-acidity as using force constant changes following the development of the Cotton-Kraihanzel force technique.[5] This gave a slightly different order of π-acidity. A major difference being that PF_3 was found to be a better π-acceptor

than CO. This observation was later reinforced by photoelectronspectroscopy studies on $Ni(CO)_4$ and $Ni(PF_3)_4$.[6]

Bigorgne[7] opposed the idea that the P(III) ligands could be involved in any form of π-back bonding. He measured the B_1 ν(CO) stretching vibration for a series of $Ni(CO)_3L$ and $Ni(CO)_2L_2$ complexes where L=PMe_3, PEt_3, PPh_3, $P(C{\equiv}CPh)_3$, $P(CF_3)_3$ and PF_3 and plotted this as a function of the Taft inductive constant, σ, and obtained a straight line correlation. Tolman[8] repeated this work using a larger set of ligands and used the A_1 ν(CO) stretching vibration as a measure of the electronic effect. Tolman refers to the stretching vibration parameter, ν(CO), as a measure of the electron donor-acceptor property of the tertiary P(III) ligand rather than the π-acceptor strength. The results showed that the values for alkyl, aryl, alkoxy and aryloxy P(III) ligands tend to correlate with σ, however those for PF_3, PH_3 and $P(CF_3)_3$ do not.

The oxidation state of the metal is also important regarding the nature of the bonding present between the metal and the P(III) ligand. When the metal centre is in a low oxidation state the ligand may be involved in π-back bonding whereas if the oxidation state is high then it is likely to be involved only in σ-donation.

From the above discussion it is apparent that it is not necessary to explain the bonding characteristics of all P(III) ligands in terms of π-back bonding.

Attempts have been made to separate quantitatively σ- and π-effects. Angelici[9] studied a series of cis-$Mn(CO)_3L_2$ complexes where L=tertiary P(III) ligand, amine. A linear

correlation between pK_a[10] and the $\nu(CO)$ stretching vibration for all P(III) ligands was observed. Essentially pK_a is a measure of the σ-donicity of the ligand. Thus it was concluded that all the P(III) ligands studied showed no π-effects. Graham[11] and then Treichel[12] used force constants to separate σ- and π-effects. Their results were however debatable as they showed P^nBu_3 to be as good a π-acceptor as $P(OPh)_3$. On the whole these earlier studies have been unsatisfactory, mainly due to the limited range of compounds studied. More recent studies by Golovin[13] have proved more successful and will be discussed later.

Molecular orbital calculations have been carried out to determine the electronic nature of the frontier molecular orbitals of PH_3, PMe_3 and PF_3.[14] As expected the LUMO of PF_3 was found to have π-accepting properties whereas PMe_3 did not. Surprisingly however the results showed that the low-lying π-acceptor orbitals consisted primarily of phosphorous orbitals with substantial 3p character and the ordering of the LUMOs in energy terms is:

$$PF_3 < PH_3 < PMe_3$$

Thus calculations predict back bonding to PF_3 is enhanced over PMe_3 due to the character of the LUMO and its more favourable energy. Further theoretical work has also shown that the d-orbitals on phosphorous are not necessary for a quantitative description of π-bonding effects.[15] The π-acceptor orbitals in this study were also shown to consist mainly of phosphorous 3p character.

So far only the electronic effects of P(III) ligands have been discussed. In addition to these it has been

observed that steric effects are at least as important.[16]

Steric effects are the result of non-bonding forces between different parts of a molecule and may be altered by changing the angle between parts of a molecule either by repulsive interactions or by structural constraints. Electronic effects are transmitted along a chemical bond and may be altered by changing the electronegativity of the substituents on the ligand.[17,18] This can be represented as follows:[17]

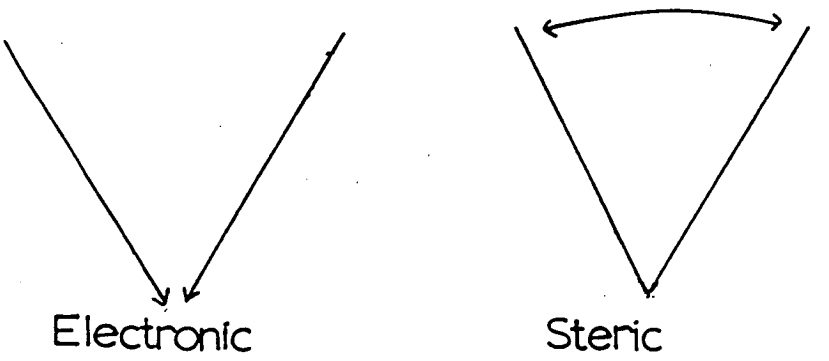

For example,[18]

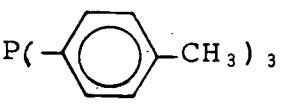 and 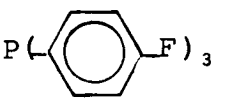 have different electronic effects but are sterically similar whereas the opposite holds for

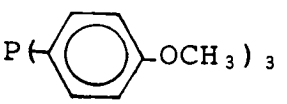 and 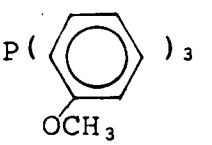

These effects are often difficult to separate. Tolman has however quantified both steric and electronic parameters for a wide range of P(III) ligands.

Steric effects have been quantified as the ligand cone angle, θ. θ is defined as "the angle of the cone with the apex at the metal which just encloses the Van der Waals surface of all the substituent atoms on the P(III) ligands, assuming that the bond length TM-P = 2.28Å".

This can be shown as follows:

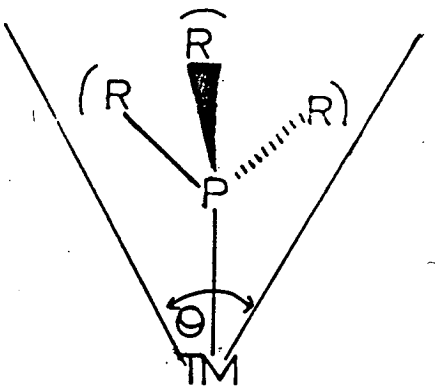

These have been measured using molecular models. There has been some controversy over the method used to measure θ for bulky ligands such as tricyclohexylphosphine and ligands of the type PR_2R' and PRR'R".

For bulky ligands Alyea[19] introduced the concept of ligand profiles which are plots of θ/2 versus φ, where φ is the angle of rotation about the M-P bond:

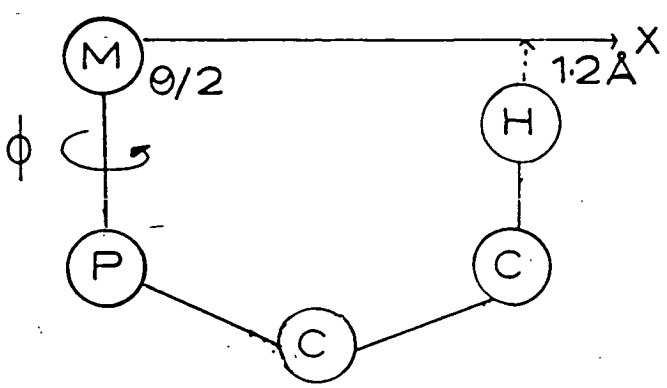

This allows visualization of ligand sizes. It was observed that the P(III) ligands do not behave like regular solid cones.

For ligands of the type PR_2R' and PRR'R" Tolman[20] used the following method for calculation of θ.

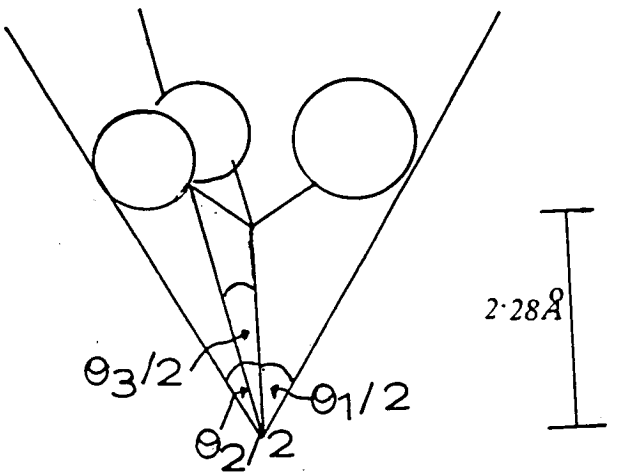

$$\text{where} \quad \theta = 2/3 \sum_{i=1}^{3} \theta_i/2$$

De Santo[21] et al. used the method of ligand profiles together with molecular orbital calculations to calculate cone angles. They calculate θ for all low energy conformations of some P(III) ligands and consider these individually and as a contribution to overall weighted average cone angles rather than choosing the single conformer which minimizes θ as Tolman did. Tolman has however measued θ values for a much wider range of ligands and these are more widely accepted. Tolman's θ values will therefore be used in this work.[16,17]

Electronic properties have been quantified as discussed

previously,[8,17] that is by measuring the A_1 carbonyl mode of a range of $Ni(CO)_3L$ complexes, where L=P(III) ligand. When $L=P^tBu_3$, the lowest value of the ν(CO) stretching vibration was observed, ν=2056.1 cm^{-1}. It was observed that successive replacement of one substituent on phosphorous by another causes the ν(CO) stretching vibration to change by almost constant increments. Tolman stated that for $PX_1X_2X_3$:

$$\nu = 2056.1 + \sum_{i=1}^{3} \chi_i$$

where χ_i is a measure of the substituent contribution to the electronic effect of the ligand. χ_i is obtained for species of the type PR_3 by $(\nu(CO) - 2056.1)/3 = \chi_i$. For ligands of the type PR_2R' and PRR'R" an overall χ value can therefore be obtained by adding substituent contributions or unknown ν(CO) stretching vibration values can be predicted.

Bodner[22] determined electronic parameters for a number of tertiary P(III) ligands using ^{13}C n.m.r. chemical shifts. These were found to be in close agreement with those of Tolman. In this work the electronic parameter, χ, of a particular P(III) ligand is taken to be:

ν(CO)(for $Ni(CO)_3L$) - 2056.1 = χ, L=P(III) ligand

using the ν(CO) stretching vibration values obtained by Tolman.

There are many examples where the behaviour of a particular series of TM-P complexes can be attributed to one or other of these effects.

1. Electronic effects

There are many cases where electronic effects can dominate. For a series of NiL_4 complexes, where L=tertiary P(III) ligand,

it was found that as the electronic parameter of the ligand increased the observed band maximum in the electronic spectrum moved to higher energy.[20] Electrochemical results also correlate with the electronic properties of the phosphine ligand. In a group of $Mn(\eta C_5H_4Me)(CO)_2L$[23] complexes, where $L=P(OPh)_3$, PPh_3 and PEt_3, there is a linear relationship between the $\nu(CO)$ stretching vibration (i.e. electronic parameter) and their oxidation potentials. The redox properties of a series of $[Mn(CO)_5L]^+$[24] complexes, which undergo a one-electron reduction also vary with the electronic parameter of L, the tertiary phosphine ligand, with the reduction becoming easier as L becomes more electron withdrawing.

Extensive studies by Golovin[13] have shown that the oxidation potential for complexes of the type of $MeCp(CO)_2MnL$ varies linearly with Tolman's electronic parameter of the tertiary phosphine ligand, L. He has classified the ligands studied into three groups to give more satisfactory results than the earlier work of Graham.

Class 1: σ-donor / π-donor

PR_3, R=Et, Bu, Cy

Class 2: σ-donor

PMe_3, $PR_{3-x}Ph_x$

x=1,2 R=Et, Me

$(pXPh)_3P$, X=H, Me, OMe

Class 3 σ-donor / π-acceptor

$P(pClPh)_3$, $P(OR)_3$

R = Ph, Me, Et, iPr, $P(OMe)Ph_2$

This classification was drawn up on the basis of a correlation of the oxidation potential, $E_2^{o'}$, with the pK_a values of R_3PH^+. Complexes with Class II ligands give a straight line correlation for pK_a versus $E_2^{o'}$; Class III ligands lie to the right of the line and Class I ligands to the left.

For Class II compounds the ease of oxidation must depend entirely on the σ-donicity of the ligand. For Class I, the complexes are easier to oxidise than implied by the pK_a values of the P(III) ligands. This is thought to be due to the π-basicities of the ligands. Members of Class III show the opposite effect i.e. the ligands are poorer overall electron donors than expected by their pK_a values; this is attributed to the onset of π-acidity.

It is important to note that pK_a values are dependent upon interactions between P and the hard acid, H^+, rather than a soft acid such as a low valent metal.

More recent studies by the same group have attempted to separate σ- and π-effects without relying on pK_a values.[25] The electronic properties of tertiary phosphines were analysed using the ν(CO) stretching vibrations and E_2^o (reduction potential) values of the family of complexes ηCpFe(CO)LCOMe, ηCpFe(CO)LMe and ηCp'FeL(CO)COMe where Cp' = $MeC_5H_4^-$ and L = tertiary phosphine. A linear correlation of E_2^o versus the ν(CO) stretching vibration was obtained for pure σ-donors (Class 2 ligands); when π-effects are present there is considerable scatter (Class 1 or 3 ligands).

2. Steric Effects

Steric effects dominate in many cases, for example, rates of reaction, equilibrium constants, UV/VIS spectra, electrochemistry and molecular structures can all be correlated with θ.

The monomeric family of complexes, RuX_2L_n, where X= halogen, n = 3 or 4 and L = tertiary phosphine ligand, when dissolved in polar solvents such as methanol participate in several equilibria to form binuclear species of the type $[L_3Ru(\mu\text{-}X)_3RuL_3]^+$.

However, for bulky ligands such as PPh_3 only the mononuclear species is observed.[26]

It has been observed in a series of $NiBr_2L_2$[27] complexes where L = $PMePh_2$, $PEtPh_2$ and $PPh_2(^tBu)$, that as the size of the tertiary phosphine ligand increases the lowest frequency transition in the electronic spectrum shifts to lower energy; being at 11,680 cm^{-1} for L=$PMePh_2$ and 10,800 cm^{-1} for L = $PPh_2(^tBu)$.

Electrochemical results have also been explained using steric effects. $[Co(salen)L_2]^+$ and $[Co(DH)_2L_2]^+$,[28] where salen = N,N'-ethylene bissalicylidene-iminato and DH = dimethylgloximato, L = tertiary phosphine, both undergo a one-electron reduction, which shifts anodically as the size of L increases. For $[Co(DH)_2L_2]^+$, when L = PPh_3 the reduction of Co(III) to Co(II) occurs at $E_{\frac{1}{2}}$ = -0.14V versus SCE; when L = $PMePh_2$ the same reduction process occurs at -0.61V (also versus SCE).

We set out to explore the effects of varying the terminal tertiary P(III) ligand on a series of compounds of type I, which were first made by Chatt,[29]

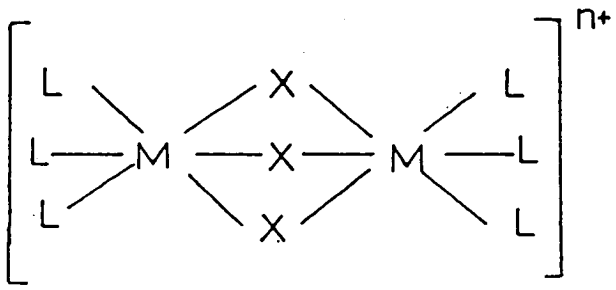

I

where M=Ru, Os; X^- = Cl^-; n = oxidation state and L is a variety of tertiary P(III) ligands. Species of this type undergo two reversible one-electron oxidations as previously discussed, i.e.

$$[M(II)M(II)]^{+} \overset{-e^-}{\rightleftharpoons} [M(II)M(III)]^{2+} \overset{-e^-}{\rightleftharpoons} [M(III)M(III)]^{3+}$$

As before the M(II)M(III) state is of particular interest as this is the mixed-valence state. All species of this type studied to date by spectroelectrochemical methods have been shown to be delocalised systems i.e. the metal centres are strongly interacting. We wanted to determine whether varying the tertiary P(III) ligand could alter the extent of the metal-metal interaction.

Crystal structures of the species $[L_3M(\mu\text{-}X)_3ML_3]^{n+}$ where L = PEt_2Ph, [30] PMe_2Ph[31] and PMe_3[32]; X = Cl; n = 1 and M = Ru have been determined previously. The metal-metal distances and Ru-Cl-Ru angles in these complexes vary; both are smallest when L = PMe_3 (3.28Å, 82°) and largest with PEt_2Ph (3.44Å, 87.9°). This suggested to us that different P(III) ligands may show different degrees of metal-metal

interaction. We wished to probe this interaction for many different terminal tertiary phosphine ligands by spectro-electrochemical techniques.

A spectroelectrochemical study of the related complex $[(NH_3)_3Ru(\mu\text{-}Cl)_3Ru(NH_3)_3]^{2+}$ in acetonitrile gave two absorption bands at 17,150 cm^{-1} (strong) and 7,140 cm^{-1} (weak).[33] This result was compared with $[(PEt_2Ph)_3Ru(\mu\text{-}Cl)_3\text{-}Ru(PEt_2Ph)_3]^{2+}$ which exhibited one band at 4350 cm^{-1}.[33,34] It was suggested on the basis of these results that the greater the degree of π-basicity exhibited by the terminal ligands then the greater the extent of electron delocalisation between the two metal centres i.e. the metal-metal interaction increases. A similar argument has been applied to explain the crystal structure data i.e. the more basic the P(III) ligand then the shorter the metal-metal distance. The results can be correlated with the steric parameter, θ, of the ligand. The data available were extremely limited and it was therefore difficult to say if the observed effects were due to π-basicity, steric parameter or a combination of the two factors.

No data are available for Osmium complexes.

4.2 RESULTS AND DISCUSSION

A range of binuclear ruthenium and osmium species $[L_3M(\mu\text{-}X)_3ML_3]^+$ has been prepared using standard literature preparations[26,29,35,36] where L = $PMePh_2$, PMe_2Ph, PMe_3, $PEtPh_2$, PEt_3, P^nPr_3, $P(OMe)Ph_2$, $P(OMe)_2Ph$, $P(OMe)_3$; X^- = Cl^-; M = Ru; L = PMe_2Ph, $PEtPh_2$, $P(OMe)Ph_2$, $P(OMe)_2Ph$, $P(OMe)_3$; X^- = Br^-; M = Ru and L = $PMePh_2$, PM_2Ph, $PEtPh_2$, PEt_2Ph, PEt_3,

P^nPr_3, $P(OMe)Ph_2$; X^- = Cl^-; M = Os. The counterion used in every case was PF_6^- except when L = PEt_2Ph; X^- = Cl^-; M = Ru, where BF_4^- was used.

Several new binuclear species were prepared M = Ru; L = $P(OMe)_3$; X^- = Cl^-, Br^-; M = Ru, L = $P(OMe)Ph_2$, $P(OMe)_2Ph$, X^-=Br^-; M = Os, L = $P(OMe)Ph_2$, X^-= Cl^-; using the standard preparations available.[26,35,36] The complex where L = PMe_3, M = Ru, X^-=Cl^- had been previously prepared by Wilkinson[32] involving the reaction of cis-$RuClMe(PMe_3)_4$ with $AgBF_4$. We however found that the method of Stephenson[26,36] could be used with better results. This method involves the interaction of $RuCl_2(PPh_3)_3$ with PMe_3 in methanol. Wilkinson had previously stated that $[(PMe_3)_3Ru(\mu\text{-}Cl)_3Ru(PMe_3)_3]^+$ was stable in air over a period of several days. However using our preparation the PMe_3 containing complex was found to be indefinitely stable. Schemes 4.2.1 and 4.2.2 detail the methods used for preparing the ruthenium and osmium complexes respectively.

It should be noted that the binuclear osmium complexes proved much more difficult to make than those of ruthenium thereby limiting the range available for study.

The electrochemical, spectroelectrochemical and theoretical results will now be discussed.

4.2.1 Electrochemistry

(a) M = Ruthenium

Electrochemical studies were carried out as previously described in methylene chloride/0.5M $TBABF_4$ when X^- = Cl^- and acetone/0.1M $TBABF_4$ when X^- = Br^-. All complexes studied

Scheme 4.2.1: Methods used for Preparation of Complexes of the Type $[L_3Ru(\mu\text{-}X)_3RuL_3]^+$ where L = tertiary phosphine ligand and X^- = Cl^-, Br^-

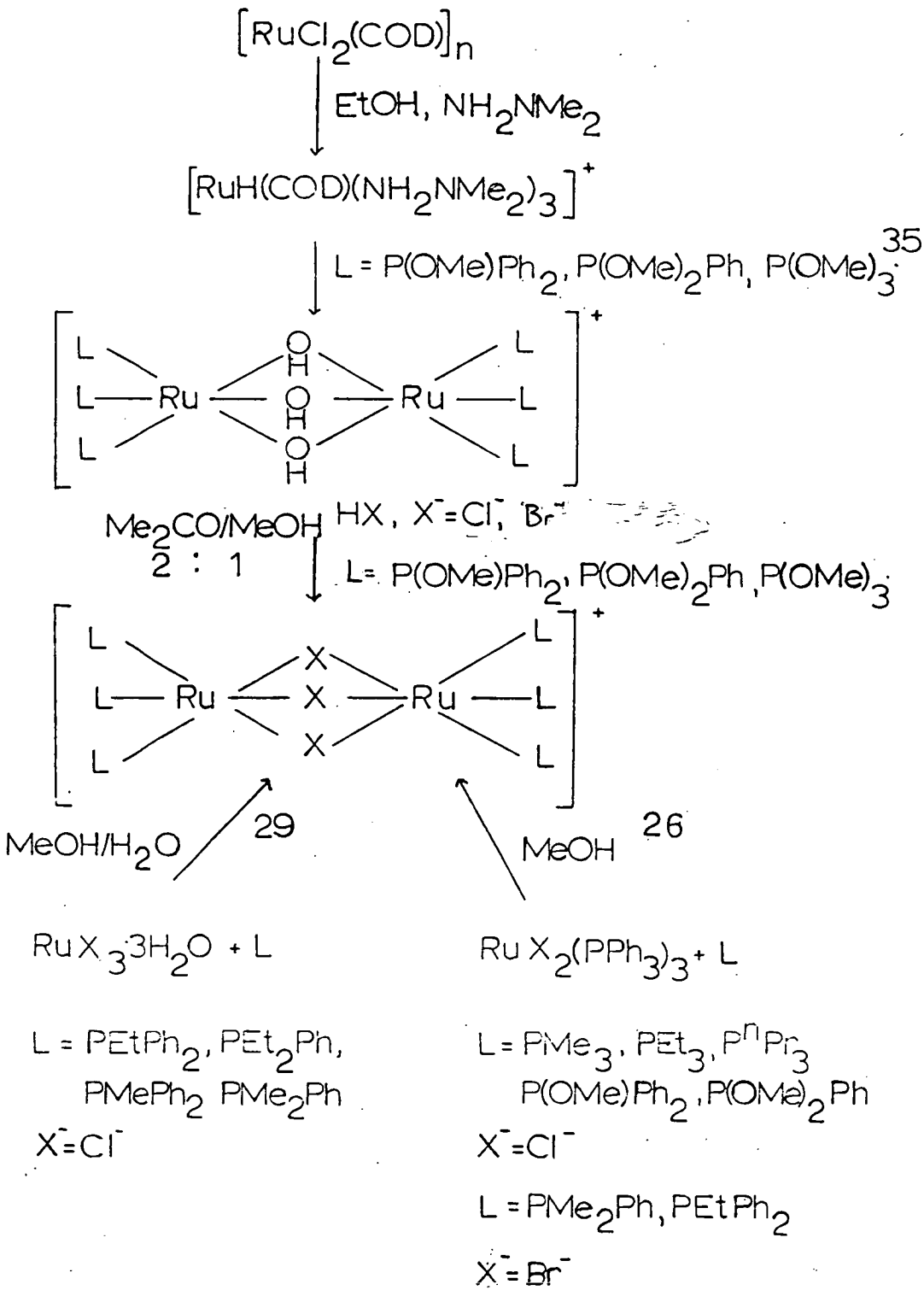

Scheme 4.2.2: Methods used for Preparation of Complexes of the Type $[L_3Os(\mu\text{-}Cl)_3OsL_3]^+$ where L = tertiary phosphine ligand

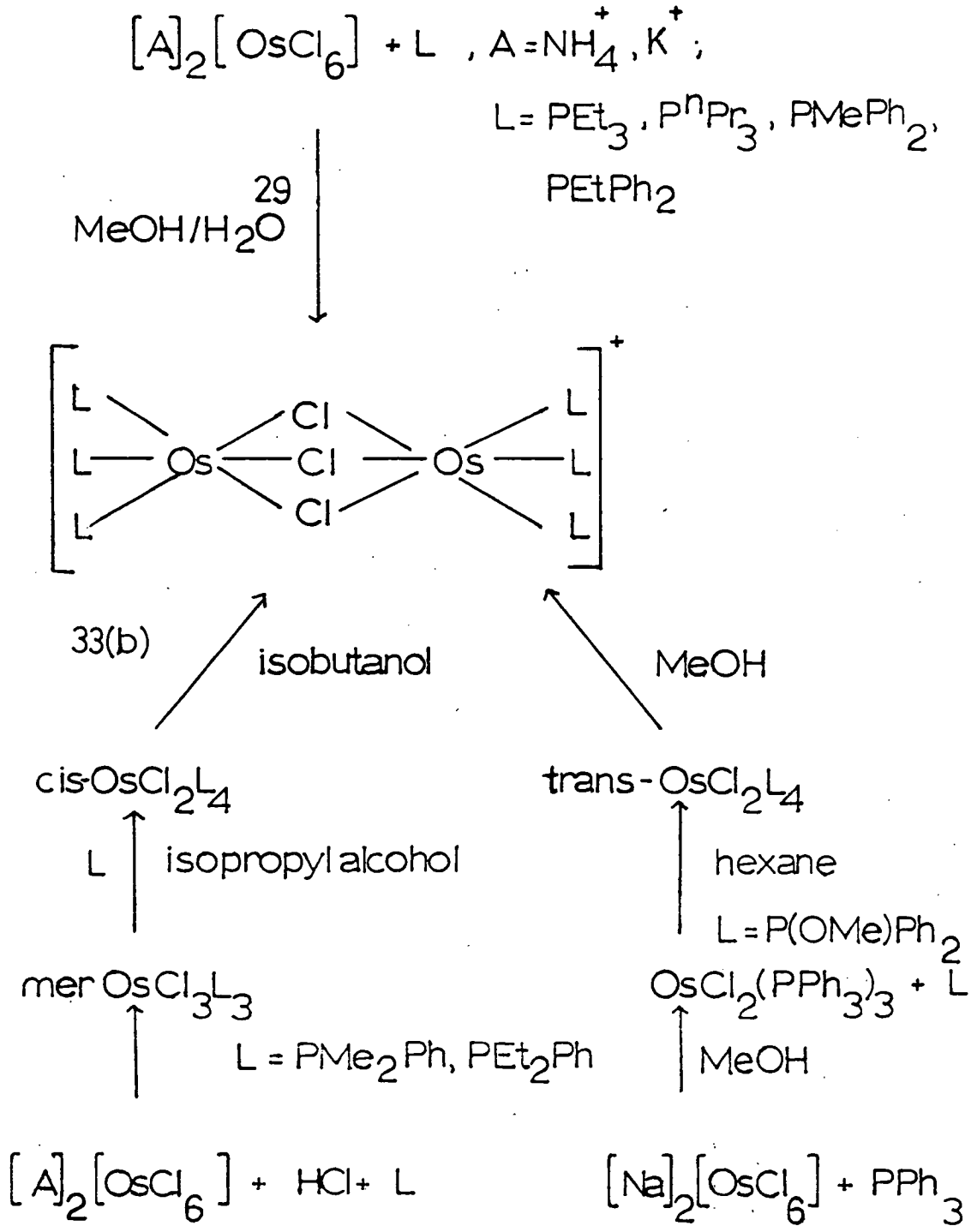

undergo two one-electron oxidations. The cyclic voltammogram and a.c. voltammogram for L = PEt_3, X^-=Cl^-, M = Ru are shown in Figure 4.2.1.

The oxidation potential values for $[L_3Ru(\mu\text{-}Cl)_3RuL_3]^+$ are given in Table 4.2.1 which also includes the difference in anodic and cathodic peak potentials for each redox process (ΔE_p). It is immediately obvious from the results that the terminal ligand L greatly influences the potentials of the metal-based redox steps. The potential of the first oxidation process $[L_3Ru(\mu\text{-}Cl)_3RuL_3]^{+/2+}$ can be shifted 470V more negative by replacing L = $P(OMe)_3$ by PEt_3. The ΔE_p values for the first oxidation process range from 60-70mV indicating electrochemical reversibility; those for the second oxidation process are larger ranging from 80-120mV. This may be due to a larger structural change occurring in the complex on further oxidation or due to the fact that these oxidations occur close to the breakdown of the solution.

It can be shown that the first oxidation potential of each species is directly dependent on the electronic parameter of the tertiary phosphine ligand. This is shown in Figure 4.2.2. There is no simple linear relationship between the redox behaviour and the steric parameter, θ, of the phosphine ligand.

The electrochemical results for the species where X^- = Br^- display the same behaviour, that is, we observe two one-electron oxidation process whose potential is dependent upon L. This is shown in Table 4.2.2 and Figure 4.2.3.

Studies carried out in this laboratory[37] on monomeric

Figure 4.2.1: Cyclic Voltammogram (c.v.) and a.c. Voltammogram of $[(PEt_3)_3Ru(\mu\text{-}Cl)_3Ru(PEt_3)_3]^+$ in Methylene Chloride / 0.5M $TBABF_4$. T = 290K.

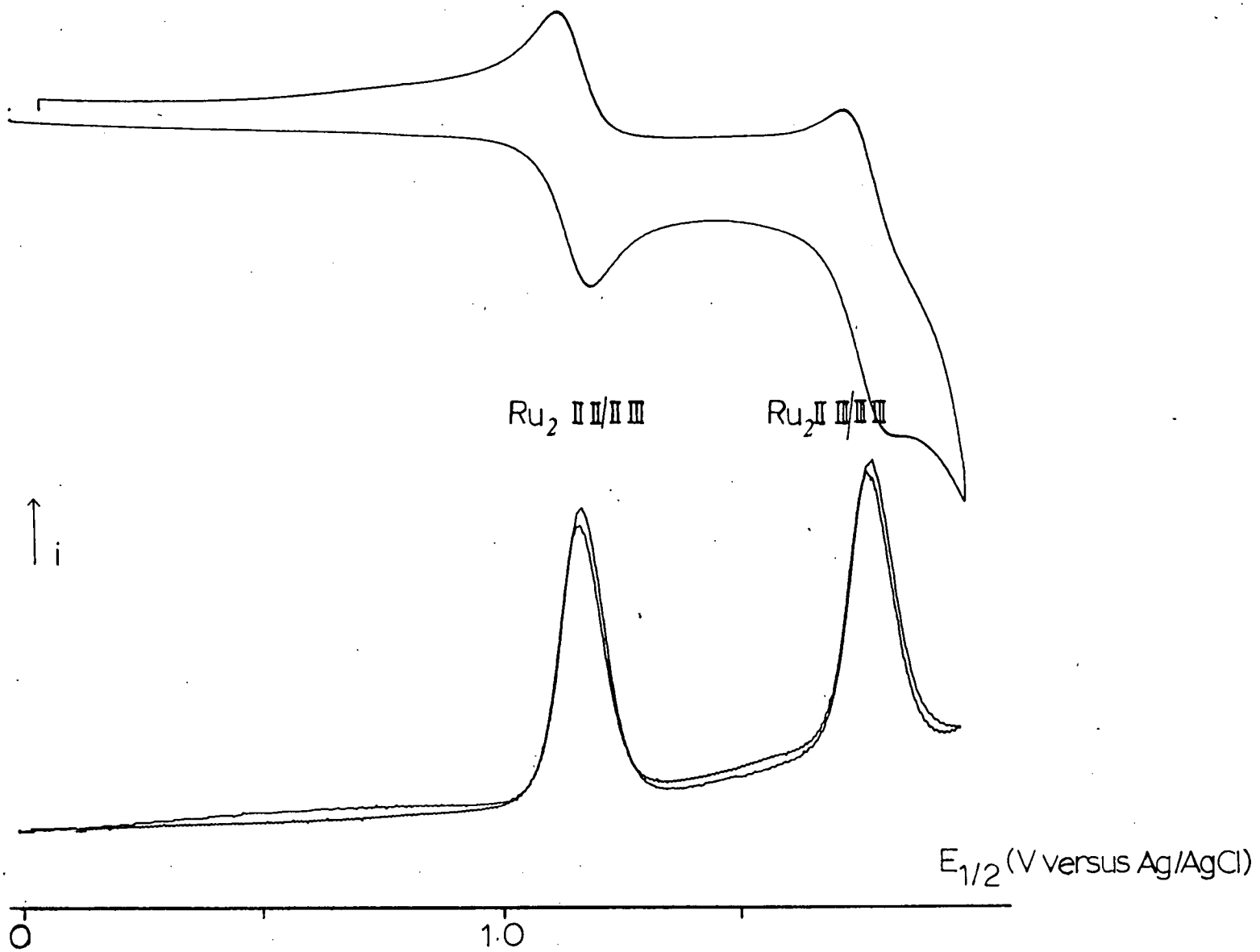

Table 4.2.1: $E_{\frac{1}{2}}$ (V) values for $[L_3Ru(\mu\text{-}Cl)_3RuL_3]^+$ in Methylene Chloride / 0.5M $TBABF_4$

L	$E_{1/2}$(V versus Ag/AgCl) [a,b]			
	II,II / II,III		II,III / III,III	
$PMePh_2$	1.36	(0.070) [c]	1.78	(0.100)
PMe_2Ph	1.23	(0.070)	1.75	(0.100)
PMe_3	1.21	(0.060)	1.74 [d]	
$PEtPh_2$	1.23	(0.060)	1.79	(0.080)
PEt_2Ph	1.20	(0.070)	1.74	(0.100)
PEt_3	1.12	(0.060)	1.71	(0.080)
P^nPr_3	1.20	(0.070)	1.80	(0.090)
$P(OMe)Ph_2$	1.41	(0.070)	1.91 [e]	
$P(OMe)_2Ph$	1.48	(0.080)	1.85	(0.100)
$P(OMe)_3$	1.59	(0.060)	1.94	(0.100)

a. Ferrocene/Ferrocinium = +0.56V

b. T = 290K

c. $E_p^F - E_p^R$ values are shown in brackets in V (where E_p^F and E_p^R are the potentials at the maximum of the forward and reverse curves respectively).

d. $[(PMe_3)_3Ru(\mu\text{-}Cl)_3Ru(PMe_3)_3]^{3+}$ coats the electrode

e. Irreversible even at low temperatures (T=233K)

Figure 4.2.2: Graph of $\chi(cm^{-1})$ versus $E_{1/2}(V)$ for $[L_3Ru(\mu\text{-}Cl)_3RuL_3]^+$ in Methylene Chloride / 0.5M $TBABF_4$ at T = 290K.

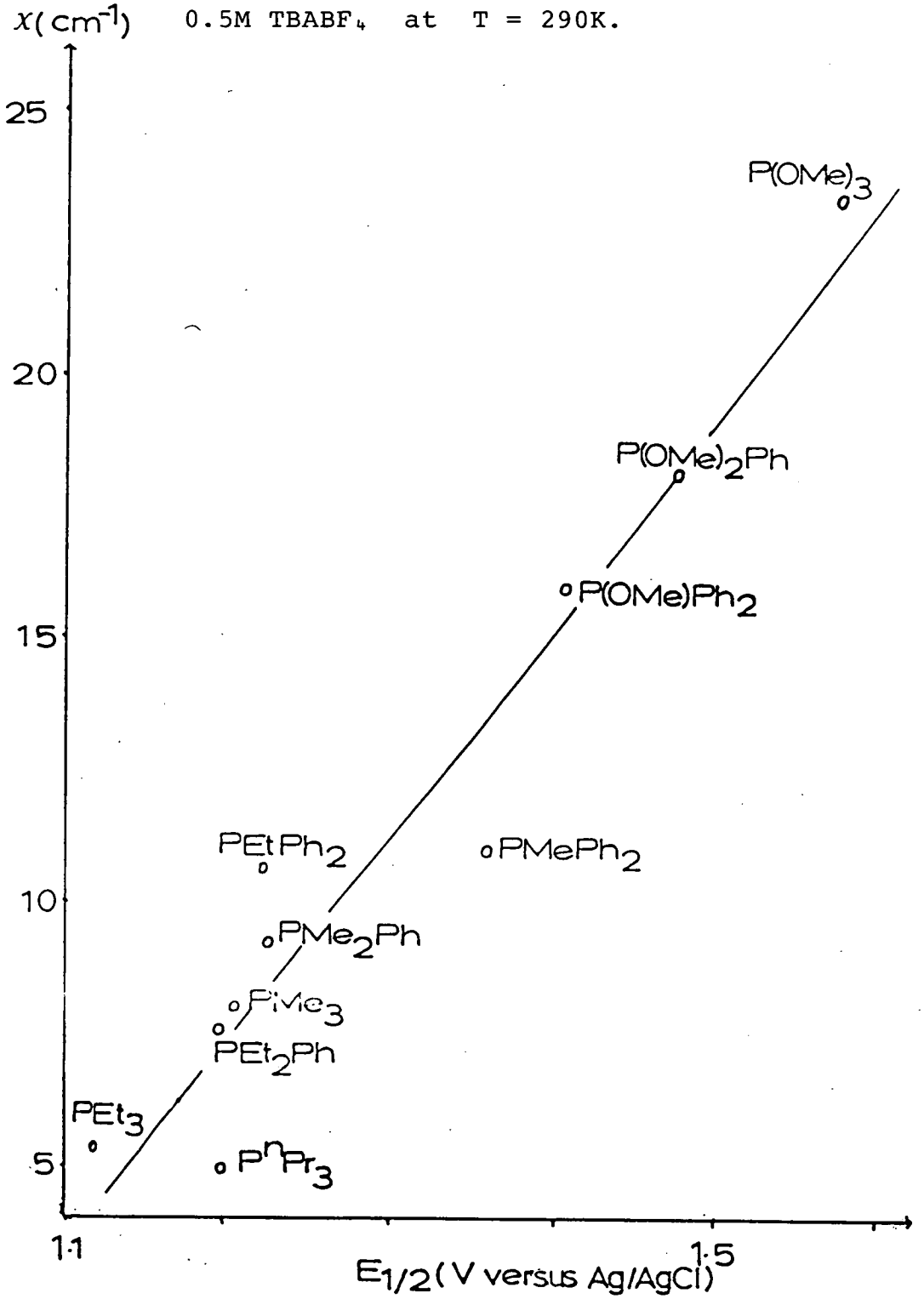

Table 4.2.2: $E_{\frac{1}{2}}$ (V) values for $[L_3Ru(\mu\text{-}Br)_3RuL_3]^+$ in acetone / 0.1M $TBABF_4$

L	$E_{1/2}$ (V versus Ag/AgCl) [a,b]			
	II,II / II,III		II,III / III,III	
$PEtPh_2$	1.8	(0.060) [c]	1.75	(0.080)
PMe_2Ph	1.22	(0.060)	1.23	(0.080)
$P(OMe)Ph_2$	1.39	(0.070)	1.88 [d]	
$P(OMe)_2Ph$	1.45	(0.070)	1.79	(0.090)
$P(OMe)_3$	1.51	(0.060)	1.86	(0.080)

a. Ferrocene/Ferrocinium at +0.56V

b. T = 290K

c. $E_p^F - E_p^R$ values are shown in brackets

d. Irreversible even at T = 233K

Figure 4.2.3: Graph of $\chi(cm^{-1})$ versus $E_{1/2}$ (V versus Ag/AgCl) for $[L_3Ru(\mu\text{-}Br)_3RuL_3]^{+/2+}$, at T = 290K in Acetone / 0.1M $TBABF_4$

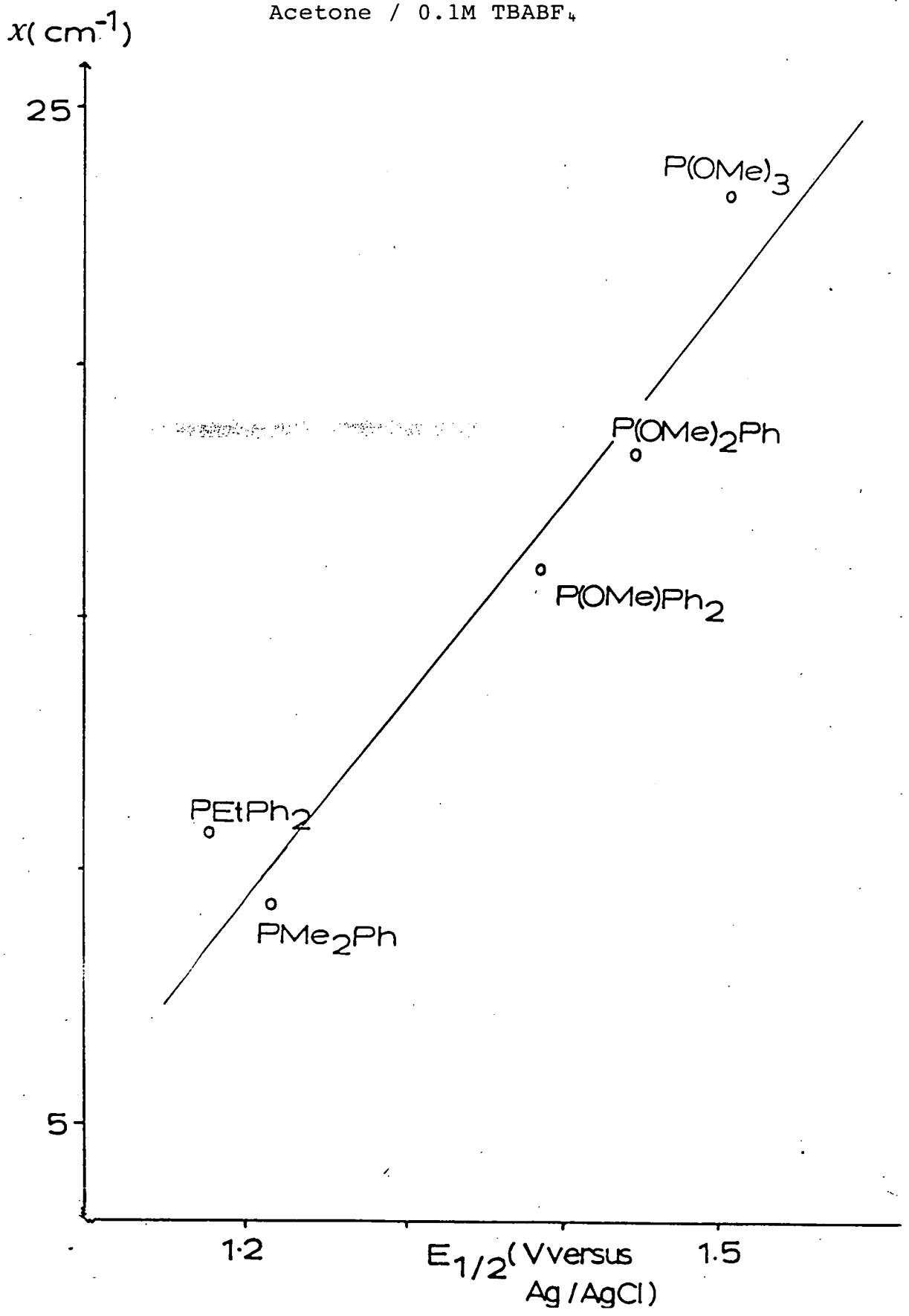

complexes of the type $RuCl_3L_3$ where L = PEt_3, PMe_2Ph, PEt_2Ph showed that the metal based reduction potential was dependent on the pK_a value of the tertiary phosphine ligand i.e. as the pK_a value increases the reduction became more difficult. In our studies of the binuclear complexes an attempted correlation between the redox potential and the pK_a[10] value is shown in Figure 4.2.4. On the basis of the studies by Golovin et al. discussed previously we would expect the $E_{\frac{1}{2}}$ values for the complexes with L = PMe_3, PMe_2Ph, $PMePh_2$, PEt_2Ph and $PEtPh_2$ to show a straight line correlation with the pK_a values. The complex with L = PEt_3 would be expected to lie to the left of the line and those with L = $P(OMe)Ph_2$, $P(OMe)_2Ph$ and $P(OMe)_3$ to the right. We observe that the complexes where L = $P(OMe)_2Ph$ and $P(OMe)_3$ show the greatest deviation from the straight line indicating that these ligands exhibit a degree of π-character in their bonding. The other ligands are behaving purely as σ donors. The use of pK_a values as a measure of σ-donicity is however suspect as discussed in Section 4.1. We maintain that a more meaningful relationship is obtained using the electronic parameter versus the electrode potential.

It has been previously stated (see Chapter 1) that the separation between the first and second oxidation for symmetric binuclear complexes is approximately 0.5V for X^- = Cl^-, Br^-. Table 4.2.3 gives the values for X^- = Cl^-. It can be seen, however, that the separation varies with different terminal tertiary phosphine ligands being 0.6V when L = P^nPr_3 and only 0.35V when L = $P(OMe)_3$. A plot of the electronic parameter, χ, against the separation in

Figure 4.2.4: Graph of pK_a versus $E_{1/2}$(V) for $[L_3Ru(\mu\text{-}Cl)_3RuL_3]^+$ in Methylene Chloride / 0.5M $TBABF_4$ at T = 290K

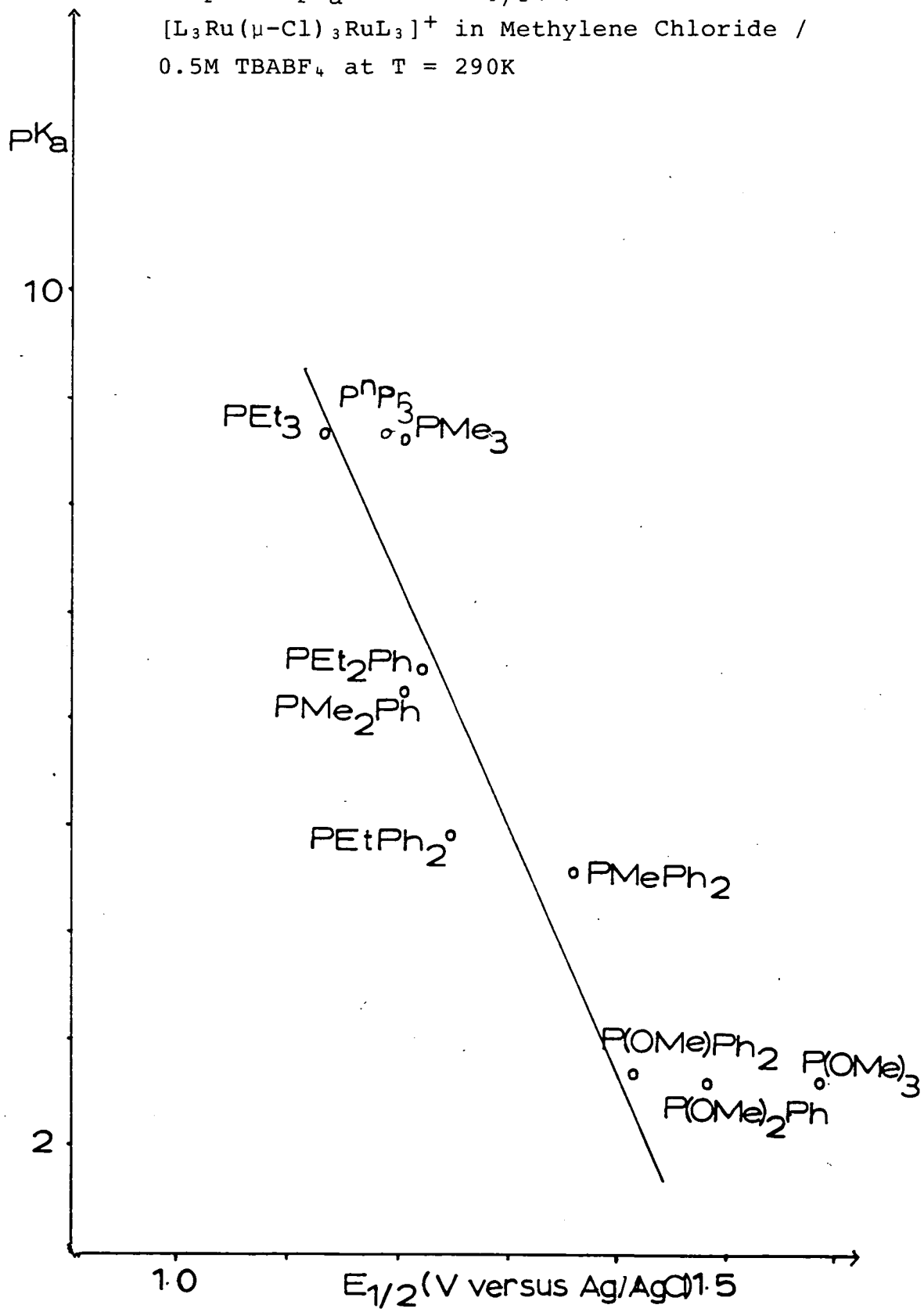

Table 4.2.3: Separation (ΔE (V)) Between the First and Second Oxidation Potentials for $[L_3Ru(\mu\text{-}Cl)_3RuL_3]^+$ in Methylene Chloride / 0.5M $TBABF_4$ at T = 290K

L	ΔE (V)
$PMePh_2$	0.42
PMe_2Ph	0.52
PMe_3	0.53
$PEtPh_2$	0.56
PEt_2Ph	0.54
PEt_3	0.59
P^nPr_3	0.60
$P(OMe)Ph_2$	0.50
$P(OMe)_2Ph$	0.37
$P(OMe)_3$	0.35

Figure 4.2.5: Graph of $\chi(cm^{-1})$ versus the Separation between the Two Oxidation Potentials (ΔE) in V of $[L_3Ru(\mu\text{-}Cl)_3RuL_3]^+$ in Methylene Chloride / 0.5M $TBABF_4$ at T = 290K

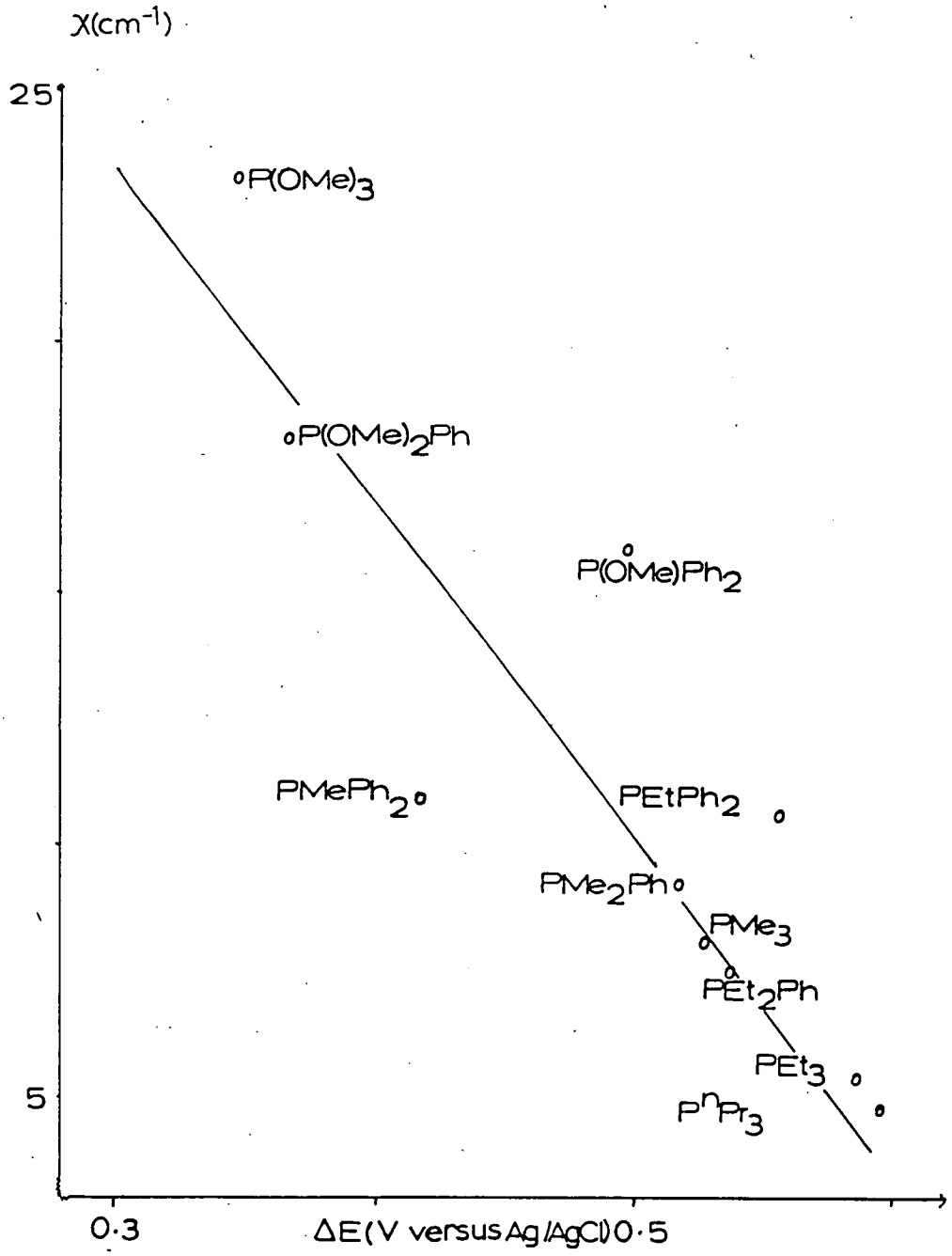

oxidation potentials is given in Figure 4.2.5 which shows that the separation tends to decrease as the ligand becomes more electron withdrawing. We conclude that a 0.5V separation between the two redox processes is not necessarily indicative of electron delocalisation between the two metal centres.

(b) M = Osmium

Electrochemical studies on the binuclear osmium complexes were carried out in the same manner as in (a).

The osmium species all showed similar electrochemical behaviour to that of equivalent ruthenium complexes. Table 4.2.4 shows the redox potentials and Figure 4.2.6 shows the correlation of the redox potentials with the electronic parameter, χ, of the tertiary phosphine ligand. We observe once again a linear relationship between the electronic parameter and the oxidation potential with a similar gradient as for the ruthenium analogues. All oxidations occurred at $\sim$0.2V less positive than the analogous ruthenium complexes (see Chapter 2).

(c) Conclusions

The redox behaviour of the binuclear ruthenium and osmium complexes studied is dependent on the electronic properties of the tertiary phosphine terminal ligand present. A good correlation between the electronic parameter, χ and the first metal-based oxidation potential has been achieved. Thus by altering M, L and χ we can fine tune the redox chemistry of these binuclear complexes over a 0.69V range

Table 4.2.4: $E_{\frac{1}{2}}$ (V) values for $[L_3Os(\mu\text{-}Cl)_3OsL_3]^+$ in Methylene Chloride / 0.5M $TBABF_4$

L	$E_{\frac{1}{2}}$ (V versus Ag/AgCl) [a,b]			
	II,II / II,III		II,III / III,III	
$PMePh_2$	1.18	(0.060) [c]	1.51	(0.080)
PMe_2Ph	1.06	(0.060)	1.56	(0.080)
$PEtPh_2$	1.04	(0.060)	1.58	(0.060)
PEt_2Ph	1.02	(0.070)	1.58	(0.080)
PEt_3	0.90	(0.060)	1.46	(0.070)
P^nPr_3	0.95	(0.060)	1.53	(0.070)
$P(OMe)Ph_2$	1.26	(0.060)	1.78	(0.080)

a. Ferrocene/Ferrocinium at +0.56V

b. T = 290K

c. $E_p^F - E_p^R$ values are shown in brackets

Figure 4.2.6: Graph of $\chi(cm^{-1})$ versus $E_{1/2}$ (V) for $[L_3Os(\mu\text{-}Cl)_3OsL_3]^+$ in Methylene Chloride / 0.5M $TBABF_4$ at T = 290K

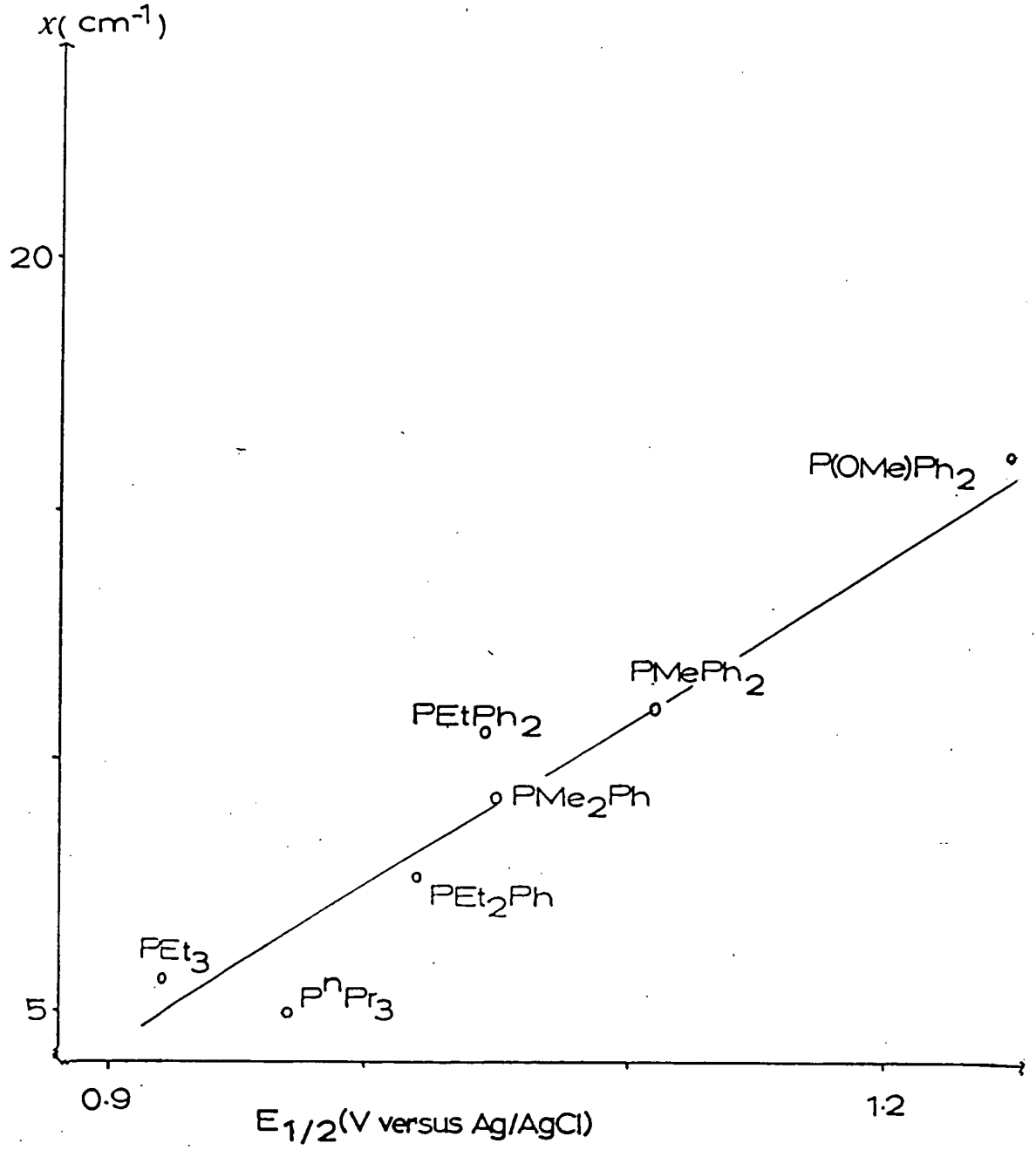

for the first oxidation process and 0.48V for the second oxidation.

4.2.2 Spectroelectrochemistry

In order to probe the metal-metal interactions in the symmetric binuclear complexes further we studied, by spectroelectrochemical techniques, the one-electron oxidation product of all the compounds discussed in section 4.2.1.

The $[L_3M(\mu\text{-}X)_3ML_3]^{2+}$ mixed-valence state was electrogenerated in situ for each species in methylene chloride/0.5M $TBABF_4$ when X^- = Cl^- and acetone/0.1M $TBABF_4$ when X^- = Br^-, at a suitable potential using the O.T.T.L.E. cell as described previously (usually 0.2V beyond the redox process). The temperature was kept constant for each experiment, within the range 263-269K depending on the complex under study. (A typical study is shown in Figure 4.2.7.)

The only species where $[L_3Ru(\mu\text{-}X)_3RuL_3]^{3+}$ could be observed was when X^- = Br^- and L = $P(OMe)_3$. This was shown to be reversible for:

$$[(P(OMe)_3)_3Ru(\mu\text{-}Br)_3Ru(P(OMe)_3)_3]^{+} \underset{+e^-}{\overset{-e^-}{\rightleftharpoons}} [(P(OMe)_3)_3Ru(\mu\text{-}Br)_3\text{-}Ru(P(OMe)_3)_3]^{2+} \underset{+e^-}{\overset{-e^-}{\rightleftharpoons}} [(P(OMe)_3)_3Ru(\mu\text{-}Br)_3Ru(P(OMe)_3)_3]^{3+}$$

(T = 265K)

Several attempts were made to observe the $[L_3Ru(\mu\text{-}X)_3RuL_3]^{3+}$ species for complexes containing other tertiary phosphine ligands. However decomposition took place even at very low temperatures (T = 223K) as observed by a failure to regenerate the starting material spectrum. All $[L_3Os(\mu\text{-}Cl)_3OsL_3]^{3+}$ species could be reversibly generated. Initially we thought the difference in behaviour between

Figure 4.2.7: Electronic Absorption Spectrum showing the Conversion of $[(PEtPh_2)_3Ru(\mu\text{-}Cl)_3Ru(PEtPh_2)_3]^+ \rightarrow [(PEtPh_2)_3Ru(\mu\text{-}Cl)_3Ru(PEtPh_2)_3]^{2+}$ in Methylene Chloride / 0.5M $TBABF_4$

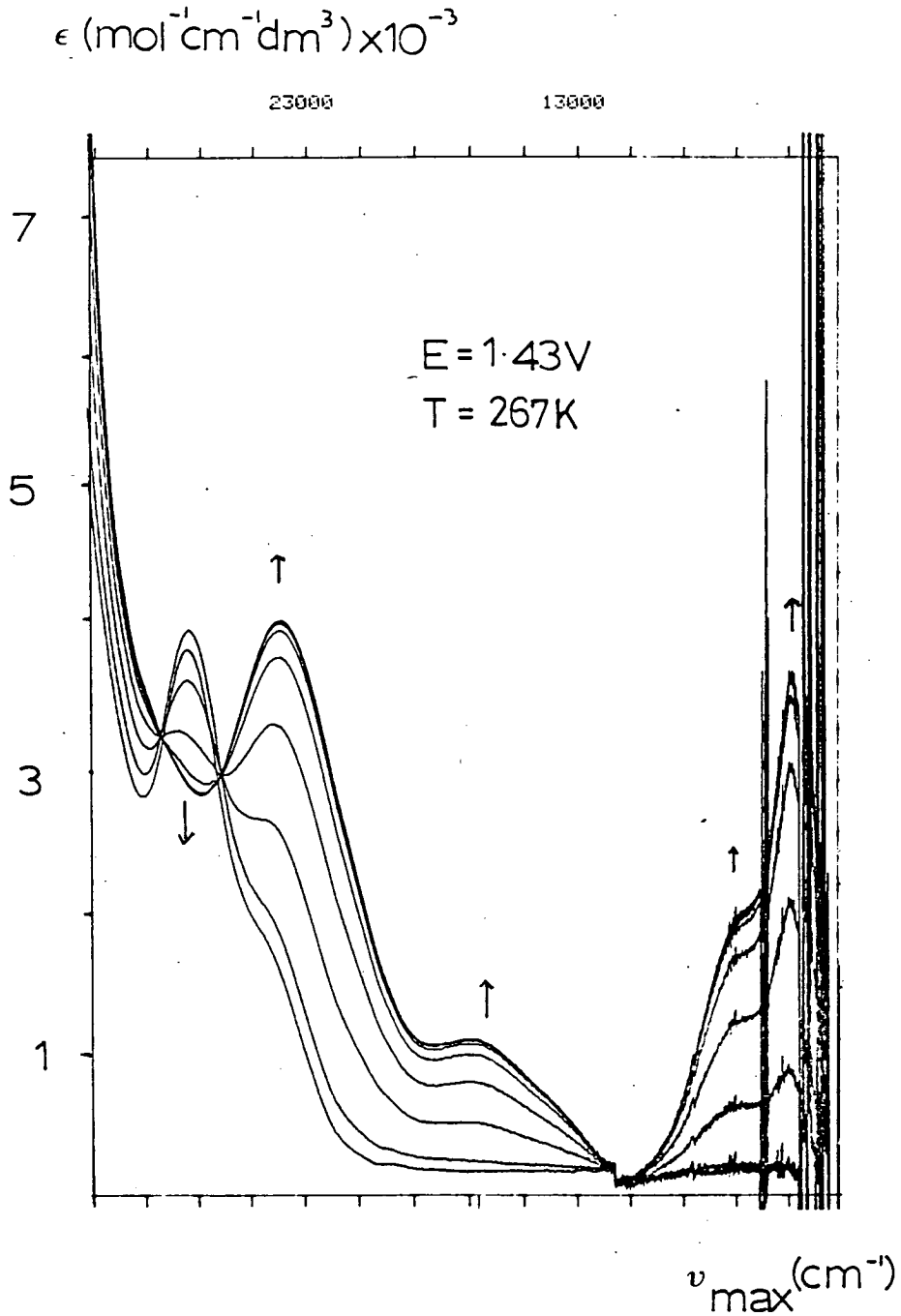

analogous ruthenium and osmium binuclear complexes was due to the more accessible oxidation potentials of the osmium complexes. However when M = Os, L = $P(OMe)Ph_2$ and X^-= Cl^- the second oxidation occurs at +1.78V which is similar to the ruthenium species for L = PMe_2Ph and X^- = Cl^- (E=+1.75V) and in this case $[L_3Ru(\mu\text{-}Cl)_3RuL_3]^{3+}$ could not be observed.

Furthermore in the $[(P(OMe)_3)_3Ru(\mu\text{-}Br)_3Ru(P(OMe)_3)_3]^+$ complex the first and second oxidation potentials are at +1.51 and 1.86V respectively. Thus there must be some other factor governing the stability of the $[L_3M(\mu\text{-}X)_3ML_3]^{3+}$ (vide infra).

The oxidation states will now be discussed in turn.

(a) $[L_3M(\mu\text{-}X)_3ML_3]^+$

The spectra for analogous $[L_3Ru(\mu\text{-}X)_3RuL_3]^+$ and $[L_3Os(\mu\text{-}X)_3OsL_3]^+$ species are very similar. All spectra are dominated by a high energy band at approximately 30,000 cm^{-1} ($\varepsilon\sim5000$ $mol^{-1}cm^{-1}dm^3$) which in most cases has a shoulder at lower energy. Tables 4.2.5 - 4.2.7 give the position of the observed bands. Figure 4.2.8 shows the spectrum of $[(PEtPh_2)_3Ru(\mu\text{-}Cl)_3Ru(PEtPh_2)_3]^+$ which is typical of all species.

We assign the band as an intraligand transition of the tertiary phosphine ligand for the following reasons.

1. It does not change significantly in either position or intensity upon oxidation which would be expected if it were due to a charge transfer transition.

Table 4.2.5: Positions of Bands (ν_{max}) in the Electronic Absorption Spectrum of $[L_3Ru(\mu\text{-}Cl)_3RuL_3]^+$ in Methylene Chloride / 0.5M $TBABF_4$ at T = 266K ± 3K

L	ν_{max} (cm^{-1})	ε ($mol^{-1}cm^{-1}dm^3$)
$PMePh_2$	25,600 (sh)	3,548
	27,965	4,489
PMe_2Ph	27,000 (sh)	3,484
	29,551	4,057
PMe_3	29,241	2,330
	32,100	2,282
$PEtPh_2$	24,400 (sh)	1,766
	27,473	4,010
PEt_2Ph	25,700 (sh)	1,431
	28,936	2,294
PEt_3	27,000 (sh)	1,709
	30,000	2,279
P^nPr_3	26,900 (sh)	2,047
	30,267	2,831
$P(OMe)Ph_2$	27,778	5,878
$P(OMe)_2Ph$	31,000	6,946
$P(OMe)_3$	33,335	2,460

Table 4.2.6: Positions of Bands (ν_{max}) in the Electronic Absorption Spectrum of $[L_3Ru(\mu\text{-}Br)_3RuL_3]^+$ in acetone / 0.1M $TBABF_4$ at T = 266K ± 3K

L	ν_{max} (cm^{-1})	ε ($mol^{-1}cm^{-1}dm^3$)
PMe_2Ph	26,700 (sh)	3,247
	28,736	3,477
$PEtPh_2$	27,262	4,448
$P(OMe)Ph_2$	26,882	4,984
$P(OMe)_2Ph$	30,340 [a]	7,965
$P(OMe)_3$	32,176 [a]	4,733

a. In Methylene Chloride / 0.5M $TBABF_4$ at T = 266K to observe high energy band.

Table 4.2.7: Position of Bands (ν_{max}) in the Electronic Absorption Spectrum of $[L_3Os(\mu\text{-}Cl)_3OsL_3]^+$ in Methylene Chloride / 0.5M $TBABF_4$ at T = 266K ± 3K

L	ν_{max} (cm^{-1})	ε ($mol^{-1}cm^{-1}dm^3$)
$PMePh_2$	25,000 (sh)	992
	31,018	5,705
PMe_2Ph	32,638	5,703
$PEtPh2_2$	24,400 (sh)	1,033
	30,230	7,573
PEt_2Ph	32,342	6,987
PEt_3	31,500 (sh)	3,163
	32,200	4,486
P^nPr_3	31,800 (sh)	3,274
	34,200	5,135
$P(OMe)Ph_2$	33,000	13,246

Figure 4.2.8: Electronic Absorption Spectrum of $[(PEtPh_2)_3Ru(\mu\text{-}Cl)_3Ru(PEtPh_2)_3]^+$ in Methylene Chloride at T = 293K

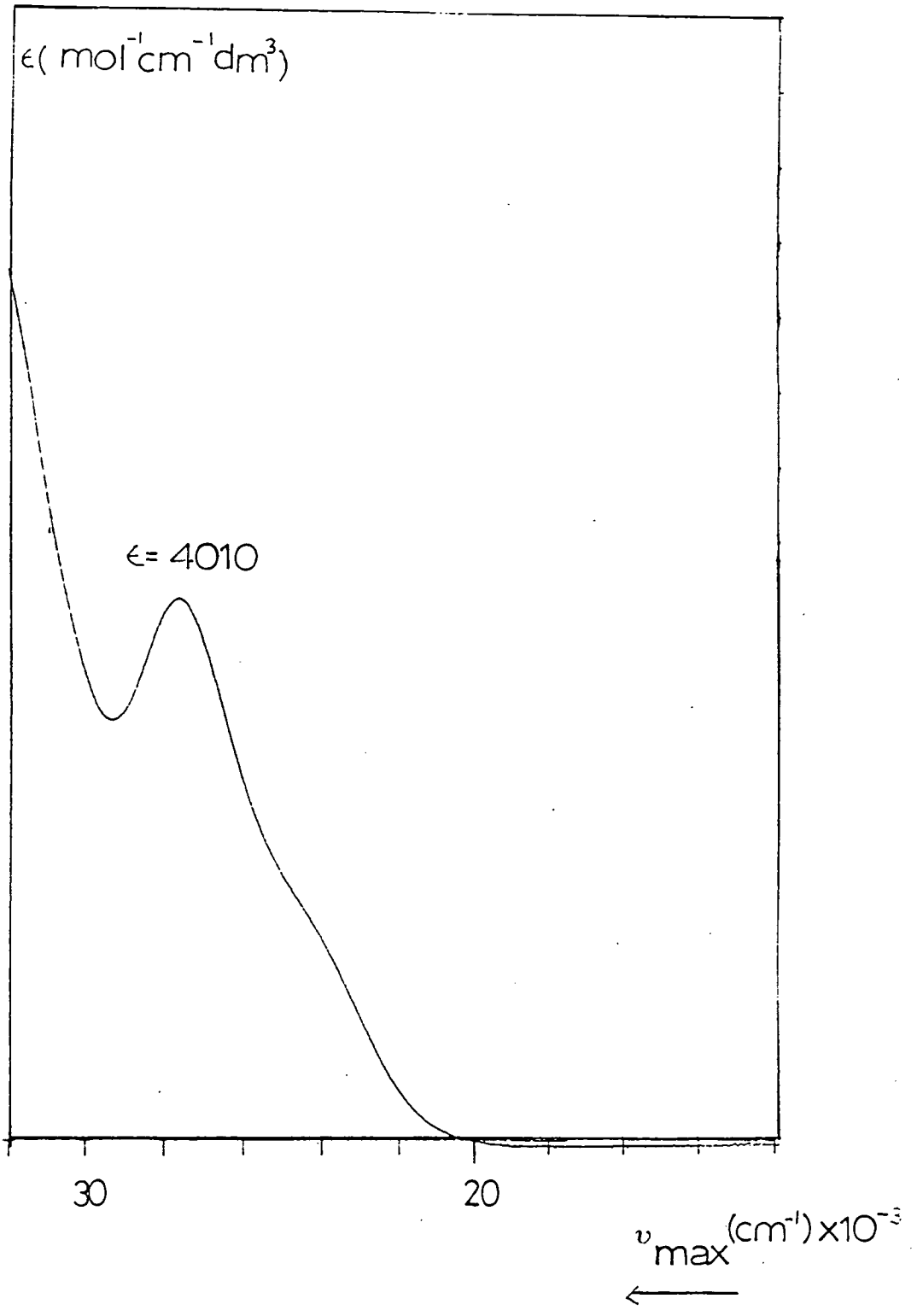

2. Monomeric species of the type MX_2L_4, where M = Os, X^-=Cl^- and L = tertiary phosphine ligand, show a band at a similar energy with similar intensity, which also behaves in an analogous manner on oxidation.

There are three points to note about this band:

1. As the ligand becomes bulkier i.e. the size of the cone angle, θ, increases the band tends to move to lower energy.

In a series of $CrL_2(NCS)_4$[38] complexes, where L is a tertiary phosphine ligand, the position of the L, ligand field band shows a similar effect. When L = PMe_3 (θ=118°) it is observed at 19,950 cm^{-1}, L = PEt_3 (θ=132°) at 19,500 cm^{-1} and L = PEt_2Ph (θ=136°) at 19,050 cm^{-1}.

2. The positions of the bands are found to be lower in energy when X^- = Br^- than when X^- = Cl^- for the same tertiary phosphine ligand. Studies on some NiX_2L_2[39] complexes where L = tertiary phosphine ligand, X^- = Br^-, Cl^- show a band at ∿25,000 cm^{-1} which decreases in energy on replacing Cl^- by Br^-. For example, a band is observed at 25,000 cm^{-1} for X^-= Cl^-; when X^- = Br^- this band shifts to 24,650 cm^{-1}.

3. The bands move to higher energy when the metal centre changes from Ru to Os.

We observe no other bands in this region of the spectrum.

(b) $[L_3M(\mu\text{-}X)\ ML_3]^{2+}$

For all $[L_3M(\mu\text{-}X)_3ML_3]^{2+}$ species studied there are:

1. Two bands observed in the near infra-red region of the electronic spectrum.
2. A weak broad band in the visible region which is displayed by most complexes.
3. A more intense band at higher energy.

Tables 4.2.8 - 4.2.10 show the positions of these bands. Figure 4.2.9 shows a typical $[L_3M(\mu\text{-}X)_3ML_3]^{2+}$ spectrum.

1. Near Infra-Red Bands

In all cases the band positions, ν_{max}, do not vary with solvent, the band halfwidth values, $\Delta_{\frac{1}{2}}$, are 5000 cm^{-1} and are insensitive to altering the temperature. It was therefore concluded that all systems studied are delocalised i.e. there is a strong metal-metal interaction and the bands are due to transitions within the molecular orbital framework (Chapter 1). The two bands are expected on the basis of the molecular orbital calculations discussed previously (Chapter 1). They arise from the following transitions

$$a_1' \rightarrow a_2'' \qquad z \text{ allowed}$$

$$\text{and} \quad e'' \rightarrow a_2'' \qquad x, y \text{ allowed}$$

As discussed in Chapter 1 the $a_1' \rightarrow a_2''$ transition is likely to be the most intense and this is taken as a measure of the metal-metal interaction.

The results for each metal will be discussed in turn.

Table 4.2.8: Positions of Bands (ν_{max}) in the Electronic Absorption Spectrum of $[L_3Ru(\mu\text{-}Cl)_3RuL_3]^{2+}$ in Methylene Chloride / 0.5M $TBABF_4$ at T = 266K ± 3K

L	ν_{max} (cm^{-1})	ε ($mol^{-1}cm^{-1}dm^3$)
$PMePh_2$	4,500	4,917
	4,920	4,276
	14,600	1,283
	16,000	1,496
	24,000	5,815
PMe_2Ph	5,000	2,613
	7,770	2,864
	17,000	955
	27,200	4,869
PMe_3	6,000	1,997
	9,340	6,610
	17,000	237
	24,000 (sh)	1,189
	28,400	4,042
$PEtPh_2$	4,958	3,679
	7,000	1,987
	16,700	809
	23,992	3,863
PEt_2Ph	4,675	1,780
	7,000	995
	15,000 (sh)	404
	17,000	587
	26,179	2,569
	29,800	2,358

/ continued

Table 4.2.8: continued

L	ν_{max} (cm^{-1})	ε ($mol^{-1}cm^{-1}dm^3$)
PEt_3	4,700	3,052
	7,246	2,523
	15,300	353
	26,969	4,988
P^nPr_3	4,700	3,463
	7,032	2,797
	16,000	478
	27,203	5,015
$P(OMe)Ph_2$	5,500	1,641
	8,460	1,383
	14,800	926
	27,400	5,839
$P(OMe)_2Ph$	6,500	597
	10,350	3,231
	16,600	1,050
	22,000	727
	31,300	11,134
$P(OMe)_3$	7,000	469
	11,350	2,460
	34,400	2,152

Table 4.2.9: Positions of Bands (ν_{max}) for $[L_3Ru(\mu\text{-}Br)_3RuL_3]^{2+}$ in acetone / 0.1M $TBABF_4$ at T = 266K ± 3K

L	ν_{max} (cm^{-1})	ε ($mol^{-1}cm^{-1}dm^3$)
$PEtPh_2$	4,997	3,674
	7,000	1,412
	17,100	1,431
	23,946	4,564
PMe_2Ph	5,000	1,917
	7,330	1,534
	17,000	630
	27,100	3,746
$P(OMe)Ph_2$	4,500	3,410
	7,500	1,311
	15,200	1,407
	26,970	4,827
$P(OMe)_2Ph$	6,600 [a]	1,210
	10,468	3,632
	31,686	6,690
$P(OMe)_3$	7,400 [a]	1,017
	12,007	4,733
	25,000	4,379
	33,378	1,636

a. In Methylene Chloride / 0.5M $TBABF_4$ to observe high energy bands at T = 266K.

Table 4.2.10: Positions of Bands (ν_{max}) in the Electronic Absorption Spectrum of $[L_3Os(\mu\text{-}Cl)_3OsL_3]^{2+}$ in Methylene Chloride / 0.5M $TBABF_4$ at T = 266K ± 3K

L	ν_{max} (cm^{-1})	ε ($mol^{-1}cm^{-1}dm^3$)
$PMePh_2$	4,938	3,522
	7,716	1,091
	18,643	1,208
	24,300 (sh)	1,510
	30,377	5,384
PMe_2Ph	4,991	4,875
	9,000	650
	18,000	810
	32,000	5,062
$PEtPh_2$	4,712	4,062
	7,718	1,377
	18,600	1,377
	29,275	5,577
PEt_2Ph	5,100	2,717
	8,700	621
	18,200	776
	32,300	6,404
PEt_3	4,895	4,831
	7,800	805
	19,201	748
	25,600	1,553
	31,889	4,946

/ continued

Table 4.2.10: continued

L	ν_{max} (cm^{-1})	ε ($mol^{-1}cm^{-1}dm^3$)
P^nPr_3	4,902	4,762
	7,708	832
	19,040	832
	25,100	1,844
	31,848	5,608
$P(OMe)Ph_2$	5,272	7,827
	8,400	1,491
	16,046	2,047
	32,217	2,276

Figure 4.2.9: Electronic Absorption Spectrum of $[(PEtPh_2)_3Ru(\mu\text{-}Cl)_3Ru(PEtPh_2)_3]^{2+}$ in Methylene Chloride / 0.5M $TBABF_4$

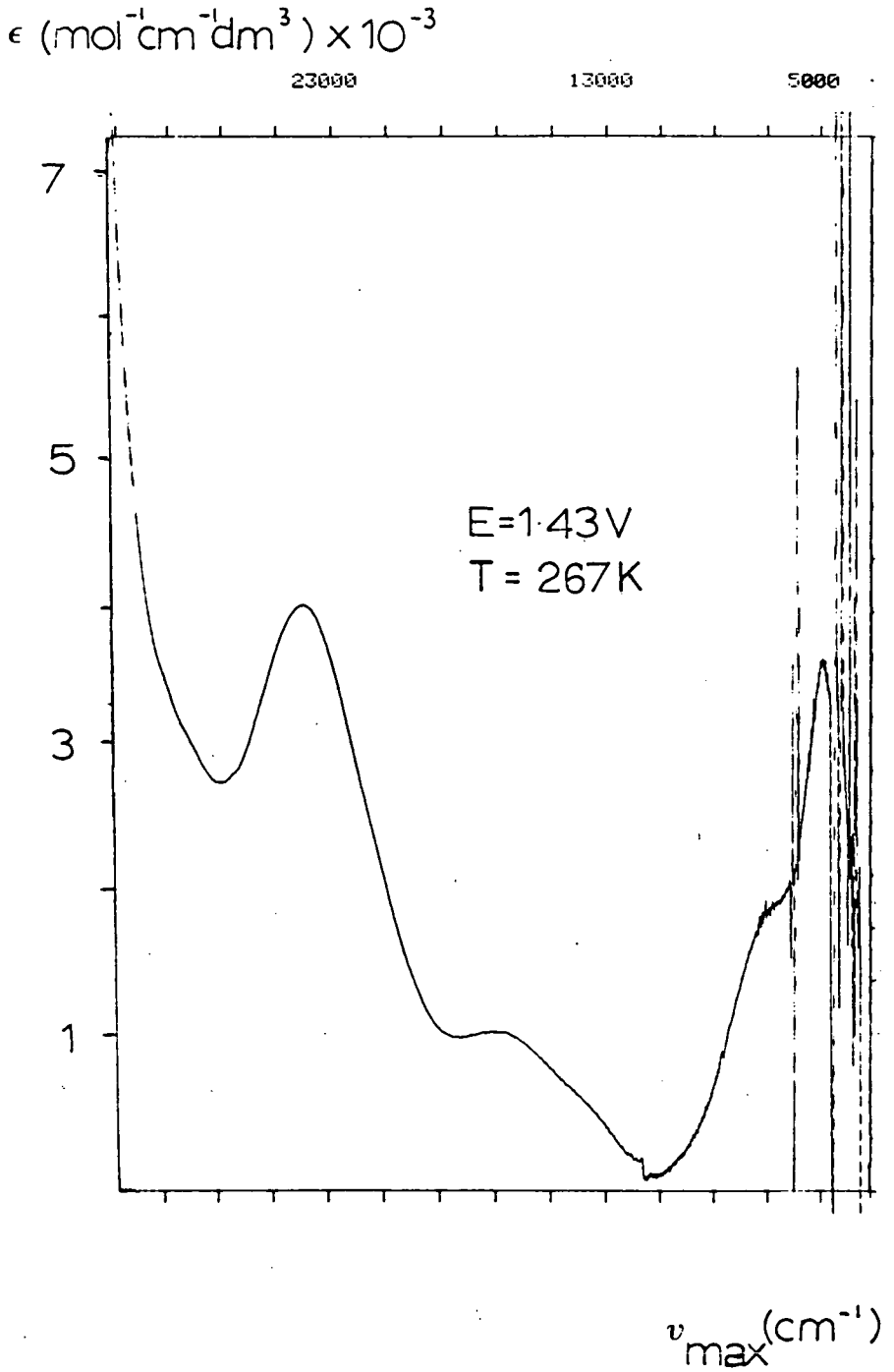

(i) M=Ruthenium

All the complexes $[L_3Ru(\mu\text{-}X)_3RuL_3]^{2+}$ studied have been determined to be delocalised systems, however the degree of the strong metal-metal interaction can be altered by using different tertiary phosphine ligands. For $X^- = Cl^-$, the energy of the most intense band ($a_1' \rightarrow a_2''$) varies over a wide range from 4,500 cm^{-1} - 11,350 cm^{-1} (see Table 4.2.8 on p153/4) as L is altered. If the position of this band, ν_{max}, is plotted as a function of the electronic parameter, χ, of the tertiary phosphine ligand as in section 4.2.1 no direct correlation is observed as shown in Figure 4.2.10. If however ν_{max} is plotted as a function of the steric parameter, θ, of the ligand then a straight line correlation is observed. This is shown in Figure 4.2.11. This indicates that the extent of metal-metal interaction is governed by the size of the ligand. In addition as the size of the ligand increases the separation between the bands decreases (there are some anomalies e.g. with $L=PEtPh_2$ which has the largest θ, but this is a general trend).

It has been previously suggested that the degree of metal-metal interaction in ruthenium complexes is dependent on the degree of π-basicity of the terminal ligand, L.

Our evidence does not bear this out e.g. PEt_3 and PMe_3 have similar basicities; their pK_a values being 8.69 and 8.65 respectively. When $L=PEt_3$, bands are observed at 4700 (ε = 3052 $mol^{-1}cm^{-1}dm^3$) and 7246 cm^{-1} (2523 $mol^{-1}cm^{-1}dm^3$) whereas when $L=PMe_3$ the bands are observed at 6000 (ε = 1997 $mol^{-1}cm^{-1}dm^3$) and 9340 cm^{-1} (ε = 6610 $mol^{-1}cm^{-1}dm^3$). Thus we would argue that there are different amounts of

Figure 4.2.10: Graph of $\nu_{max}(cm^{-1})$ versus $\chi(cm^{-1})$ for $[L_3Ru(\mu\text{-}Cl)_3RuL_3]^{2+}$ at T = 266K in Methylene Chloride / 0.5M $TBABF_4$

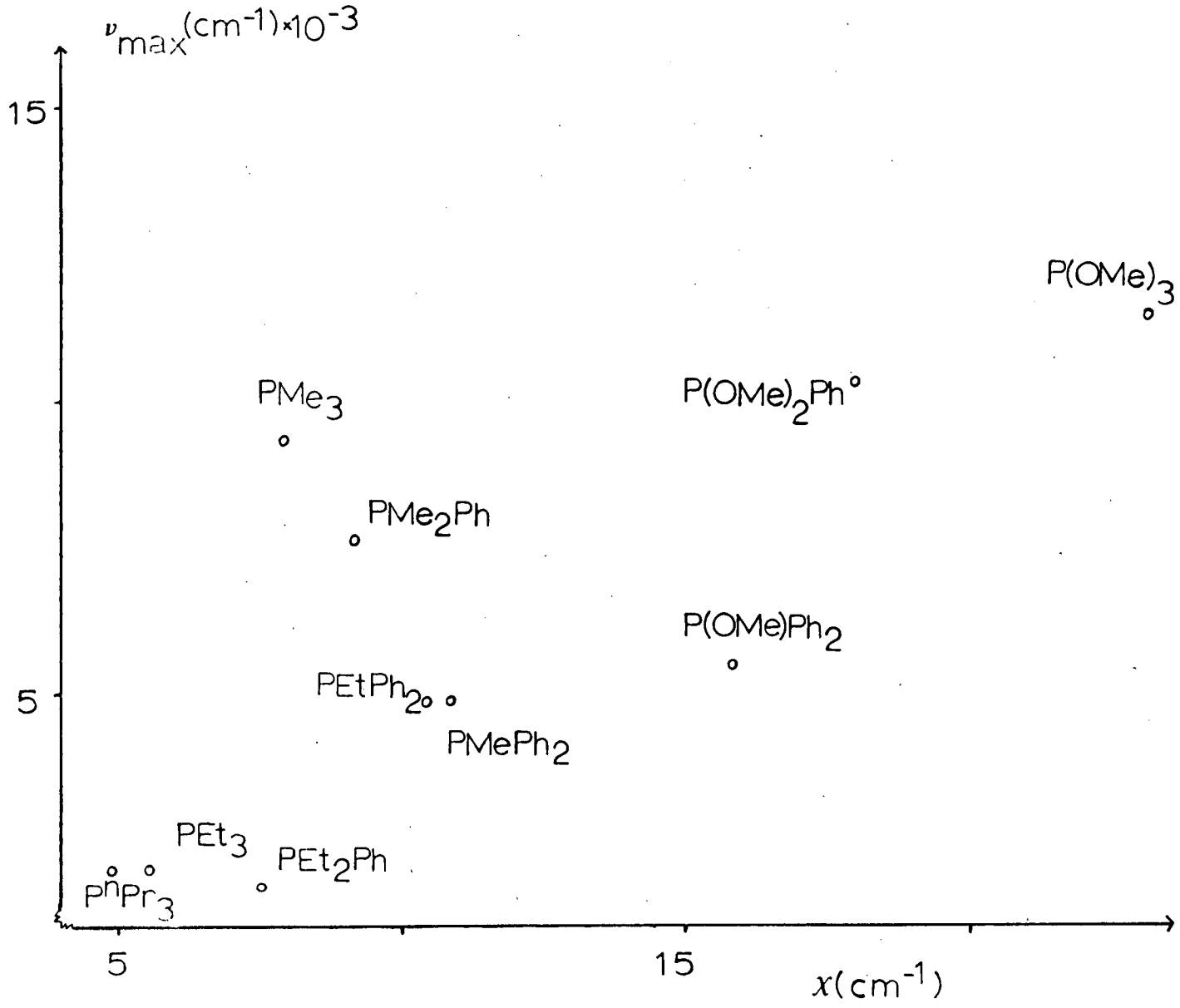

Figure 4.2.11: Graph of ν_{max} (cm^{-1}) versus θ(°) for $[L_3Ru(\mu\text{-}Cl)_3RuL_3]^{2+}$ at T = 266K in Methylene Chloride / 0.5M $TBABF_4$

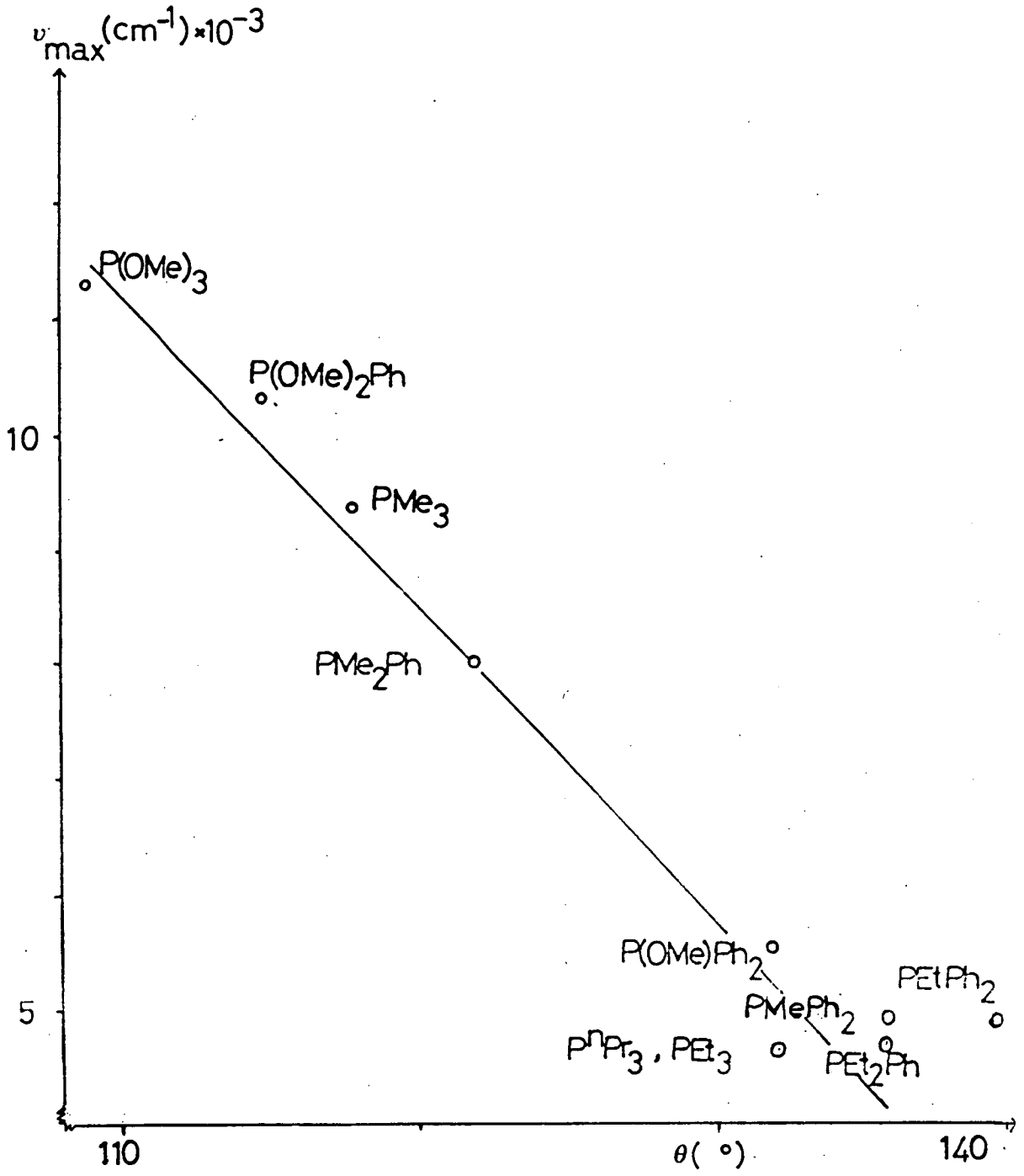

delocalisation for these two compounds; the greatest being for the slightly less basic L=PMe_3. When L=$P(OMe)_3$, which is the least basic ligand used in the study, the most intense near infra-red absorption lies at the highest energy observed (11,350 cm^{-1}). There is a correlation within the group of $PR_{3-x}Ph_x$, x = 0, 1, 2 ligands which is shown in Figure 4.2.12; the interaction decreasing as the basicity decreases as suggested (c.f. relation of ν_{max} to electronic parameter). The steric parameter does however also decrease as the basicity decreases within these groups of ligands.

We conclude therefore that the steric parameter, θ, of the tertiary phosphine ligand is the major factor contributing to the extent of metal-metal interaction in these complexes. Interestingly, the spectrum of the related complex $[(NH_3)_3Ru(\mu\text{-}Cl)_3Ru(NH_3)_3]^{2+}$ [33] can now be re-examined and interpreted on steric grounds rather than π-basicity. Thus for L=NH_3 we would expect θ to be small and hence the intense $a_1' \rightarrow a_2''$ transition to be at high energy with a large separation to the much weaker $e'' \rightarrow a_2''$ transition at lower energy. Experimentally $[(NH_3)_3Ru(\mu\text{-}Cl)_3Ru(NH_3)_3]^{2+}$ is observed to have an intense transition at 17,150 cm^{-1} and a weaker transition at 7140 cm^{-1}.

A further point to note regarding the spectra of the $[L_3Ru(\mu\text{-}X)_3RuL_3]^{2+}$ species is that the most intense band which we assign as a $a_1' \rightarrow a_2''$ transition is not always the higher energy band. For ligands with small θ, then the most intense band is at highest energy. However as θ increases so the bands become almost equal in intensity and for the largest values of θ the low energy band has greatest intensity.

Figure 4.2.12: Graph of $\nu_{max}(cm^{-1})$ versus pK_a for $[L_3Ru(\mu\text{-}Cl)_3RuL_3]^{2+}$ in Methylene Chloride / 0.5M $TBABF_4$ at T = 266K

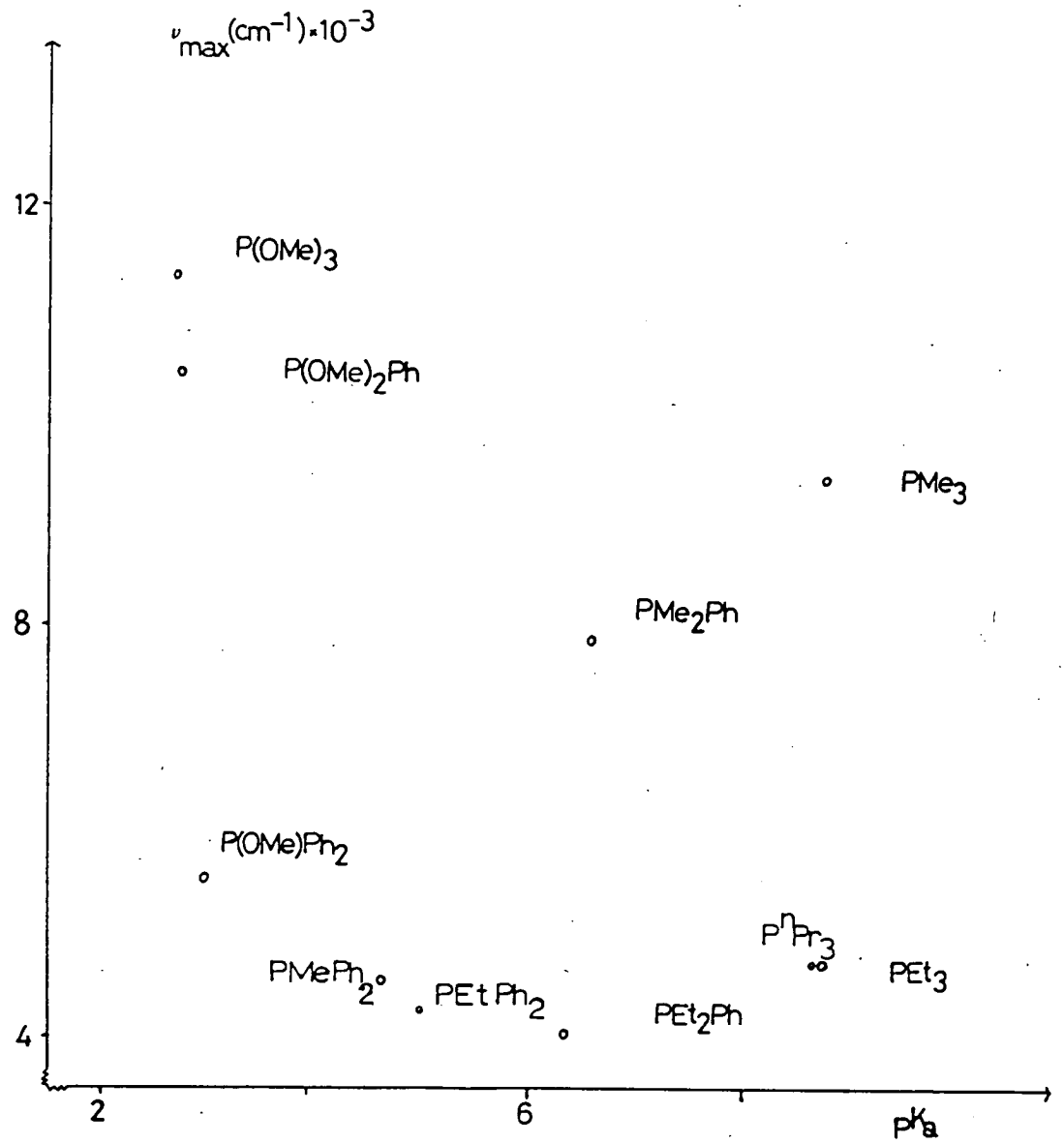

Figure 4.2.13 illustrates this, showing the spectra observed for the species where L=PMe_3 (θ=118°), PMe_2Ph (θ=122°) and PEt_2Ph (θ=136°). The molecular orbital scheme discussed in Chapter 1 shows the following order of energy levels

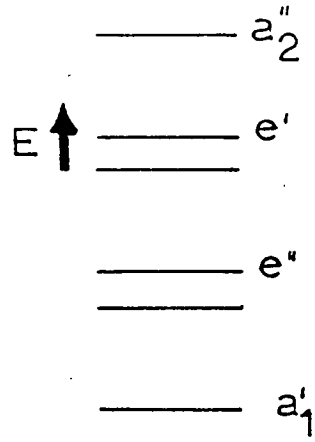

which suggests that the intense $a_1' \rightarrow a_2''$ transition should be higher in energy than the $e'' \rightarrow a_2''$ transition.

The work of Hoffman[40] on the triple chloro-bridged species $[Cl_3M(\mu\text{-}Cl)_3MCl_3]^n$ and $[(CO)_3M(\mu\text{-}Cl)_3M(CO)_3]^m$ where M=Fe, Re; n, m = charge of complex, calculated that as the M-$\hat{Cl}$-M angle increases the e" and a_1 orbitals cross over in energy. See Figure 4.2.14. We therefore considered that a similar crossing of orbitals might be occurring in our systems, thus explaining the phenomenon noted above.

The crystal structures of several $[L_3Ru(\mu\text{-}Cl)_3RuL_3]^+$ species where L=PEt_2Ph, PMe_2Ph and PMe_3 show that as the size of the ligand increases, the Ru-$\hat{Cl}$-Ru angle and the metal-metal distance also increase reinforcing the above suggestion.

Thus for tertiary phosphine ligands with small values of θ and hence an overall structure close to the model system, we would predict the intense $a_1' \rightarrow a_2''$ transition at

Figure 4.2.13: Electronic Absorption Spectra of $[L_3Ru(\mu\text{-}Cl)_3RuL_3]^{2+}$ where L = PMe_3, PMe_2Ph and PEt_2Ph in Methylene Chloride / 0.5M $TBABF_4$

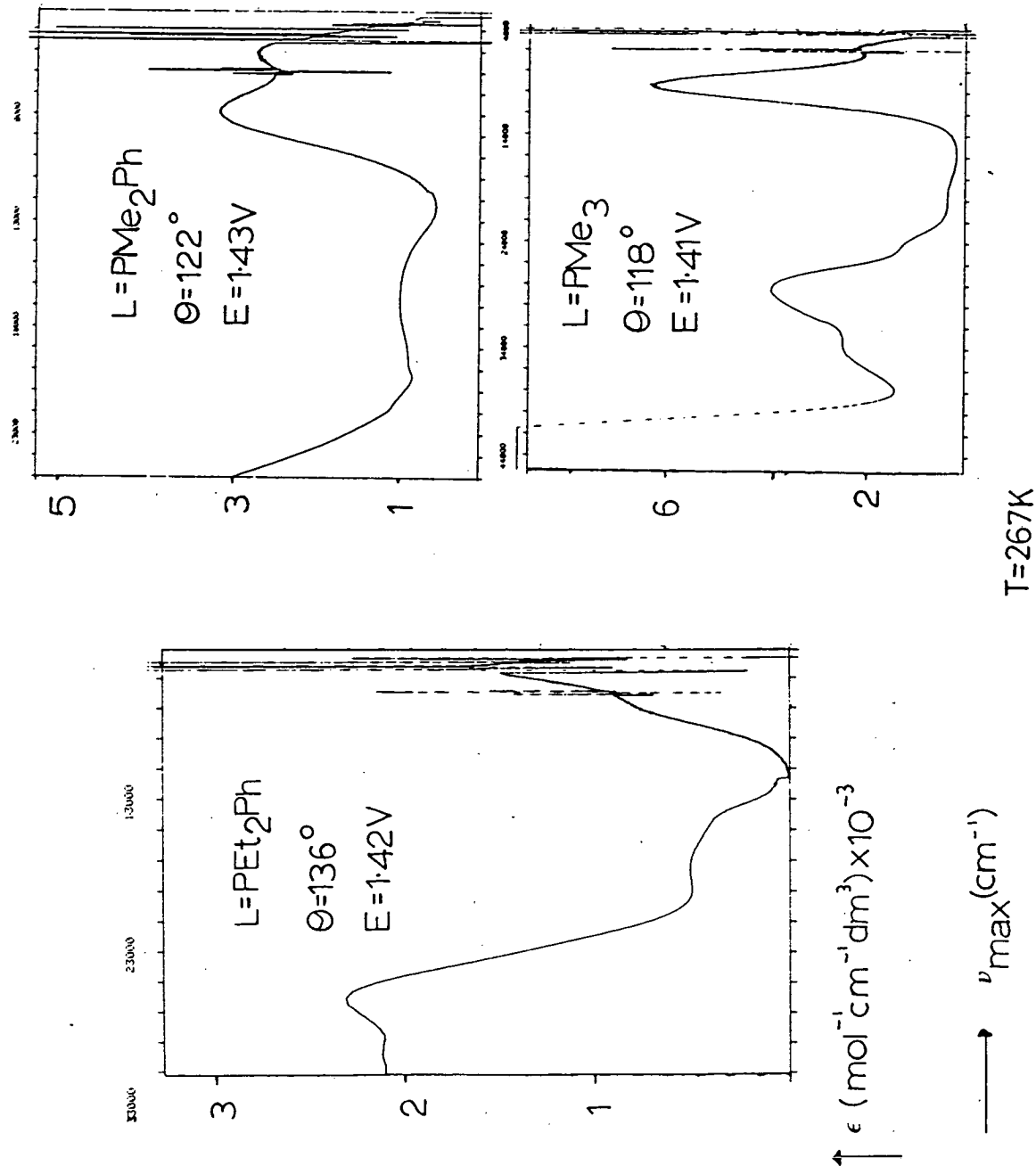

Figure 4.2.14: Difference in Energy between Some Energy Levels of $(CO)_3M(\mu\text{-}Cl)_3M(CO)_3$ and $(CO)_3MM(CO)_3$ as a Function of M-$\hat{Cl}$-M angle

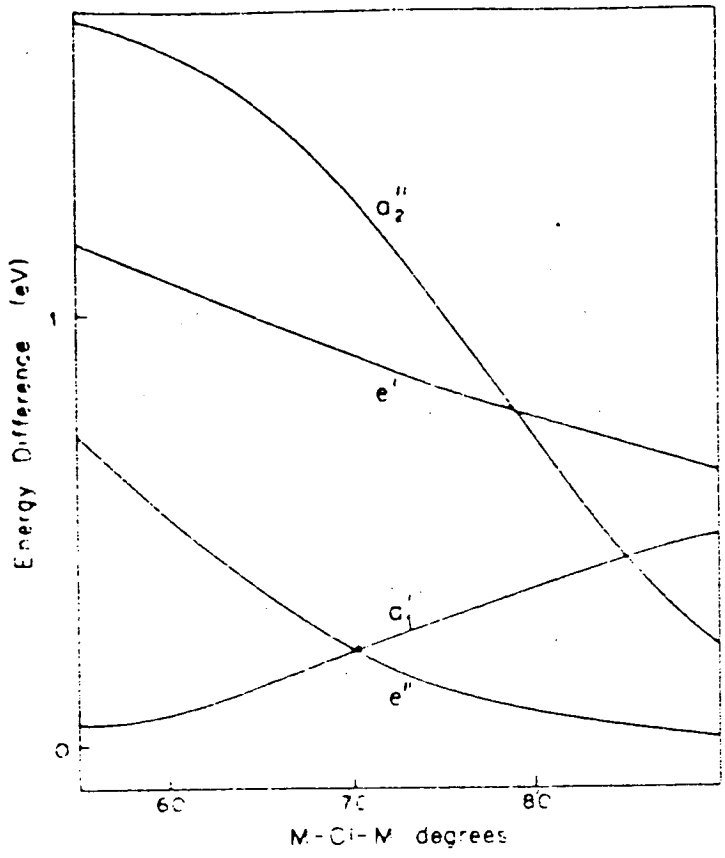

(from Hoffman, 1979, reference 40)

higher energy than the weaker $e'' \rightarrow a_2''$ transition. As θ increases so the two transitions become energetically more equivalent until for large values of θ the weaker $e'' \rightarrow a_2''$ transition is higher in energy than the $a_1' \rightarrow a_2''$ transition.

A similar argument can be applied to the complexes studied in Chapter 3 where as the size of the bridging ligand increased the $a_1' \rightarrow a_2''$ transition decreased in energy and the $e'' \rightarrow a_2''$ transition increased.

When $X^- = Br^-$ we observe analogous behaviour. The results are given in Table 4.2.9. Figure 4.2.15 shows the graph of ν_{max} versus θ. For L=$PEtPh_2$, PMe_2Ph and $P(OMe)Ph_2$ the most intense near infra-red band ($a_1' \rightarrow a_2''$ transition) is at lower energy than when $X^- = Cl^-$ (or approximately the same) indicating weaker metal-metal interaction (or approximately the same). Rather surprisingly, however when L = $P(OMe)_2Ph$ and $P(OMe)_3$ the most intense near infra-red band is observed at higher energy than when $X^- = Cl^-$ indicating stronger metal-metal interaction. This may be a consequence of the smaller size of these terminal ligands together with the larger size of the bridging ligand Br^- giving rise to more efficient packing.

(ii) <u>M=Osmium</u>

In contrast with the ruthenium compounds the position of the most intense near infra-red band in the diosmium species shows no correlation with either the electronic parameter, χ, or the steric parameter, θ, of the phosphine ligand. This is shown in Figures 4.2.16 and 4.2.17 i.e. the extent of metal-metal interaction is not dependent on either

Graph 4.2.15: Graph of $\nu_{max}(cm^{-1})$ versus $\theta(°)$ for $[L_3Ru(\mu\text{-}Br)_3RuL_3]^{2+}$ at T = 267K in Acetone / 0.1M $TBABF_4$

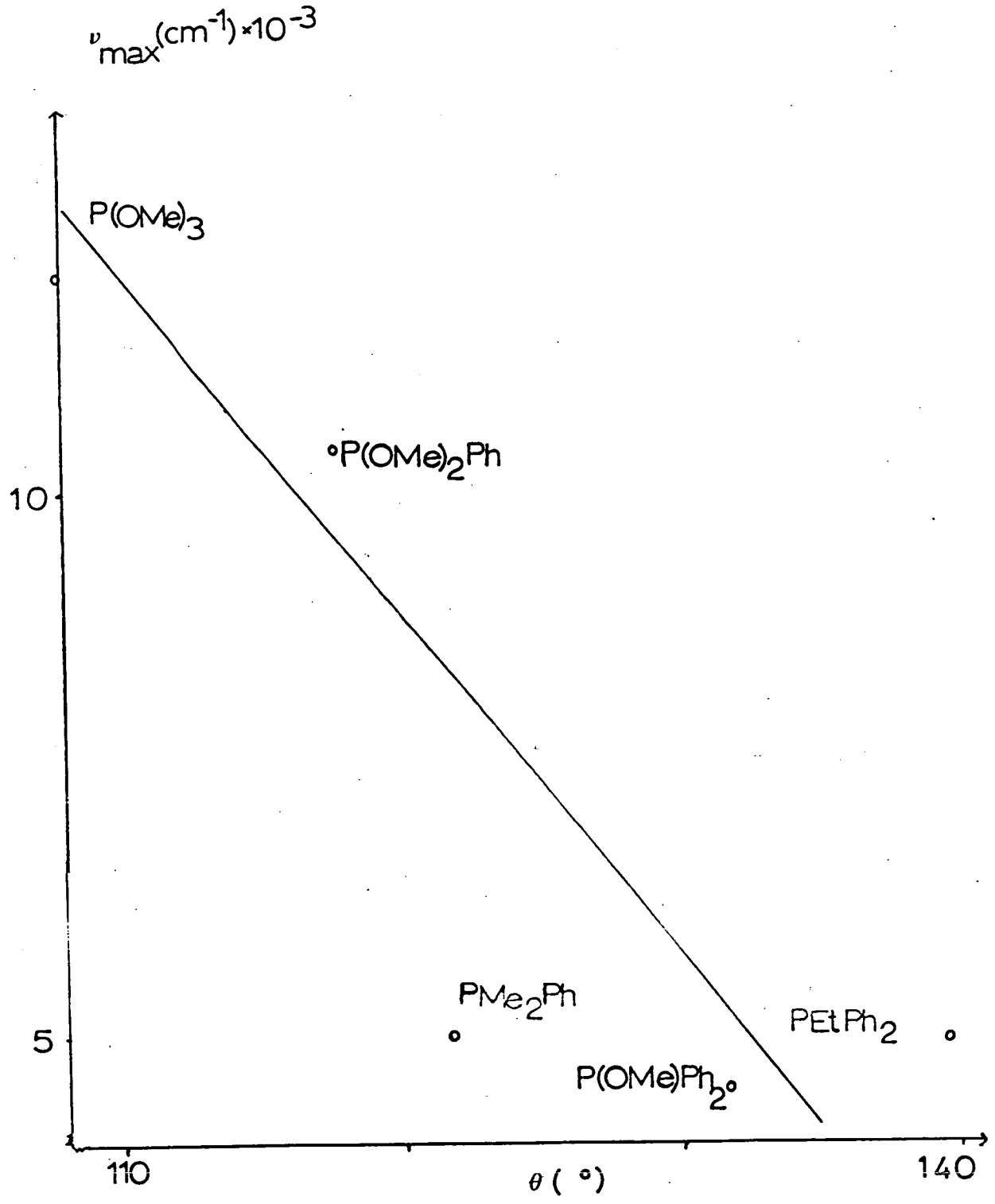

Figure 4.2.16: Graph of $\nu_{max}(cm^{-1})$ versus $\chi(cm^{-1})$ for $[L_3Os(\mu\text{-}Cl)_3OsL_3]^{2+}$ where L = tertiary phosphine ligand at T = 266K in Methylene Chloride / 0.5M $TBABF_4$

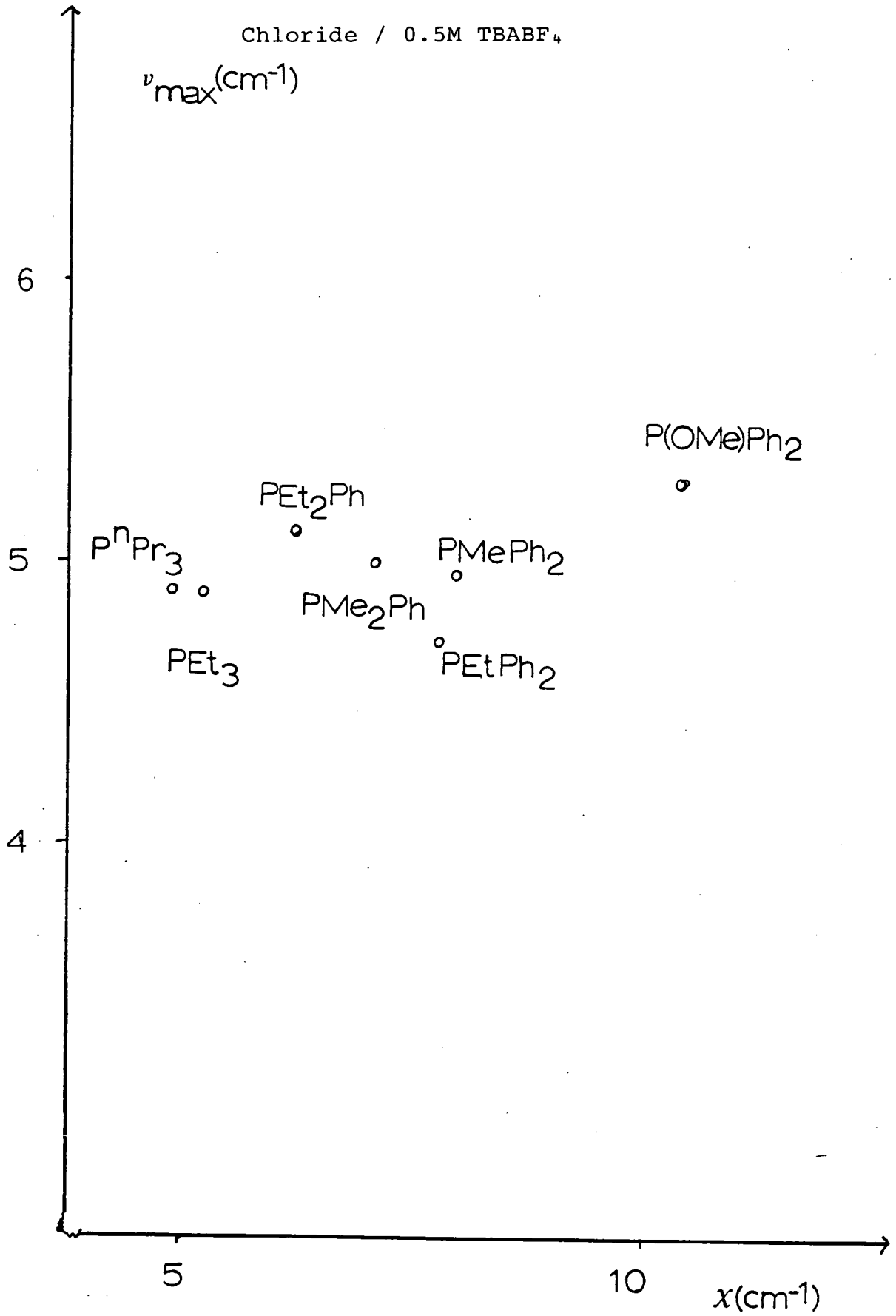

Figure 4.2.17: Graph of $\nu_{max}(cm^{-1})$ versus $\theta(°)$ for $[L_3Os(\mu\text{-}Cl)_3OsL_3]^{2+}$, where L = tertiary phosphine ligand, at T = 266K in Methylene Chloride / 0.5M $TBABF_4$

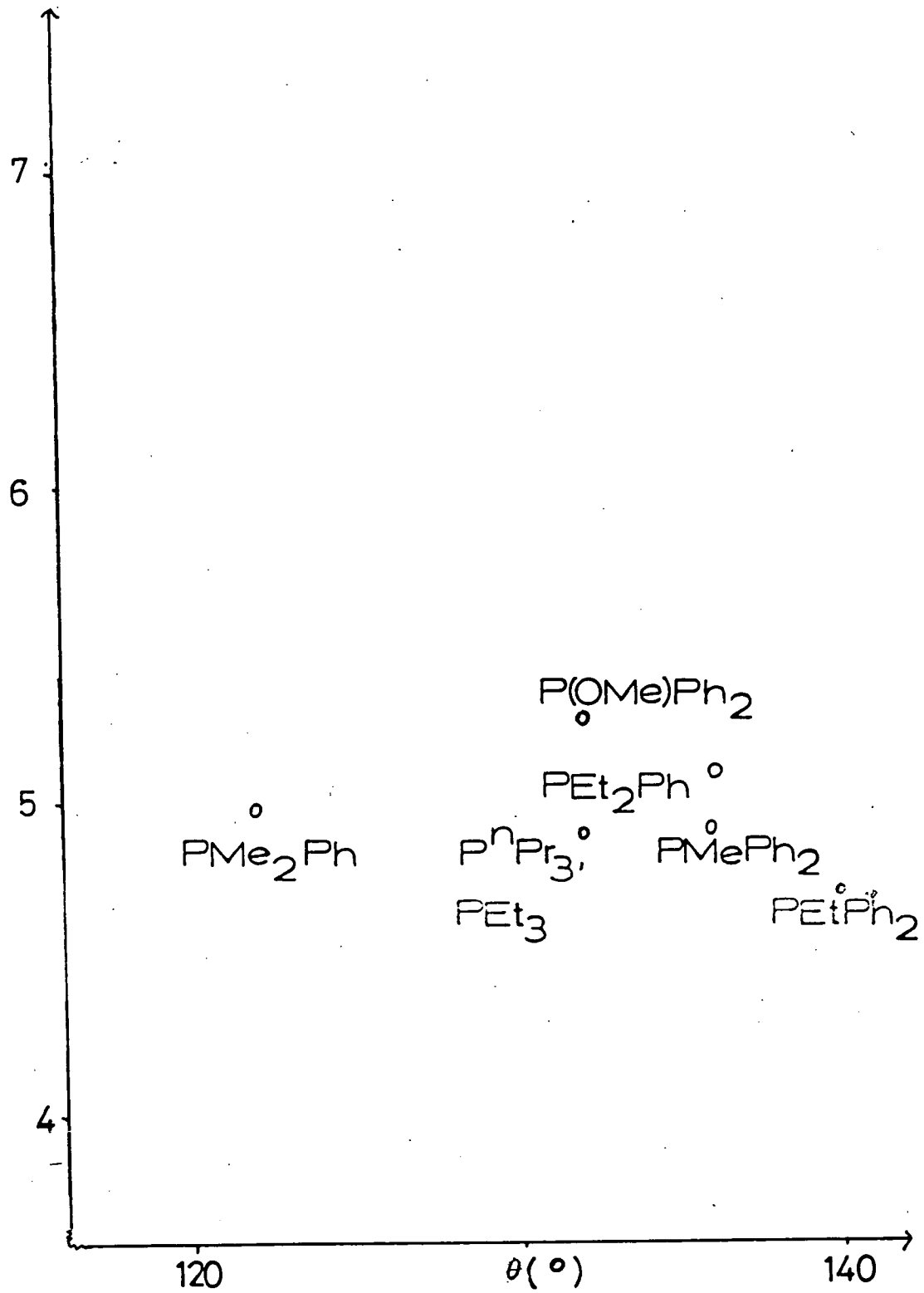

the electronic or steric effect of the terminal tertiary phosphine ligand. It was also observed that the most intense band is always at lower energy regardless of the size of the tertiary phosphine ligand. This is shown in Figure 4.2.18. The range in energy of this band is very small from 4700-5300 cm^{-1}.

The triple bridged species all have a confacial bioctahedral structure but the angles and distances are dependent on the tertiary phosphine ligand present. As the ligand geometry departs from that of an ideal octahedron then the amount of overlap of the d-orbitals will decrease. Since the 5d orbitals of osmium are more diffuse than the 4d ruthenium orbitals the difference in geometry will be more obviously felt in the diruthenium species.

The crystal structure of the osmium species where L=PEt_3 has been discussed in Chapter 2. The Os--Os distance, the average Os-$\hat{Cl}$-Os and P-$\hat{Os}$-P angles are shown below together with those of the related species where L=PMe_2Ph.

L	Os--Os(Å)	Os-$\hat{Cl}$-Os(°)	P-$\hat{Os}$-P(°)
PEt_3	3.473 (1)	88.25	96.68
PMe_2Ph	3.440 (1)	87.00	95.64

Similar trends to those present in the ruthenium systems are apparent i.e. as the terminal ligand becomes bulkier the Os--Os distance, the Os-$\hat{Cl}$-Os and P-$\hat{Os}$-P angles all increase. The P-$\hat{Os}$-P angles show a greater effect than in the ruthenium complexes (see section 4.3). Thus in the solid state when M=Os, we do see geometric changes on altering the terminal ligand, L.

Figure 4.2.18: Electronic Absorption Spectra of $[L_3Os(\mu\text{-}Cl)_3OsL_3]^{2+}$ where L = PMe_2Ph and $PEtPh_2$ in Methylene Chloride / 0.5M $TBABF_4$

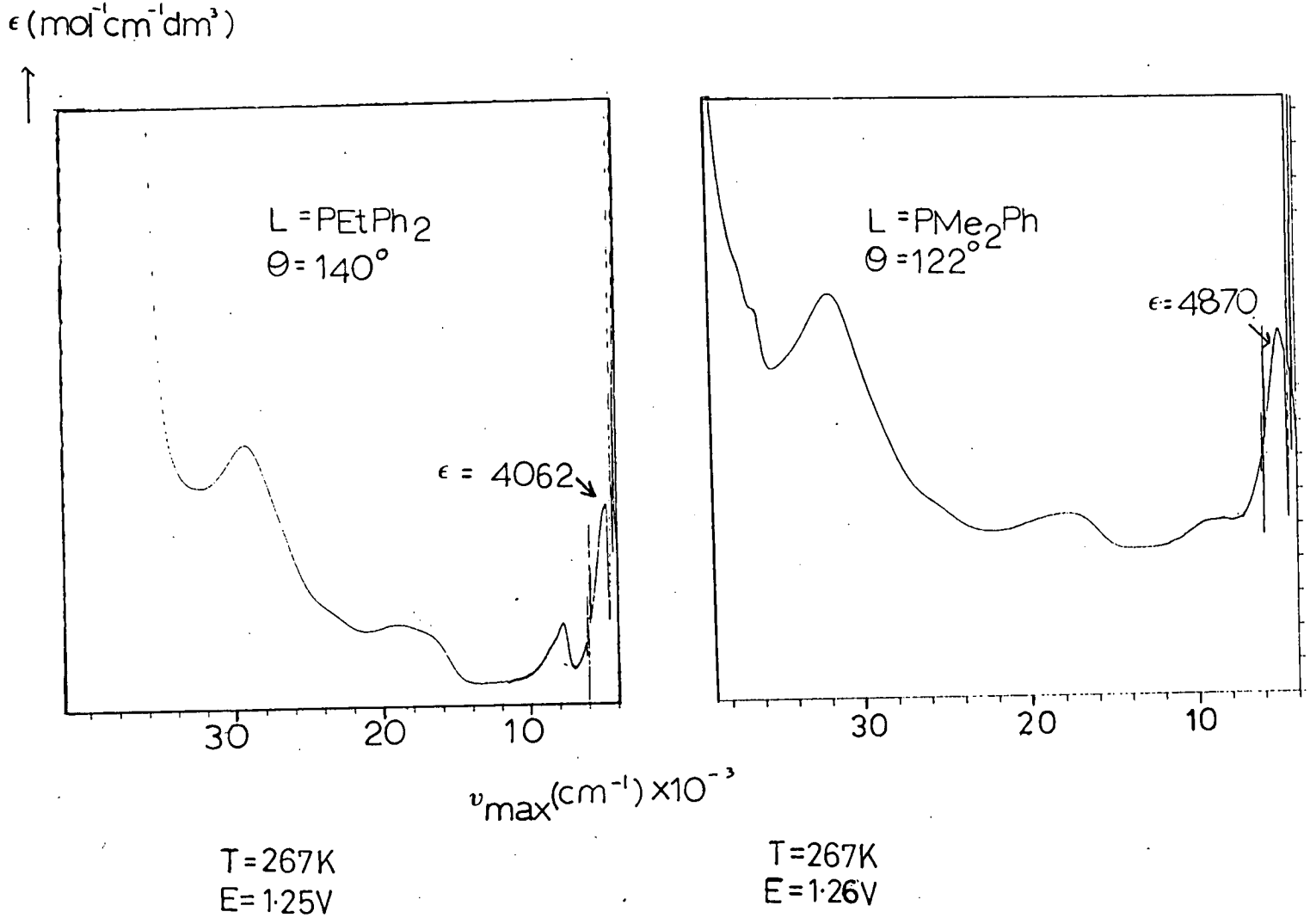

2. Visible and UV Bands

The weak broad band ($\Delta\sim8000$ cm^{-1}) between 15,000 - 18,000 cm^{-1} which in some compounds is split into more than one band is assigned as a tertiary phosphine $\pi \rightarrow a_2''$ transition. The band position shifts on changing the tertiary phosphine ligand but there is no relation between the position and the steric or electronic parameter of the ligand.

The higher energy band centred around 25,000 cm^{-1} is thought to be due to a tertiary phosphine intraligand absorption similarly assigned in the $[L_3M(\mu\text{-}X)_3ML_3]^+$ species. As mentioned previously this does not shift appreciably upon oxidation as expected for intraligand absorption (see Chapter 1, section 1.1).

(c) $[L_3M(\mu\text{-}X)_3ML_3]^{3+}$

On oxidation to the +3 oxidation state all osmium complexes showed a shift of the two near infra-red bands to higher energy. The spectra are once again almost invariant with terminal ligand, L. The values are shown in Table 4.2.11. In most cases the bands become more intense as the complex is oxidised from $[L_3Os(\mu\text{-}Cl)_3OsL_3]^{2+}$ to $[L_3Os(\mu\text{-}Cl)_3OsL_3]^{3+}$, see Figure 4.2.19. Both of these factors indicate an increase in metal-metal interaction upon oxidation. The positions of the bands exhibit no direct correlation with either the steric parameter, θ, or the electronic parameter, χ, of the tertiary phosphine ligand. The increased metal-metal interaction will probably result in a smaller metal-metal distance which may have caused

Table 4.2.11: Positions of Bands (ν_{max}) in the Electronic Absorption Spectrum of $[L_3Os(\mu\text{-}Cl)_3OsL_3]^{3+}$ in Methylene Chloride / 0.5M $TBABF_4$ at T = 243K

L	ν_{max} (cm^{-1})	ε ($mol^{-1}cm^{-1}dm^3$)
$PMePh_2$	10,955	7,441
	15,075	2,113
	30,600	5,635
PMe_2Ph	11,483	7,220
	14,934	2,116
	32,051	5,421
$PEtPh_2$	10,753	12,463
	14,863	2,654
	29,400	6,433
PEt_2Ph	11,343	3,478
	17,000	3,043
PEt_3	11,939	10,575
	14,900	770
	18,464	1,030
	20,200	858
	21,600	927
	31,606	4,669
P^nPr_3	11,814	10,273
	15,000	8,504
	18,200	1,276
	20,000	1,276
	21,132	1,343
	31,929	5,237

/ continued

Table 4.2.11: continued

L	ν_{max} (cm^{-1})	ε ($mol^{-1}cm^{-1}dm^3$)
$P(OMe)Ph_2$	10,965	6,788
	14,277	3,674
	31,800	9,424

Table 4.2.12: Positions of Bands (ν_{max}) in the Electronic Absorption Spectrum of $[(P(OMe)_3)_3Ru(\mu\text{-}Br)_3Ru(P(OMe)_3)_3]^{3+}$ in CH_2Cl_2 / 0.5M $TBABF_4$ at T = 267K

L	ν_{max} (cm^{-1})	ε ($mol^{-1}cm^{-1}dm^3$)
$P(OMe)_3$	25,330	5,794
	33,400	5,142

Figure 4.2.19: Electronic Absorption Spectrum showing Conversion of $[(PMePh_2)_3Os(\mu\text{-}Cl)_3Os(PMePh_3)_3]^{2+}$ → $[(PMePh_2)_3Os(\mu\text{-}Cl)_3Os(PMePh_2)_3]^{3+}$ in Methylene Chloride / 0.5M $TBABF_4$

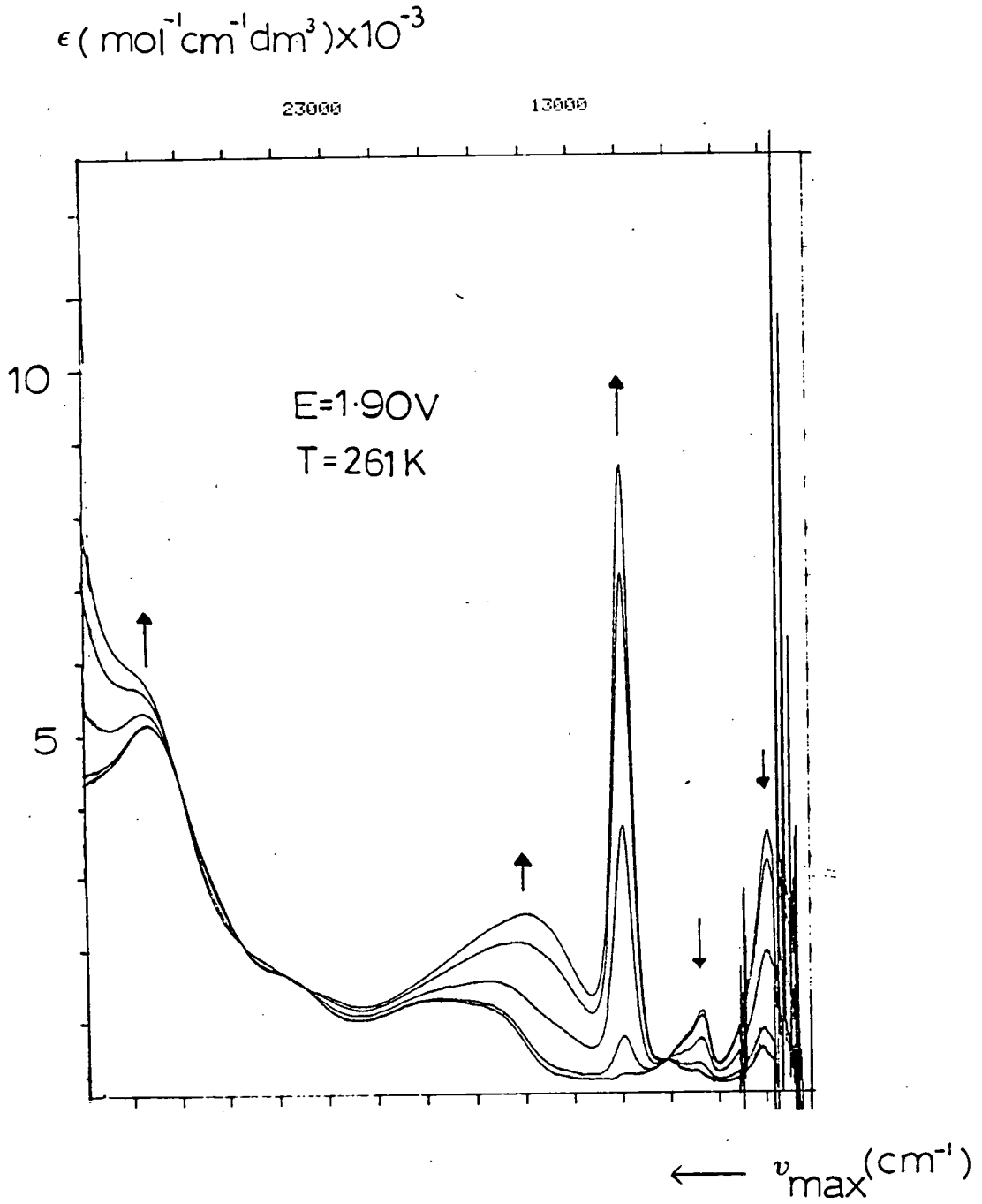

the steric effect to become important but this does not seem to be the case.

Oxidation of $[(P(OMe)_3)_3Ru(\mu\text{-}Br)_3Ru(P(OMe)_3)_3]^{2+}$ to $[(P(OMe)_3)_3Ru(\mu\text{-}Br)_3Ru(P(OMe)_3]^{3+}$ showed a similar effect to that in the osmium complexes, but only one broad band was observed. This was however found to shift to a greater extent than in the osmium complexes, shifting by 13,000 cm^{-1} for M=Ru, but only 6,000 cm^{-1} for M=Os. See Figure 4.2.20 and Table 4.2.12 The related $[(NH_3)_3Ru(\mu\text{-}Cl)_3Ru(NH_3)_3]^{3+}$ species has been observed and shows analogous behaviour. The shift in ν_{max} in this case is 11,000 cm^{-1}.[33(b)]

The fact that no other species of the type $[L_3Ru(\mu\text{-}X)_3RuL_3]^{3+}$, where L = tertiary phosphine ligand, was observed is significant. $P(OMe)_3$ is the smallest tertiary phosphine ligand used in our studies and only $[(P(OMe)_3)_3Ru(\mu\text{-}Br)_3Ru(P(OMe)_3)_3]^{3+}$ is stable on a timescale long enough for study. All other ruthenium species decomposed in the +3 oxidation state even when $L=P(OMe)_3$ and $X^-=Cl^-$. However we note that $[(NH_3)_3Ru(\mu\text{-}Cl)_3Ru(NH_3)_3]^{3+}$, which contains a smaller terminal ligand than $P(OMe)_3$, is stable. This suggests that steric influences are important in determining the stability of the +3 oxidation state when M=Ru. In addition the increased size of the bridging ligand, Br^- rather than Cl^- is a further factor in stabilising the $[(P(OMe)_3)_3Ru(\mu\text{-}Br)_3Ru(P(OMe)_3)_3]^{3+}$ species. Thus oxidation to $[L_3Ru(\mu\text{-}X)_3RuL_3]^{3+}$, which is accompanied by increased metal-metal interaction, will result in the metal centres becoming too close together to allow the bridging halides and terminal tertiary phosphine ligands sufficient

Figure 4.2.20: Electronic Absorption Spectrum showing
(a) Conversion of
$[(P(OMe)_3Ru(\mu\text{-}Br)_3Ru(P(OMe)_3)_3]^{2+} \rightarrow$
$[(P(OMe)_3Ru(\mu\text{-}Br)_3Ru(P(OMe)_3)_3]^{3+}$
and Final Spectrum of
$[(P(OMe)_3)_3Ru(\mu\text{-}Br)_3Ru(P(OMe)_3)_3]^{3+}$
in Methylene Chloride / 0.5M $TBABF_4$

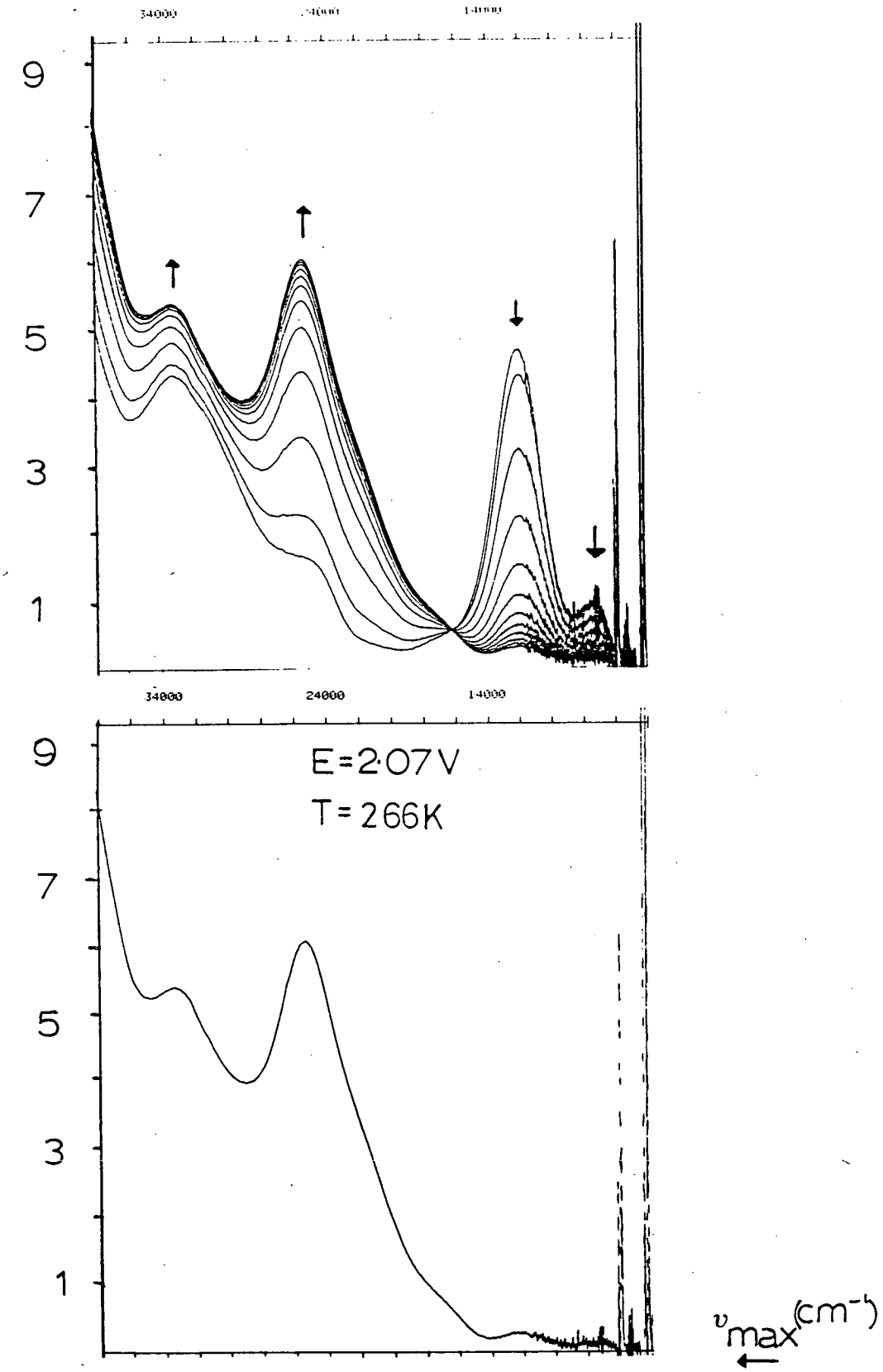

space to retain the confacial bioctahedral environment and hence decomposition takes place. A further point to note is that in the crystal structures of $[(PEt_3)_3Os(\mu\text{-}Cl)_3Os(PEt_3)_3]^{+/2+}$ discussed in Chapter 2, the average M-P bond length increased on oxidation of the monocation to the dication. It is possible that in the ruthenium binuclear species an oxidation to $[L_3M(\mu\text{-}X)_3ML_3]^{3+}$ the M-P bond has to be very long for bulkier ligands in order to retain the confacial bioctahedral structure and thus leads to decomposition.

It is unfortunate that the second oxidations of the bridging iodide species are all irreversible.

(d) Conclusions

Every symmetric triple bridged binuclear species studied of general formula $[L_3M(\mu\text{-}X)_3ML_3]^{2+/3+}$ is delocalised with strong metal-metal interactions. The extent of metal-metal interaction in ruthenium complexes is dependent on the bulk of the terminal tertiary phosphine ligand. In osmium complexes the metal-metal interaction is independent of the terminal tertiary phosphine ligand.

4.3 EXTENDED HÜCKEL MOLECULAR ORBITAL CALCULATIONS

These were carried out using the ICON 8[41] program. The atomic coordinates for the three known $[L_3Ru(\mu\text{-}Cl)_3RuL_3]^+$ crystal structures where L=PMe_3, PMe_2Ph, PEt_2Ph were used to model ideal D_{3h} systems for each of the above species (details are given in section 4.4). Each tertiary P(III) ligand had H atoms attached to it rather than the alkyl/aryl

groups actually present as the main limitation of the ICON 8 program is that it can only be used for compounds of up to fifty atoms of which only forty can be non-hydrogen. The replacement of PR_2R' or PR_3 by PH_3 is not considered to be a simplification in the first instance since we have already shown that the electronic properties of the terminal ligand do not significantly influence the metal-metal interaction. The geometric orientation of the ligands is important and we have taken this into account by imposing real experimental values on the system rather than model ones as was the case in the molecular orbital calculations described in Chapter 1. In each idealised system the average of the Ru-$\hat{Cl}$-Ru and P-$\hat{Ru}$-P angles and the Ru--Ru distance had the same values as those found crystallographically. The molecule was given a charge of +2 in the program. It is important to note that the coordinates used are for the $[L_3Ru(\mu\text{-}Cl)_3RuL_3]^+$ so it is unlikely that accurate results can be obtained but trends should become apparent.

The energies of the molecular orbitals were calculated and the orbitals were assigned using symmetry consideration for a complex with overall D_{3h} symmetry. The results are shown in Table 4.3.1.

Experimentally we observe two NIR bands. The intense band was assigned to the $a_1' \rightarrow a_2''$ transition and the weaker band to the $e'' \rightarrow a_2''$ transition. For ligands with small θ the intense band is at high energy and for large θ it is at low energy compared to the weaker band. Thus we hoped to observe a cross over in energy of the a_1' and e" orbitals in the calculations for the three real examples

Table 4.3.1: Energies of the Orbital Sets from E.H.M.O. Calculations for $[L_3Ru(\mu\text{-}Cl)_3RuL_3]^{2+}$

L	E (eV) e"	a_1'	e'	$a_2"$	Av Ru-$\hat{Cl}$-Ru(°)
PEt_2Ph	-13.63170	-13.35850	-13.30378	-13.31467	87.9
PMe_2Ph	-13,63648	-13.41356	-13.32350	-13.27932	86.0
PMe_3	-13.63493	-13.49574	-13.32887	-13.17470	82.8
Theoretical Model	-13.53675	-13.76855	-13.24585	-12.93602	76.0

above with the a_1' orbitals moving to higher energy as the size of L increases and vice versa for e". The calculations are in good agreement with this (see Figure 4.3.1). However they predict that the e" orbital should be lower in energy than a_1' for all systems studied. The e" → a_1' difference does however decrease as L becomes smaller indicating the possibility of a cross over at a smaller Ru-$\hat{Cl}$-Ru angle. Both the a_1' → a_2" and e" → a_2" differences increase in the order $PEt_2Ph<PMe_2Ph<PMe_3$.

In these systems the Ru--Ru distance is found to be directly proportional to the Ru-$\hat{Cl}$-Ru angle (see Figure 4.3.2). We decided to extrapolate from this and hence model a system with a smaller Ru--Ru distance and Ru-$\hat{Cl}$-Ru angle. Again it must be stressed that our model is based on the species $[L_3Ru(\mu\text{-}Cl)_3RuL_3]^+$ where each ruthenium centre has the oxidation state II and they are not interacting. For the $[L_3Ru(\mu\text{-}Cl)_3RuL_3]^{2+}$ species both the ruthenium centres have an oxidation state of 2.5 and there is a strong interaction present. The related complex $[(PEt_3)_3Os(\mu\text{-}Cl)_3Os(PEt_3)_3]^+$ has been shown to have analogous behaviour. We have shown in Chapter 2 that the oxidation of $[(PEt_3)_3Os(\mu\text{-}Cl)_3Os(PEt_3)_3]^+$ to $[(PEt_3)_3Os(\mu\text{-}Cl)_3Os(PEt_3)_3]^{2+}$ leads to a decrease of 6pm in the metal-metal distance. The extrapolation is therefore valid.

The related mixed-valence complexes $Cl(P^nBu_3)_2Ru(\mu\text{-}Cl)_3Ru(P^nBu_3)Cl$,[42] $[(NH_3)_3Ru(\mu\text{-}Cl)_3Ru(NH_3)_3]^{2+}$[43] and $[(NH_3)_3Ru(\mu\text{-}Br)_3Ru(NH_3)_3]^{2+}$[44] have been characterised crystallographically and the Ru--Ru distances and Ru-$\hat{X}$-Ru angles are respectively: 3.12Å, 79.3°; 2.753Å, 70.2° and

Figure 4.3.1: Walsh Diagram showing the variation in the Energies (eV) of the Orbitals as the Ru-$\hat{Cl}$-Ru angle(°) increases

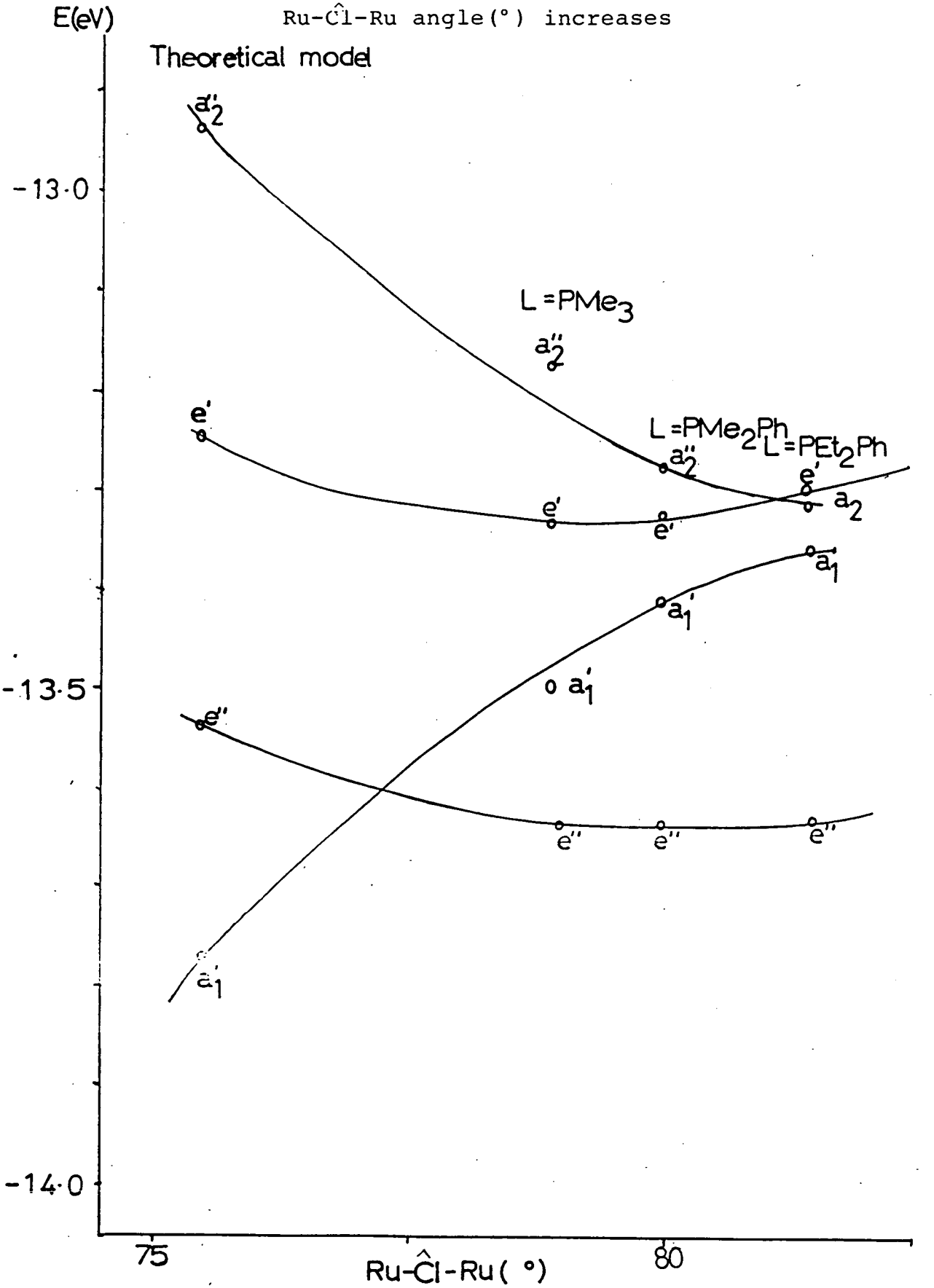

Figure 4.3.2: Graph of Ru-$\hat{Cl}$-Ru angle(°) versus Ru--Ru Distance for Three Structurally Characterised Species of the type $[L_3Ru(\mu\text{-}Cl)_3RuL_3]^+$ where L = PEt_2Ph, PMe_2Ph and PEt_3

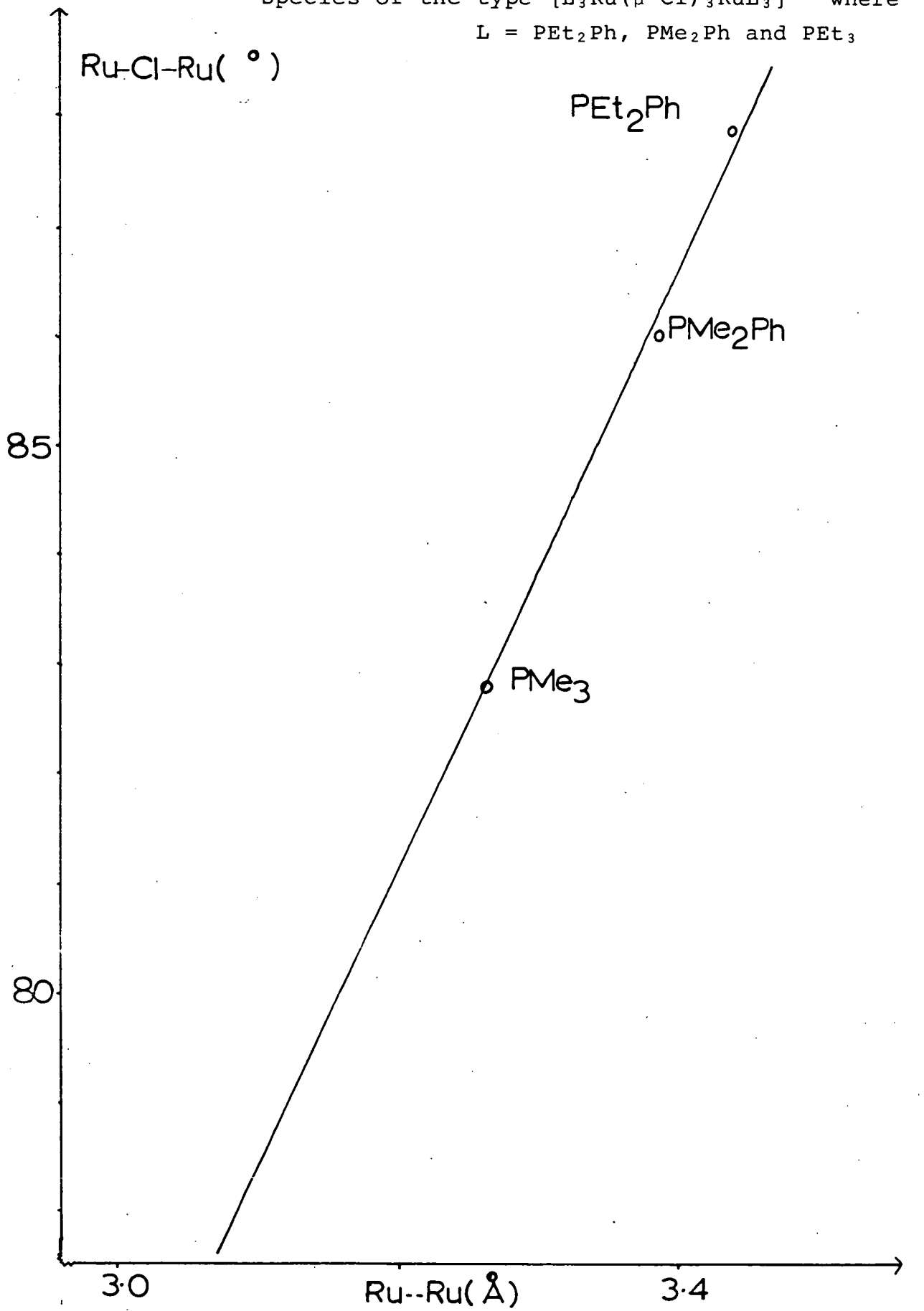

2.852Å, 68.5°, thus reinforcing the above argument.

On extrapolation an Ru-$\hat{Cl}$-Ru angle of 78° was obtained for an Ru--Ru distance of 3.09Å. A model was constructed to obtain atomic coordinates for an ideal D_{3h} system with these geometric parameters. The energies obtained are shown in Table 4.3.1. The a_1' energy level is now lower in energy than the e" i.e. we have observed a cross over of the e" and a_1' orbitals. A Walsh diagram was constructed for all four species to show this effect. This is shown in Figure 4.3.1. Drawings of the orbitals are shown in Figure 4.3.3. From the Walsh diagram the e" and a_1' orbitals cross over when Ru-$\hat{Cl}$-Ru = 79.5° and Ru--Ru = 3.14Å.

Further points of interest from the Walsh diagram together with the drawings of the orbitals are:

1. The a_1' and a_2'' orbitals are metal-based and represent the bonding and antibonding interactions of the d_{z^2} orbitals respectively along the metal-metal axis. The a_1' increases dramatically in energy i.e. becomes less stable as the Ru-$\hat{Cl}$-Ru angle increases (or as the Ru--Ru distance increases). This effect is expected, as the overlap between the atomic orbitals is decreasing. The opposite effect occurs for the antibonding a_2'' orbital.
2. The e' and e" bonding and antibonding orbitals consist mainly of contributions from the $d_{x^2-y^2}$ and d_{xy} atomic orbitals on each ruthenium centre. The e' and e" orbitals vary only slightly in energy as the Ru-$\hat{Cl}$-Ru angle alters. This is as expected because the extent of orbital overlap is smaller than with the a set.

Figure 4.3.3: Drawing of the Frontier Molecular Orbitals of $[L_3Ru(\mu\text{-}Cl)_3L_3]^{2+}$

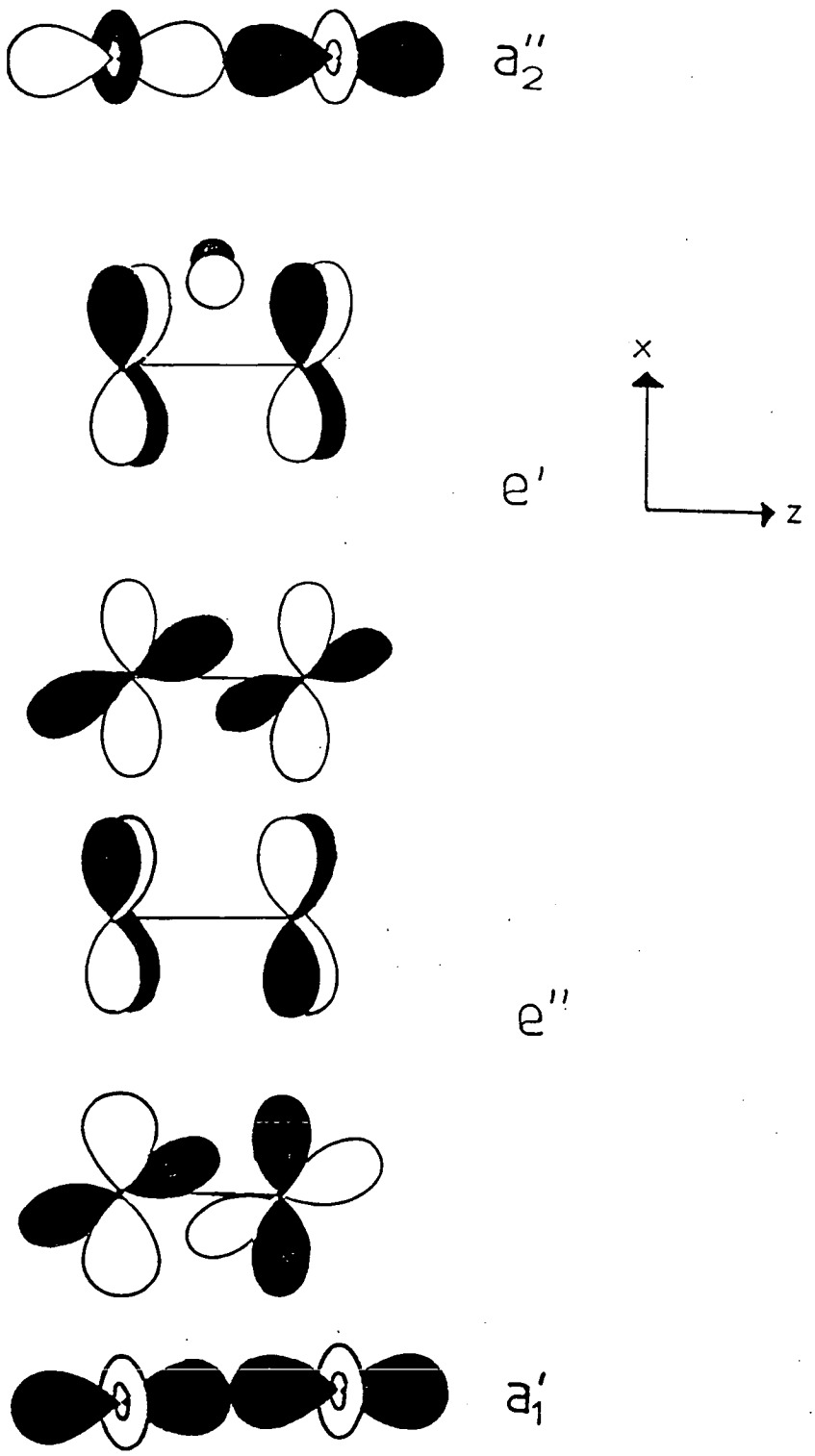

The molecular orbitals of a symmetry result due to σ-overlap whereas the e set result from δ overlap.

The e' pair is primarily metal-based with an antibonding Cl⁻Py contribution; the e" pair however were shown by symmetry to be entirely metal-based. This accounts for the higher energy of the e' pair compared to the e" pair. The e" orbital becomes more stable as the metal-metal distance increases as expected for an antibonding molecular orbital. The e' set however decrease then increase again and become even higher in energy than the a_2" orbital. This is thought to be a consequence of two interacting factors which result from increasing the metal-metal distance.

(i) The Cl⁻Py antibonding interaction decreases, hence the e' orbital is stabilised.

(ii) The metal bonding interaction decreases so the e' orbital is destabilised.

Finally in all systems studied the P-$\hat{Ru}$-P angle does not vary by much.

P	P-$\hat{Ru}$-P (form crystal structure)	P-$\hat{Ru}$-P (models)
PEt_2Ph	96.8°	96.6°
PMe_2Ph	95.3°	95.9°
PMe_3	95.4°	95.4°
Theoretical Model	-	94.2°

The calculations therefore suggested that the steric effect results from the terminal ligands at one metal centre interacting with those of the other end. Space filling diagrams[45] were constructed for the three known systems. These are

shown in Figures 4.3.4 - 4.3.6. It is clear from the diagrams that this effect is indeed occurring and that for bulky ligands as the species are oxidised and the metal-metal distance becomes smaller we would expect there to be severe crowding of the terminal ligands between the metal centre or for the M-P bond lengths to increase to counteract this effect; thus accounting for the lack of success in generating the $[L_3Ru(\mu\text{-}X)_3RuL_3]^{3+}$ species.

Conclusions

The EHMO calculations give support to the trends obtained experimentally. The steric effect results from the interaction of the terminal ligands across the bridge rather than at the metal centre.

4.4 EXPERIMENTAL

Electrochemical studies were carried out as described previously using the PAR model 170 potentiostat and programmer.

Spectroelectrochemical studies were carried out using the O.T.T.L.E. cell as previously described. The Perkin-Elmer Lambda 9 spectrophotometer was employed for these studies. Spectra were recorded over the range 3125-50000 cm^{-1}. The temperature was controlled as described previously. Elemental analyses were performed by the Chemistry Department, University of Edinburgh.

F.A.B. mass spectra were recorded by the Chemistry Department, University of Edinburgh, using the Kratos-50TC Spectrometer, using 3-nitrobenzylalcohol (3-NOBA) as the matrix.

Figure 4.3.4: Space Filling Diagram[45] of $[(PMe_3)_3Ru(\mu\text{-}Cl)_3Ru(PMe_3)_3]^+$

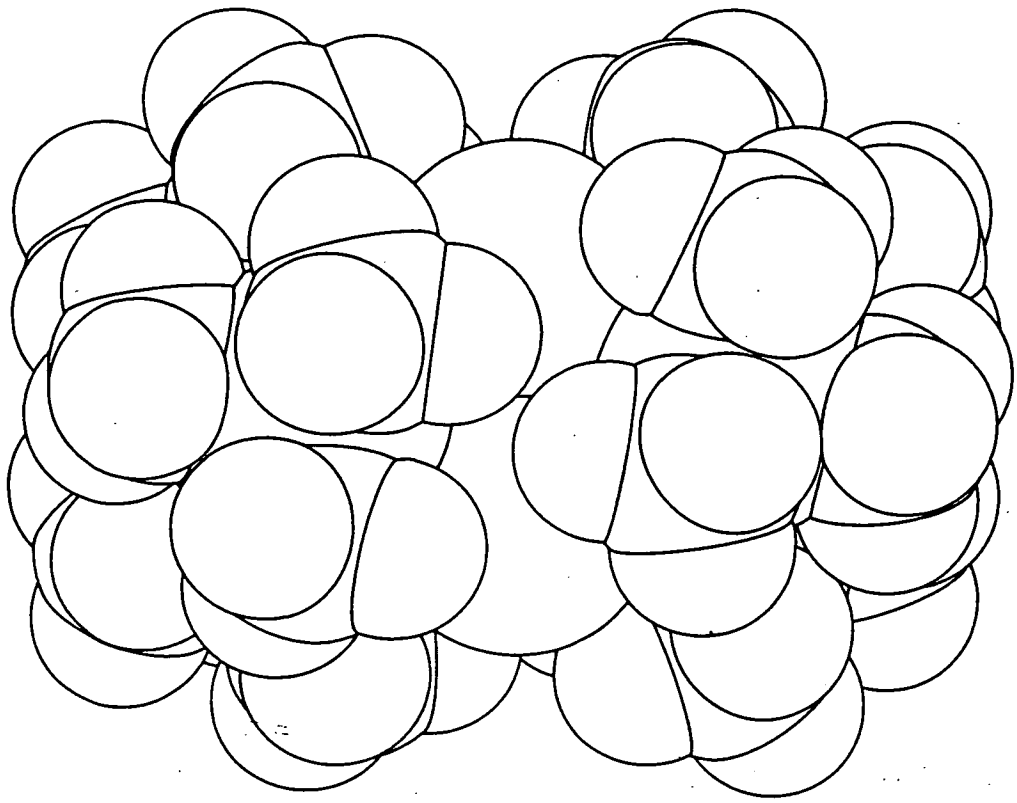

L = PMe_3

$\Theta = 118°$

Figure 4.3.5: Space Filling Diagram[45] of $[(PMe_2Ph)_3Ru(\mu\text{-}Cl)_3Ru(PMe_2Ph)_3]^+$

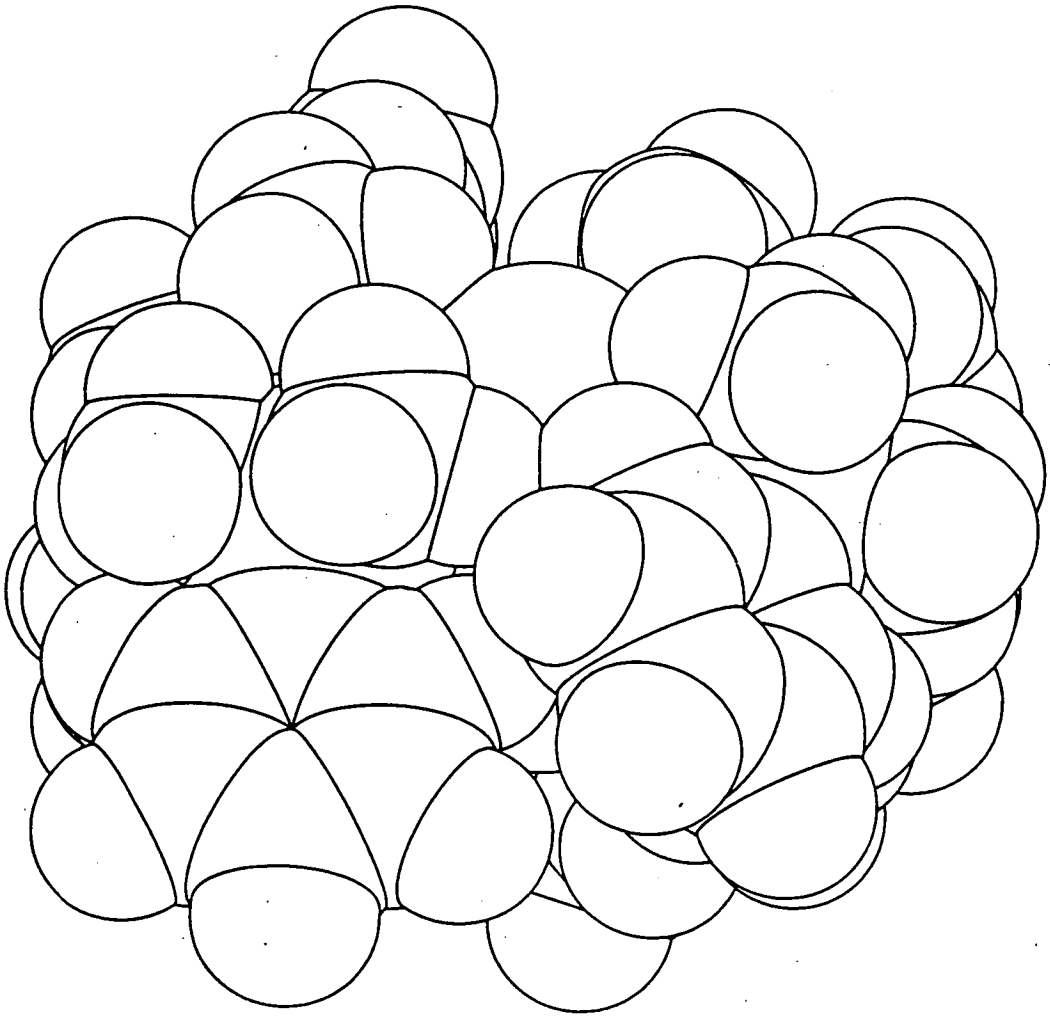

Figure 4.3.6: Space Filling Diagram[45] of

$[(PEt_2Ph)_3Ru(\mu\text{-}Cl)_3Ru(PEt_2Ph)_3]^+$

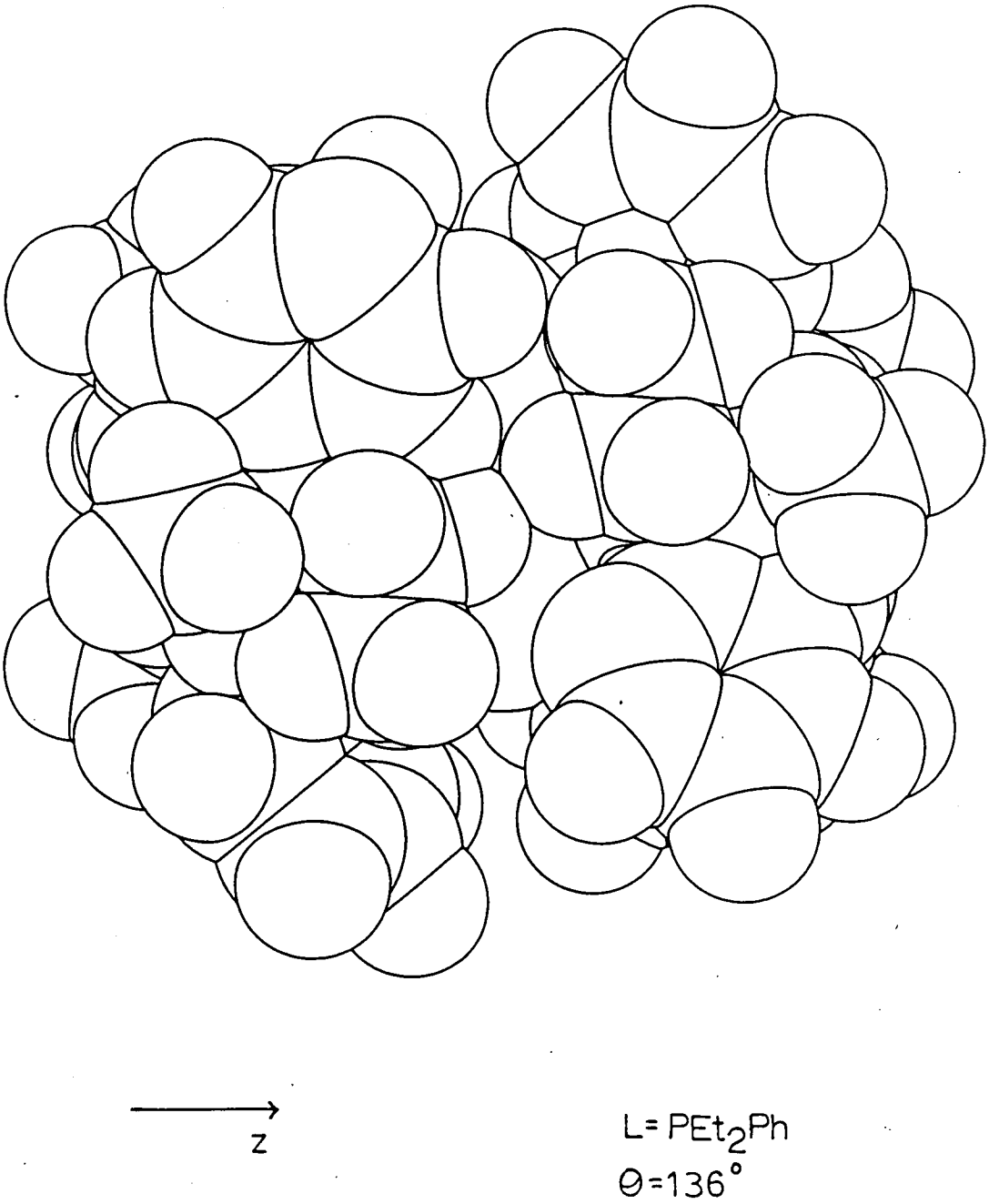

Materials

Methylene chloride was purified as described previously. All other solvents were used as supplied without further purification.

$RuCl_3$-$3H_2O$, K_2OsCl_6, Na_2OsCl_6 were obtained from Johnson Matthey.

$TBABF_4$ was prepared as previously described.

PPh_3, PEt_3, P^nPr_3, PMe_3, $P(OMe)Ph_2$, $P(OMe)_2Ph$ and $P(OMe)_3$ were obtained from Aldrich.

$PEtPh_2$, PEt_2Ph, $PMePh_2$, PMe_2Ph were prepared according to the literature method.[46]

The compounds where M=Ru, $X^-=Cl^-$, $L=PMe_2Ph$, $PMePh_2$, PEt_2Ph, $PEtPh_2$; M=Os, $X^-=Cl^-$, $L=PMePh_2$, $PEtPh_2$, PEt_3, P^nPr_3 were prepared according to the method of Chatt.[29]

M=Ru, $X^-=Cl^-$, $L=PMe_3$, PEt_3, P^nPr_3, $P(OMe)Ph_2$, $P(OMe)_2Ph$; M=Ru, $X^-=Br^-$, $L=PMe_2Ph$, $PEtPh_2$ using the method of Stephenson.[26,36]

M=Ru, $X^-=Cl^-$, $L=P(OMe)_3$; M=Ru, $X^-=Br^-$, $L=P(OMe)Ph_2$, $P(OMe)_2Ph$, $P(OMe)_3$ by extension of the method of Ashworth.[35]

M=Os, $X^-=Cl^-$, $L=PMe_2Ph$, PEt_2Ph by the method of Coombe and Stephenson.[33(b)]

M=Os, $X^-=Cl^-$, $L=P(OMe)Ph_2$ by extension of the method of Stephenson.[26,36]

1. Preparation of Tri-μ-Chlorohexakis(trimethyl phosphite) diruthenium (II,II) hexafluorophosphate.

This complex is prepared via the triply hydroxy-bridged species.

(a) Preparation of Tri-μ-hydroxyhexakis(trimethyl phosphite)diruthenium (II,II) hexafluorophosphate.

$[RuH(COD)(NH_2NMe_2)_3]PF_6$ (0.35g) was added to a degassed mixture of acetone (36.8ml) and methanol (18.4ml). To this PMe_2Ph (0.212ml) was added. This was heated to reflux under N_2. After 30 minutes degassed water (10ml) was added to the pale yellow solution. No change in colour of the solution occurred. After a short while a precipitate formed. The reaction was continued for a further two hours then the solution was cooled and filtered. The white compound resulting was washed with cold methanol then diethyl ether and dried in vacuo (0.310g, 83%).

Elemental Analysis: Found C: 18.43%, H: 4.50%, N: 0%

calculated for $C_{18}H_{43}O_{21}P_7F_6Ru_2$

C: 18.96%, H: 4.74%, N: 0%

FAB Mass Spectrum: Found $M^+ = 996$ (100%)

calculated for $[(P(OMe)_3)_3Ru(\mu\text{-}(OH)_3)Ru(P(OMe)_3)_3]^+$

$M^+ = 994$

(b) Tri-μ-hydroxyhexakis(trimethylphosphite)diruthenium (II,II) hexafluorophosphate (0.1g) was dissolved in acetone (5ml). To this an excess of concentrated HCl was added. This was shaken for ten minutes then left for

2-3 days, after which colourless crystals formed. These were filtered and washed with cold methanol and diethylether. Due to the vast excess of Cl^- present the white crystals were dissolved in methylene chloride and methanol/excess NH_4PF_6 was added. Colourless crystals formed after slow evaporation of the methylene chloride. These were filtered and washed with cold methanol and diethylether and dried in vacuo (0.083g, 79%).

Elemental Analysis: Found C: 17.80%, H: 4.45%, N: 0%

Calculated for $C_{18}H_{54}O_{18}P_7F_6Cl_3Ru_2$

C: 18.01%, H+ 4.51%, N: 0%

FAB Mass Spectrum: Found M^+ = 1054 (100%)

Calculated for $[(P(OMe)_3)_3Ru(\mu\text{-}Cl)_3Ru(P(OMe)_3)_3]^+$

M^+ = 1049

2. Preparation of Tri-μ-bromohexakis(methyldiphenyl phosphonite) diruthenium (II,II) hexafluorophosphate

As 1, but using the appropriate phosphine, $P(OMe)Ph_2$ and HBr (0.072g, 65%).

Elemental Analysis: Found C: 48.91%, H: 4.05%, N: 0%

Calculated for $C_{78}H_{78}O_6P_7F_6Br_3Ru_2$

C: 49.79%, H: 4.15%, N: 0%

FAB Mass Spectrum: Found M^+ = 1886 (0.5%), 1741 (100%)

Calculated for $[P(OMe)Ph_2)_3Ru(\mu\text{-}Br)_3Ru\text{-}(P(OMe)Ph_2)_3]PF_6$

M^+ = 1883

and $[(P(OMePh_2)_3Ru(\mu\text{-}Br)_3Ru\text{-}(P(OMe)Ph_2)_3]^+$

M^+ = 1738

3. Preparation of Tri-μ-bromohexakis(dimethylphenyl phosphinite) diruthenium (II,II) hexafluorophosphate.

As 1, but using the appropriate phosphine, $P(OMe)_2Ph$ and HBr (0.081g, 72%).

Elemental Analysis: Found C: 35.25%, H: 4.00%, N: 0%

Calculated for $C_{48}H_{66}O_{12}P_7F_6Br_3Ru_2$

C: 35.84%, H: 4.11%, N; 0%

FAB Mass Spectrum: Found M^+ = 1607 (0.1%), 1466 (100%)

Calculated for $[(P(OMe)_2Ph)_3Ru(\mu\text{-}Br)_3Ru\text{-}(P(OMe)_2Ph)_3]PF_6$

M^+ = 1607

and $[(P(OMe)_2Ph)_3Ru(\mu\text{-}Br)_3Ru\text{-}(P(OMe)_2Ph)_3]^+$

M^+ = 1466

4. Preparation of Tri-μ-bromohexakis(trimethylphosphite) diruthenium (II,II) hexafluorophosphate.

As 1 using the appropriate phosphine, $P(OMe)_3$ and HBr (0.082g, 70%).

Elemental Analysis: Found C: 15.70%, H: 4.11%, N: 0%

Calculated for $C_{18}H_{43}O_{18}P_7F_5Br_2Ru_2$

C: 16.27%, H: 4.07%, N: 0%

FAB Mass Spectrum: Found M^+ = 1335 (0.5%), 1188 (100%)

Calculated for $[(P(OMe)_3)_3Ru(\mu\text{-}Br)_3Ru\text{-}(P(OMe)_3]PF_6$

M^+ = 1333

and for $[(P(OMe)_3)_3Ru(\mu\text{-}Br)_3Ru(P(OMe)_3)_3]^+$

M^+ = 1188

5. Preparation of Tri-μ-Chlorohexakis(methyldiphenyl phosphonite) diosmium (II,II) hexafluorophosphate:

trans $OsCl_2(P(OMe)Ph_2)_4$ (0.3g), prepared as in Appendix 2, was heated to reflux in degassed methanol (40ml) under N_2 for 6 hours. During this time a number of colour changes took place. The initial pale green colour changed to orange then to deep orange/red after ∿10 minutes. After a further 20 minutes the colour was golden brown. Finally the colour was green. After 6 hours the solution was cooled. On reduction of the volume of solvent a green solid formed. This was filtered to yield a yellow solution which on further evaporation of solvent gave a yellow/brown solid. This was dried in vacuo (0.151g, 65%). Elemental analysis suggested that this species was the expected binuclear complex so the Cl^- counterion was exchanged for PF_6^- as described previously (see 1).

Elemental Analysis: Found C: 49.10%, H: 4.29%, N: 0%

Calculated for $C_{78}H_{78}P_6O_6Cl_4Os_2$

C: 51.5%, H: 4.49%, N: 0%

and Found C: 47.80%, H: 4.08%, N:0%

Calculated for $C_{78}H_{78}P_7O_6F_6Cl_3Os_2$

C: 48.47%, H: 4.04%, N: 0%

FAB Mass Spectrum: Found $M^+ = 1786$

Calculated for $[(P(OMe)Ph_2)_3Os(\mu\text{-}Cl)_3Os\text{-}(P(OMe)Ph_2)_3]^+$

$M^+ = 1782$

6. Preparation of Tri-μ-chlorohexakis(trimethylphosphine) diruthenium (II,II) hexafluorophosphate.

A suspension of $RuCl_2(PPh_3)_3$ (0.15g) was heated to reflux in degassed methanol (0.30ml) with PMe_3 (0.1 ml) under N_2 for 3 hours. On warming $RuCl_2(PPh_3)_3$ dissolves gradually and reacts with PMe_3. The colour of the solution becomes golden yellow. NH_4PF_6 (excess) was added after 2.5 hours. After cooling the volume of methanol was reduced then diethylether was added. A pale yellow precipitate formed. This was filtered and washed with cold methanol, diethylether and hexane and dried in vacuo (0.055g, 77%).

Elemental Analysis: Found C: 23.24%, H: 5.50%, N: 0%

Calculated for $C_{28}H_{54}P_7F_6Cl_3Ru_2$

C: 23.75%, H: 5.94%, N: 0%

FAB Mass Spectrum: Found $M^+ = 764$ (100%)

Calculated for $[(PMe_3)_3Ru(\mu\text{-}Cl)_3Ru(PMe_3)_3]^+$

$M^+ = 764$

Method Used for E.H.M.O. Calculations

The structures were first idealised as D_{3h} systems. This was achieved used the FORTRAN programs CALC[47] and ROTATE[48] by the following method:

(1) CALC was used on the X-ray determined model to calculate the following distances and angles.

Ru--Ru
Average Ru-Cl
Average Ru-P
Average P-$\hat{Ru}$-P

Having obtained these parameters, the Ru-$\hat{Cl}$-Ru, Cl-$\hat{Ru}$-Ru, Cl-$\hat{Ru}$-Cl and P-$\hat{Ru}$-Cl angles can all be calculated.

(2) Ru1, Ru2 and Cl1 were set up trigonometrically with both ruthenium centres lying on the z-axis and Cl1 on the x-axis. This leads to Ru1 and Ru2 having coordinates 0, 0, +z and 0, 0, -z respectively and Cl1; x, 0, 0.

(3) By using CALC, P1 was generated. From this the atoms H11-H13 were obtained (torsion angle Ru2-Ru1-P1-H is 180°).

(4) The program ROTATE was then used to generate Cl2, Cl3, $P2H_3$ and $P3H_3$.

(5) The z coordinates are then inverted to generate the remainder of the molecule; $P4H_3$, $P5H_3$ and $P6H_3$.

The theoretical model was constructed as follows:

(1) By extrapolation of the graph of Ru--Ru distance versus the average Ru-$\hat{Cl}$-Ru angle shown in Figure 4.3.2 an Ru-$\hat{Cl}$-Ru angle of 78° was obtained for an Ru--Ru distance of 3.09Å.

(2) The Ru-Cl distance was calculated using trigonometry.

(3) The difference in Ru--Ru distance for L=PEt_2Ph and L=PMe_3 is approximately the same as that between L=PMe_3 and the theoretical model. The Ru-P distances follow similar trends so using this assumption, Ru-P distances and Ru-Ru-P angles were calculated using CALC.

Once the above parameters are obtained the method described for the X-ray determined models can be followed.

After setting up the models, charge iteration was carried out on the model obtained from the species where L=PMe_2Ph. This uses the H_{ii}'s for ruthenium and refines them to give the best values appropriate for systems of this type i.e. those of lowest energy. These were then used for the other compounds. The initial and corrected H_{ii}'s are given below for ruthenium in eV

	s	P	d
Initial	-10.4	-6.87	-14.9
Corrected	-9.9760	-4.9571	-13.3355

4.5 REFERENCES

1. J. Chatt, Nature (London); 1950, 165, 637.
2. E.W. Abel, M.A. Bennett and G. Wilkinson, J.Chem.Soc.A, 1959, 2325.
3. W.D. Horrocks Jr and R.C. Taylor, Inorg.Chem., 1963, 2, 723.
4. F.A. Cotton, Inorg.Chem., 1964, 3, 702.
5. F.A. Cotton and C.S. Kraihanzel, J.Am.Chem.Soc.; 1962, 84, 4432.
6. J.C. Green, D.I. King and J.H.D. Eland, J.Chem.Soc., Chem.Comm.; 1970, 1121.
7. M. Bigorgne, J.Inorg.Nucl.Chem.; 1964, 26,107, and references therein.
8. C.A. Tolman, J.Am.Chem.Soc.; 1970, 92, 2593.
9. R.J. Angelici, J.Inorg.Nucl.Chem.; 1966, 28, 2627.
10. C.A. Streuli, Anal.Chem.; 1960, 32, 985.
11. W.A. Graham, Inorg.Chem.; 1968, 7, 315.
12. P.M. Treichel, Inorg.Chem.; 1968, 7, 1942.
13. M.N. Golovin, Md.M. Rahman, J.E. Belmonte and W.P. Giering, Organometallics; 1985, 4, 1981.
14. X.X. Shen, W.C. Trogler, P.C. Ellis and Z. Berbovitch-Yellin, J.Am.Chem.Soc.; 1983, 105, 7033.
15. D.S. Marynick, J.Am.Chem.Soc.; 1984, 106, 4064.
16. C.A. Tolman, J.Am.Chem.Soc.; 1970, 92, 2953.
17. C.A. Tolman, Chem.Res.; 1977, 313.
18. C.A. Tolman, Fundamen.Res.Organomet.Chem.Proc. (China-Jpn.-U.S.); 1982, 483.
19. G. Ferguson, P.J. Roberts, E.C. Alyea and M. Khan, Inorg.Chem.; 1978, 17, 2965.

20. C.A. Tolman, W.C. Seidel and L.W. Gosser, J.Am.Chem. Soc.; 1974, 53.

21. J.T. DeSanto, J.A. Mosbo, B.N. Starhoff, P.L. Bock and R.E. Bloss, Inorg.Chem.; 1980, 19, 3086.

22. G.M. Bodner, C. Gagnon and D.N. Whittern, J.Organomet. Chem.; 1983, 243, 305.

23. N.G. Connelly and M.D. Kitchen, J.Chem.Soc., Dalton Trans.; 1977, 931.

24. D.J. Kuchynka, C. Amatore and J.K. Kochi, Inorg.Chem.; 1986, 25, 4087.

25. Md.M. Rahman, H-Y. Liu, K. Eriks, A. Prock, W.P. Giering, Organometallics; 1989, 1.

26. P.W. Armit, A.S.F. Boyd and T.A. Stephenson, J.Chem. Soc., Dalton Trans., 1975, 1663.

27. L. Que, Jr, and L.H. Pignolet, Inorg.Chem.; 1973, 12, 156.

28. C.W. Smith, G.W. Vanloon and M.C. Baird, J.Coord.Chem.; 1976, 6, 89.

29. J. Chatt and R.G. Hayter, J.Chem.Soc.; 1961, 896.

30. K.A. Raspin, J.Chem.Soc.A; 1969, 461.

31. M. Laing and L. Pope, Acta.Cryst.; 1976, B32, 1567.

32. J.A. Statler, G. Wilkinson, M. Thornton-Pett and M.B. Hursthouse, J.Chem.Soc., Dalton Trans.; 1984,1731.

33. (a) N.S. Hush, J.K. Beattie, V.M. Ellis, Inorg.Chem.; 1984, 23, 3339, and

(b) V.T. Coombe, Ph.D. Thesis, University of Edinburgh, 1985.

34. G.A. Heath, A.J. Lindsay, T.A. Stephenson and D.K. Vattis, J.Organomet.Chem.; 1982, 233, 353.

35. T.V. Ashworth, N.J. Nolte, and E. Singleton, J.Chem. Soc., Chem.Comm.; 1977, 936.

36. W.J. Sime and T.A. Stephenson, J.Organomet.Chem.; 1978, 161, 245.

37. R. Contreras-Zarate, Ph.D. Thesis, University of Edinburgh 1981.

38. M.A. Bennett, R.J.H. Clark and A.D.J. Goodwin, Inorg. Chem.; 1967, 6, 1625.

39. G. Giacommetti and A. Turco, J.Inorg.Nucl.Chem.; 1960, 15, 242.

40. R.H. Summerville and R.J. Hoffmann, J.Am.Chem.Soc.; 1979, 101, 3821.

41. ICON 8: J. Howell, A. Rossi, D. Wallace, K. Haraki and R. Hoffmann, Quantum Chemistry Program Exchange, University of Indiana.

42. G. Chiccola, J.J. Daly and J.K. Nicholson, Angew.Chem.; Int.Ed.Engl.; 1968, 7, 131.

43. M.N. Hughes, D. O'Reardon, R.K. Poole, M.B. Hursthouse and M. Thornton-Pett, Polyhedron; 1987, 6, 1711.

44. J.K. Beattie, P. Del Favero, T.W. Hambley and N.S. Hush, Inorg.Chem.; 1988, 27, 2000.

45. PLUTO: W.D.S. Motherwell, University of Cambridge, England.

46. W.C. Davies and W.J. Jones, Chem.Soc. Journal; 1929, 1, 33.

47. CALC: "A program for molecular geometry calculations", R.O. Gould and P. Taylor, University of Edinburgh, 1985.

48. ROTATE: "A program for molecular rotations", A.J. Welch, University of Edinburgh, 1984.

C H A P T E R 5

SPECTROELECTROCHEMICAL STUDIES OF AN ASYMMETRIC BINUCLEAR RUTHENIUM COMPLEX

5.1 INTRODUCTION

This thesis has so far concentrated on symmetric, cationic, binuclear species of the type $[L_3M(\mu\text{-}X)_3ML_3]^{n+}$ where L = tertiary phosphine ligand; x = bridging ligand e.g. Cl^- ; M = Ru, Os and n = 1,2,3.

A wide range of asymmetric triply chloro-bridged complexes are also known, mainly for M=Ru, although there are some examples for M=Os.

A. M(II)M(II)

The neutral species $(PEt_2Ph)_3Ru(\mu\text{-}Cl)_3RuCl(PEt_2Ph)_2$ was first prepared by Alcock et al.,[1] by the pyrolysis of the symmetric binuclear complex $[(PEt_2Ph)_3Ru(\mu\text{-}Cl)_3Ru(PEt_2Ph)_3]Cl$ in methylacetate or n-propylpropionate. An X-ray crystallographic study has been carried out on this complex by Raspin[2] confirming the confacial bioctahedral, triply chloro-bridged structure. The Ru--Ru distance was found to be 3.367Å compared to 3.44Å in the related ionic binuclear complex from which it is formed. Since the preparation of this complex species of the type where $L=PMePh_2$ and $PEtPh_2$[3] have also been prepared by this method. Other methods of preparation have since been developed, mainly by Stephenson et al. For $L=PEt_2Ph$ and $PClPh_2$,[4] the reaction of L with $RuCl_2(PPh_3)_3$ in a non-polar solvent such as hexane gives the required species. When $L=PEtPh_2$,[4] the monomeric species, $RuCl_2(PEtPh_3)_3$ is isolated first. By dissolving this in cold degassed methylene chloride and adding petroleum ether (B.P. 60-80°C) the neutral binuclear $(PEtPh_2)_3Ru(\mu\text{-}Cl)_3RuCl(PEtPh_2)_3$ complex is obtained. The chemical reduction of

of mer-$RuCl_3L_3$[5] where L=PMe_2Ph, PEt_3 affords the appropriate $L_3Ru(\mu\text{-}Cl)_3RuL_2Cl$ complex, thus extending the series of complexes of this type to the more basic phosphines. A further method involves the use of UV light (λ = 254nm) on cis $RuCl_2L_4$ (L=PMe_2Ph) in benzene.[6]

A related complex where L=Me_2SO is known.[7] Tayim et al.[8] reported that the only product obtained from heating $RuCl_2(Me_2SO)_4$ in toluene was the binuclear species $Ru_2Cl_4(Me_2SO)_5$. They proposed that the complex had two bridging chloride ligands and one bridging Me_2SO group. Further studies in our laboratory[8] however revealed this to have the familiar triple-chloro bridged structure with all the Me_2SO groups bonded through the sulphur atom.

The reaction of $(PEt_2Ph)_3Ru(\mu\text{-}Cl)_3RuCl(PEt_2Ph)_2$ with a 1:1 molar ratio of acetonitrile and sodium tetraphenylborate in methylene chloride leads to the replacement of the terminal Cl^- ligand giving $[(PEt_2Ph)_3Ru(\mu\text{-}Cl)_3Ru(PEt_2Ph)_2(MeCN)]BPh_4$.[7]

A number of complexes of the type $L_2YRu(\mu Cl)_3RuL_2Cl$ have been prepared where (a) Y=CO, CS; L=PPh_3, $P(\underline{p}\text{-tol})_3$[9,10,11] and (b) Y=$N_2$,[12] $N_2B_{10}H_8SMe_2$[13]; L=PPh_3. Complexes of type (a) are prepared by the direct reaction of the appropriate monomeric species $RuCl_2L_3$ and $RuCl_2YL_2(DMF)$ in refluxing acetone or ethanol where L and Y are as before. This method can be extended to prepare mixed ligand or mixed metal complexes[14] i.e. $(PPh_3)_2ClRu(\mu\text{-}Cl)_3RuY(P(\underline{p}\text{-tol})_3)_2$; Y=CO, CS and $(PPh_3)_2ClRu(\mu\text{-}Cl)_3Os(CO)(PPh_3)_2$. $(PPh_3)_2ClRu(\mu\text{-}Cl)_3Ru(CS)(PPh_3)_2$ has also been prepared in low yield by the direct reaction of $RuCl_2(PPh_3)_3$ and CS_2.[15] The structure of this complex has been carried out thus confirming that the species

is triply-chloro bridged.[16] The Ru--Ru distance in this case was found to be 3.35Å, slightly shorter than that observed for the related $(PEt_2Ph)_3Ru(\mu\text{-}Cl)_3RuCl(PEt_2Ph)_2$ complex.

To obtain the species where $Y=N_2$, $L=PPh_3$ (type b) reverse osmosis of $RuCl_2(PPh_3)_3$ and N_2 in THF is carried out. Reaction of this with $N_2B_{10}H_8SMe_2$ gives $(PPh_3)_2ClRu(\mu\text{-}Cl)_3Ru(N_2B_{10}H_8SMe_2)(PPh_3)_2$.

Complexes of the type $RuCl_2YL_2(MeOH)$; L= $PEtPh_2$, PPh_3, $P(p\text{-tol})_3$; Y=CO, CS have been found to undergo a self-condensation reaction in non-polar media giving a mixture of three geometric isomers, $L_2YRu(\mu\text{-}Cl)_3RuYClL$.[10,11] The isomeric forms are:-

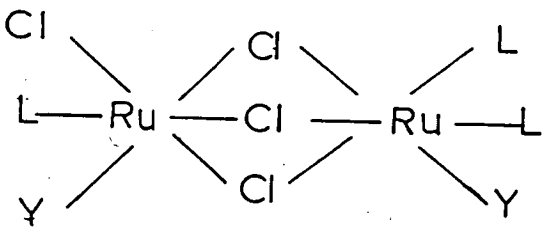

I

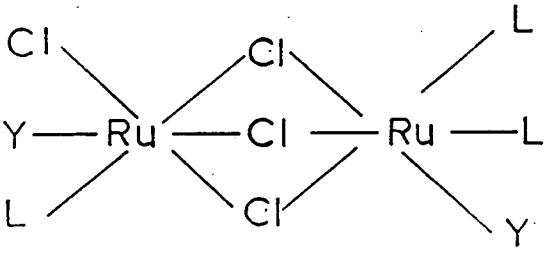

II

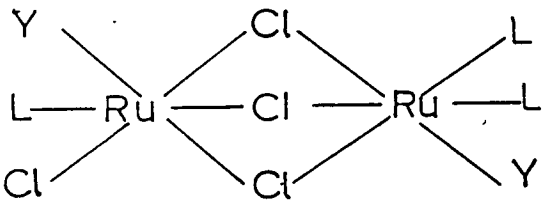

III

This class of complexes can also be prepared by the reaction of $RuX_2(CO)(PPh_3)_3$, X = Cl,[17] H[18] with gaseous HCl in benzene or by the reaction of $PhCH_2PPh_3[RuCl_3(CO)norb]$

in methylene chloride with an excess of PPh_3.[10]

A related hydrido species to that mentioned above, $RuH_2(PF_3)(PPh_3)_3$, has been found to react with HCl to give an isomeric mixture of $Cl(PPh_3)(PF_3)Ru(\mu\text{-}Cl)_3Ru(PPh_3)_2(PF_3)$.[18] This compound can be prepared by a number of other methods. These are detailed in scheme 5.1.1. The analogous PF_2NMe_2 complex can be prepared using methods 3, 4 and 5 in this scheme. These species can be compared directly with $Cl(PPh_3)YRu(\mu\text{-}Cl)_3(PPh_3)_2Y$, Y=CO, CS, discussed previously.

Other related complexes where $L=PF_3$ can be prepared; for example mono-PF_3 complex,[18] $(PPh_3)_2(PF_3)Ru(\mu\text{-}Cl)_3RuCl(PPh_3)_2$ is obtained from the reaction of $RuCl_2(PPh_3)_3$ with PF_3 in a 2:1 molar ratio. The mixed complex[18] $(PF_3)(PPh_3)ClRu(\mu\text{-}Cl)_3Ru(PPh_3)_2(CO)$ is prepared by the 1:1 reaction of $(CO)(PPh_3)_2Ru(\mu\text{-}Cl)_3Ru(PPh_3)_2Cl$ and PF_3.

$(PPh_3)_2(CO)Ru(\mu\text{-}Cl)_3Ru(SnCl_3)(PPh_3)(CO)$ [19] and $(SnCl_3)(CO)_2Ru(\mu\text{-}Cl)_3Ru(CO)_3$ [20] are reported to be formed by a rearrangement reaction of the monomeric species $RuCl(SnCl_3)(CO)(PPh_3)_2(acetone)\cdot acetone$ and $RuCl(SnCl_3)(CO)_4$ respectively.

$(SnCl_3)(CO)_2Ru(\mu\text{-}Cl)_3Ru(CO)_3$ [20] has been characterised crystallographically confirming the triple chloro-bridged structure. The Ru--Ru distance in this species is 3.157Å.

B. M(II)M(III)

A characteristic reaction of complexes of the type $L_2ClRu(\mu\text{-}Cl)_3RuL_3$ where $L=PEt_2Ph$, PMe_2Ph, $PEtPh_2$, $PMePh_2$ and $L_2YRu(\mu\text{-}Cl)_3RuClL_2$ where $L=PPh_3$, P(p-tolyl)$_3$; Y=CO, CS; is aerial oxidation in the presence of concentrated hydrochloric

Scheme 5.1.1: Methods of Preparing

$[CL(PPh_3)LRu(\mu\text{-}Cl)_3RuL(PPh_3)_2]$ where

$L = PF_3$, PF_2NMe_2

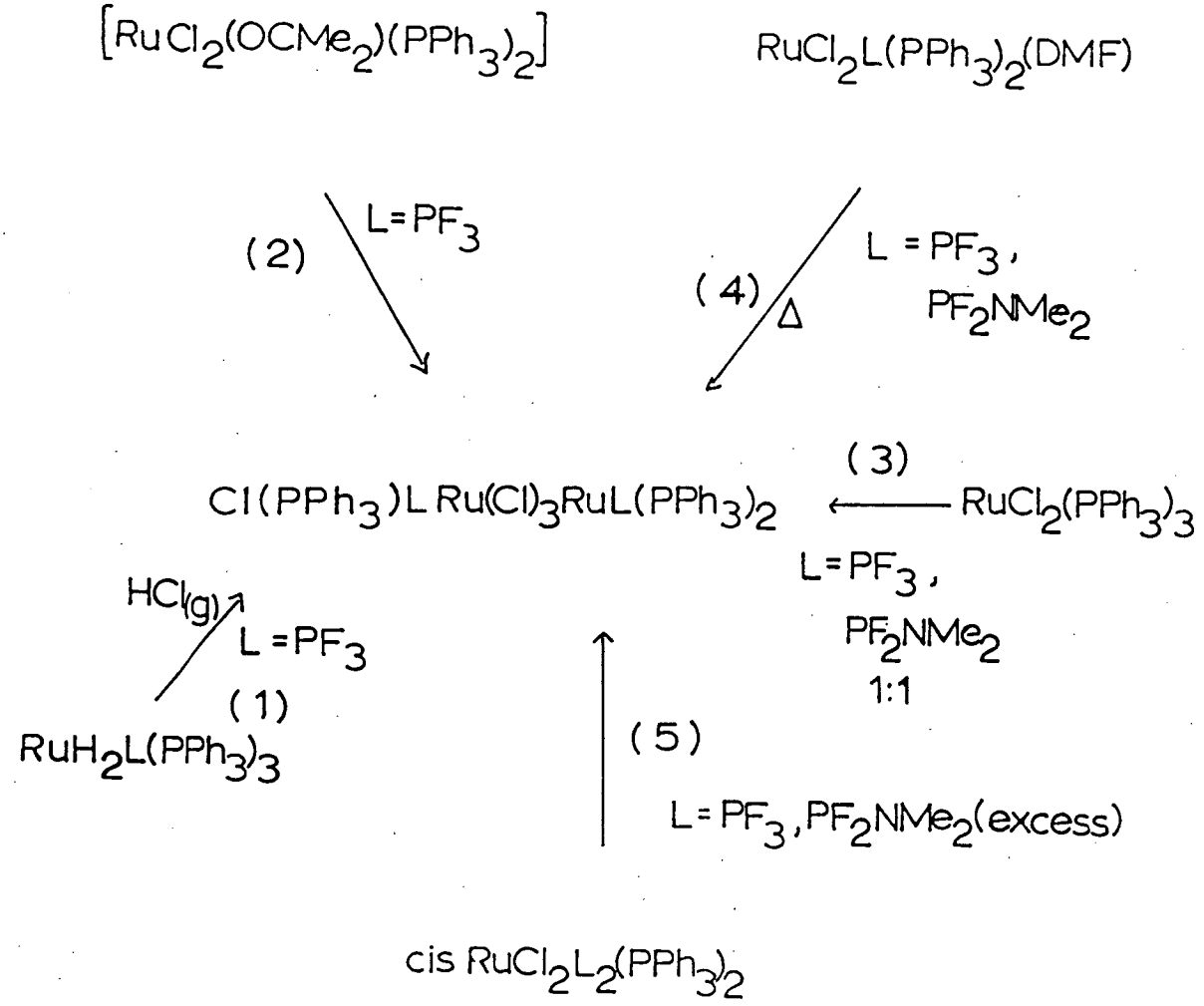

acid to give mixed-valence complexes of the type $L_3Ru(\mu\text{-}Cl)_3RuCl_2L$[5,7] and $L_2YRu(\mu\text{-}Cl)_3RuCl_2L$ respectively.[14]

Related mixed-valence asymmetric complexes of the above form are known where M=Ru, L=As(p-tolyl)$_3$, As(p-ClPh)$_3$ and M=Os, L=PPh_3, As(p-tolyl)$_3$, $AsPh_3$.[5] These are made by the direct reaction of $RuCl_3 \cdot 3H_2O$ and Na_2OsCl_6 respectively with the ligand, L, in an appropriate solvent.

The complex $(PEt_2Ph)_3Ru(\mu\text{-}Cl)_3RuCl_2(PEt_2Ph)$ has been characterised crystallographically by Gould et al.[21] The Ru--Ru distance was found to be 3.28Å. This is shorter than in the related $(PEt_2Ph)_3Ru(\mu\text{-}Cl)_3RuCl(PEt_2Ph)_2$ complex. As the degree of asymmetry increases the metal-metal distance decreases. In the mixed-valence complex the oxidation state of one of the metal centres has been increased; this may be an additional factor causing the decrease of metal-metal distance.

C. M(III)M(III)

Cotton et al.[22] have recently isolated and characterised the complex $Cl_2(P^nBu_3)Ru(\mu\text{-}Cl)_3Ru(P^nBu_3)_2Cl$. This was obtained by the reaction of $RuCl_3 \cdot 3H_2O$ and P^nBu_3 in ethanol. An X-ray crystal structure showed the complex to have a Ru--Ru distance of 3.176Å;[22] c.f. those observed for the related Ru(II)Ru(II) and Ru(II)Ru(III) species discussed previously. The fact that a contraction in the metal-metal distance has been observed even though the charge on the metal centres has increased suggests that a single metal-metal band has been formed.

There is a wide range of triple chloro-bridged

asymmetric binuclear complexes available where M=Ru. The nature of the metal-metal interaction in the mixed-valence state in these species has not been studied to any extent.

In the symmetric species studied in this work the mixed-valence state has been extensively studied and it has been found that the metal-metal interaction can be altered by varying M, X and L but it is always a strong interaction i.e. the complexes are Class III according to the Robin and Day classification.[23]

By electrochemical synthesis several sequences of triple chloro-bridged diruthenium complexes of the general type $[L_{3-x}Cl_xRu(\mu\text{-}Cl)_3RuCl_yL_{3-y}]^{z/z+1/z+2}$ where x=0, 1, 2; y=0, 1, 2; z=-1, 0, +1 and L = soft neutral ligand, have been generated.[24] Preliminary studies on the behaviour of the metal centres in the mixed-valence state of these complexes using spectroelectrochemical techniques have suggested that as the asymmetry increases the degree of metal-metal interaction decreases; going from completely delocalised (Class III) with the symmetric complex to localised (Class II) with the most asymmetric species.[24]

Replacing tertiary P(III) ligands with π-acid ligands such as CO and CS reduces the metal-metal interaction further. We have investigated the complex $(PPh_3)_2(CS)(Ru(II)(\mu\text{-}Cl)_3\text{-}Ru(II)(PPh_3)_2Cl$. This species undergoes a reversible one-electron oxidation at +0.74V (versus Ag/AgI at which ferrocene is oxidised at +0.60V in 0.5M $LiClO_4$/THF) to give $[(PPh_3)_2(CS)Ru(II)(\mu\text{-}Cl)_3Ru(III)Cl(PPh_3)_2]^+$. We believe that it is the ruthenium centre containing Cl^- rather than CS that is oxidised first due to the π-donating character of Cl^-

which will tend to make the Ru(II) centre more susceptible to oxidation than if only tertiary phosphine ligands are present. In contrast to this, the π-accepting nature of the CS ligand will make the Ru(II) centre less likely to be oxidised than when surrounded by only tertiary phosphine ligands.

Spectroelectrochemical studies[24] on $[(PPh_3)_2(CS)Ru(\mu\text{-}Cl)_3\text{-}RuCl(PPh_3)_2]^+$ showed the oxidised species to have a weak band at 14,800 cm^{-1} in THF (ε=100 $mol^{-1}cm^{-1}dm^3$) which was absent in the parent complex spectrum. This was assigned as an intervalence charge transfer band i.e. the complex is a true Class II species with weakly interacting metal centres. In this work an in-depth study of this complex has been carried out.

5.2 RESULTS AND DISCUSSION

$Cl(PPh_3)_2Ru(\mu\text{-}Cl)_3Ru(PPh_3)_2CS$ was prepared as described in Section 5.1.

5.2.1 Electrochemical studies

Electrochemical studies were carried out as previously described in methylene chloride/0.5M $TBABF_4$. The results are as previously obtained; $E_{\frac{1}{2}}$ = +0.74V versus Ag/AgCl where ferrocene/ferrocinium = +0.56V at T=293K.

5.2.2 Spectroelectrochemical Studies

These were carried out as described previously. The oxidation of $Cl(PPh_3)_2Ru(\mu\text{-}Cl)_3Ru(PPh_3)_2(CS)$ to $[Cl(PPh_3)_2\text{-}Ru(III)(\mu\text{-}Cl)_3Ru(II)(PPh_3)_2(CS)]^+$ was monitored over a period

of time at a temperature of T=258K.

Spectra were recorded over the range 4,000-44,000 cm^{-1} in the following solvents

(1) Methylene Chloride / 0.5M $TBABF_4$

(2) Chloroform / 0.5M $TBABF_4$

(3) Propylene carbonate / 0.1M $TBABF_4$

(4) Dimethylformamide / 0.1M $TBABF_4$

It would have been advantageous to study the complex in more solvent systems, however the solubility of the compound prevented this. Table 5.2.1 gives the results obtained for each solvent.

Figure 5.2.1 shows the spectrum of $[Cl(PPh_3)_2Ru(\mu\text{-}Cl)_3\text{-}Ru(PPh_3)_2(CS)]^+$ in methylene chloride/0.5M $TBABF_4$.

Three weak low energy bands are observed (ε ranging from 710 $mol^{-1}cm^{-1}dm^3$ to 470 $mol^{-1}cm^{-1}dm^3$. We can compare these bands with the low energy bands in the spectrum of $[(PMe_2Ph)_3Ru(\mu\text{-}Cl)_3Ru(PMe_2Ph)_3]^{2+}$ where ε=2864 $mol^{-1}cm^{-1}dm^3$ for the band observed at 7700 cm^{-1}.)

In a less polar solvent ($CHCl_3$) the bands will move to a lower energy and vice versa for a more polar solvent.

Hush[25] theory for Class II mixed-valence species was introduced in Chapter 1. Application of Hush's theory to the observed spectrum of $[Cl(PPh_3)_2Ru(\mu\text{-}Cl_3)Ru(PPh_3)_2(CS)]^+$ enables us to test further the nature of the band at 14,500 cm^{-1} in methylene chloride which had previously been observed at 14,800 cm^{-1} and is assigned as an intervalence charge transfer band.

For symmetric complexes the following equations result from Hush theory:

Table 5.2.1: Positions of Bands (ν_{max}) in the Low Energy Region of the Eelctronic Absorption Spectrum for $[Cl(PPh_3)_2Ru(\mu\text{-}Cl)_3Ru(CS)(PPh_3)_2]^+$ [a] in Different Solvents at T = 258K

Solvent	$\nu_{max}(cm^{-1})$	$(mol^{-1}cm^{-1}dm^3)$	D_{op}	D_s
Methylene Chloride	14,500	470	2.028	8.9
0.5M $TBABF_4$	17,100	550		
	20,000	710		
Chloroform	12,600	450	2.085	4.7
0.5M $TBABF_4$	15,400	536		
	18,100	685		
Dimethylformamide	16,000	470	2.0458	36.7
0.1M $TBABF_4$	19,000	572		
	22,000	724		
Propylene Carbonate	15,600	484	2.0133	65.1
0.1M $TBABF_4$	18,400	546		
	21,200	714		

a. The electrogenerating potential used in each case E_{gen} = +0.94V (versus Ag/AgCl on which ferrocene is oxidised at E = +0.56V)

Figure 5.2.1: Spectrum showing (a) conversion of $[(CS)(PPh_3)_2Ru(\mu\text{-}Cl)_3RuCl(PPh_3)_2] \rightarrow [(CS)(PPh_3)_2Ru(\mu\text{-}Cl)_3RuCl(PPh_3)_2]^+$ and (b) the Final Spectrum of $[(CS)(PPh_3)_2Ru(\mu\text{-}Cl)_3RuCl(PPh_3)_2]^+$ in Methylene Chloride / 0.5M $TBABF_4$

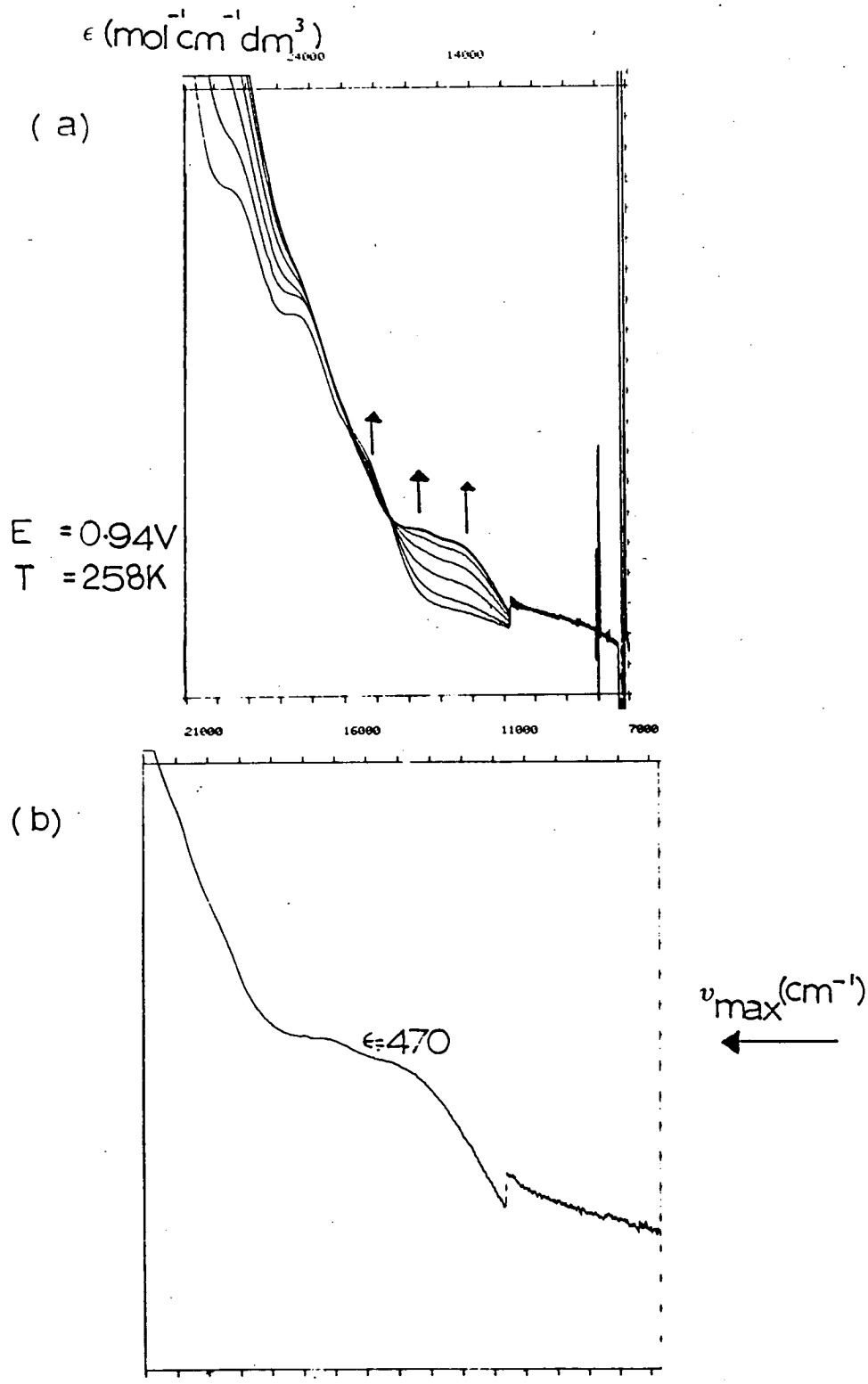

$$\nu_{max} = \lambda = 4\Delta G_{th}^{*} \qquad (1)$$

where ν_{max} is the position of the band maximum in cm^{-1}. ΔG_{th}^{*} is the free energy barrier for thermal electron transfer.

$$\Delta_{\frac{1}{2}}(calc) = [2310\ \nu_{max}]^{\frac{1}{2}} \qquad (2)$$

$\Delta_{\frac{1}{2}}(calc)$ is the calculated band halfwidth in cm^{-1}.

$\Delta_{\frac{1}{2}}(calc)$ is equal to the experimental band halfwidth, $\Delta_{\frac{1}{2}}(exp)$ (within 10% error) for an intervalence charge transfer band ($\Delta_{\frac{1}{2}} \geqslant 5000\ cm^{-1}$).

$$\alpha^2 = 4.24\times10^{-4}\,[(\varepsilon\Delta_{\frac{1}{2}})/\nu_{max}d^2] \qquad (3)$$

where α is the degree of delocalisation and $0 < \alpha < 0.25$ for a Class II system.

ε is the molar extinction coefficient, $mol^{-1}cm^{-1}dm^3$.

d is the distance between the metal centres, Å.

$$E_{op} = \nu_{max} = E_{in} + E_{out} \qquad (4)$$

where E_{in} and E_{out} are the inner sphere and outer sphere reorganisation energies respectively.

$$E_{out} = e^2\left(\frac{1}{2a_1} + \frac{1}{2a_2} - \frac{1}{d}\right)\left(\frac{1}{D_{op}} - \frac{1}{D_s}\right) \qquad (5)$$

where $a_{1,2}$ are the radii of the two coordination spheres.

d is the metal--metal distance in Å.

D_{op} is the optical dielectric constant, and

D_s is the static dielectric constant.

Thus a plot of ν_{max} versus $^1/D_{op} - {}^1/D_s$ will give a straight line with intercept E_{in} if the species is a Class II system.

By applying the above equations to the complex under study here we can obtain more information regarding the nature of the band observed at 14,500 cm^{-1}.

(a) Band halfwidth

$$\Delta_{\frac{1}{2}}(calc) = [2310\ \nu_{max}]^{\frac{1}{2}} \qquad (2)$$

The observed $\Delta_{\frac{1}{2}}(exp)$ value is 5200 cm^{-1}. The calculated value of $\Delta_{\frac{1}{2}}$ given by equation (2) is $\Delta_{\frac{1}{2}}(calc)$ = 5780 cm^{-1} and is therefore within the allowed percentage error so

$$\Delta_{\frac{1}{2}}(exp) = \Delta_{\frac{1}{2}}(calc)$$

(b) Degree of Delocalisation (α)

$$\alpha^2 = 4.24 \times 10^{-4}[(\varepsilon \Delta_{\frac{1}{2}})/\nu_{max} d^2]$$

using $d = 3.35\text{Å}$

$$\alpha = 0.07$$

The metal--metal distance, d, in $Cl(PPh_3)_2Ru(\mu\text{-}Cl)_3Ru(PPh_3)_2(CS)$ is 3.35Å. It would be expected that on oxidation this would decrease thus the value of α obtained is likely to be slightly greater.

(c) Solvent Dependence

A graph of ν_{max} versus $^1/D_{op} - {}^1/D_s$ was plotted. This is shown in Figure 5.2.2. A straight line correlation is obtained. D_{op} and D_s values for the various solvents used are given in Table 5.2.1 together with the ν_{max} values.

It can be concluded therefore that the 14,500 cm^{-1} band in $[(PPh_3)_2ClRu(\mu\text{-}Cl)_3Ru(PPh_3)(CS)]^+$ is indeed due to an intervalence charge transfer transition i.e.

$$[(PPh_3)_2(CS)Ru(II)(\mu\text{-}Cl)_3Ru(III)(PPh_3)_2Cl]^+ \xrightarrow{\nu_{max}} [(PPh_3)_2(CS)Ru(III)(\mu\text{-}Cl)_3Ru(II)Cl(PPh_3)_2]^{+*}$$

Figure 5.2.2: Graph of ν_{max} (cm^{-1}) versus $^{1}/D_{op} - {}^{1}/D_{s}$ for $[(PPh_3)_2(CS)Ru(\mu\text{-}Cl)_3RuCl(PPh_3)_2]^+$ at T = 258K in various solvents

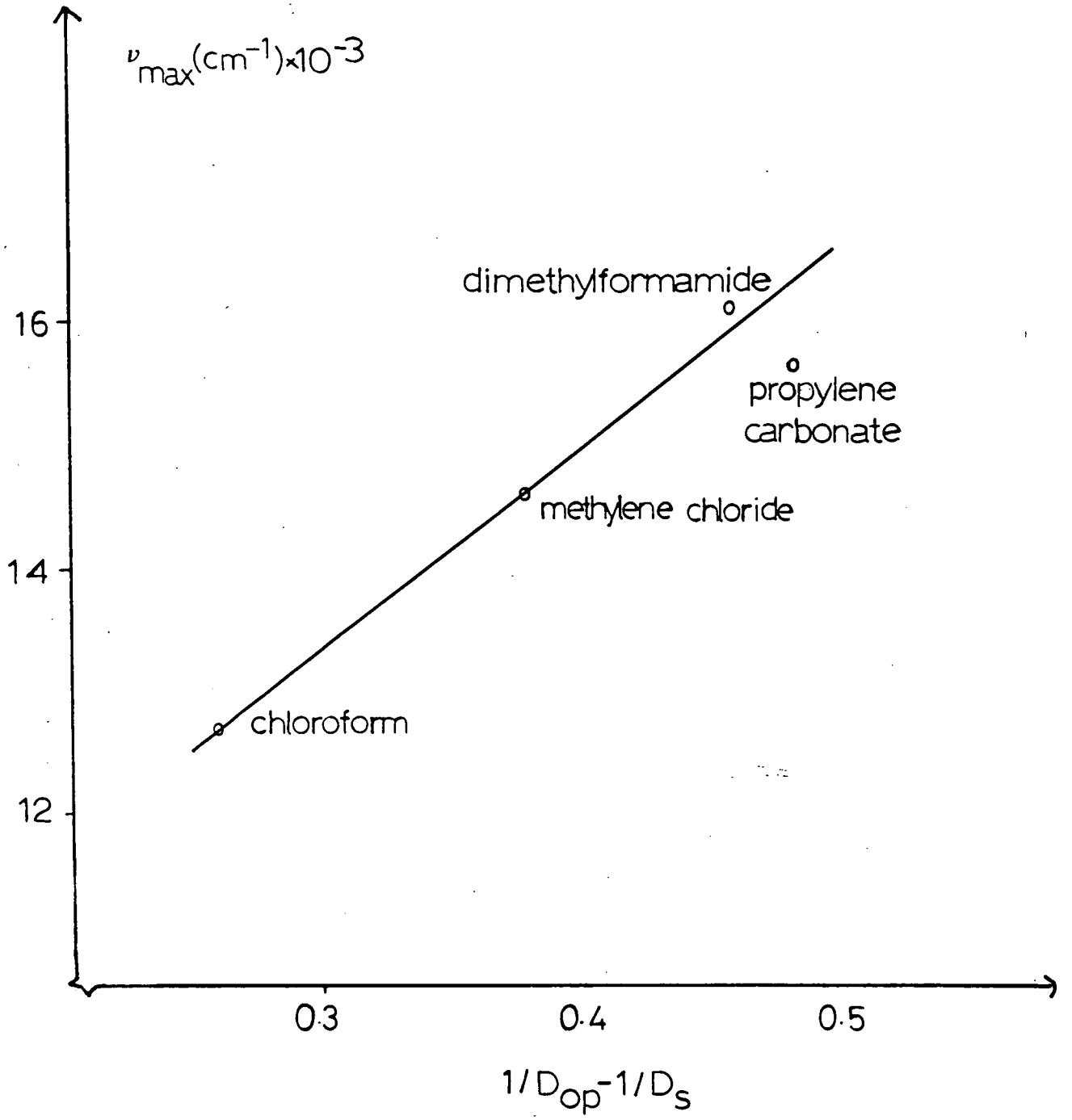

As mentioned previously a further two weak bands are observed at higher energy than the band at 14,500 cm^{-1} studied above. These bands are also thought to arise from intervalence charge transfer transitions and are a consequence of the asymmetry of the complex. Both ruthenium centres have an octahedral environment. One metal centre has the π-accepting ligand CS attached to it whereas the other has the π-donating Cl^- ligand present. This leads to the "t_{2g}" levels of each ruthenium being non-degenerate. Thus the following processes can occur:

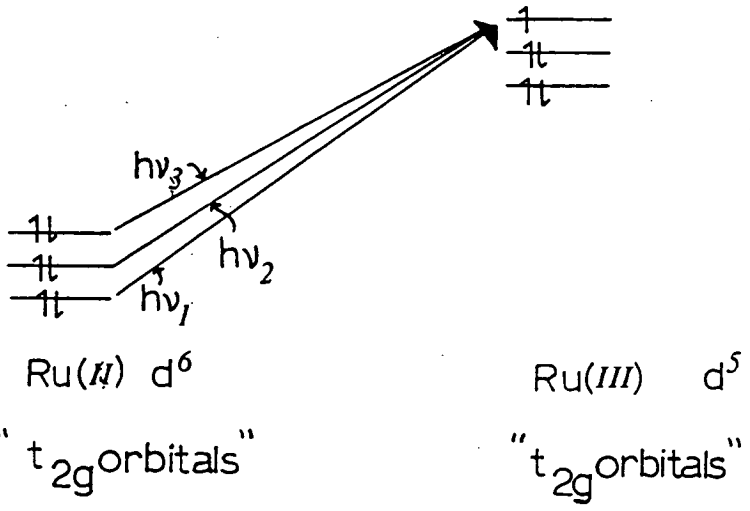

giving rise to three intervalence charge transfer bands rather than one.

Hush[25] has developed his theory further so that a number of parameters regarding the electron transfer from one ruthenium centre to another can be calculated in asymmetric mixed-valence complexes. For asymmetric systems there is an energy difference, ΔE_o, between the HOMO's on the two metal sites. The potential energy diagram for an asymmetric species is shown in Figure 5.2.3.

Figure 5.2.3: Potential Energy versus Nuclear Configuration for an Asymmetric Mixed Valence Complex

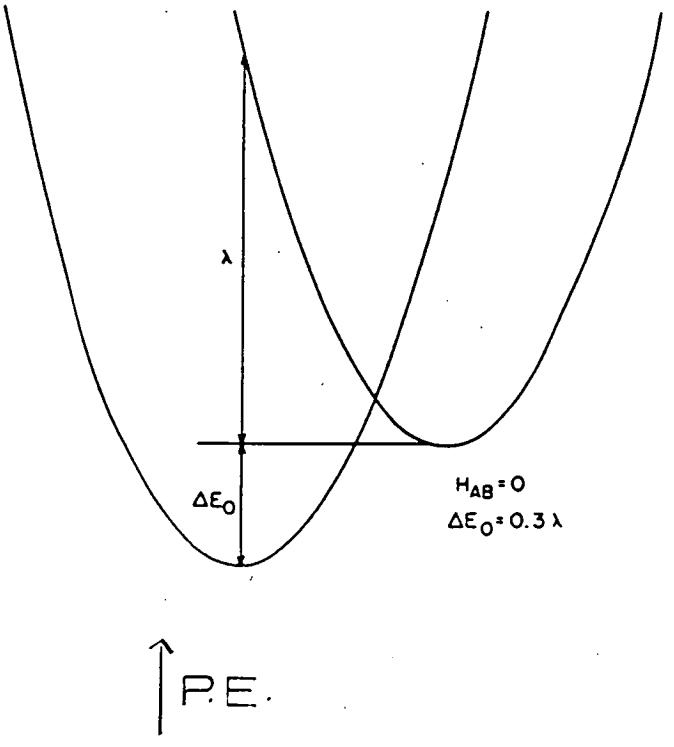

Hush Treatment for Asymmetric Species

For an asymmetric complex

$$E_{op} = \nu_{max} = \lambda + \Delta E_o = 2(\lambda E_{th}) \qquad (6a)$$

$$\Rightarrow E_{th} = (\lambda + \Delta E_o)^2/4\lambda \qquad (6b)$$

$$\nu_{max} - \Delta E_o = E_{in} + E_{out} \qquad (7)$$

A plot of $\nu_{max} - \Delta E_o$ versus $^1/D_{op} - {}^1/D_s$ should give a straight line of gradient E_{out} and intercept E_{in} for a Class II transition.

The value ΔE_o can be calculated from equation 8:

$$\nu_{max} - (\Delta_{\frac{1}{2}}(exp))^2/2310 = \Delta E_o \quad (cm^{-1}) \qquad (8)$$

i.e. it can be estimated from the intervalence charge transfer band. However, in practice this often leads to an underestimation of ΔE_o.

A more frequently used method of obtaining ΔE_o is given in equation (9):

$$\Delta E_o = 8.067\ (E_2^{o\prime} - E_1^{o\prime}) \quad (kK) \qquad (9)$$

where $E_1^{o\prime}$ is the electrode potential for the process:

$$M(II)M'(II) \xrightarrow{-e^-} [M(II)M'(III)]^+$$

and $E_2^{o\prime}$ is the electrode potential for the process:

$$M(II)M'(II) \xrightarrow{-e^-} [M(III)M'(II)]^+$$

ΔG^*_{th}, the free energy barrier for thermal electron transfer is obtained from the relationship

$$\Delta G^*_{th} = ((4\Delta G^*_\lambda + \Delta G^o)^2/16\Delta G^*_\lambda) - H_{AB} \qquad (10)$$

where $\Delta G^*_\lambda = (E_{in} + E_{out})/4$ and ΔG^o is given by ΔE^o. H_{AB} is the degree of electronic coupling between the metal

centres and is given by equation (11):

$$H_{AB} = \left(2.05\times10^{-2} \left(\frac{\varepsilon\ \Delta\nu_{\frac{1}{2}}}{\nu_{max}}\right)^{\frac{1}{2}} \nu_{max}\right) / r \quad (cm^{-1}) \qquad (11)$$

where ε is the extinction coefficient at the band maximum and r is the distance between the two metal centres.

Combining equations 1, 6b and 10 gives

$$\Delta G^{*}_{th} = E_{th} - H_{AB} \qquad (12)$$

The rate constant for the thermal electron transfer, k_{th}, can be calculated using equation (13).

$$k_{th} = (2\pi H_{AB}^{2}/\hbar)(\pi/k_B T\lambda)^{\frac{1}{2}} \exp(-\Delta G^{*}_{th}/RT) \qquad (13)$$

$$= \nu_{ET} \exp(-\Delta G^{*}_{th}/RT)$$

where ν_{ET} is the frequency factor for electron transfer

k_B is the Boltzmann constant and

T is the temperature in K.

Thus the intervalence charge transfer band profile allows us to calculate ΔE^{o}, ΔG^{*}_{th} and H_{AB} and finally to arrive at a value for the rate of an intramolecular electron transfer reaction. The above treatment will now be applied to the system under study namely $[(CS)(PPh_3)_2Ru(\mu\text{-}Cl)_3Ru\text{-}(PPh_3)_2Cl]^{+}$.

(a) Calculation of ΔE^{o} (in Methylene Chloride)

Using equation (8) ΔE^{o} was calculated where $E_1{}^{o\prime}$ is the electrode potential for the process:

$Cl(PPh_3)_2Ru(II)(\mu\text{-}Cl)_3Ru(II)(PPh_3)_2(CS) \xrightarrow{-e^-} [Cl(PPh_3)_2Ru(III)\text{-}(\mu\text{-}Cl)_3Ru(II)(PPh_3)_2(CS)]^{+}$

Electrochemically this is measured at +0.74V (versus Ag/AgCl

reference electrode on which ferrocene is oxidised at +0.56V in methylene chloride/0.5M $TBABF_4$). $E_2^{O'}$ is the electrode potential for the hypothetical process:

$$Cl(PPh_3)_2Ru(II)(\mu\text{-}Cl)_3Ru(II)(PPh_3)_2(CS) \xrightarrow{-e^-} [Cl(PPh_3)_2Ru(II)\text{-}(\mu\text{-}Cl)_3Ru(III)(PPh_3)_2(CS)]^+$$

The value of $E_2^{O'}$ is often taken from the second oxidation potential which in this case would be:

$$[Cl(PPh_3)_2Ru(III)(\mu\text{-}Cl)_3Ru(II)(PPh_3)_2(CS)]^+ \xrightarrow{-e^-} Cl(PPh_3)_2Ru(III)(\mu\text{-}Cl)_3Ru(III)(PPh_3)_2(CS)]^{2+}$$

however this is not a good approximation as the Ru(II)/Ru(III) couple is attached to a Ru(III) centre and not a Ru(II) centre as required. The related complex $[(CS)(PPh_3)_2Ru(II)(\mu\text{-}Cl)_3\text{-}Ru(II)(CS)(PPh_3)_2]^+$ [7] undergoes a one electron oxidation at +1.50V (versus Ag/AgCl reference electrode on which ferrocene is oxidised at + 0.56V) to give the species $[(CS)(PPh_3)_2Ru(II)(\mu\text{-}Cl)_3Ru(III)(CS)(PPh_3)_2]^{2+}$. This oxidation process gives a Ru(III) centre with the same coordination environment as that of the hypothetical process. $E_2^{O'}$ was therefore taken to be 1.50V.

A similar method has been used by Meyer[26] for the species $[(NH_3)_5Ru(III)(pyr)Ru(III)Cl(bipy)_2]^{5+}$. This undergoes a one electron reduction to give $[(NH_3)_5Ru(III)(pyr)Ru(II)Cl(bipy)_2]^{4+}$ and a further reduction to give $[(NH_3)_5Ru(II)(pyr)Ru(II)\text{-}Cl(bipy)_2]^{3+}$. $E_1^{O'}$ is taken to be the reduction potential for the first reduction process. $E_2^{O'}$ is however estimated to have the value of the reduction potential for the process:

$$[(bipy)_2ClRu(III)(pyr)Ru(III)(bipy)_2Cl]^{4+} \xrightarrow{-e^-} [(bipy)_2ClRu(II)(pyr)Ru(III)(bipy)_2Cl]^{3+}$$

Again this was chosen rather than the second reduction potential of the complex under study as this measures the reduction potential of a Ru(III) site adjacent to a Ru(II) site.

The lack of solubility of $[(CS)(PPh_3)_2Ru(\mu\text{-}Cl)_3Ru(CS)(PPh_3)_2]^+$ in most solvents results in $E_2^{o'}$ being measured only in methylene chloride which was then used to calculate ΔE^o from equation 9. This value of ΔE^o has been used for all solvents as it was deemed to be the most accurate method of determination.

$$\Delta E^o = 6131 \text{ cm}^{-1}$$

The values of E_{in} and E_{out} will not be strictly correct since ΔE^o is calculated only for methylene chloride and will vary slightly with solvent.

From ΔE^o, other parameters can now be calculated. These are tabulated in Table 5.2.2. A graph of $\nu_{max} - \Delta E^o$ versus $^1/D_{op} - {}^1/D_s$ is shown in Figure 5.2.4. From this E_{in} and E_{out} are obtained. These are shown in Table 5.2.3. Calculations of this type have been carried out on a series of ruthenium binuclear mixed-valence complexes with a single conjugated bridging ligand of the type L = pyrazine, 4,4 bipyridine and 1,2 bis (4 - pyridyl)ethene.[27] In order to make comparisons with our triple chloro-bridged binuclear species these values have been included in Table 5.2.2.

In the triple chloro-bridged species under study both ν_{max} and ΔG^*_{th}, the free energy barrier to the thermal process, are greater than in the single bridged complexes. This is thought to be a consequence of the greater asymmetry of the

Table 5.2.2: Electron Transfer Parameters Calculated from Intervalence Charge Transfer Bands

Complex	$\nu_{max}(cm^{-1})$	$\lambda(cm^{-1})$	$H_{AB}(cm^{-1})$	$\nu_{et}(S^{-1})$	$\Delta G^{*}_{th}(V)$	$k(s^{-1})$
1. $[Cl(PPh_3)_2Ru(\mu\text{-}Cl)_3Ru(CS)(PPh_3)_2]^{+}$ [a]	14,500	8,369	1,135	2.08×10^{15}	0.64	2.9×10^{4}
2. $[L_2ClRu(pyz)RuClL_2]^{3+}$ [b,c]	7,340	7,340	129	2.5×10^{14}	0.23	3.9×10^{10}
3. $[(NH_3)_5Ru(pyz)RuClL_2]^{4+}$ [b,c]	10,406	8,417	573	5.2×10^{14}	0.41	5.7×10^{7}
4. $[L_2ClRu(bpe)RuClL_2]^{3+}$ [b,c]	10,809	10,809	129-185	$(2.3\text{-}4.8)\times10^{7}$	0.34	$5.1\text{-}10\times10^{7}$
5. $[L_2ClRu(4,4'bipy)RuClL_2]^{3+}$ [b,c]	10,163	10,163	137-214	$(2.7\text{-}5.9)\times10^{3}$	0.32	$(1.0\text{-}2.8)\times10^{8}$

a. In methylene chloride

b. In acetonitrile

c. L = 2,2'-bipyridine, pyz = pyrazine, bpe = 1,2 bis(bipyridyl)ethene

4,4'bipy = 4,4'-bipyridine

Table 5.2.3: Inner and Outer Sphere Electron Transfer Energies

Complex	E_{in}(eV)	E_{out}(eV)
$[(NH_3)_5Ru(4,4bipy)Ru(NH_3)_5]^{5+}$ a 29	0.43	0.67
$[(bipy)_2ClRu(pyz)RuCl(bipy)_2]^{3+}$ a 28	0.73	0.26
$[(NH_3)_5Ru(4,4\ bipy)RuCl(bipy)_2]^{4+}$ a 30	0.56	0.43
$[(NH_3)_5Ru(pyz)RuCl(bipy)_2]^{4+}$ a 28	0.56	0.43
$[Cl(PPh_2)\ Ru(\mu\text{-}Cl)_3Ru(CS)(PPh_3)_2]^{+}$ b	0.30	2.0

a. In acetonitrile

b. In methylene chloride

Figure 5.2.4: Graph of ν_{max} (cm^{-1}) - $\Delta E°$ (cm^{-1}) versus $^{1}/D_{op}$ - $^{1}/D_{s}$ for $[(PPh_3)_2(CS)Ru(\mu\text{-}Cl)_3RuCl(PPh_3)_2]^+$ at T = 258K, in various solvents

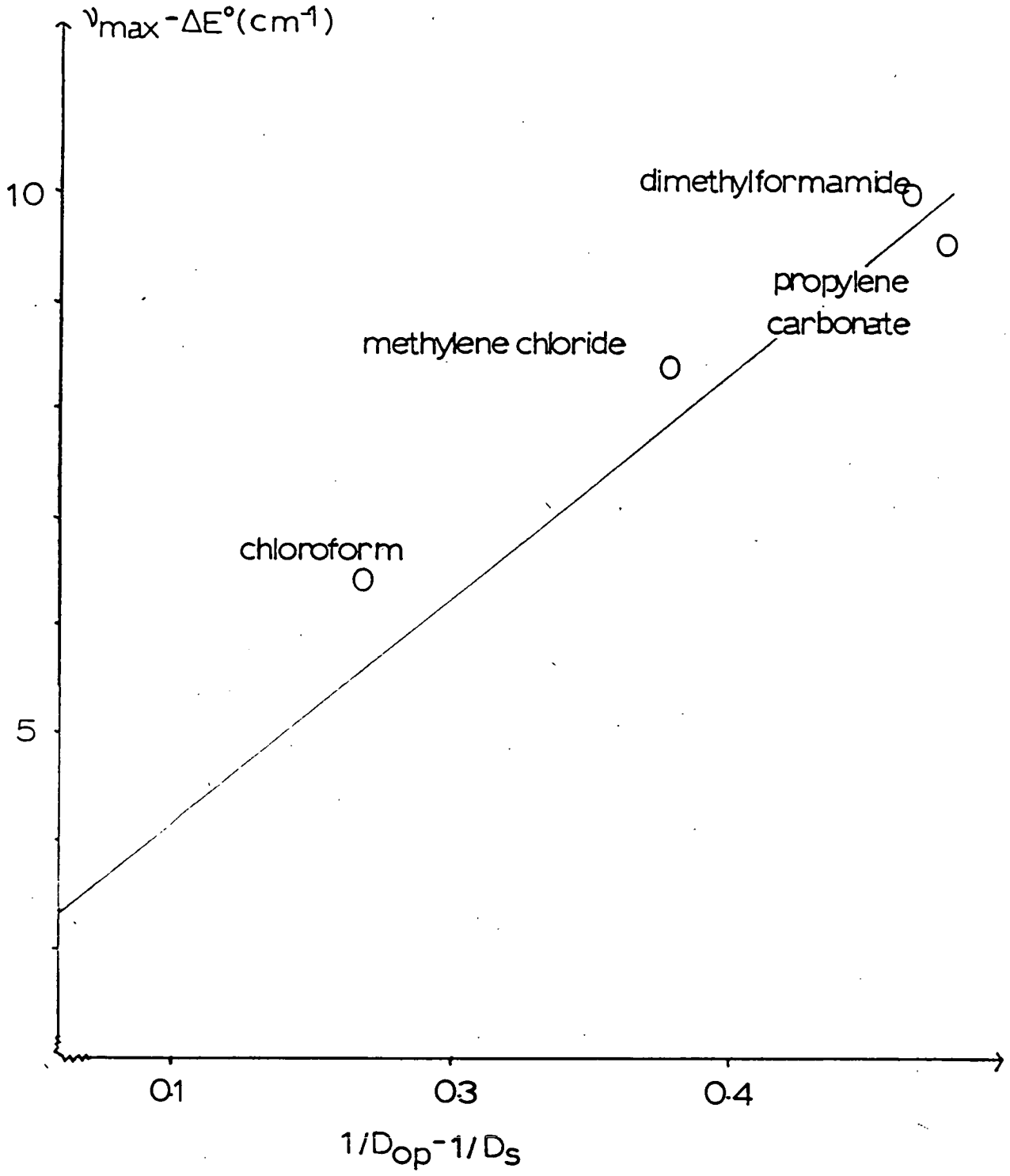

two metal centres in the triply bridged species than in the singly bridged compounds. The singly bridged species are known to undergo electron transfer via an inner sphere mechanism via the bridge. In the triply-chloro bridged complex, the thermal electron transfer rate constant is smaller than those calculated for the singly bridged species. The electron transfer is thought to occur by an inner sphere mechanism, but through direct d-orbital overlap rather than via the bridge in the singly bridged species.

The E_{in} value calculated for the triple chloro-bridged complex is comparable with those calculated for the N-donor bridged complexes, 0.3eV compared with range of 0.43-0.73eV. Table 5.2.3 shows the E_{in} and E_{out} values for four complexes where the bridging ligand is pyrazine[28] or 4,4' bipyridine[29,30] together with the values for the complex under study. E_{out} however is much greater than in these complexes, 2.0eV compared with 0.26-0.67eV. We believe that this may be the result of a greater amount of solvent reorganisation being required.

5.3 CONCLUSIONS

The mixed-valence compound $[Cl(PPh_3)_2Ru(\mu\text{-}Cl)_3Ru(PPh_3)_2(CS)]^+$ is a Class II complex with weak interaction between the metal centres whether it be light or thermally induced. Electron transfer occurs via an inner sphere mechanism. The magnitude of the electron transfer rate makes it amenable to study by variable temperature e.p.r. methods and thereby allow us to probe the electron transfer reaction by two independent techniques.

It would have been interesting to study a wider range of complexes of this type to enable the above type of calculations to be carried out and compared. The related complex where CS is replaced by CO proved to be too unstable in solution to enable spectroelectrochemical studies.

The mixed-valence complex $Cl_2(PPh_3)Ru(III)(\mu\text{-}Cl)_3Ru(II)(PPh_3)_2(CS)$ was prepared, as determined by an electrochemical study, but we were unable to obtain pure samples. The starting complex $Cl(PPh_3)_2Ru(II)(\mu\text{-}Cl)_3Ru(II)(PPh_3)_2CS$ was always present in the mixture. The mixed-valence species $Cl_2(PPh_3)Ru(\mu\text{-}Cl)_3Ru(PPh_3)_2(CS)$ was previously reported to have a reversible one-electron reduction at -0.02V (versus an Ag/AgI reference electrode) at which ferrocene is oxidised at +0.56V).[7] We also observed this redox process together with two previously unreported oxidations at (a) +1.58V and (b) +1.78V (versus an Ag/AgCl reference electrode at which ferrocene is oxidised at +0.56V). We believe that these oxidation processes may be formulated as follows:

(a) $Cl_2(PPh_3)Ru(III)(\mu\text{-}Cl)_3Ru(II)(PPh_3)_2(CS) \xrightarrow{-e^-}$

$[Cl_2(PPh_3)Ru(III)(\mu\text{-}Cl)_3Ru(III)(PPh_3)_2(CS)]^+$

(b) $Cl_2(PPh_3)Ru(III)(\mu\text{-}Cl)_3Ru(III)(PPh_3)_2(CS) + \xrightarrow{-e^-}$

$[Cl_2(PPh_3)Ru(IV)(\mu\text{-}Cl)_3Ru(III)(PPh_3)_2(CS)]^{2+}$

This mixed-valence complex is therefore worthy of further extended spectroelectrochemical study since it should provide two mixed-valence oxidation states of the same complex.

5.4 EXPERIMENTAL

Electrochemical studies were performed as described previously using the PAR model 170 potentiostat and programmer.

Spectroelectrochemical studies were carried out as previously described using the Perkin-Elmer Lambda 9 spectrophotometer. Temperature control was achieved as previously described. $Cl(PPh_3)_2Ru(\mu\text{-}Cl)_3Ru(PPh_3)_2CS$ was prepared as described in the literature.[10]

Materials

PPh_3 and CS_2 were obtained from Aldrich.

$RuCl_3 \cdot 3H_2O$ from Johnson Matthey.

Methylene chloride was purified as described previously.

All other solvents were used as obtained without further purification.

$TBABF_4$ was made as described previously.

5.5 REFERENCES

1. R.H. Prince and K.A. Raspin, J.Inorg.Nucl.Chem.; 1969, 31, 695.
2. N.W. Alcock and K.A. Raspin, J.Chem.Soc. A; 1968, 2108.
3. P.W. Armit, Ph.D. Thesis, University of Edinburgh, 1977.
4. P.W. Armit, A. Boyd and T.A. Stephenson, J.Chem.Soc., Dalton Trans.; 1975, 1663.
5. R.C. Zarate, Ph.D. Thesis, University of Edinburgh, 1981.
6. T. Easton, Ph.D. Thesis, University of Edinburgh, 1985.
7. A.J. Lindsay, Ph.D. Thesis, University of Edinburgh, 1982.
8. H.A. Hudali, J.V. Kingston and H.A. Tayim, Inorg.Chem.; 1979, 18, 1391.
9. R.O. Gould, C.L. Jones, W.J. Sime and T.A. Stephenson, J.Chem.Soc., Dalton Trans.; 1977, 669.
10. P.W. Armit, W.J. Sime and T.A. Stephenson, J.Chem.Soc., Dalton Trans.; 1976, 2121.
11. P.W. Armit, W.J. Sime, T.A. Stephenson and L. Scott, J.Organomet.Chem.; 1978, 161, 391.
12. L.W. Gosser, W.H. Knoth and G.W. Parshall, J.Am.Chem.Soc.; 1973, 95, 3436.
13. L.W. Gosser, W.H. Knoth and G.W. Parshall, J.Mol.Catal.; 1977, 2, 253.
14. T. Arthur, Ph.D. Thesis, University of Edinburgh, 1980.
15. P.W. Armit, T.A. Stephenson and E.S. Switkes, J.Chem.Soc., Dalton Trans.; 1974, 1139.
16. A.J. Fraser and R.O. Gould, J.Chem.Soc., Dalton Trans.; 1974, 1139.

17. J.A. McCleverty, D. Seddon and R.N. Whitely, J.Chem. Soc., Dalton Trans.; 1975, 839.

18. R.A. Head and J.F. Nixon, J.Chem.Soc., Dalton Trans.; 1978, 901 and references therein.

19. R.O. Gould, W.J. Sime and T.A. Stephenson, J.Chem.Soc., Dalton Trans.; 1978, 76.

20. R.K. Pomeroy, M. Elder, D. Hall and W.A.G. Graham, J.Chem.Soc., Chem.Comm.; 1969, 381.

21. R.A. Contreras-Zarate, Ph.D. Thesis, University of Edinburgh, 1981.

22. F.A. Cotton, M. Matoz and R.C. Torralba, Inorg.Chem.; 1989, 28, 1516.

23. M.B. Robin and P. Day, Adv.Inorg.Chem. and Radiochem.; 1967, 10, 247.

24. G.A. Heath, A.J. Lindsay, T.A. Stephenson, D.K. Vattis, J.Organomet.Chem.; 1982, 233, 353.

25. N.S. Hush, Prog.Inorg.Chem.; 1967, 8, 391.

26. M.J. Powers, R.W. Callahan, D.J. Salmon and T.J. Meyer, Inorg.Chem.; 1976, 15, 1457.

27. T.J. Meyer, Chem.Phys.Lett.; 1979, 64, 417 and references therein.

28. R.W. Callahan, F.R. Keene, T.J. Meyer and D.J. Salmon, J.Am.Chem.Soc.; 1977, 99, 1064 and R.W. Callahan and T.J. Meyer, Chem.Phys.Lett.; 1976, 39, 82.

29. G.M. Tom, C. Creutz and H. Taube, J.Am.Chem.Soc.; 1974, 96, 7827, and C. Creutz, Inorg.Chem.; 1978, 17, 3123.

30. M.J. Powers, R.W. Callahan, D.J. Salmon and T.J. Meyer, Inorg.Chem.; 1976, 15, 1457.

C H A P T E R 6

ELECTROCHEMICAL AND SPECTROELECTROCHEMICAL STUDIES OF SINGLE CN BRIDGED BIRUTHENIUM COMPLEXES

6.1 INTRODUCTION

The emphasis in this thesis has been on triply-bridged Ruthenium and Osmium binuclear complexes. Only by introducing asymmetry into the terminal ligand sets of the complexes of this type did we observe Class II type behaviour in the mixed-valence, M(II)M(III), M=Ru, state. An alternative approach to binuclear species with weak metal-metal interactions is to consider complexes with a singly bridging ligand rather than three. Much work has been carried out on Ruthenium mixed-valence complexes of this type and Class I, II and III species have all been observed.

A. Pyrazine Bridged Species

The Creutz-Taube ion,[1] $[(NH_3)_5Ru(pyz)Ru(NH_3)_5][C_7H_7SO_3]_5 \cdot 3H_2O$, pyz = pyrazine, has been a subject of much controversy over the years. The complex is prepared by the reaction of $[(NH_3)_5Ru(H_2O)]^{2+}$ with pyrazine in a 2:1 mole ratio. This gives the $[(NH_3)_5Ru(pyz)Ru(NH_3)_5]^{4+}$ complex which on oxidation with either Ce(IV) or Ag(I) yields the mixed-valence complex of interest.

This species was originally considered to be a Class II complex by Creutz and Taube on the basis of the electronic spectrum obtained. An absorption band is observed at 6350 cm^{-1} (ε=5000 $mol^{-1}cm^{-1}dm^3$) and was assigned as an intervalence charge transfer band on the basis that it was not observed in either the $[Ru(II)Ru(II)]^{4+}$ or $[Ru(III)Ru(III)]^{6+}$ species. Since this early study the complex has been the subject of intensive investigations. Studies by Hush[2] opposed the original conclusions and suggested that the complex is in

fact a Class III species. He observed that the low energy band under study is very intense and the band halfwidth is six times narrower than predicted by theory. The position of the band, ν_{max}, was found to be independent of the solvent used.

Crystallographic studies by Ludi[3] of $[(NH_3)_5Ru(pyz)Ru(NH_3)_5]^{5+}$ are consistent with there being two equivalent Ruthenium centres thus supporting the conclusions made by Hush.

Substituted derivatives of the Creutz-Taube ion have been prepared.[4] These are of the general type $[(NH_3)_4LRu(pyz)Ru(NH_3)_5]^{n+}$ where L=D_2O, pyridine and pyrazine n=5; L=Cl^-, n=4. All these complexes also show a band in the low energy region of the electronic spectrum. For L=D_2O this band is at a slightly lower energy (6540 cm^{-1}) than for L=NH_3 whereas the other ligands L=pyridine, pyrazine, Cl^- all cause the band to move to higher energy.

Substitution of the NH_3 ligands at both ends of the molecule to give complexes of the type $[(NH_3)_4LRu(pyz)RuL(NH_3)_4]^{5+}$ and $[(NH_3)_3L_2'Ru(pyz)RuL_2'(NH_3)_3]^{5+}$ where L=pyridine and L_2'=2,2'-bipyridine cause the near infra-red band to move to lower energy, 6060 cm^{-1} in the case of L=pyridine and 5810 cm^{-1} in the case of L=2,2'-bipyridine. In all the pyrazine bridged complexes these bands were initially assigned as intervalence charge transfer bands i.e. the mixed-valence pyrazine bridged complexes all exhibit Class II type behaviour.

Related complexes of the type $[(bipy)_2XRu(pyz)RuY(bipy)_2]^{n+}$ and $[(bipy)_2XRu(pyz)Ru(NH_3)_5]^{n+}$, n=2,3,4,5, have been

prepared[1,4] where X,Y=Cl, NO_2; bipy=2,2'-bipyridine. These are prepared by routes detailed in scheme 6.1.1. The mixed-valence Ru(II)Ru(III) state has been studied in detail for these complexes. The electronic spectrum of the symmetric $[(bipy)_2ClRu(pyz)RuCl(bipy)_2]^{3+}$ complex shows a low energy band at 7690 cm^{-1} in acetonitrile. This band can be assigned as occurring due to an intervalence charge transfer transition by application of Hush Theory.[5] The complex has thus been designated as a Class II species. A similar treatment was applied to the complex $[(bipy)_2ClRu(pyz)Ru(NH_3)_5]^{4+}$ which confirmed that the observed band at 10,400 cm^{-1} in acetonitrile is also due to an intervalence charge transfer transition.

B. Other N-donor Bridging Ligands

A similar series of complexes where the bridging ligand is 4,4'-bipyridine have been prepared by Meyer et al.[6] The complex $[(bipy)_2(py)Ru(4,4'-bipy)Ru(py)(bipy)_2]^{5+}$ has been prepared by the oxidation of the tetrapositive species, $[(bipy)(py)Ru(4,4'-bipy)Ru(py)(bipy)_2]^{4+}$. The parent complex is prepared by the reaction of $[Ru(bipy)_2(NO)(py)](PF_6)_3$ in an acetone/methanol mixture with KN_3 and 4,4'-bipyridine. The low energy region of the absorption spectrum of the oxidised species $[(bipy)_2(py)Ru(4,4'-bipy)Ru(py)(bipy)_2]^{5+}$ in acetonitrile is dominated by a band at 7,900 cm^{-1}. The band successfully fits Hush's criteria for an intervalence charge transfer transition and thus this species is categorised as a Class II complex.

Several related complexes have been synthesised and

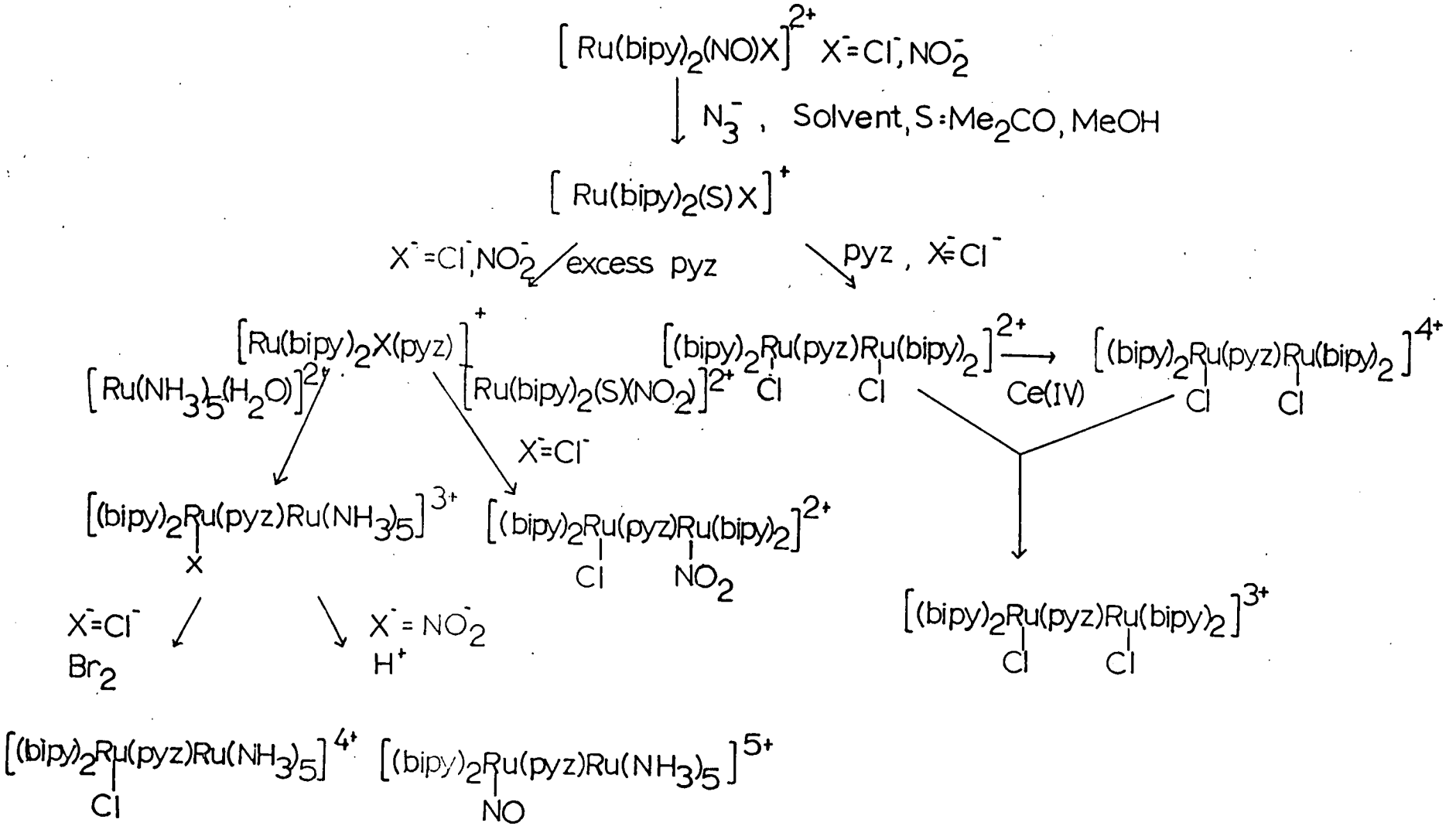

Scheme 6.1.1: Routes for Preparation of Some Ruthenium Binuclear Complexes with Pyrazine as a Bridging Ligand

studied. They broadly fall into four main categories as follows:

(a) $[(bipy)_2RuLM(bipy)_2]^{4+}$ [7]

M = Ru, Os

L = 2,2'-bipyrimidine (bpym), 1.

(b) $[(bipy)_2ClRuL'M(bipy)_2]^{2+}$

M = Ru, Os

L' = pyrazinecarboxylate anion (pyzc), 2.

(c) $[(bipy)_2ClRuL"RuCl(bipy)_2]^{2+}$ [8]

L" = pyrimidine (pym), 3; trans 1,2 bis (4-bipyridyl) ethane (bpe), 4; 1,2 bis (4-pyridyl) ethane (bpea), 5.

(d) $[(NH_3)_5RuL'''Ru(NH_3)_5]^{4+}$

L''' = 3,5; 1,2 bis (4-pyridyl) methane (bpm), 6; 3,3'-dimethyl-4,4'- bipyridine (3,3'-Me_2-4,4'-bipy), 7; bis (4-pyridyl) sulphide (bps), 8; diazapyrene (dap)[9], 9; cyanogen (NC-CN)[10], 10; tetrabutylmalonitrile (bmnH)[11], 11; p-benzoquinonedimmine (bqd)[12], 12.

The structures of the bridging ligands 1-12 are shown in figure 6.1.1.

Complexes of type (a), (b) and (c) are prepared in general by allowing a monomeric complex of the bridging ligand e.g. $[(bipy)_2M(pyzc)](PF_6)$, M=Ru, Os to react with 1.3 equivalents of $cis(bipy)_2Cl_2Ru\cdot 2H_2O$ in an ethanol/water

Figure 6.1.1: Structures of Bridging Ligands

1·bpym

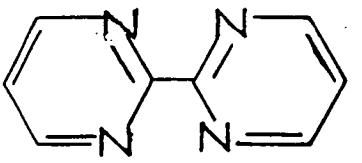

2·pyzc

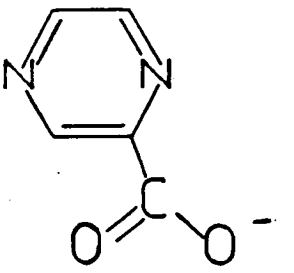

3·pym

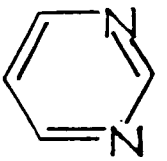

4·bpe

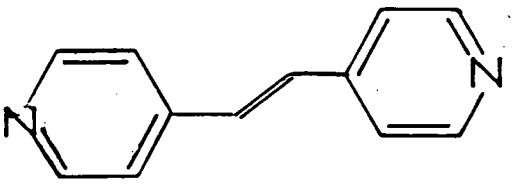

5·bpea

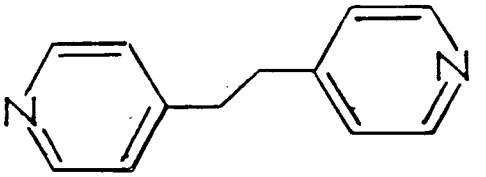

6·bpm

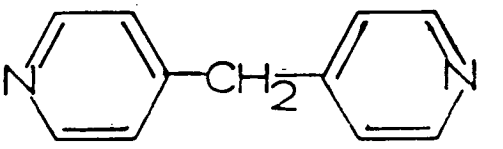

Figure 6.1.1: Structures of Bridging ligands

7. 3,3'-Me_2-4,4'-bipy

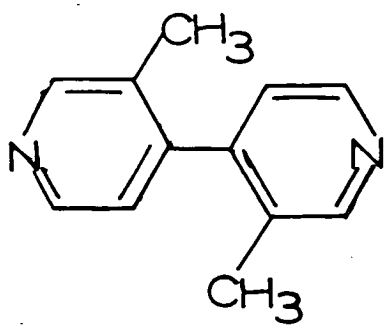

8. bps

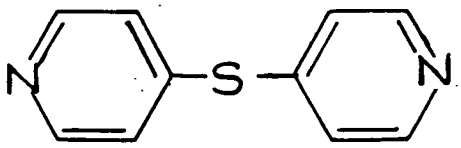

9. dap

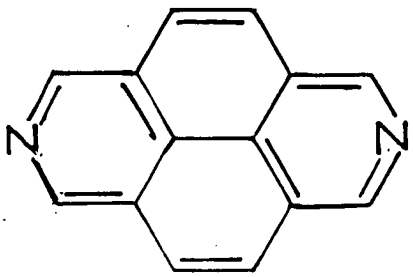

10. NC-CN

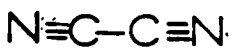

11. bmnh

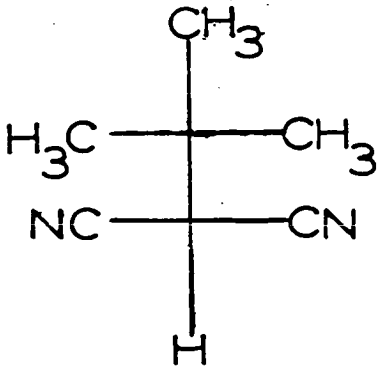

12. bdq

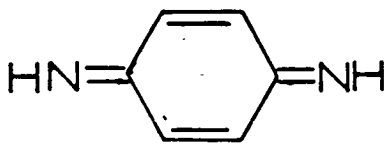

mixture for a period of 12-48 hours. The mixed-valence species are all prepared by electrochemical oxidation of the parent species.

Type (d) complexes where L'''=pym, bpea, bpm, 3,3'-Me_2-4,4'-bipy, bps, dap, NC-CN, bmnH, are prepared by analogous routes to the related pyrazine bridged complex previously discussed. Mixed-valence complexes of the type $[(NH_3)_5RuLRu(NH_3)_5]^{5+}$ are prepared by reduction of $[(NH_3)_5RuLRu(NH_3)_5]^{6+}$ to $[(NH_3)_5RuLRu(NH_3)_5]^{4+}$ by zinc amalgam and then mixing equimolar amounts of the tetrapositive and hexapositive ions.

Where L'''=bqd, $[(NH_3)_5RuLRu(NH_3)_5]^{5+}$ is prepared by the oxidation of $Ru(NH_3)_5(H_2O)^{2+}$ in the presence of p-phenylene-dihydrochloride, keeping the pH at 7 ± 0.5.

All mixed-valence species discussed above with the exception of L"=bpea, L'''=bpea, bpm exhibit an absorption in the low energy region of the electronic spectrum. The absorption spectrum of the complexes where L"=bpea, L'''= bpm and bpea show no low energy band and have thus been assigned as Class I species.

Analysis of the observed low energy bands according to Hush theory of the complexes where L=bpym, L'=pyzc, L"=pym, bpe, and L'''=bpe, 3,3'-Me_2-4,4'-bipy, bps, dap, show that they arise due to an intervalence charge transfer process and are thus Class II species. Complexes with asymmetric terminal ligation tend to have intervalence charge transfer bands at higher energy than the corresponding symmetric species. Replacing one ruthenium centre for osmium shifts

the band to higher energy. Both of these observations are a consequence of the energy difference, ΔE_o, increasing between the two sites (see Chapter 5).

When L''' = NC-CN, the low energy transition is observed at 6990 cm^{-1} in acetonitrile. The position of the low energy band does not vary with solvent. Only one ν(CN) stretching vibration is observed in the infra-red spectrum at 2330 cm^{-1} which is 50 cm^{-1} higher than in the case of the reduced complex and 120 cm^{-1} lower than for the oxidised species. These observations suggest that this complex is a Class III species i.e. the metal centres are strongly interacting. It is thought that complexes with L''' = bdq and bmnh are also of the Class III type.

C. Other Bridging Ligands

Recently complexes where L=NCX; x=S, Se have been prepared.[13,14,15] There are two Classes of these complexes:

(a) $[Cl(bipy)_2Ru(NCX)Ru(bipy)_2Z]^{n+}$ [13,14]

$Z = Cl^-, NO_2^-, NCS^-$

$n = 1, 2, 3$

$X = S, Se$

(b) $[(NH_3)_5Ru(NCX)Ru(NH_3)_5]^{4+}$ [15]

$X = S$

Scheme 6.1.2 details the syntheses of type (a) complexes. Complex (b) is prepared by the reaction of $[Ru(NH_3)_5N_2]Br_2$ with $[Ru(NH_3)_5SCN]Br_2$ in water.

Studies have shown that complex (b) is a Class III species. By changing the terminal ligands from NH_3 to bipy

Scheme 6.1.2: Routes for Preparation of Some Binuclear Ruthenium Complexes of the type $[Cl(bipy)_2RuXRu(bipy)_2Y]^{3+}$ where $X^- = NCS^-$, $NCSe^-$ and $Y = Cl^-$, NCS^-, NO_2^-

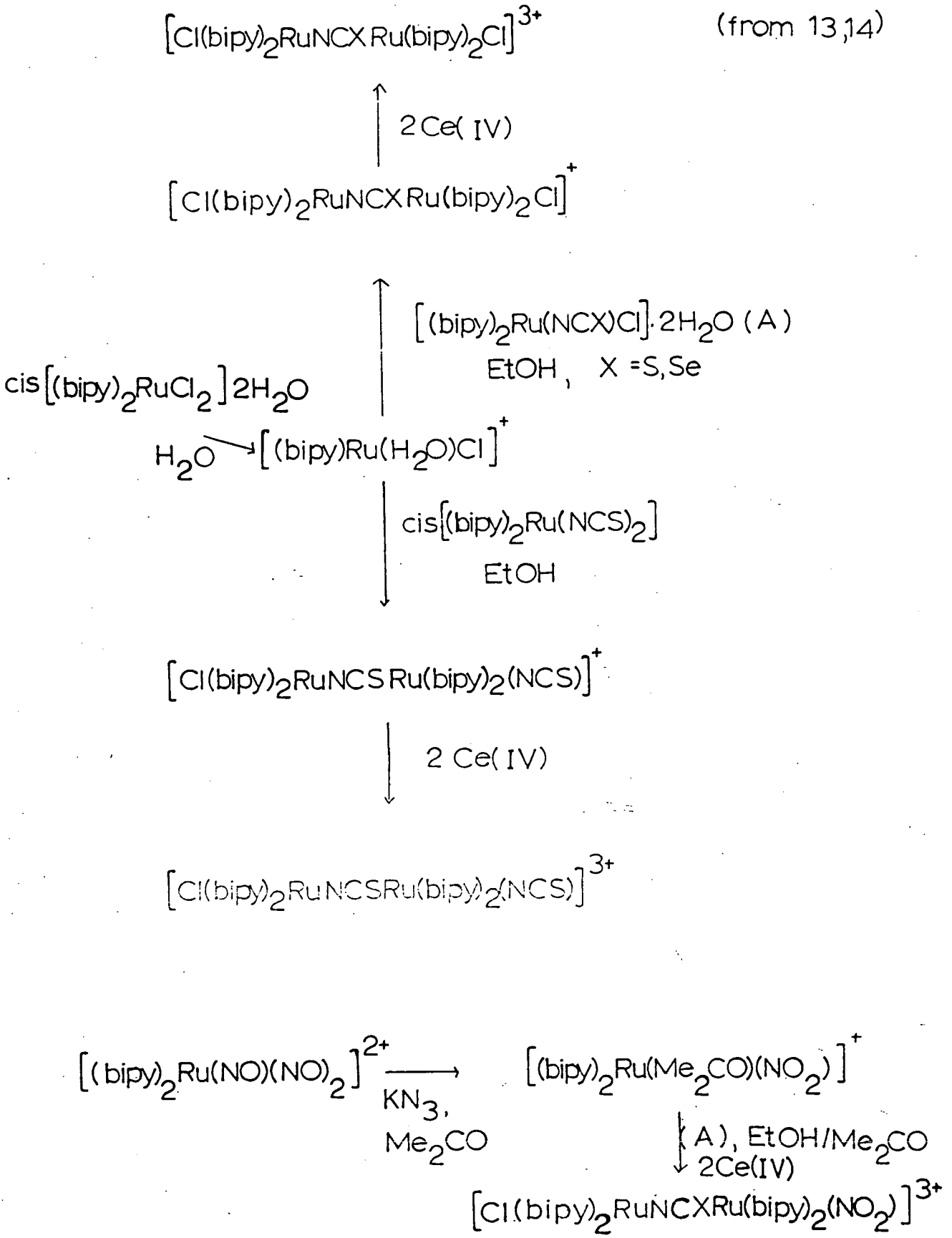

as in Type (a) species leads to the extent of metal-metal interaction decreasing in the mixed-valence state. Thus these complexes have been determined to exhibit Class II type behaviour.

This present study involves cyano-bridged complexes of the type $[CpL_2Ru(II)-C\equiv N-Ru(II)L_2Cp]PF_6$[16] where L is a soft neutral ligand. The complexes are shown below:

(1) $[Cp(PPh_3)_2Ru-C\equiv N-Ru(PPh_3)_2Cp]PF_6$

(2) $[Cp(PPh_3)_2Ru-C\equiv N-Ru(Ph_2P(CH_2)_2PPh_2)Cp]PF_6$

(3) $[Cp(Ph_2P(CH_2)_2PPh_2)Ru-C\equiv N-Ru(PPh_3)_2Cp]PF_6$

(4) $[Cp(PPh_3)(^tBuNC)Ru-C\equiv N-Ru(PPh_3)_2Cp]PF_6$

(5) $[Cp(PPh_3)_2Ru-C\equiv N-Ru(PPh_3)(CO)Cp]PF_6$

Cyano-bridged mixed valence complexes of the type $[(NH_3)_5Ru-N\equiv C-M(CN)_5]^-$ [17] where M=Fe, Os and $[(CN)_5Fe-C\equiv N-Fe(CN)_5]^{6-}$ [18] have been studied previously and all were shown to exhibit Class II behaviour.

Complexes (1)-(5) are prepared by the reaction of the monomeric cyano-species $CpRuL_2CN$ with the relevant monomer $CpRuClL_2$ where L is as before.

Complex (3) has been characterised crystallographically confirming the binuclear structure with a bridging cyano group.[16] The central four atoms Ru(1), N(1), C(1) and Ru(2) are almost colinear with an angle of 168° at N(1) and 175° at C(1). The Ru-C(1) bond length of 2.03Å is longer than that found in monomeric ruthenium isonitrile complexes e.g. $[RuCl_2(CO)(PPh_3)_2(CNC_6H_4Cl\text{-}\underline{p})]\cdot EtOH$ has a Ru-C distance of 1.94Å.[19] The Ru-N distance is however shorter than observed for typical Ru-N donor complexes, being 2.07Å compared with 2.165Å in $[Ru(\eta^4C_8H_{12})Cl_2(CO)(NCMe)]$.[20] This observation

suggests that the positive charge is localised on the ruthenium centre bearing the nitrogen. An electrochemical study of these cyano-bridged complexes was carried out to determine the redox processes available in these complexes. Any mixed-valence Ru(II)Ru(III) state at accessible potential will be probed by spectroelectrochemical methods to determine the nature of the metal-metal interactions.

6.2 RESULTS AND DISCUSSION

Complexes (1)-(5) were supplied by Dr. S.J. Simpson, University of Salford.

(a) Results:

6.2.1 Electrochemistry

Electrochemical studies were carried out as previously described. The results are shown in Table 6.2.1. Figure 6.2.1 shows the cyclic voltammogram obtained for complex (1).

Complex (1) undergoes two one-electron oxidations in methylene chloride/0.5M $TBABF_4$. The first is reversible at 290K; the second however is only reversible at T=243K.

Complexes (2), (3) and (4)* also show two oxidations. The first one-electron process is reversible whereas the second in every case is irreversible regardless of the temperature and scan rate used.

Complex (5) shows only one, one-electron oxidation at +1.22V which is more positive than the other first

* Complex (4) shows an additional oxidation at +0.88V as a shoulder of that at 1.03V. It is thought that this occurs due to cis/trans isomerism.[21]

Table 6.2.1: $E_{\frac{1}{2}}$ (V) values for Complexes (1) - (5) in Methylene Chloride / 0.5M $TBABF_4$ (T = 290K)

Compound	$E_{\frac{1}{2}}$ (V versus Ag/AgCl) [a]			
	II,II / II,III		II,III / III,III	
1	1.00	(0.060) [d]	1.58 [b]	(0.060)
2	0.86	(0.060)	1.44 [c]	
3	0.93	(0.060)	1.49 [c]	
4	1.03	(0.070)	1.56 [c]	
5	1.22	(0.060)	-	

a. Ferrocene/Ferrocinium at +0.56V

b. Reversible at T = 243K

c. Irreversible even at low temperatures

d. $E_pF - E_pR$ values are shown in brackets (where E_pF and E_pR are potentials at the maximum of the forward and reverse scans respectively.

Figure 6.2.1: Electrochemistry of [1] in Methylene Chloride / 0.5M $TBABF_4$ at T = 243K

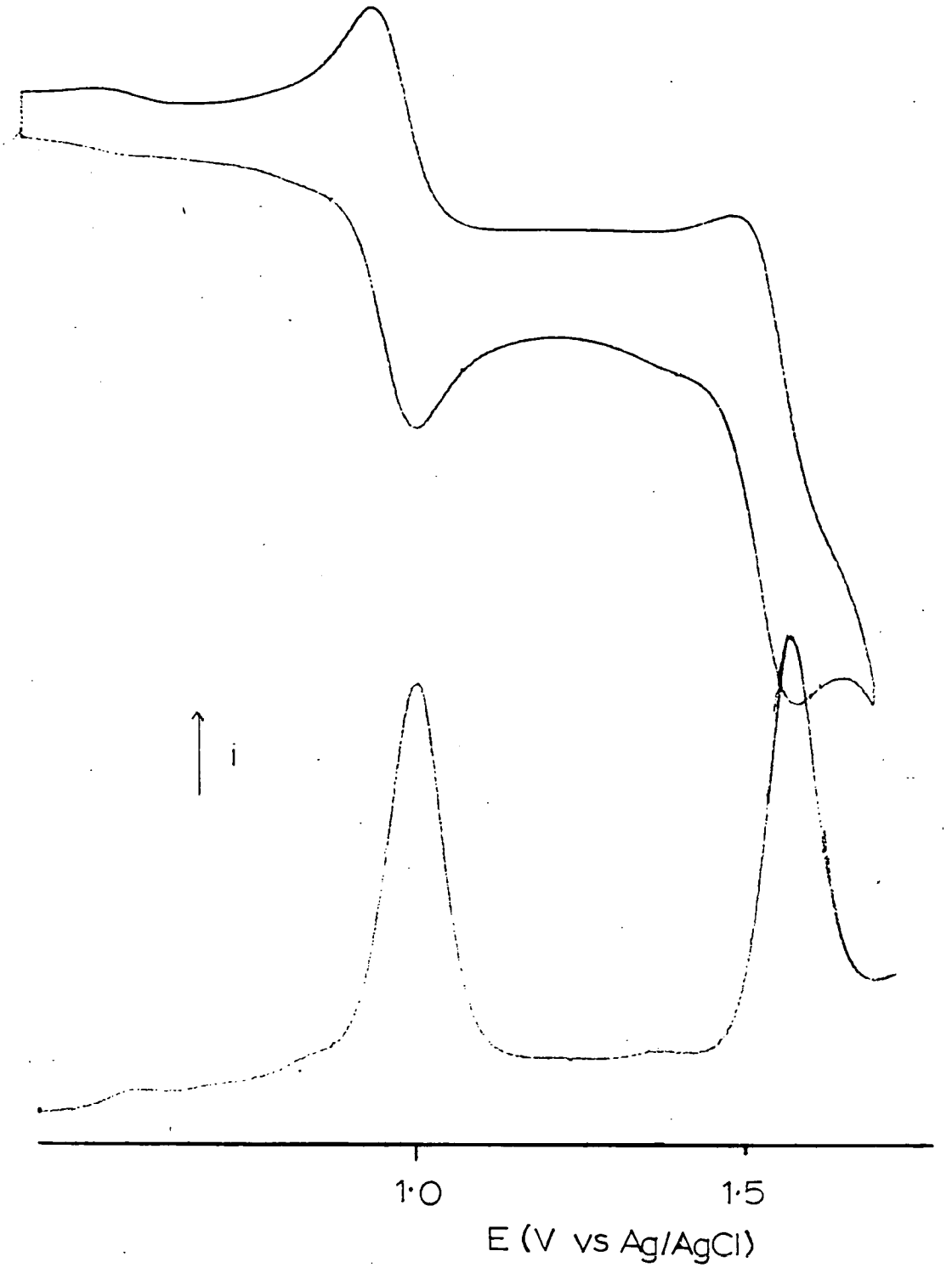

oxidation processes observed. No other redox processes were observed. We note that the oxidation at +1.22V is fully reversible which is unusual in transition metal complexes with coordinated CO.

The separation between the first and second oxidation processes is between 0.5 and 0.6V which is similar to that observed for the symmetric triply bridged complexes discussed in Chapters 1-4.

6.2.2 Spectroelectrochemistry

Spectroelectrochemical studies were carried out as described previously for complexes (1)-(5).

The mixed-valence Ru(II)Ru(III) $[A]^{+}$, where A=complexes (1)-(5), state was electrogenerated *in situ* for each species in methylene chloride/0.5M $TBABF_4$ at a suitable potential using the O.T.T.L.E. cell ($\sim$ 0.2V beyond the redox process). The temperature was maintained at T=243K for complexes (1)-(4) and 272K for complex (5). The absorption spectra were recorded over the range 4000-40,000 cm^{-1}.

Only complex (1) displayed a reversible second oxidation, therefore the species $[1]^{2+}$ was electrogenerated using the O.T.T.L.E. cell at a potential of E=+1.85V. In this case the temperature was maintained at T=233K.

Of interest to us is the low energy region of the spectrum, since it is this region which is diagnostic of mixed-valence behaviour. Therefore, only the near infra-red region of the absorption spectrum will be discussed.

1. [A] , where A = Complexes (1)-(5)

All species, [A] show no bands in the low energy region of the electronic spectrum.

2. $[A]^+$

On oxidation to $[A]^+$ when A=complexes (1)-(4) a very intense band forms in the low energy region of the electronic spectrum with extinction coefficients ranging from 5704 to 7332 $mol^{-1}cm^{-1}dm^3$. The results are shown in Table 6.2.2. Figure 6.2.2 shows the spectrum obtained for the oxidation of $[1] \rightarrow [1]^+$.

In the cases of complexes (2) and (3) this band is asymmetric. Complex (2) has a shoulder at low energy and (3) one at higher energy. Figure 6.2.3 shows the spectra obtained for $[2]^+$ and $[3]^+$.

In complexes $[1]^+$, $[2]^+$ and $[3]^+$ the position of this band, ν_{max}, was found to be independent of the solvent used. Figure 6.2.4 shows the graph of ν_{max} versus $^1/D_{op} - ^1/D_s$ for $[1]^+$. The solvents used were:-

(1) Chloroform / 0.5M $TBABF_4$

(2) Methylene Chloride / 0.5M $TBABF_4$

(3) Acetone / 0.1M $TBABF_4$

(4) Acetonitrile / 0.1M $TBABF_4$

ν_{max} varies from 10,024 cm^{-1} in the least polar solvent, chloroform, to 9952 cm^{-1} in the most polar solvent, acetonitrile. The band halfwidth, $\Delta_{\frac{1}{2}}$, which in all cases is < 5000 cm^{-1} varies from 3200 cm^{-1} for complex (3) to 4200 cm^{-1} for complex (2) and does not vary with temperature. Both indicate that the metal centres are strongly interacting

Table 6.2.2: Band Positions (ν_{max}) in the Near Infra-Red Region of the Electronic Absorption Spectrum for Complexes (1) - (5) in Methylene Chloride / 0.5M $TBABF_4$

	II,II		II,III		III,III	
Compound	$\nu_{max}(cm^{-1})$	$\varepsilon(mol^{-1}cm^{-1}dm^3)$	$\nu_{max}(cm^{-1})$	$\varepsilon(mol^{-1}cm^{-1}dm^3)$	$\nu_{max}(cm^{-1})$	$\varepsilon(mol^{-1}cm^{-1}dm^3)$
1 [a]	-	-	9,773	7,332	12,309	3,503
2 [a]	-	-	11,568	5,704	-	-
3 [a]	-	-	9,994	7,320	-	-
4 [a]	-	-	10,052	6,677	-	-
5 [b]	-	-	15,200	1,344	-	-

a. T = 243K
b. T = 272K

Figure 6.2.2: Spectrum showing the Conversion of [1] → $[1]^+$ in Methylene Chloride / 0.5M $TBABF_4$

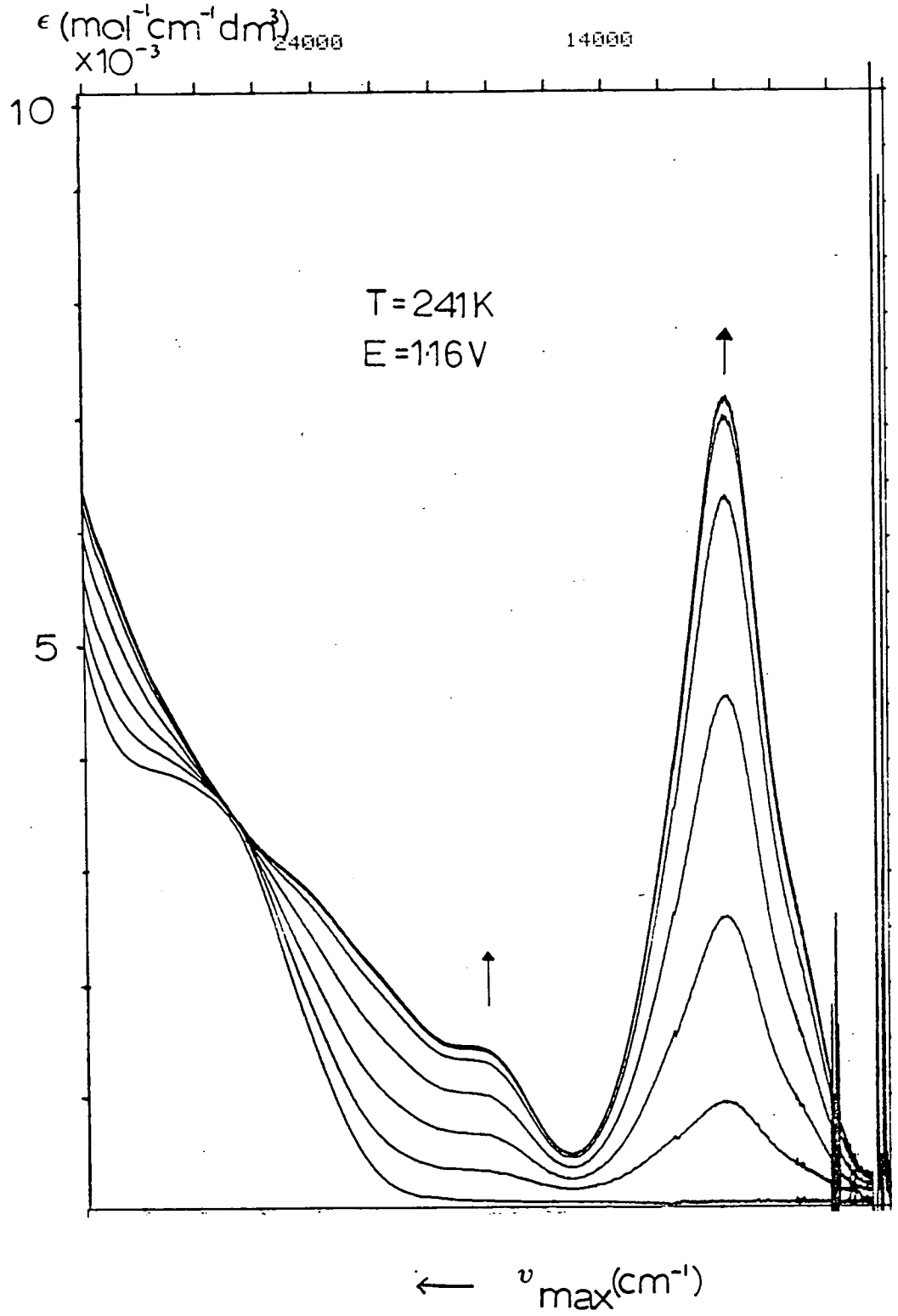

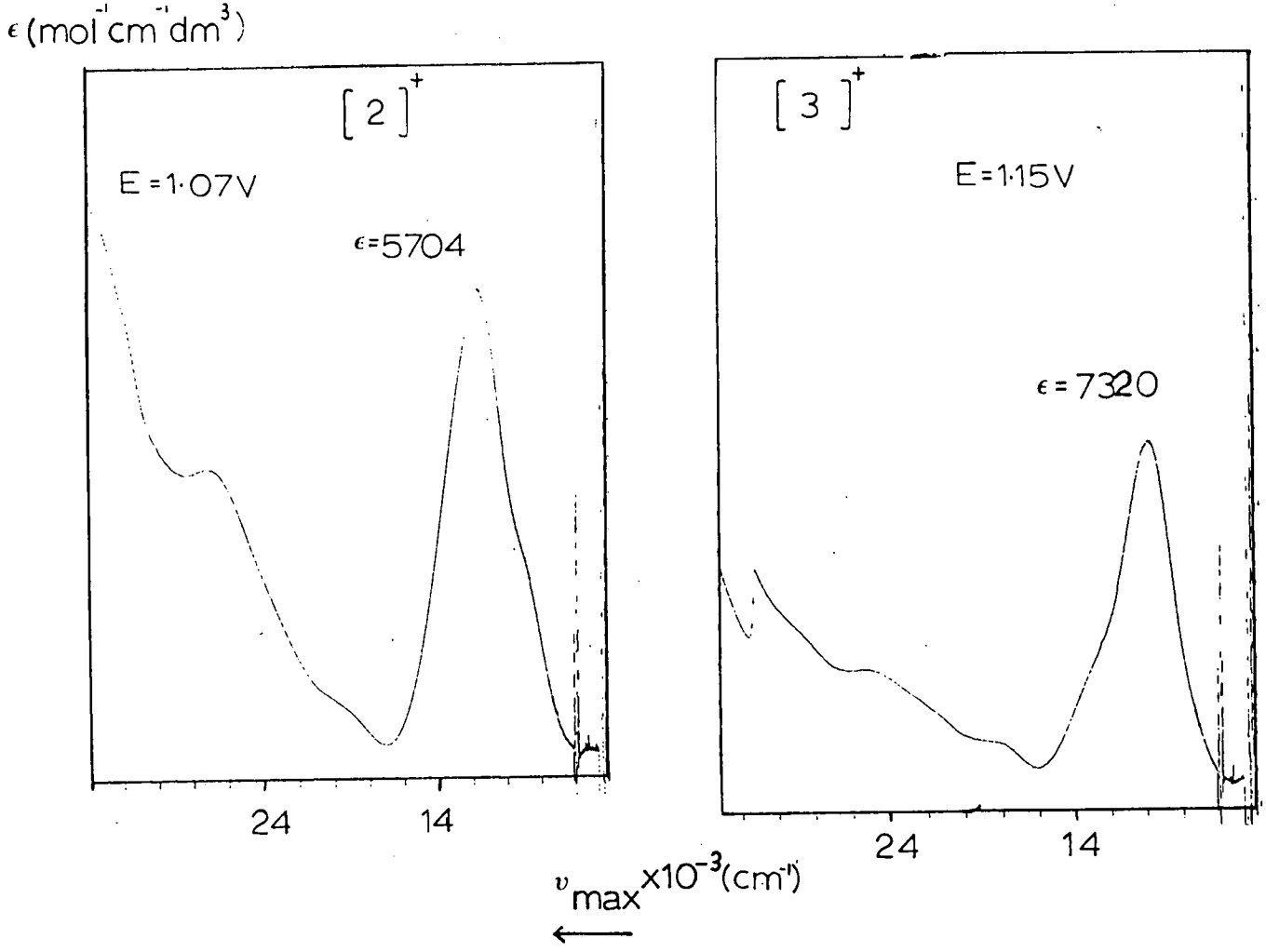

Figure 6.2.3: Spectra of $[2]^+$ and $[3]^+$ in Methylene Chloride / 0.5M $TBABF_4$ at T = 243K

Figure 6.2.4: Graph of ν_{max} (cm^{-1}) versus $^{1}/D_{op} - {}^{1}/D_{s}$ for $[1]^{+}$ in Methylene Chloride / 0.5M $TBABF_4$ at T = 243K

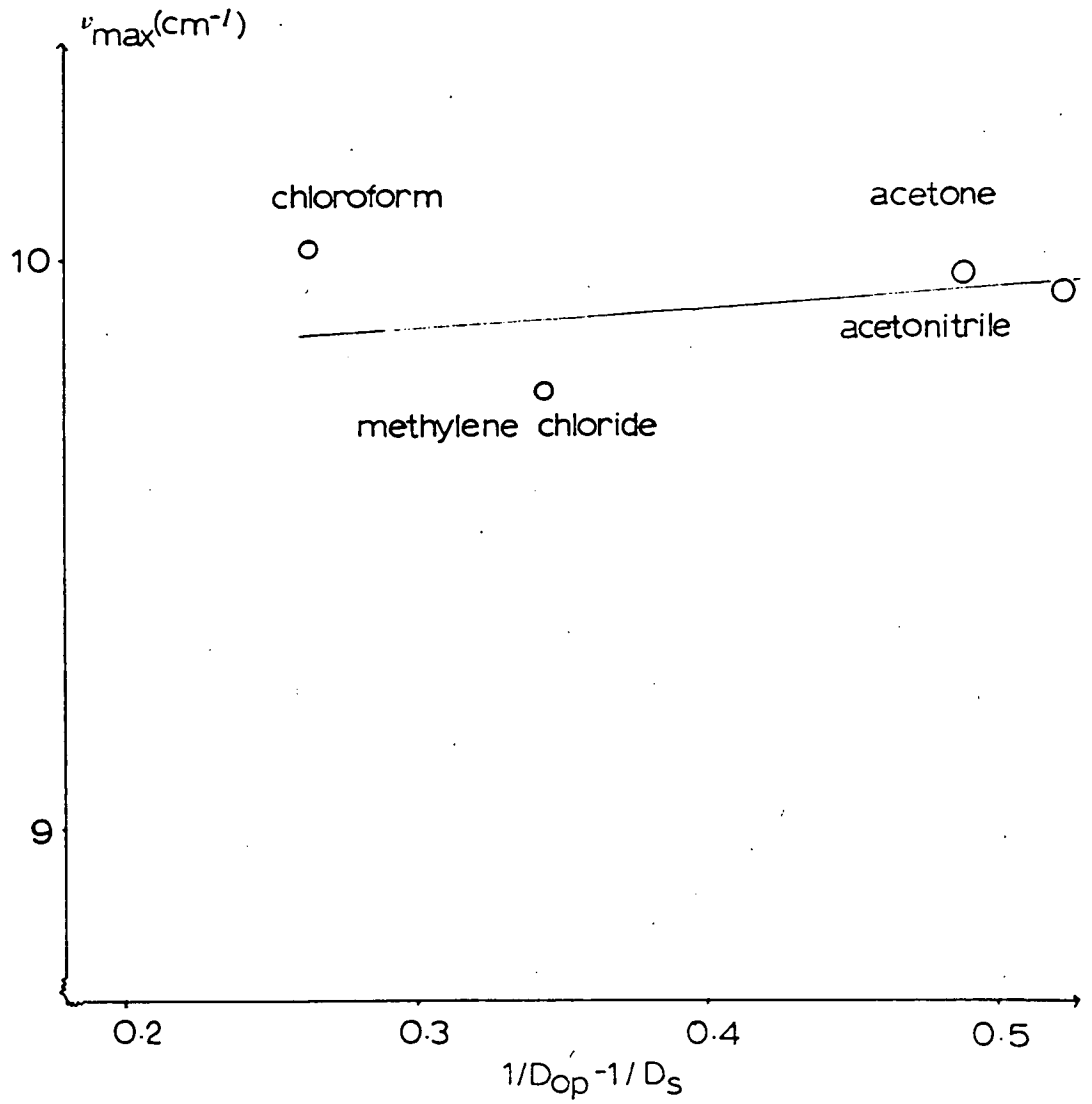

and that the species are Class III compounds.

The largest extinction coefficient is observed with complex $[1]^+$ i.e. that of lowest energy and the smallest with complex $[2]^+$, which has the highest energy band. The bands with larger extinction coefficients tend to have lower $\Delta_{\frac{1}{2}}$ values and vice versa for those with smaller extinction coefficients. All bands will therefore have similar values of oscillator strength, f ($f=4.6\times10^{-9}\varepsilon_{max}\Delta_{\frac{1}{2}}$), which is a measure of the integrated intensity under the absorption profile.

Complex (5) shows very different behaviour from (1)-(4). The results are shown in Table 6.2.2. A much weaker band ($\varepsilon=1344$ $mol^{-1}cm^{-1}dm^3$) is observed at 15,200 cm^{-1} in methylene chloride/0.5M $TBABF_4$. The band halfwidth does vary with temperature, decreasing from 2900 cm^{-1} at 282K to 2200 cm^{-1} at 203K. Figure 6.2.5 shows the observed spectrum for $[5] \rightarrow [5]^+$.

Attempts were made to study this complex in other solvents. In acetonitrile and chloroform the species decomposed to give an unknown compound. In acetone a band was observed at 15,200 cm^{-1} for $[5]^+$. From this very limited information it appears that the position of the band, ν_{max}, is independent of the solvent used. Further studies in other solvents are therefore required providing suitable ones can be found in which the complex in either oxidation state does not decompose. Temperature and solvent studies therefore give conflicting results. On the basis of the extinction coefficient, compared with those for complexes (1)-(4), the fact that it is higher in energy than

Figure 6.2.5: (a) Electronic Absorption Spectrum of the conversion of [5] → $[5]^+$ and (b) Final Spectrum of $[5]^+$ in Methylene Chloride / 0.5M $TBABF_4$

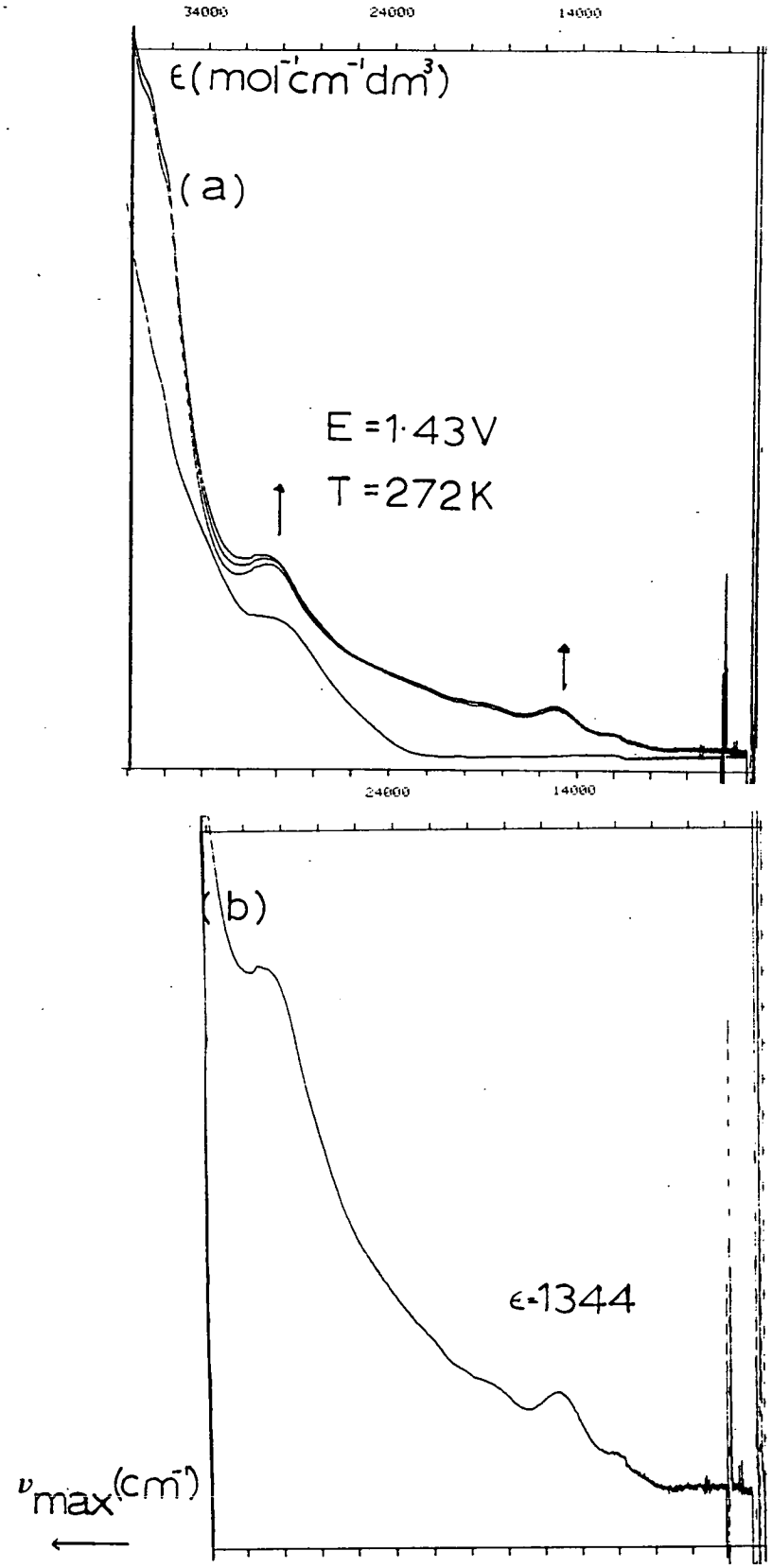

those observed for complexes (1)-(4) and that [5] shows no such band suggests we may be observing an intervalence charge transfer band.

3. $[A]^{2+}$

This was only observed for complex (1). The position of the bands are given in Table 6.2.2. Figure 6.2.6 shows the spectrum obtained for the oxidation of $[1]^{+} \rightarrow [1]^{2+}$ together with the final spectrum of $[1]^{2+}$.

Two bands are observed at 12,309 cm^{-1} and 16,015 cm^{-1}, which are weaker than that observed in $[1]^{+}$ (ε=3503 and 3113 $mol^{-1}cm^{-1}dm^{3}$ respectively).

(b) Discussion

Spectroelectrochemical results of the oxidised species $[A]^{+}$, A=(1)-(4) indicate that the two Ru centres are strongly interacting. The X-ray crystallographic study of [3] shows that the Ru-C≡N-Ru linkage is almost linear which suggests that the metal-metal interaction is either through direct d-d orbital overlap or involves orbitals on the CN bridging ligand. The electrochemical results would tend to favour the first suggestion since the oxidation potential of the process $[A] \rightarrow [A]^{+}$ occurs at very similar values to those of the triply bridged complexes discussed in Chapters 1-4. The qualitative molecular orbital calculations on the triple chloro-bridged binuclear species (Chapter 4) showed that the HOMO orbital had no contribution from the bridging ligands and was solely metal based. We therefore propose a similar interaction in these CN bridged complexes. Further consideration of the structure of [3] indicated that the

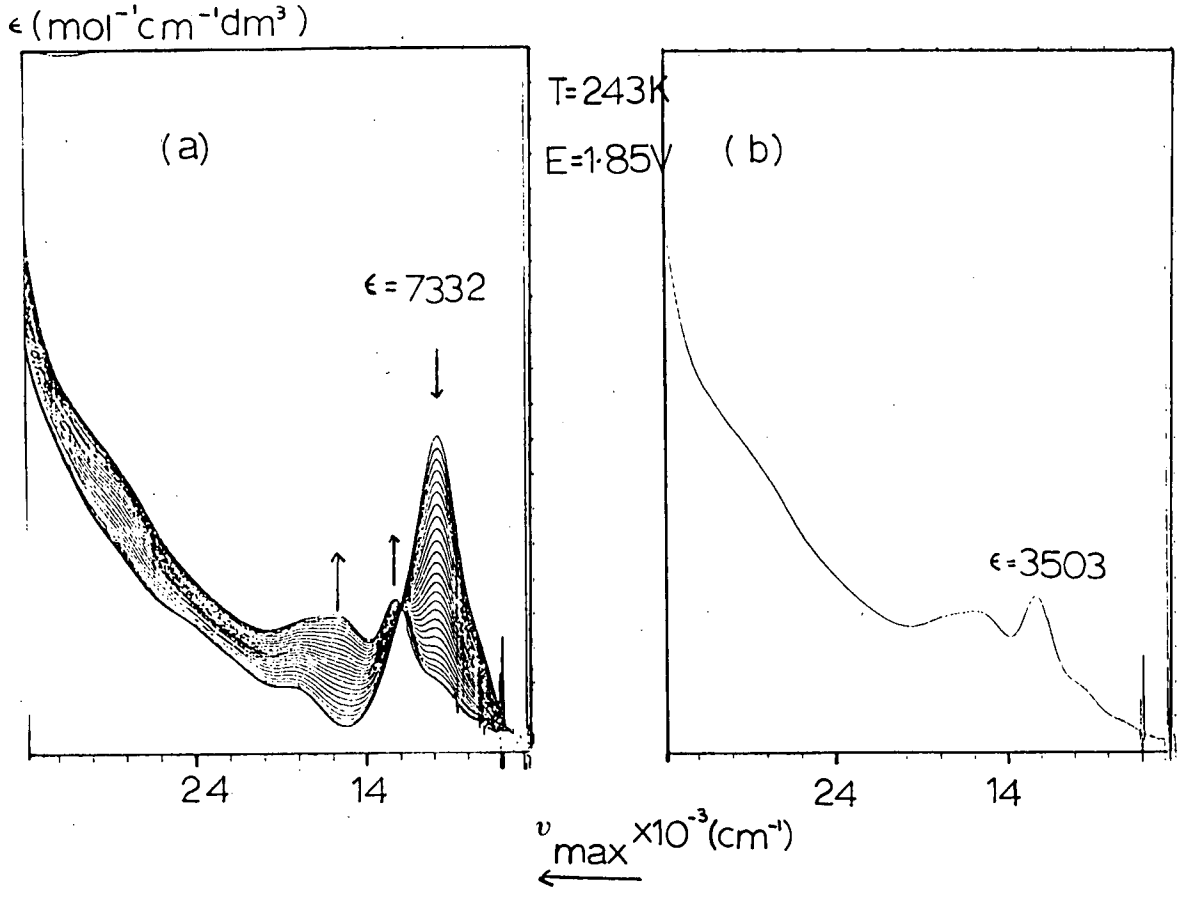

Figure 6.2.6: (a) Electronic Absorption Spectrum of the conversion of $[1]^{+} \rightarrow [1]^{2+}$ and (b) The Final Spectrum of $[1]^{2+}$

important orbital overlap between the two ruthenium centres will be via the d_{z^2} orbitals giving a σ and σ^* molecular orbital.

Complexes (1)-(4) all involve some degree of asymmetry and therefore there will be an energy difference between both ruthenium centres. It has been argued that in [3] the positive charge of the complex is localised on the ruthenium centre attached to the nitrogen end of the CN bridging ligand (henceforth referred to as the Ru-N end).

Thus we would expect the Ru(II) centre attached to the carbon of the CN ligand (the Ru-C end) to be stabilised towards Ru(III) compared with the Ru-N end. The electronic influence of negatively charged ligands in stabilising the Ru(III) centre is well documented. For example if we compare the potentials for the Ru(II) → Ru(III) process on $[Ru(bipy)_2(py)Cl]^+$ at +0.76V and $[Ru(bipy)_2Cl_2]$ at +0.31V (both versus S.C.E. reference electrode),[22] then the latter complex oxidises at less positive potentials than the former.

A qualitative molecular orbital diagram for $[1]^+$ is shown over page.

The molecular orbital σ^* which is the HOMO of the complex has predominantly d-orbital character at the Ru-C end and the σ orbital will have predominantly d-orbital character at the Ru-N end. Upon oxidation of [1] → $[1]^+$, we envisage removal of one electron from the σ^* orbital and the near infra-red absorption is assigned to the $\sigma \rightarrow \sigma^*$ transition.

In order to rationalise the electrochemical and spectro-electrochemical results for complexes (1)-(5) we have

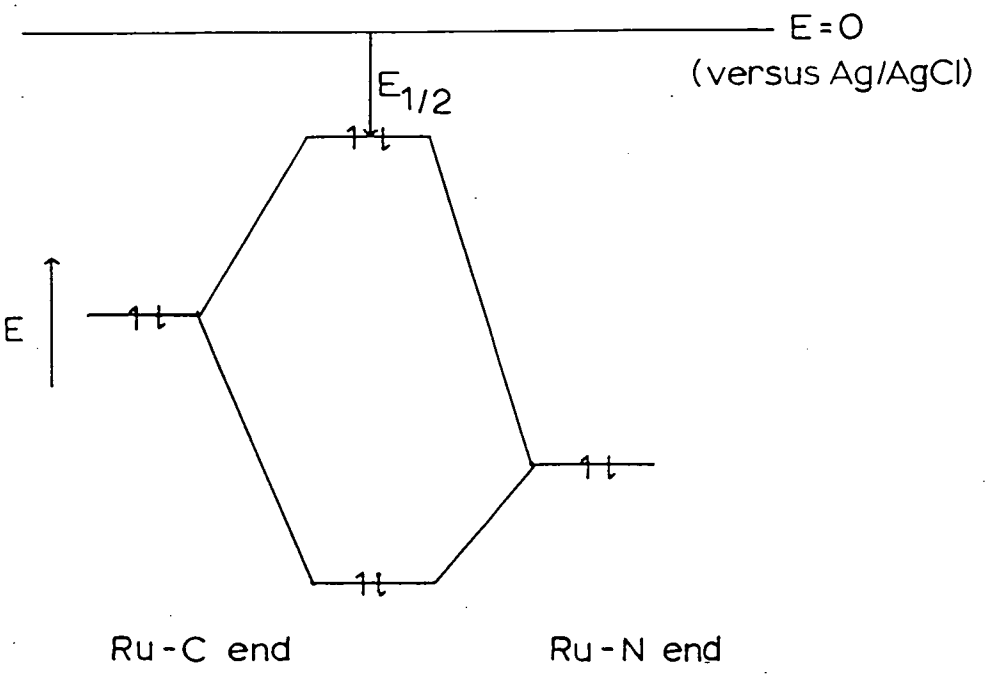

constructed a molecular orbital diagram. This is shown in Figure 6.2.7 in which complexes (2)-(5) are energetically related to complex (1). In complex (2) the Ru-N end has the bidentate $Ph_2P(CH_2)_2PPh_2$ ligand replacing two monodentate PPh_3 ligands in [1]. Although there are no literature values for the electronic parameter of the bidentate phosphine ligand we would expect it to be more electron releasing than the two PPh_3 ligands as it has only four electron withdrawing phenyl groups as opposed to six. This should stabilise the Ru-N end towards oxidation thereby making the two ruthenium centres energetically more equivalent which will result in a stronger interaction in $[2]^+$ than $[1]^+$. This is indeed observed experimentally as ν_{max} in $[2]^+$ is at higher energy than $[1]^+$. Furthermore the stronger interaction should result in a smaller $E_{\frac{1}{2}}$ value for $[2]^+$ compared to $[1]^+$ which is in agreement with experiment.

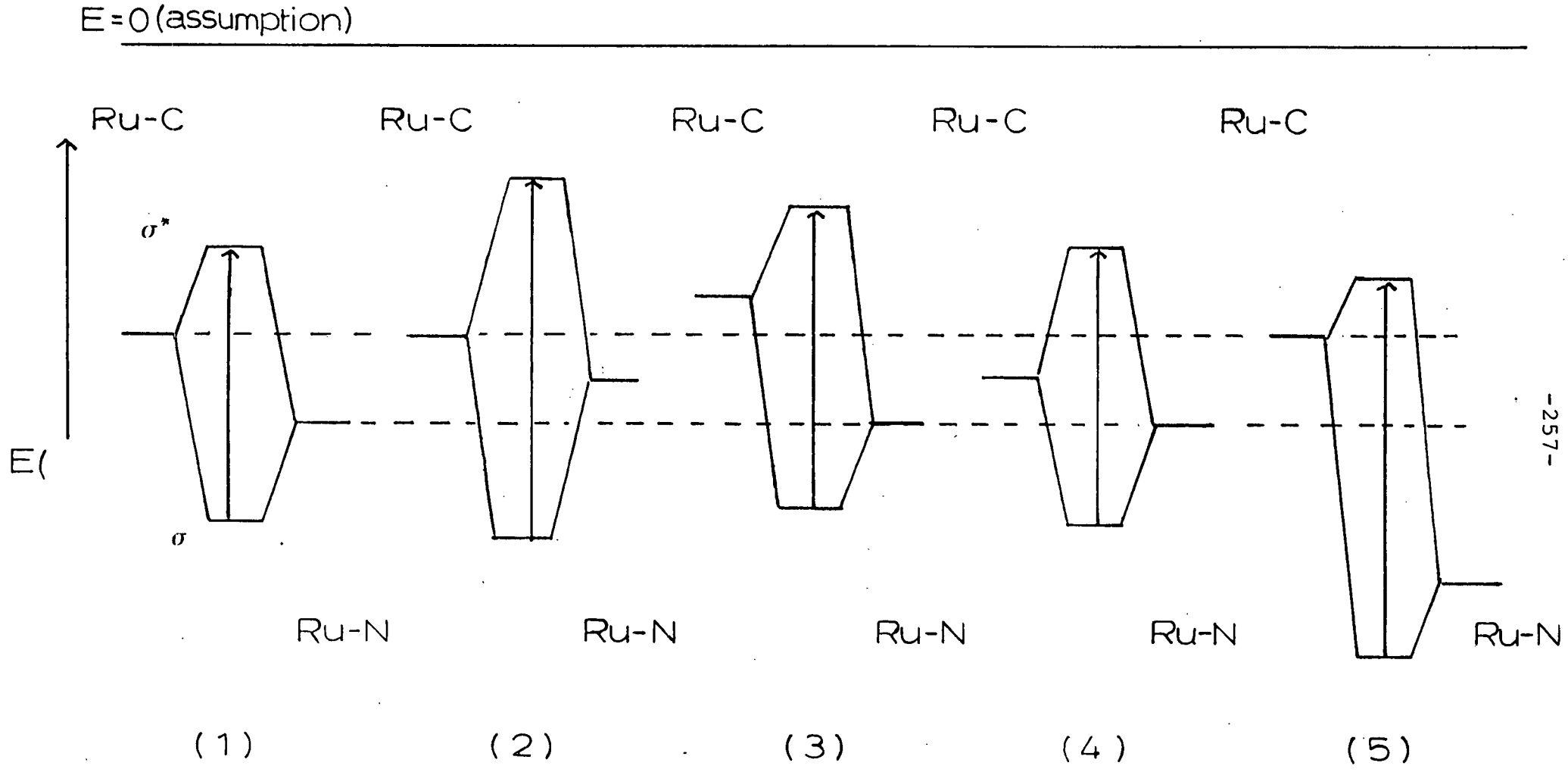

Figure 6.2.7: Molecular Orbital Diagram Energetically Relating Complexes 2 - 5 to 1

A similar argument applies to complex [3] in which the bidentate phosphine ligand is attached to the Ru-C end thereby making it more accessible to oxidation than in [1]. In this case the two ruthenium centres are less favourably energetically matched than in [1]. Experimental results indicate that the energy mismatch between the ruthenium centres is such that the oxidation process is easier than in [1] and we therefore conclude that the degree of interaction is less in $[3]^+$ than $[1]^+$; it is still however a strong interaction.

In complex [4], one PPh_3 group, at the Ru-C end of [1], has been replaced by the π-accepting ligand ^tBuNC (∿50% effective as the CO ligand).[23] This would be expected to destabilise the Ru-C end towards oxidation and therefore lead to a stronger interaction between the two ruthenium centres. This is observed spectroelectrochemically as ν_{max} for $[4]^+$ is higher in energy than for $[1]^+$. The oxidation potential for $[4] \rightarrow [4]^+$ is similar to that for $[1] \rightarrow [1]^+$ which indicates that the strong interaction in $[4]^+$ is almost negated by the "lowering" of the Ru-C end.

In complex [5], one of the PPh_3 ligands of the Ru-N end of [1] is replaced by the strongly π-accepting CO ligand. The spectroelectrochemical results were best explained using Class II type behaviour, that is a weakly interacting system. The electronic effect of the CO ligand is such that the energy mismatch between the two ruthenium centres is sufficient for the σ* orbital to have little or no contribution from the orbital on the Ru-N end, and the σ orbital has a similar contribution from the orbital on the Ru-C end.

The results and molecular orbital discussion combine to suggest that complexes $[2]^+$ and $[4]^+$ have the strongest metal-metal interaction and $[5]^+$ has the weakest.

A further one electron oxidation involves removal of an electron from an antibonding σ^* orbital which should result in the σ orbitals moving to lower energy and ν_{max} to higher energy as is observed. The work in previous Chapters showed that oxidation of, for example, the mixed-valence $[(P(OMe)_3)_3Ru(\mu\text{-}Br)_3Ru(P(OMe)_3)_3]^{2+}$ to $[(P(OMe)_3)_3Ru(\mu\text{-}Br)_3Ru(P(OMe)_3)_3]^{3+}$ led to an increase in metal-metal interaction. The bands observed in the low energy region of the electronic spectrum of $[(P(OMe)_3)_3Ru(\mu\text{-}Br)_3Ru(P(OMe)_3)_3]^{2+}$ move to higher energy and become more intense upon oxidation to $[(P(OMe)_3)_3Ru(\mu\text{-}Br)_3Ru(P(OMe)_3)_3]^{3+}$. The band observed in the low energy region of the electronic spectrum of $[1]^+$ is however weaker. It is important to remember that in the single CN bridged complexes the geometry of the bridge prevents the two ruthenium centres becoming much closer to one another. Thus, although electronic considerations favour an increased metal-metal interaction, steric considerations do not.

6.3 CONCLUSIONS

Complexes (1)-(4) are all Class III complexes with strongly interacting metal centres. Changing the ligands at each ruthenium centre alters the energy difference between the two metal centres which is reflected in the differing degree of metal-metal interactions observed.

Complex (5) is a Class II complex with weakly interacting metal centres.

It would be interesting to study a wider range of complexes of this type. Examples are shown below.

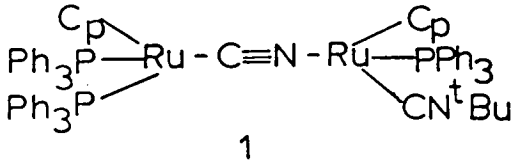

1

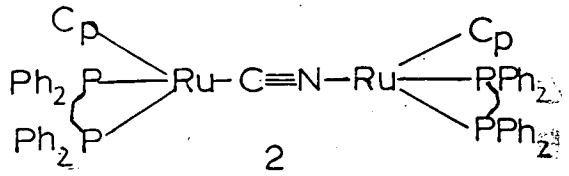

2

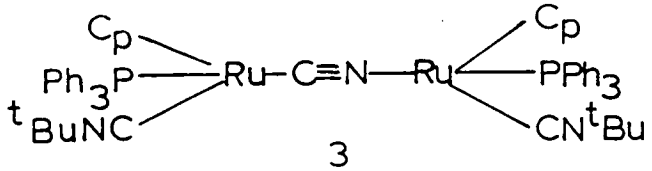

3

6.4 EXPERIMENTAL

Electrochemical studies were performed using the PAR model 170 potentiostat and programmer as described previously.

Spectroelectrochemical studies were carried out using the optically transparent thin layer electrode of the previously described design. The Perkin-Elmer Lambda 9 spectrophotometer was employed for these studies. Spectra

were recorded over the range 4000 cm^{-1} - 40,000 cm^{-1}. Temperature control was achieved as previously described.

Materials

Complexes (1)-(5) were supplied by Dr. S.J. Simpson, University of Salford.

Methylene chloride was purified as described previously. All other solvents were used as obtained, without further purification.

$TBABF_4$ was prepared as described previously.

6.5 REFERENCES

1. C. Creutz and H. Taube, J.Am.Chem.Soc.; 1969, 91, 3988.
2. J.K. Beattie, N.S. Hush and P.R. Taylor, Inorg.Chem.; 1976, 15, 992.
3. U. Furholz, S. Joss, H. Beat-Bürghi and A. Ludi, Inorg. Chem.; 1985, 24, 943.
4. C. Creutz and H. Taube, J.Am.Chem.Soc.; 1973, 95, 1086.
5. N.S. Hush, Prog.Inorg.Chem.; 1967, 8, 391.
6. M.J. Powers and T.J. Meyer, Inorg.Chem.; 1978, 17, 1785.
7. K.A. Goldsby and T.J. Meyer, Inorg.Chem.; 1984, 23, 3002.
8. M.J. Powers and T.J. Meyer , J.Am.Chem.Soc.; 1980, 102, 1289.
9. H. Fischer, G.M. Tan and H. Taube, J.Am.Chem.Soc.; 1976, 98 5512.
10. G.M. Tan and H. Taube, J.Am.Chem.Soc.; 1975, 97, 5310.
11. H. Krentzien and H. Taube, J.Am.Chem.Soc.; 1976, 98, 6379.
12. S. Joss, H. Beat-Bürghi and A. Ludi, Inorg.Chem.; 1985, 24, 949.
13. V. Palaniappan, S. Sathiah, H. Dutt-Bist, and U. Chandra-Agarwala, J.Am.Chem.Soc.; 1988, 110, 6403.
14. V. Palaniappan and U. Chandra-Agarwala, Inorg.Chem.; 1988, 27, 3568.
15. S.K.S. Yadav and U. Chandra-Agarwala, Polyhedron; 1985, 4, 1457.

16. G.J. Baird, S.G. Davies, S.D. Moon, S.J. Simpson and R.H. Jones, J.Chem.Soc., Dalton Trans.; 1985, 1479.

17. A. Ludi, Chimia; 1972, 26, 647.

18. R. Glauser, U. Hauser, F. Herren, A. Ludi, P. Roder, E. Schmidt, H. Siegenthaler and H. Wenk, J.Am.Chem.Soc.; 1973, 95, 8457.

19. G.R. Clark, Acta Cryst., Sect. B; 1982, 38, 2256.

20. R.O. Gould, C.L. Jones, D.R. Robertson and T.A. Stephenson, J.Chem.Soc., Dalton Trans.; 1977, 129.

21. N. Connelly, Chem.Soc. Reviews; 1989, 18, 153.

22. B. Durham, J.L. Walsh, C.L. Carter and T.J. Meyer, Inorg.Chem.; 1980, 19, 860.

23. A.C. Sarapu and R.F. Fenske, Inorg.Chem.; 1975, 14, 247, and 1972, 11, 3021.

A P P E N D I X 1

A.1 ELECTROCHEMICAL TECHNIQUES

Electrochemical studies have been carried out throughout this work. A brief outline of the apparatus and techniques used will now be given.[1] Electrodes, cell design, solvent and supporting electrolyte will be considered first.

A.1.1 Electrodes

In all the systems studied organic solvents were used, which all have a high intrinsic solution resistance. A three electrode configuration is commonly employed under such conditions: a working electrode (w.e.), a reference electrode (r.e.) and a counter (auxiliary) electrode (c.e.). A potential difference is measured between the r.e. and the w.e. and a current is monitored between the w.e. and c.e. The r.e. maintains a constant reference potential throughout the experiment and any change in applied potential appears across the w.e. solution interface. No current flows to the r.e., which is therefore left unpolarised and stable.

The reference electrode must meet certain requirements:

1. Be reversible and obey the Nernst equation.
2. The potential must not change with time and temperature and the resistance of this component must be relatively high.
3. It must not cause contamination of the test solution. (In experiments a Salt bridge is employed to avoid this effect).

The most commonly used reference electrodes are Ag/Ag^+ where polar solvents such as acetonitrile are the solvent and

Ag/AgCl in non polar solvents, for example, methylene chloride.

In organic media, Pt is the most commonly used w.e. as it is stable over a wide potential range. The c.e. is usually made of an inert material such as Pt and should have a large area compared with the w.e.

A.1.2 Solvent

The solvent used is dictated by the sample solubility and stability. There are however a number of other important features to consider. These are: usable potential range, dielectric constant, accessible temperature range, vapour pressure, viscosity, toxicity, donor or coordinating properties and ease of purification. For spectroelectrochemical experiments the onset of absorption of the solvent in the UV region is also important.

A.1.3 Supporting Electrolyte

The electrolyte is present to increase the conductivity of the solution and is present in concentrations of between 0.1 and 0.5M. This decreases the resistance between the w.e. and c.e. and also minimizes the error in potential measurement due to the uncompensated solution resistance, iR_u. It largely determines the structure of the double layer immediately adjacent to the electrode. The vast excess of ions present in the electrolyte compared with the test species eliminates migration as a mode of mass transport for the electroactive species.

A.1.4 Cell

A suitable cell must satisfy the following requirements:

1. It must have as low a resistance as possible which is particularly important with organic solvents and high currents. In order to achieve this the three electrodes are placed reasonably close to each other and the w.e. is kept small (so that all points on the surface of the electrode will be essentially equidistant from the much larger counter electrode).
2. A symmetric electical field must be established at the w.e. by optimizing the electrode geometry.
3. The temperature must be controlled.
4. It must be protected from air, water etc.
5. It must be easily dismantled.
6. The facility for separation of w.e. and c.e. during bulk electrosynthesis must be easily incorporated (in practice use a different cell design).

Figure A.1.1 shows a typical cell arrangement for conventional electrochemistry and Figure A.1.2 shows a three compartment cell for bulk electrosynthesis experiments.

Before discussing the techniques used to study electrode processes it is important to define certain terms used to describe types of charge transfer processes.

1. Reversible: The electron transfer to or from the electrode occurs more rapidly than the rate of diffusion of the redox active material to the electrode surface.
2. Quasi-Reversible: The electron transfer process is

Figure A.1.1: Typical Cell Arrangement for Conventional Electrochemistry

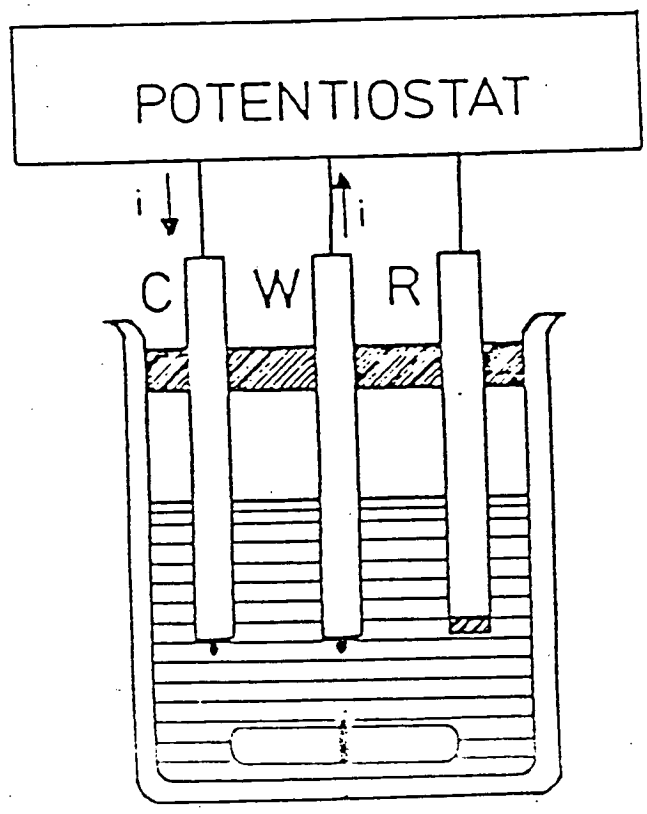

C, counter electrode

W, working electrode

R, reference electrode

Figure A.1.2: Three Compartment Cell for Controlled Potential Electrolysis

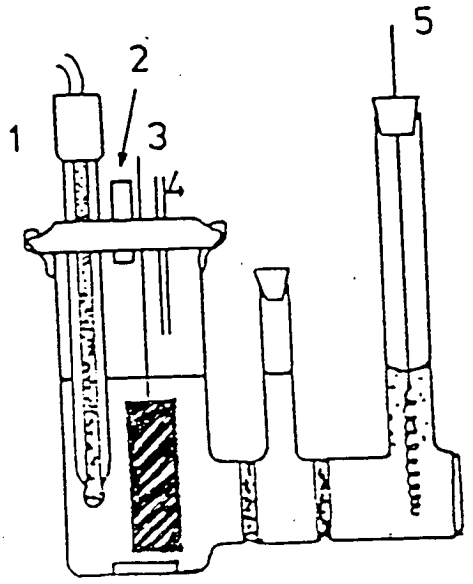

1 Reference Electrode

2 N_2 Inlet

3 Working Electrode

4 N_2 Outlet

5 Counter Electrode

governed by both diffusion and charge transfer kinetics.

3. Irreversible: The charge transfer process is much slower than the diffusion rate.

A.1.5 Cyclic Voltammetry

In cyclic voltammetry a stationary electrode is used in a quiet (unstirred) solution. The vast concentration of supporting electrolyte in solution and the thermostatically controlled cell means that the effects of mass transport due to convection and migration can be eliminated from further discussion. Diffusion is therefore the only means of mass transport of reactants and products between the bulk solution and the solution/electrode interface.

The potential of the electrode is varied linearly with time; the rate at which the potential is changed being the scan rate, ν (typically 20-500 mVs^{-1}). The current, i, is measured as a function of potential, E.

A typical cyclic voltammogram for a reversible process is shown in Figure A.1.3.

The current response is of an asymmetric peaked form, the increase in current occurring when the potential of the electrode is scanned into the range where the reactant begins to be reduced (or oxidised) at the electrode. The rate of this reaction increases rapidly as E increases. This leads to most of the reactant near to the surface of the electrode being consumed. The current is therefore limited by the rate at which additional reactant can diffuse to the electrode from the bulk solution. The current maximum occurs when the

tendency towards increasing current, because of the increasingly favourable potential, is just matched by the trend towards decreasing current which is imposed by the depletion of reactant near the electrode. Beyond the peak the latter of these effects occurs. Upon reaching a pre-set value, the "switching potential", the voltage scan is reversed to the starting value using the same scan rate, ν, as in the forward scan. The reversal current has a shape much like that of the forward peak for essentially the same reasons but in the opposite direction. The position of the peak of the reverse wave is not at the same potential as the forward peak and is shifted to more positive potentials in the case of a reduction and vice versa for an oxidation.

The parameters obtained from the cyclic voltammogram of most interest are the peak current, i_p^F, the potential at the maximum of the forward curve, E_p^F and the corresponding parameters for the reverse curve (i_p^R and E_p^R). By using these parameters we can determine the nature of a charge transfer process as shown in Table A.1.1. Figure A.1.3 indicates how the parameters are obtained from a cyclic voltammogram.

A.1.6 Voltammetry in a Stirred Solution

In order to determine if a redox process is an oxidation or a reduction stirred linear voltammetry can be used. Figure A.1.4 shows a typical stirred and unstirred voltammogram for a complex that undergoes both a reduction and oxidation. Conventionally processes with current traces

Figure A.1.3: Typical Cyclic Voltammogram for a Reversible Process

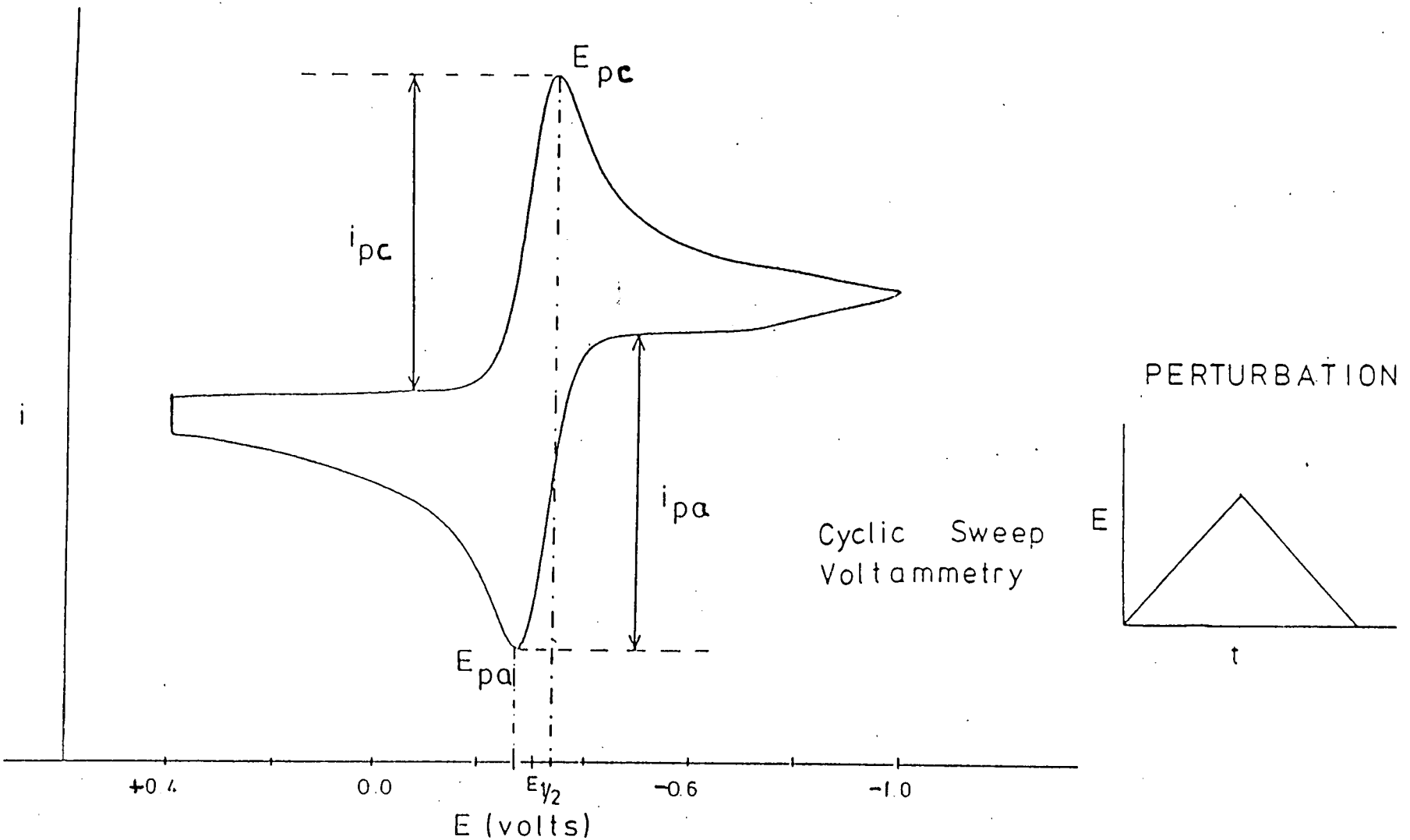

Table A.1.1: Cyclic Voltammetric Criteria for Reversible, Quasi-Reversible, Partially Reversible and Irreversible Charge Transfer Processes at 298K

Reversible	E_p is independent of ν
	$E_p^F - E_p^R = 59/n$ mV and is independent of ν
	$\frac{1}{2}[E_p^F + E_p^R] = E_{1/2}$, independent of concentration
	$i_p/\nu^{1/2}$ (current function) is independent of ν
	$i_p^R/i_p^F = 1$ and independent of ν
Quasi-reversible	E_p shifts with ν
	$E_p^F - E_p^R$ increases as ν increases
	$i_p/\nu^{1/2}$ is independent of ν
	i_p^R/i_p^F generally = 1
Partially-reversible (i.e. irreversible chemical reaction following charge transfer)	E_p increases by 30/n mV for a ten fold increase in ν, at low ν
	$i_p/\nu^{1/2}$ is independent of ν
	i_p^R/i_p^F increases towards 1 as ν increases
Irreversible	E_p shifts with ν
	$i_p/\nu^{1/2}$ is independent of ν
	There is no current on reverse scan.

ν = sweep rate in mVs^{-1}

n = number of electrons involved in the redox process

Figure A.1.4: Typical Stirred and Unstirred Voltammogram

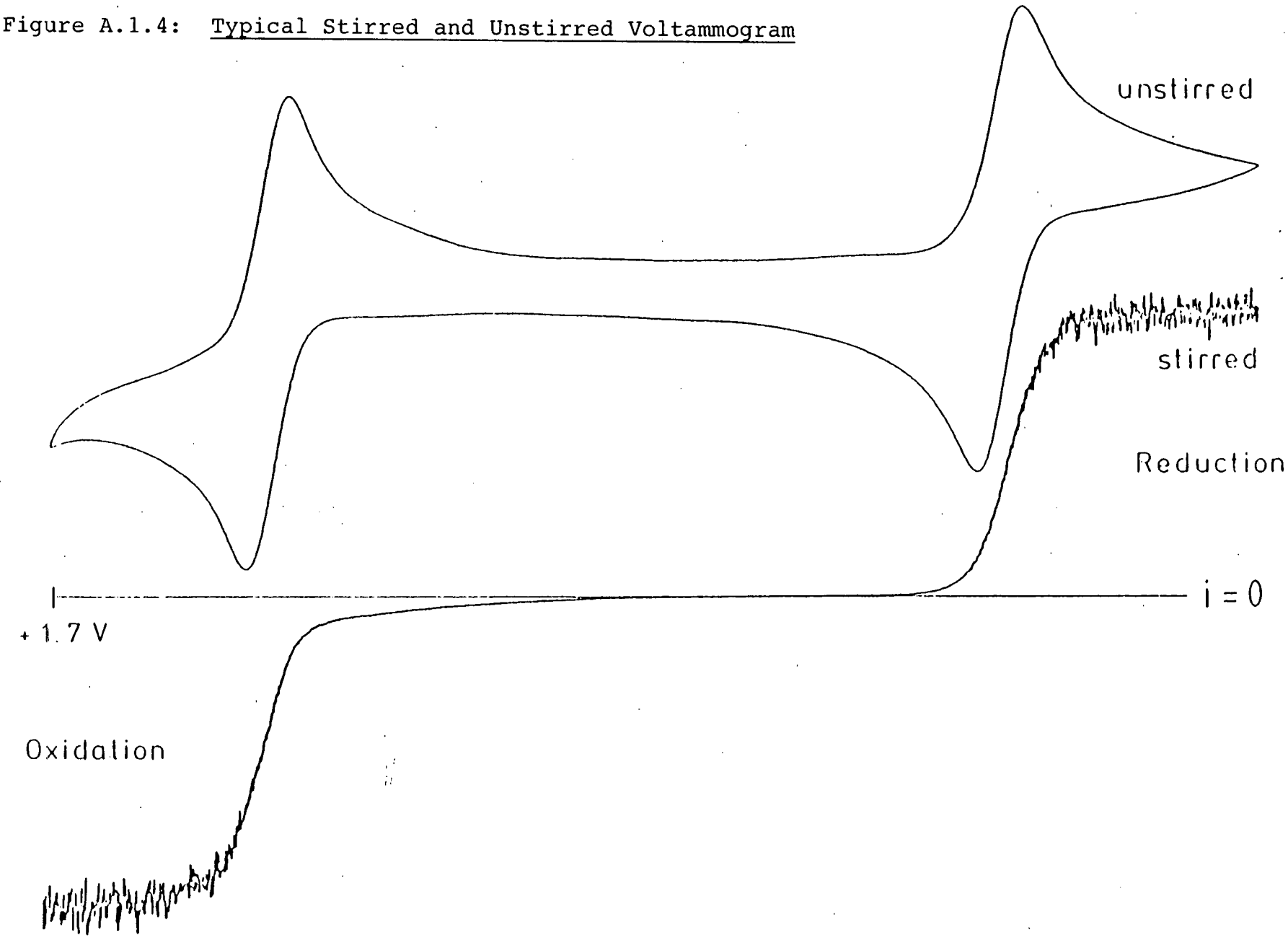

above the i = 0 line are reductions and those below are oxidations. In this type of voltammetry the mass transport is carried out by both convection and diffusion. For efficient stirring a rotating disc electrode (R.D.E.) and a slow scan rate should be used.

The RDE consists of a disc of the electrode material imbedded into a rod of insulating material. For example a Pt wire is surrounded by teflon or epoxy resin. The shaft of the RDE is linked directly to a motor and an electrical contact. The variable parameter of interest is the angular velocity, $\omega(s^{-1})$ where $\omega = 2\pi f$. A typical RDE is shown in the diagram below.

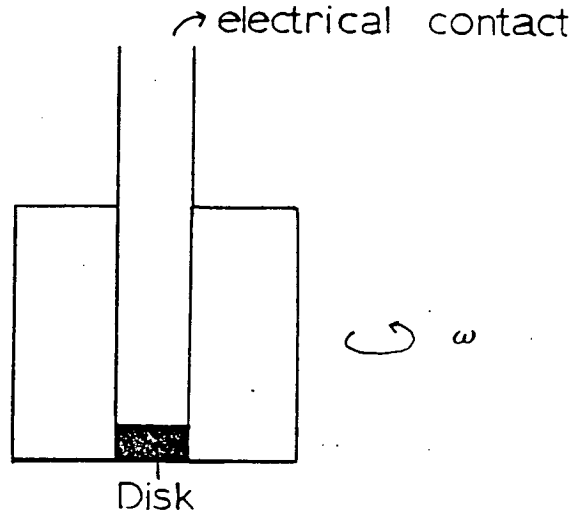

Access of the solution to all the electrode surface is uniform if the electrode radius is small compared with the insulating surround. The rate of mass transport to the electrode can be varied over a wide range and in a controlled way. For potentials where the surface concentration of

electroactive species is zero, the equation that relates the limiting current density and the rotation rate has been derived by Levich:

$$i_{i,c} = 0.620nFA\, D_O^{2/3}\, \omega^{1/2}\, \nu^{-1/6}\, C_O^*$$

where
- n = number of electrons
- F = Faradays constant (96487 $Cmol^{-1}$)
- A = area of electrode, cm^2
- D_O = diffusion coefficient, cm^2s^{-1}
- ν = kinematic viscosity, cm^2s^{-1}
- ω = angular frequency of rotation s^{-1} (2π x rotation rate)
- C_O^* = initial bulk concentration mol cm^{-3}

This equation is often used to test that the current is entirely mass transport controlled. A plot of i versus $\omega^{1/2}$ should be linear and pass through the origin. The slope may be used to determine the diffusion coefficient for the electroactive species.

A.1.7 a.c. Voltammetry

Alternating current (a.c.) voltammetry essentially involves the superposition of a small amplitude, relatively high frequency alternating potential upon a linearly scanning d.c. potential. The superimposed voltage is usually periodic in time such as a sinusoidal wave. Thus in addition to the d.c. potential an alternating current also flows. The net alternating current component is recorded as a function of the linear d.c. potential. For a reversible redox step the output current signal recorded is a symmetric peak centred

upon $E_{1/2}$ of the corresponding d.c. polarogram. Figure A.1.5 shows a typical reversible a.c. voltammogram.

A range of frequencies, ω, from about 10Hz-1000Hz can be used.

In a simple model, if the cell is considered as a capacitor-resistor network to which the sinusoidal voltage superimposed on a linear potential ramp is applied, the shape of the a.c. wave follows straightforwardly from considering it as the "first derivative" of the d.c. wave. However, although this argument gives an understanding of the shape of the wave, it should be treated with caution. It would be misleading to regard the a.c. voltammogram as merely a first derivative presentation. The a.c. experiment contains additional information; a new experimental variable, ω, is available which effectively controls the "timescale" of the experiment thus making the experiment a more sensitive test of the departure from reversibility than the d.c. mode. Similarly, the model fails to explain the dependence of peak height on the frequency of the a.c. voltage.

An additional advantage with a.c. is that under normal conditions the technique discriminates against the background "residual" or capacitive current. This is possible because of the differing phase relationships which the two current components, faradaic and capacitive currents, have with the applied voltage. Thus by phase sensitive detection the faradaic current can be measured exclusively, thus increasing the sensitivity to analyte concentrations of 10^{-6} - 10^{-7}M (the d.c. mode requires concentrations of 10^{-4} - 10^{-6}M).

A further advantage of using a.c. is that it is possible

Figure A.1.5: Typical a.c. Voltammogram for a Reversible Process

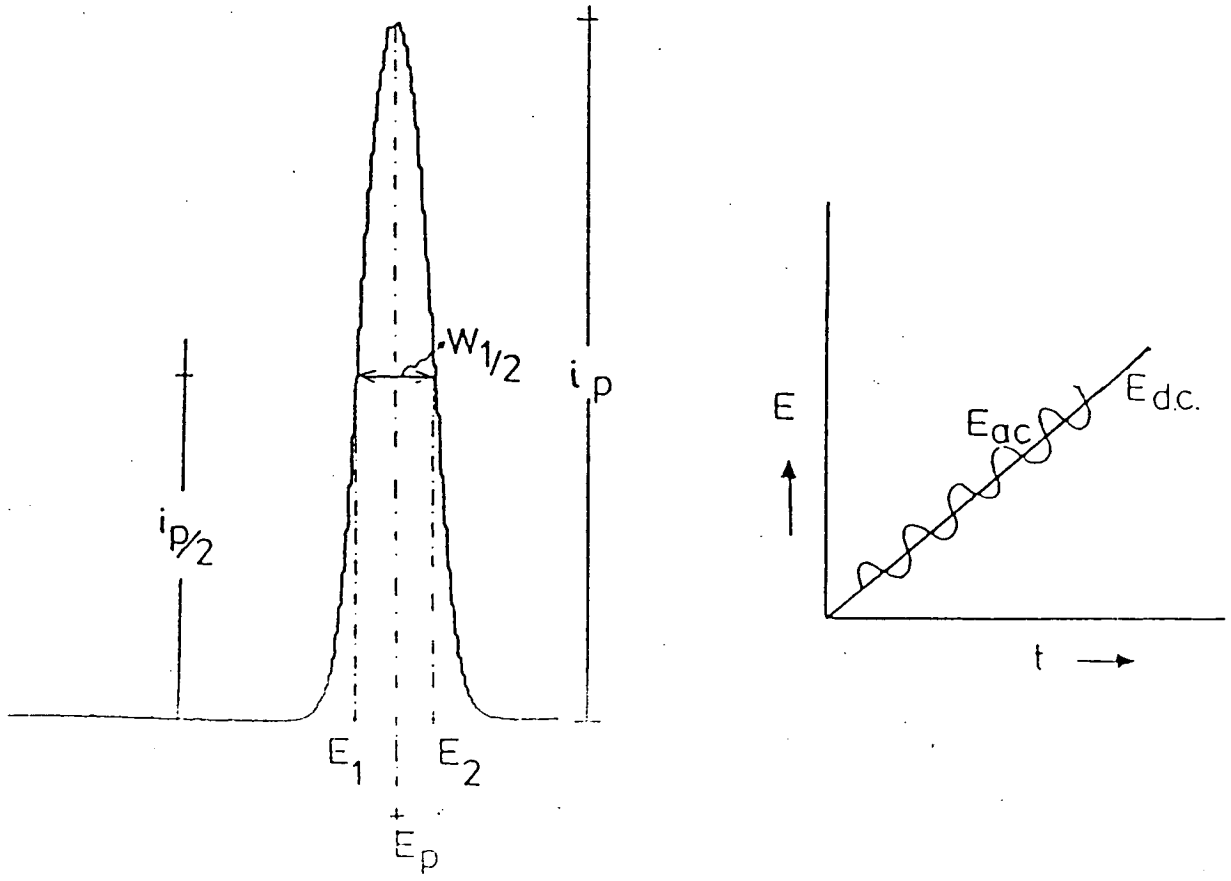

to resolve waves which are separated by as little as 40mV (150mV separation is required for d.c. voltammetry).

Reversibility criteria for a.c. voltammetry are:

(a) Potential

"E_p" is independent "ω".
$W_{1/2}$ = 90/n mV at 25° and independent of "ω".

(b) Current

A plot of "i_p" versus $\omega^{1/2}$ gives a straight line through the origin.

A.1.8 Electrosynthesis - Coulometry

Preparative scale electrolyses fall into two classes:

(a) Controlled Current (galvanostatic)

(b) Controlled Potential (potentiostatic)

The controlled potential method is the more often used. It consists simply of an experiment in which an electrochemical reaction is allowed to proceed at an electrode, the potential of which is held constant. The fixed potential must be more than 60mV past $E_{1/2}$ for 100% conversion.

The currents passing through the solution are relatively large and it is therefore necessary to work with a three electrode cell. A typical cell is shown in Figure A.1.2.

The w.e. and c.e. must be separated in this type of experiment otherwise products formed at each electrode would self cancel.

The current is measured as a function of time, with the solution stirred throughout. Figure A.1.6 shows a typical i versus t graph. The area under the curve gives the total quantity of electrical charge which has passed during

electrolysis (Q). Thus:

$$Q = \int_0^t i\,dt \qquad (1)$$

but $Q = nFM$ (2)

where m = number of moles of product, n = number of electrons and F = Faradays constant. Thus from an electrosynthesis experiment, assuming 100% efficiency, we can determine n, the number of electrons involved in the redox step.

A.1.9 REFERENCES

1. A.J. Bard and L.R. Faulkner, "Electrochemical Methods", John Wiley and Sons Inc. (New York), 1980.

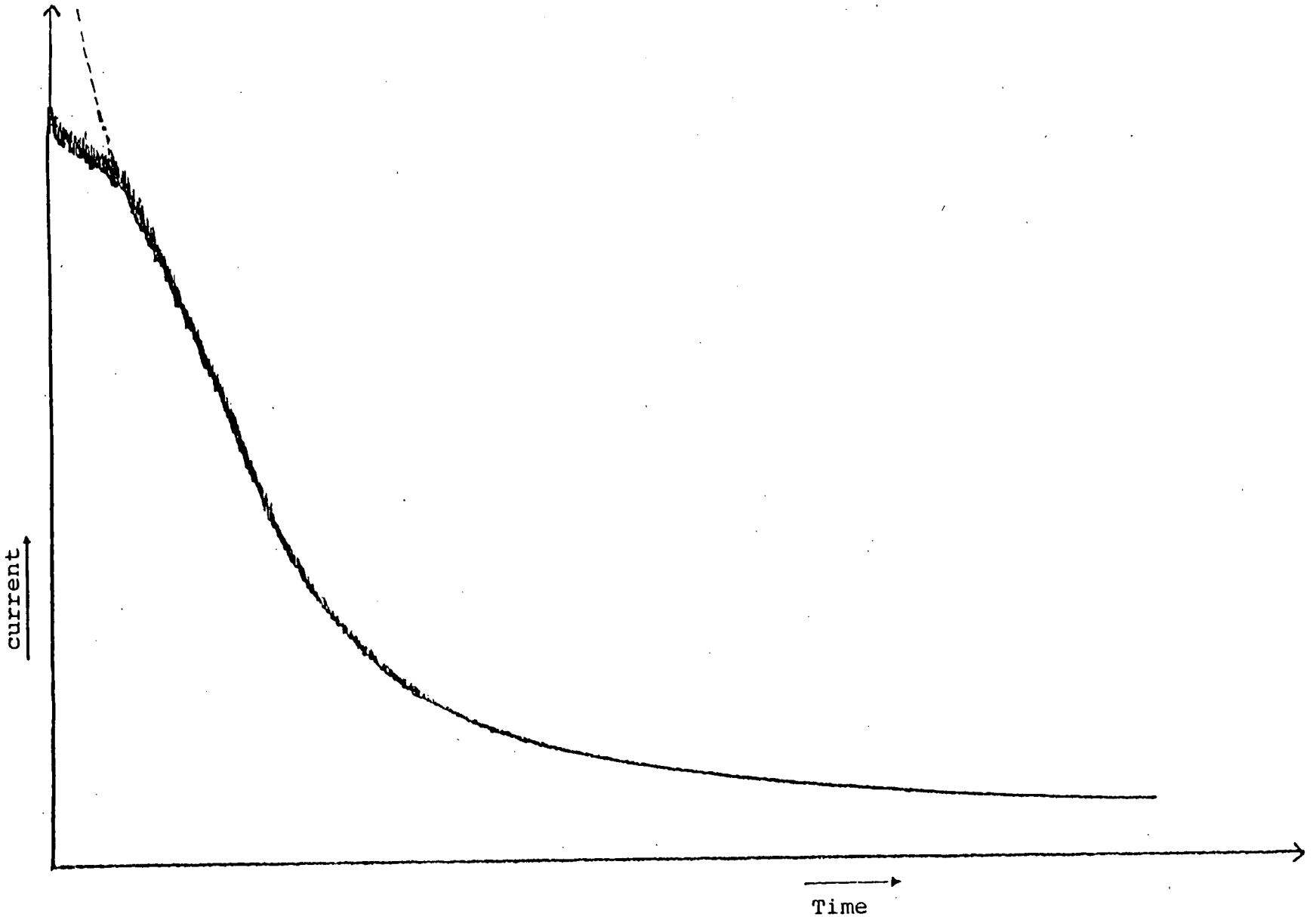

Figure A.1.6: Characteristic Current-Time Response for Controlled Potential Electrolysis

A P P E N D I X 2

A.2.1 STUDIES ON TWO MONOMERIC OSMIUM COMPLEXES

Attempts were made to prepare $[(PMe_2Ph)_3Os(\mu\text{-}Cl)_3Os(PMe_2Ph)_3]Cl$ by Chatt's method[1] i.e. by the interaction of $[OsCl_6]^{2-}$ with PMe_2Ph in methanol. A yellow solid was always obtained which was initially assumed to be the binuclear species. Addition of methanol/excess NH_4PF_6 to a dichloromethane solution of this in order to exchange the Cl^- anion yielded some yellow solid material together with a purple solution, from which purple crystals formed. The yellow material analysed as the expected $[(PMe_2Ph)_3Os(\mu\text{-}Cl)_3Os(PMe_2Ph)_3]PF_6$ species.

Microanalysis and the FAB mass spectrum of the purple crystals suggested that this complex was $[OsCl_2(PMe_2Ph)_4]PF_6$. Electrochemical studies showed that it had the trans isomeric form. The neutral monomeric species, trans $OsCl_2(PMe_2Ph)_4$[2] undergoes two one-electron oxidations at +0.28V and +1.55V (versus Ag/AgCl) whereas cis $OsCl_2(PMe_2Ph)_4$ undergoes one, one-electron oxidation at +0.74V. The complex under study showed a one-electron reduction at +0.28V and a one-electron oxidation at +1.55V (determined using stirred cyclic voltammetry. Appendix 1 gives details of this technique). Thus it was assigned to be $[Os(III)Cl_2(PMe_2Ph)_4]PF_6$.

The related complex $OsCl_2(P(OMe)Ph_2)_4$ was prepared as an intermediate in the preparation of $[(P(OMe)Ph_2)_3Os(\mu\text{-}Cl)_3Os(P(OMe)Ph_2)_3]PF_6$ by the reaction of $OsCl_2(PPh_3)_3$ and $P(OMe)Ph_2$ in degassed hexane. This complex was confirmed to have trans chloride ligands by a $^{31}P\{H\}$ n.m.r. study which showed a singlet at 85.3 ppm over a range of temperatures.

Electrochemical studies showed this complex to have two one-electron oxidations at +0.35V and +1.53V (versus Ag/AgCl). The first oxidation being slightly more difficult than in the case of the species where L = PMe_2Ph; this is likely to be an effect of the electronic properties of the P(III) ligands as discussed in Chapter 4.

Spectroelectrochemical studies were carried out as previously described. The generation of the Os(III) species from Os(II) was carried out at a suitable electrogeneration potential. The temperature was maintained at 243K. The spectra were recorded over the range 4,000-40,000 cm^{-1}. The positions of the bands observed and their extinction coefficients are given in Table A.2.1. Figure A.2.1 a, b and c shows the spectra of $Os(II)Cl_2(P(OMe)Ph_2)_4$, $Os(II)Cl_2(P(OMe)Ph_2)_4 \rightarrow [Os(III)Cl_2(P(OMe)Ph_2)_4]^+$ and $[Os(III)Cl_2(P(OMe)Ph_2)_4]^+$ respectively.

The electronic spectrum of trans $[OsCl_2(PMe_2Ph)_4]PF_6$ is very similar to that of trans $[OsCl_2(P(OMe)Ph_2)_4]^+$ (see Figure A.2.2).

The major bands in the oxidised species are at higher energy when L = PMe_2Ph than when L = $P(OMe)Ph_2$. It is thought that the band at approximately 30,000 cm^{-1} is due to an intraligand transition because of its intensity ($\varepsilon \sim 2000$ $mol^{-1}cm^{-1}dm^3$) and its very small energy shift on oxidation. The lower energy band is only present in the Os(III) state and is assigned to a $Cl^- \rightarrow$ Os(III) ligand to metal charge transfer transition since it varies little with changing phosphine ligand. We note that in neither case is there a NIR absorption band similar to that observed in the

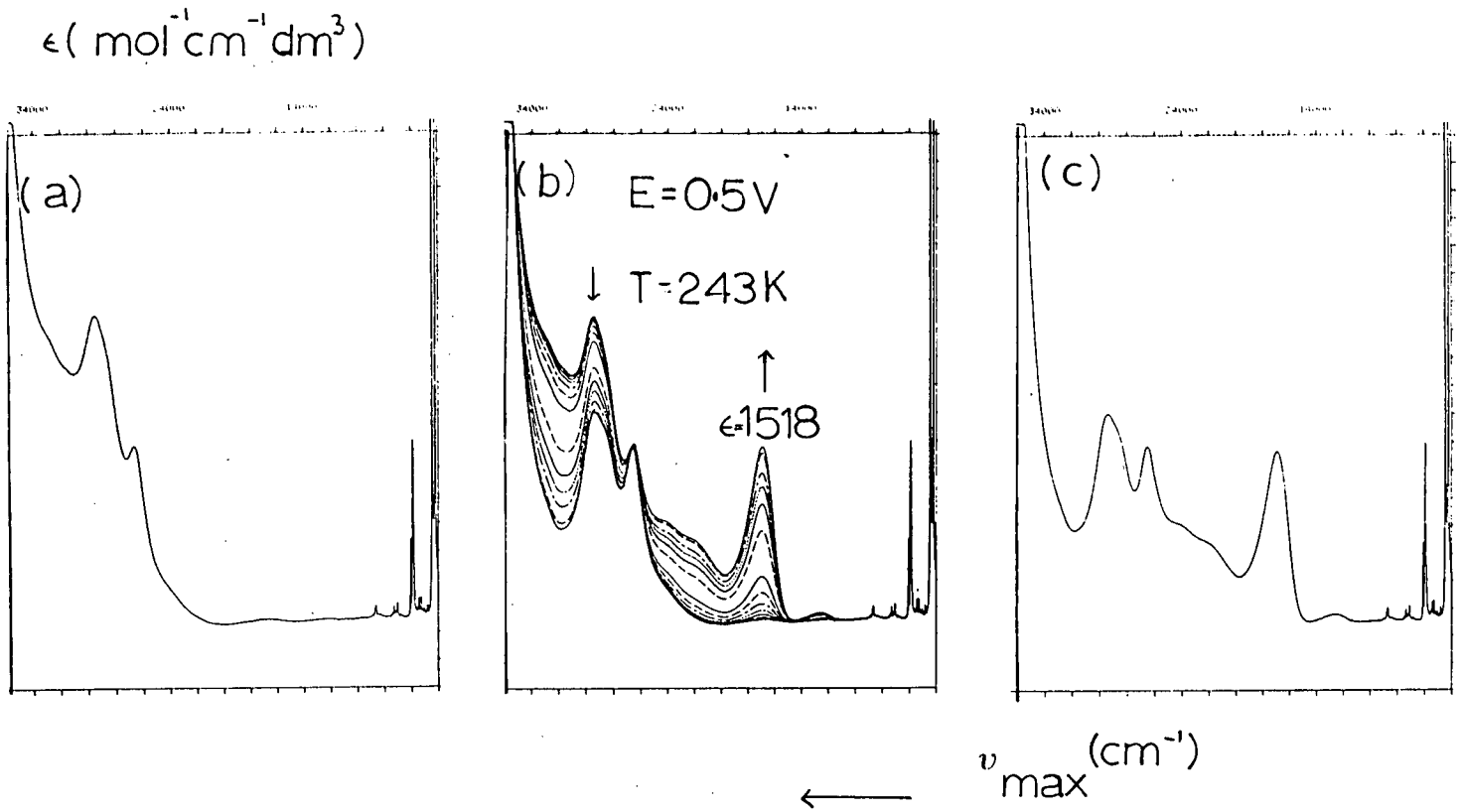

Figure A.2.1: Electronic Absorption Spectrum of (a) $OsCl_2(P(OMe)Ph_2)_4$, (b) $[OsCl_2(P(OMe)Ph_2)_4] \rightarrow [OsCl_2(P(OMe)Ph_2)_4]^+$ and (c) $[OsCl_2(P(OMe)Ph_2)_4]^+$ in Methylene Chloride / 0.5M $TBABF_4$

Figure A.2.2: Electronic Absorption Spectrum of $[OsCl_2(PMe_2Ph)_4]PF_6$ in Methylene Chloride at T = 293K

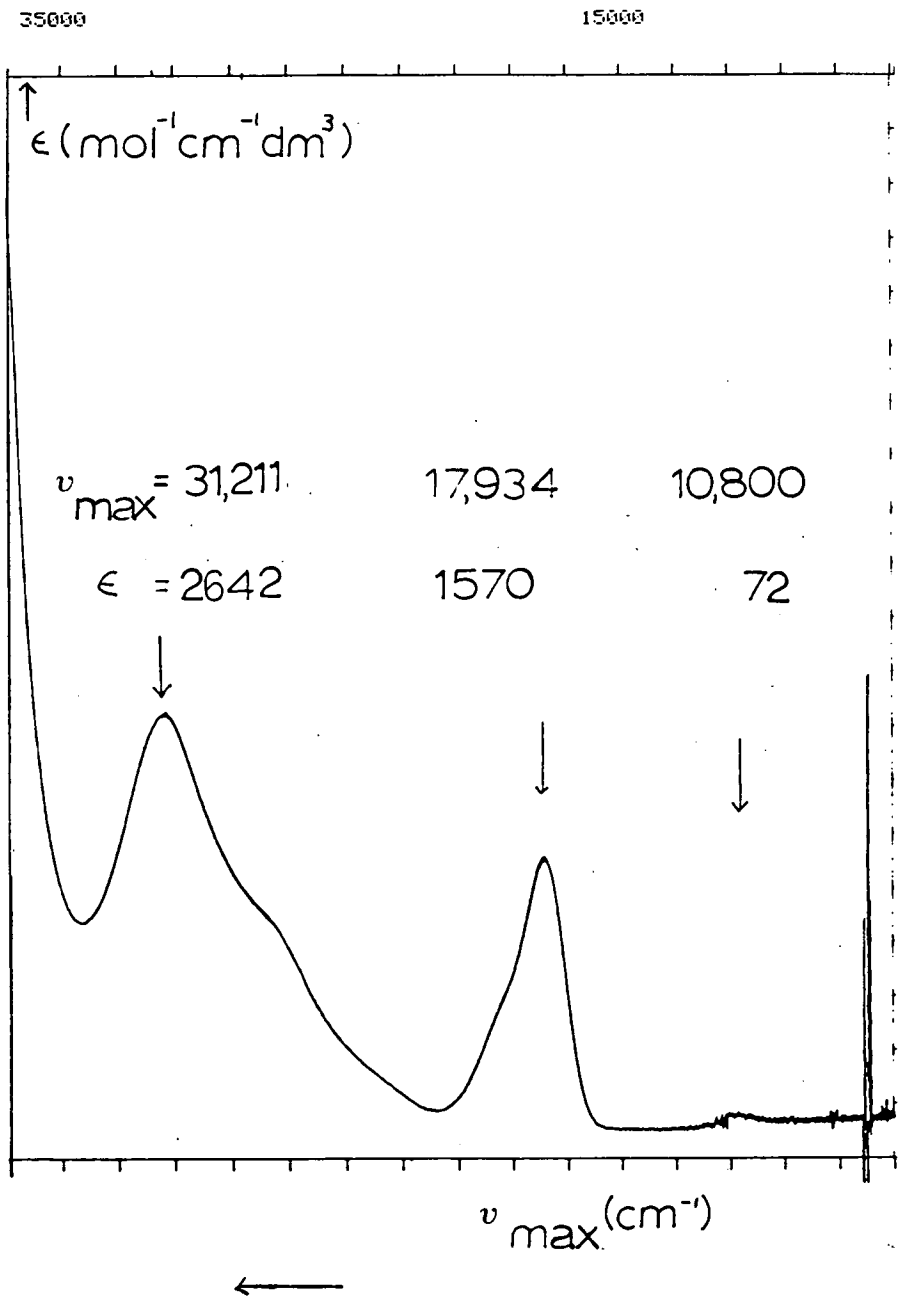

Table A.2.1: Values of ν_{max} for $OsCl(P(OMe)Ph_2)_4$ and $[OsCl_2(P(OMe)Ph_2)_4]^+$ in Methylene Chloride /0.5M TBABF at T = 243K

	ν_{max} (cm^{-1})	ε ($mol^{-1}cm^{-1}dm^3$)
$OsCl_2(P(OMe)Ph_2)_4$	26,700	1578
	29,600	2665
$[OsCl_2(P(OMe)Ph_2)_4]^+$	13,000	68
	17,000	1518
	26,700	1585
	29,600	1856

related binuclear species.

Earlier studies[2] into the behaviour of trans $OsCl_2(PMe_2Ph)_4$ suggested that the species was not a genuine trans $[OsCl_2(PMe_2Ph)_4]$ complex but had only three of its phosphine ligands bound conventionally to the Os(II) centre with the further phosphine ligand being only loosely bound. This was concluded on the basis of:

1. n.m.r. studies
2. Electrochemical Studies

1. The trans isomer would be expected to exhibit a singlet in the $^{31}P\{H\}$ n.m.r. spectrum as all P nuclei are equivalent. At room temperature a broad singlet is observed. As the temperature is reduced another resonance becomes apparent until at 193K the spectrum exhibits a very sharp singlet superimposed on a complex pattern of resonances. This suggests that more than one P environment is present in the molecule.

2. All other trans $OsCl_2(PMe_2Ph)_3L$ complexes, where L = MeCN, dmf, dmso, PhCN, C_2H_4, N_2, studied showed redox potentials almost superimposable on those of the cis complexes. The redox couples of the first oxidation of cis and trans $OsCl_2(PMe_2Ph)_4$ are however separated by 0.46V.

Unfortunately attempts to obtain a single crystal, suitable for X-ray structural studies, of the trans $OsCl_2(PMe_2Ph)_4$ species failed. It was therefore decided to

carry out a structural study of $[OsCl_2(PMe_2Ph)_4]PF_6$ to determine if this exhibits any differences in Os-P bond lengths.

A view of the cation (without H-atoms) is shown in Figure A.2.3. Table A.2.2 gives a selection of bond lengths and angles.

The X-ray crystal structure confirms the trans arrangement of the chloride ligands. Both Os-Cl distances are identical. Two of the trans Os-P distances are very similar 2.436 and 2.441Å whereas the other two show a greater difference being 2.416Å and 2.460Å. The complex trans $[Os(II)(CHO)(CO)(dppe)_2]SbF_6$,[3] where dppe = diphenylphosphinoethane, also has two such Os-P pairs. The first having bond lengths of 2.429 and 2.380Å and the other 2.414 and 2.389Å. The observation of one longer Os-P bond in $[OsCl_2(PMe_2Ph)_4]^+$ suggests that one phosphine ligand is in fact more loosely bound and hence is easily displaced by other ligands. The phenyl rings attached to P_1 and P_4 are separated by only 3.83Å and the angle between the two phenyl planes is 8.79°. This suggests that there may be an interaction between the two rings. No such interaction is evident between the other phenyl rings.

A.2.2 EXPERIMENTAL

Electrochemical studies were performed using the PAR model 170 potentiostat and programmer as described previously. The temperature was controlled as described previously.

Spectroelectrochemical studies were carried out as described previously using the O.T.T.L.E. cell and the Perkin

Figure A.2.3: View of the $[OsCl_2(PMe_2Ph)_4]^+$ Cation

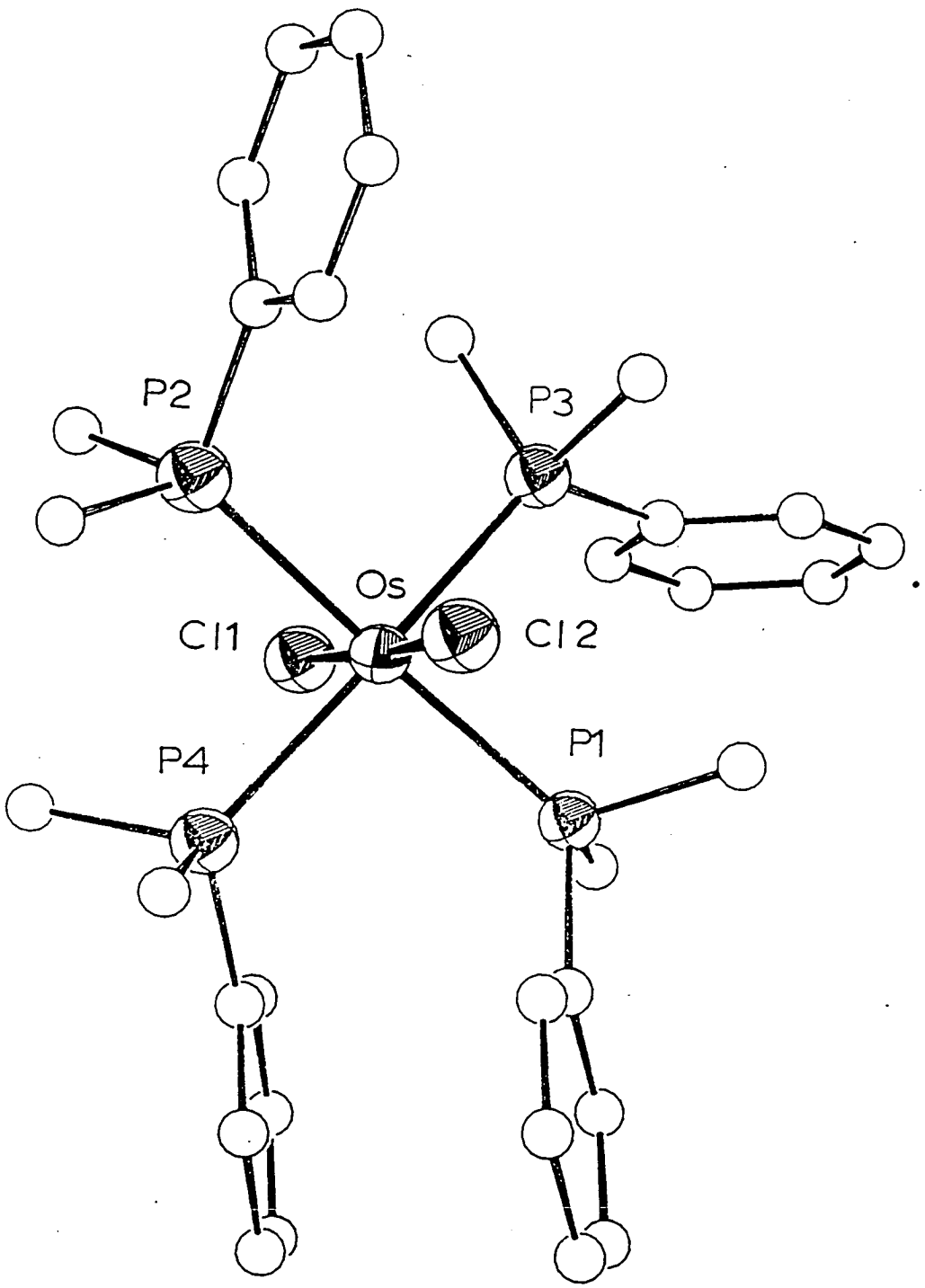

Table A.2.2: Selected Bond Lengths and Angles for

$[OsCl_2(PMe_2Ph)_4]^+$

Bond Lengths(A) with standard deviations

Os	-Cl(1)	2.340(3)	P(2)	-C(211)	1.844(7)
Os	-Cl(2)	2.340(3)	P(2)	-C(221)	1.811(12)
Os	- P(1)	2.416(3)	P(2)	-C(231)	1.810(14)
Os	- P(2)	2.460(3)	P(3)	-C(311)	1.844(7)
Os	- P(3)	2.441(3)	P(3)	-C(321)	1.801(11)
Os	- P(4)	2.436(3)	P(3)	-C(331)	1.839(12)
P(1)	-C(111)	1.845(7)	P(4)	-C(411)	1.842(7)
P(1)	-C(121)	1.807(11)	P(4)	-C(421)	1.805(11)
P(1)	-C(131)	1.802(11)	P(4)	-C(431)	1.829(12)

Angles(degrees) with standard deviations

Cl(1)	-	Os	-Cl(2)	177.06(9)
Cl(1)	-	Os	- P(3)	84.00(9)
Cl(1)	-	Os	- P(4)	85.48(9)
Cl(1)	-	Os	- P(1)	96.52(9)
Cl(1)	-	Os	- P(2)	92.02(9)
Cl(2)	-	Os	- P(3)	94.95(9)
Cl(2)	-	Os	- P(4)	95.62(9)
Cl(2)	-	Os	- P(1)	86.21(9)
Cl(2)	-	Os	- P(2)	85.24(10)
P(3)	-	Os	- P(4)	169.40(9)
P(3)	-	Os	- P(1)	89.82(9)
P(3)	-	Os	- P(2)	90.59(10)
P(4)	-	Os	- P(1)	90.15(9)
P(4)	-	Os	- P(2)	91.00(10)
P(1)	-	Os	- P(2)	171.45(9)

Elmer Lambda 9 Spectrophotometer. The temperature was controlled as previously described.

Elemental analyses were carried out by the Department of Chemistry, University of Edinburgh.

FAB mass spectra were recorded by the Department of Chemistry, University of Edinburgh, using the Kratos 50-TC spectrometer and 3-nitrobenzylalcohol (3-NOBA) as the matrix.

Materials

Na_2OsCl_6, K_2OsCl_6 were obtained from Johnson Matthey.

PMe_2Ph[4] was made according to the literature preparation.

$P(OMe)Ph_2$ was obtained from Aldrich.

Methylene chloride was purified as described previously. All other solvents were used as obtained without further purification.

1. Preparation of $[OsCl_2(PMe_2Ph)_4]PF_6$

K_2OsCl_6 (0.15g) in degassed water (3.5ml) and PMe_2Ph (0.18ml) in degassed ethanol (15.8ml) were mixed together and heated under N_2. After 30 minutes yellow solid formed. There was no change after a further 30 minutes so the mixture was cooled and filtered. The yellow solid was washed with ethanol and diethylether. This was then dissolved in methylene chloride and to this methanol/NH_4PF_6 were added. After a short while yellow solid formed. This was filtered and the remaining solution set aside. On leaving overnight, purple crystals formed. These were filtered and washed with cold methanol and diethylether and dried in vacuo (0.113g, 38%).

Elemental Analysis: Found C:40.7%, H: 4.79%, N: 0%

Calculated for $C_{32}H_{44}F_6P_5Cl_2Os$

C: 40.1%, H: 4.59%, N: 0%

FAB Mass Spectrum: Found $M^+ = 814$ (100%)

$M^+ = 676$ (90%)

Calculated for $[OsCl_2(PMe_2Ph)_4]^+$

$M^+ = 812.9$

$[OsCl_2(PMe_2Ph)_3]^+$

$M^+ = 675.$

Single Crystal Structure of $[OsCl_2(PMe_2Ph)_4]PF_6$

Crystal Data: $[C_{32}H_{44}Cl_2Os\ P_4]PF_6$, M = 958.61, monoclinic space group $P2_1/c$, a = 11.4149(13), b = 26.5376(21), c = 12.6375(8), β = 92.580(7), V = 3824.3Å (from setting angles for 38 reflections with $27 < 2\theta < 28$, λ = 0.71073Å), Z = 4, D_{calc} = 1.995g cm^{-3}, T = 293K, purple plates, 0.12 x 0.23 x 0.62mm, μ = 70.48 cm^{-1}, $F(000)$ = 1900.

Data Collection and Processing: Stöe STADI-4 diffractometer, graphite monochromated Mo - K_α X-radiation, T = 293K, $\omega/2\theta$ scans using learnt profile method,[5] 5113 data collected ($2\theta_{max}$ = 45°, h -12 -11, 1 0 28, l -8 -8), 5113 unique data (R_{int} = 0.0000) giving 4913 with $F > 6\sigma(F)$ for use in all calculations. No significant crystal decay or movement. Initial corrections for absorption based on ψ scans were applied, minimum and maximum transmission factors are 0.1021 and 0.2179 respectively.

Structure Solution and Refinement: A Patterson synthesis located the Os atom and subsequent iterative cycles of least squares refinement and difference Fourier synthesis located the positions of all non-H atoms. These were refined by least squares refinement using SHELX-76 with anisotropic thermal parameters for Os, P, Cl and F. DIFABS[6] absorption correction was carried out with minimum correction = 0.898 and maximum correction = 1.168. The H atoms were fixed in calculated positions by AFIX. Phenyl rings were constrained to be rigid hexagons. At final convergence $\underline{R}$ = 0.0488, $\underline{R}_w$ = 0.0608, $\underline{S}$ = 1.036 for 207 refined parameters and the final ΔF synthesis showed no peak above 0.887eA^{-3}. The weighting scheme $\underline{W}^{-} = \sigma^2(F) + 0.000063F^2$ gave satisfactory analyses and in the final cycle $(\Delta/\sigma)_{max}$ = 0.039. Atomic scattering factors were inlaid[7] or taken from reference 8.

The figure was produced using ORTEP.[9]

2. Preparation of $OsCl_2(P(OMe)Ph_2)_4$

$OsCl_2(PPh_3)_3$ (0.140g) and $P(OMe)Ph_2$ (0.127g) were heated under reflux in degassed hexane (30ml) under N_2. The initial dark green solution gradually became paler in colour. After heating for 1 hour the colour was pale green. After 3 hours the pale green solution was cooled. Pale green crystals formed on cooling. This was filtered and washed with hexane and diethylether and dried in vacuo (0.102g, 68%).

Elemental Analysis: Found C: 55.47%, H: 4.62%, N: 0%

Calculated for $C_{52}H_{52}P_4O_4Cl_2Os$

C: 56.23%, H; 4.93%, N: 0%

FAB Mass Spectrum: Found $M^+ = 1126$ (10%)

$M^+ = 910$ (100%)

Calculated for $OsCl_2(P(OMe)Ph_2)_4$

$M^+ = 1124.9$

$OsCl_2(P(OMe)Ph_2)_3$

$M^+ = 909$

$^{31}P\{^1H\}$ n.m.r. 85.33 ppm - singlet

A.2.3 REFERENCES

1. J. Chatt and R.G. Hayter, J.Chem.Soc.; 1961, 896.
2. V.T. Coombe, Ph.D. Thesis, University of Edinburgh, 1985. V.T. Coombe, G.A. Heath, T.A. Stephenson, J.D. Whitelock and L.J. Yellowlees, J.Chem.Soc., Dalton Trans.; 1985, 947.
3. G. Smith, D.J. Cole-Hamilton, M. ThorntonPett and M.B. Hursthouse, J.Chem.Soc., Dalton Trans.; 1985, 387.
4. W.C. Davies and W.J. Jones, Chem.Soc.Journal; 1929, 1, 33.
5. W. Clegg, Acta Cryst. A; 1981, 37, 22.
6. DIFABS: N.G. Walker and D. Stuart, Acta Cryst. A; 1983, 39, 158.
7. SHELX-76: "A Program for Crystal Structure Determination and Refinement". G.M. Sheldrick, University of Cambridge, England, 1976.
8. D.T. Cromer and J.L. Mann, Acta Cryst.; 1968, A24, 321.
9. ORTEP: P.D. Mallinson and K.W. Muir, J.Appl.Cryst.; 1985, 18, 51.

ABBREVIATIONS AND NOTES

ABMO	antibonding molecular orbital
2,2' bipy	2,2'-bipyridine
4,4' bipy	4,4'-bipyridine
bpea	1,2 bis (4-pyridyl)ethane
bpm	1,2 bis (4-pyridyl)methane
bps	bis (4-pyridyl) sulphide
bpym	2,2'-bipyrimidine
bqd	p-benzoquinonedimmine
^{n}Bu	normal butyl
^{t}Bu	tertiary butyl
COD	1,5 cyclooctadiene
Cy	cyclohexyl
dap	diazapyrene
DMF	dimethylformamide
D_o	diffusion coefficient
dppm	(1,2-diphenylphosphino)ethane
EHMO	extended Hückel molecular orbital
e.s.d.	estimated standard deviation
Et	ethyl
e.p.r.	electron paramagnetic resonance
FAB	fast atom bombardment
HOMO	highest occupied molecular orbital
kK	$cm^{-1} \times 10^{-3}$
LUMO	lowest unoccupied molecular orbital
M^{+}	molecular ion peak
Me	methyl

3,3'-Me_2-4,4'-bipy	3,3'-dimethyl-4,4'bipyridine
NIR	near infra-red
n.m.r.	nuclear magnetic resonance
3-NOBA	3-nitrobenzylalcohol
norb	norbornadiene
OMe	methoxy
O.T.T.L.E.	optically transparent thin layer electrode
Ph	phenyl
py	pyridine
pym	pyrimidine
pyz	pyrazine
sh	shoulder
$TBABF_4$	tetrabutylammonium tetrafluoroborate
THF	tetrahydrofuran
ppm	parts per million
p-tol	4-methylphenyl
UV	ultra violet
VIS	visible
α	charge transfer coefficient
γ	$(D_O/D_R)^{1/2}$
ε	extinction coefficient ($mol^{-1}cm^{-1}dm^3$)
ν_{max}	wavenumber of band maximum
ν_{IT}	wavenumber of intervalence charge transfer band

All E values quoted are versus Ag/AgCl on which ferrocene is oxidised at +0.56V unless otherwise stated.

LIST OF COURSES ATTENDED

Electronic Structures of Inorganic Complexes

by Drs. L.J. Yellowlees and A.J. Welch

Recent Avances in Inorganic Chemistry

by Drs. A.J. Welch, L.J. Yellowlees, S.K. Chapman and M. Schröder

Catalysis

by Drs. D.A. Whan, M.S. Spencer and J.P. Candlin: I.C.I. Staff

Industrial Management

by Professor S. Coke, Department of Business Studies, University of Edinburgh

Electroanalytical Methods

by Dr. G.A. Heath

Solving and Refining Crystal Structures

by Drs. A.J. Blake and R.O. Gould

Electrochemistry

by Drs. L.J. Yellowlees and H.H.J. Girault

Departmental Research Seminars and Colloquia

University of Strathclyde Inorganic Club Conferences 1988, 1989

Butler Postgraduate Electrochemistry Meetings 1987, 1988, 1989; University of Edinburgh

ISE Conference 1988, University of Strathclyde

R.S.C. (Dalton Division) Autumn Meeting, 1988, Birmingham